69-13,996

OLDFIELD, William Anthony, 1931-

COMPUTER MODEL STUDIES IN MATERIALS SCIENCE.

Stanford University, Ph.D., 1969
Engineering, metallurgy

University Microfilms, Inc., Ann Arbor, Michigan

COMPUTER MODEL STUDIES IN MATERIALS SCIENCE

A DISSERTATION

SUBMITTED TO THE DEPARTMENT OF MATERIALS SCIENCE

OF STANFORD UNIVERSITY

IN PARTIAL FULFILLMENT OF THE REQUIREMENTS

FOR THE DEGREE OF

DOCTOR OF PHILOSOPHY

By

William Oldfield

November 1968

I certify that I have read this thesis and that in my opinion it is fully adequate, in scope and quality, as a dissertation for the degree of Doctor of Philosophy.

William A. Tiller

I certify that I have read this thesis and that in my opinion it is fully adequate, in scope and quality, as a dissertation for the degree of Doctor of Philosophy.

G. M. Pound

I certify that I have read this thesis and that in my opinion it is fully adequate, in scope and quality, as a dissertation for the degree of Doctor of Philosophy.

Robert L. Street

Approved for the University Committee
on the Graduate Division:

Virgil K. Whitaker
Dean of Graduate Division

COMPUTER MODEL STUDIES IN MATERIALS SCIENCE

William Oldfield, Ph.D.
Stanford University, 1968

Computer models are the logical development of the "Conceptual Model" approach. The basis of the computer model method has been outlined and illustrated by a model treatment of diffusive heat flow.

The computer model technique has been used to study a number of phenomena associated with materials. The methods which have been used have been classified as those designed to apply science to technology, and those to be employed on a more basic level. A model study of the freezing of cast iron has been described as an illustration of the first class of model. A computer model of a freezing cylindrical casting has been developed which simulates the production of real castings. The model forecasts the solidification sequence for the casting, the graphite structure variation, and the change of temperature with time at various positions within the casting. It was used to estimate the changes in microstructure induced by the solidification pattern, and it forecasts behavior which had never been observed previously. Subsequent experiments confirmed the predictions. A model study of dendrite growth has also been described in some detail. The model is noteworthy as the first treatment which does not invoke the "Maximum Velocity" criterion. The behavior of the model under restrictive conditions confirmed the analytical results of Ivantsov and Temkin. Free growth of the crystal model indicated that branching is initiated near the crystal tip, and that the branching process is associated with fluctuation of the growth velocity. The predicted sequence was subsequently observed by Morris and Winegard.

The uses of computer models in several areas of Materials Science are briefly discussed and illustrated by the descriptions of a model which simulates Ostwald "ripening", and a model which synthesises the patterns produced by crystal defects under electron beam microscopy.

ACKNOWLEDGEMENTS

I was encouraged to return to the University by Professor William A. Tiller. I am deeply indebted to him for his consistent support, his guidance, and his stimulating approach to science which has made my study richly profitable. My debt of gratitude extends to the faculty of the Department of Materials Science for their patience with a difficult student, and also to H. Morrogh, F.R.S. who guided my first attempts at research and introduced me to the study of solidification.

Many other scientists influenced the development of this research. The scientific community at Owens-Illinois Technical Center introduced me to computers. G. T. Geering, who cooperated in the computer modelling work, Ron Hiskes, and others in the crystallogenics research group all provided the atmosphere in which this work could be carried forward. The management and staff at Battelle Memorial Institute also contributed in many ways to the production of this dissertation.

I wish to thank my wife, Freda, for her faith and support during the difficult years and also my children, who kept us in good heart throughout the venture. I also wish to express my gratitude to my father and to my late mother, who provided the base from which this undertaking was developed.

The Air Force Office of Scientific Research, Grant AFOSR-731-65 provided financial support.

TABLE OF CONTENTS

Page

ABSTRACT iii

ACKNOWLEDGEMENTS v

A. AN INTRODUCTION TO THE USE OF COMPUTER MODELS IN MATERIALS SCIENCE. 1

Chapter I: Introductory Ideas. 2

1. The Model Concept. 2

2. The Application of Computer Models in Materials Science. 5

Chapter II: A Comparison of the Model and Analytic Approaches. . 9

1. Model Treatment of Diffusive Flow. 9

B. A COMPUTER SIMULATION OF THE FREEZING OF A CAST IRON BAR 26

Chapter III: Conceptual Basis for the Model. 27

1. The Freezing of Cast Iron. 27

2. Treatment of Heat Flow in the Casting. 34

3. Nucleation Processes 35

4. Eutectic Solidification. 40

5. Mechanical Effects: Cell-Cell and Cell-Mold Wall Interactions 41

Chapter IV: Combination of the Separate Models Into a System: Trial Calculations. 46

1. Simulation of the Freezing of an Isothermal Cylinder . . 46

2. Freezing of a Non-Isothermal Cylinder. 49

3. The Effect of Sulphur on Solidification. 51

Chapter V: Study of Primary Phase Solidification and the Refinement of the Model 58

1. Primary Phase Solidification 58

2. The Computer Model With Primary Phase Solidification Included 62

TABLE OF CONTENTS (Continued)

Page

Chapter VI: Model Study of Casting Solidification. 69

1. Aims of the Study. 69

2. The Soundness of Cast Iron 70

3. Flake Graphite Structure 83

C. A STUDY OF DENDRITE GROWTH BY MEANS OF A COMPUTER MODEL. 85

Chapter VII: Dendrite Growth 86

1. A Description of a Growing Dendrite. 86

2. The Study of Dendrite Growth 87

3. The Need for a Model Study 91

Chapter VIII: A General Treatment of Heat Transfer by Numerical Transformation of Coordinates. 92

1. The Simulation of Dendrite Growth. 92

2. One-Dimensional Heat Transfer. 93

3. Model Calculation. 95

4. Initial Conditions 97

5. One-Dimensional Flow Channels. 100

6. Outermost Compartment. 105

7. Central Compartments 106

8. Surface Compartment. 107

9. Application of the Solid/Liquid Interface Boundary Condition. 111

10. Preparation of a New Orthogonal Network. 117

Chapter IX: Simulation of Ice and Tin Dendrites 124

1. Comparison With Ivantsov's Results 124

TABLE OF CONTENTS (Continued)

Page

2. Simulation of a Non-Isothermal Dendrite. 131

3. Modification to Increase Stability 133

4. Tin Dendrites Simulated by the Runge-Kutta Method. . . . 136

5. Long-Term Growth of Tin Dendrites. 138

Chapter X: The Development of Crystal Shape. 145

1. The Maximum Velocity Principle 145

2. "Natural Selection" of Tip Shape 145

3. Oscillatory Growth 147

Chapter XI: Special Forms of Dendrite Growth 151

1. Varieties of Dendrite Growth 151

2. Arrays and Spherulites - Discussion. 152

3. Arrays and Spherulites - Initial Conditions. 154

4. Arrays and Spherulites - Results and Discussion. 156

5. Anisotropic Crystals 159

D. GENERALIZATION OF THE IDEAS. 163

Chapter XII: Bubble Growth and Electron Beam Diffraction 164

1. The Generality of Modelling Methods. 164

2. Ostwald Ripening and Bubble Growth 165

3. The Transmission of an Electron Beam Through a Foil. . . 167

4. Extension of the Ideas 171

5. Summary and Conclusions. 173

REFERENCES 179

TABLE OF CONTENTS (Continued)

Page

APPENDIX A. MODEL FOR HEAT FLOW ACROSS A PLATE A-1

APPENDIX B. HEAT FLOW ACROSS A CYLINDER B-1

APPENDIX C. PROGRAM LISTING - MAIN PROGRAM FOR THE PLOTTING OF COOLING CURVES. C-1

Subprogram to Calculate The Amount of Austenite Liberated C-11

Typical Set of Data Cards for a Calculation C-11

APPENDIX D. SAMPLE OF OUTPUT DATA D-1

APPENDIX E. COMPUTER PROGRAM TO MODEL DENDRITE GROWTH E-1

Main Program. E-2

Line of Steepest Descent Through a Temperature Field From a Non-Isothermal Field. E-9

LIST OF TABLES

Page

TABLE 1. COMPUTER MODEL CALCULATION OF HEAT FLOW ACROSS A PLATE . . . 21

TABLE 2. RELATION BETWEEN THE NUMBER OF NUCLEI AND THE UNDERCOOLING 37

TABLE 3. CALCULATED AND EXPERIMENTAL VALUES OF UNDERCOOLING 63

TABLE 4. EFFECT OF NUCLEATION AND SULPHUR CONTENT ON THE TIME FOR THE OUTER LAYER OF THE CASTING TO BECOME SOLID 73

TABLE 5. AXIAL GROWTH VELOCITIES NEAR THE TIP 125

TABLE 6. AXIAL COMPONENT OF VELOCITY OF AN ISOTHERMAL TIN DENDRITE. . 129

TABLE 7. PHYSICAL CONSTANTS FOR TIN USED IN THE CALCULATIONS. 130

LIST OF ILLUSTRATIONS

		Page
FIGURE 1.	"COMPARTMENTATION" OF HEAT FLOW IN A PLATE; NOMENCLATURE.	12
FIGURE 2.	FLOW DIAGRAM FOR A SIMPLE HEAT-FLOW CALCULATION	20
FIGURE 3.	PREDICTED TEMPERATURE VARIATION WITH TIME AT THE PLATE SURFACE	22
FIGURE 4.	TEMPERATURE PROFILES ACROSS A CONDUCTOR	23
FIGURE 5.	THE EQUILIBRIUM DIAGRAM FOR CAST IRON EUTECTIC.	28
FIGURE 6.	THE APPEARANCE OF BARS QUENCED DURING SOLIDIFICATION. . . .	29
FIGURE 7.	THE PROGRESS OF SOLIDIFICATION (SCHEMATIC).	30
FIGURE 8.	THE RELATIONSHIP BETWEEN CELL NUMBER AND UNDERCOOLING . . .	38
FIGURE 9.	NUCLEATION PLOTTED AGAINST $(\text{UNDERCOOLING})^2$.	39
FIGURE 10.	SURFACE AREA LOST BY WALL CONTACT.	44
FIGURE 11.	FLOW CHART FOR THE COMPUTER SIMULATION OF THE FREEZING OF AN ISOTHERMAL CASTING	47
FIGURE 12.	FLOW CHART FOR A COMPUTER SIMULATION OF THE FREEZING OF A ROUND BAR SUBDIVIDED INTO N ANNULI.	50
FIGURE 13.	APPARATUS FOR FREEZING POINT DETERMINATIONS (SCHEMATIC). .	54
FIGURE 14.	MAXIMUM AND MINIMUM SOLIDIFICATION TEMPERATURES RELATED TO KINETIC CONSTANTS	55
FIGURE 15.	COMPARISON OF EXPERIMENTAL AND PREDICTED COOLING CURVES. .	57
FIGURE 16.	THE STRUCTURE OF AN INGOT QUENCHED DURING RECALESCENCE . .	61
FIGURE 17.	THEORETICAL COOLING CURVES FOR LOW SULPHUR ALLOY	64
FIGURE 18.	THEORETICAL COOLING CURVES FOR HIGH SULPHUR ALLOY.	65
FIGURE 19.	TEMPERATURE GRADIENTS ACROSS A 1.2" BAR.	66
FIGURE 20.	DISPERSED AND PROGRESSIVE SOLIDIFICATION (SCHEMATIC) . . .	72
FIGURE 21.	PROGRESS OF SOLIDIFICATION: HIGH SULPHUR ALLOY OF LOW NUCLEATION	74

LIST OF ILLUSTRATIONS (Continued)

		Page
FIGURE 22.	PROGRESS OF SOLIDIFICATION: HIGH SULPHUR ALLOY OF HIGH NUCLEATION.	75
FIGURE 23.	PROGRESS OF SOLIDIFICATION: LOW SULPHUR ALLOY OF LOW NUCLEATION	76
FIGURE 24.	PROGRESS OF SOLIDIFICATION: LOW SULPHUR ALLOY OF HIGH NUCLEATION.	77
FIGURE 25.	MEASURED PROGRESS OF SOLIDIFICATION AT LOW NUCLEATION.	78
FIGURE 26.	MEASURED PROGRESS OF SOLIDIFICATION AT HIGH NUCLEATION	79
FIGURE 27.	EFFECT OF NUCLEATION UPON AUSTENITE SOLIDIFICATION AT THE EDGE OF A BAR; LOW SULPHUR ALLOY	81
FIGURE 28.	EFFECT OF NUCLEATION UPON AUSTENITE SOLIDIFICATION AT THE EDGE OF A BAR; HIGH SULPHUR ALLOY.	82
FIGURE 29.	THE VARIATION OF FLAKE GRAPHITE SIZE WITH TIME COMPARISON OF HIGH AND LOW SULPHUR ALLOYS.	85
FIGURE 30.	HEAT FLOW AT A MOVING SOLID/LIQUID INTERFACE	88
FIGURE 31.	GRAPHICAL REPRESENTATION OF THE COUPLING EQUATION. . .	88
FIGURE 32.	SUBDIVISION OF SPACE INTO ONE-DIMENSIONAL FLOW CHANNELS	94
FIGURE 33.	FLOW CHART FOR SIMULATION OF DENDRITE GROWTH	96
FIGURE 34.	COMPARTMENTATION OF SPACE FOR ONE-DIMENSIONAL FLOW . .	101
FIGURE 35.	ORTHOGONAL PLANES FOR A BODY WITH ROTATIONAL SYMMETRY.	103
FIGURE 36.	TEMPERATURE PROFILE ALONG A RADIAL COORDINATE.	104
FIGURE 37.	FLOW CHART FOR A HEAT FLUX CALCULATION	110
FIGURE 38.	SOLUTION OF THE INTERFACE BOUNDARY CONDITIONS.	112
FIGURE 39.	SURFACE COMPARTMENT.	114
FIGURE 40.	ISOTHERM MOVEMENT.	119
FIGURE 41.	FLOW CHART FOR "MOVER"	120

LIST OF ILLUSTRATIONS (Continued)

Page

FIGURE 42. FLOW CHART FOR THE CONSTRUCTION OF ORTHOGONAL TRAJECTORIES 123

FIGURE 43. EFFECT OF NETWORK SIZE UPON THE CALCULATED DENDRITE GROWTH VELOCITY. 127

FIGURE 44. CROSS SECTION THROUGH THE ORTHOGONAL NETWORK 128

FIGURE 45. VARIATION OF PREDICTED VELOCITY WITH TIP RADIUS. 132

FIGURE 46. GROWTH VELOCITY CHANGE WITH TIME 134

FIGURE 47. VARIATION OF TIP VELOCITY AND TIP RADIUS 137

FIGURE 48. SLOWING OF A DENDRITE INITIATED AT FASTER THAN THE OPTIMUM GROWTH VELOCITY. 139

FIGURE 49. THE VARIATION OF TIP VELOCITY WITH TIME. 141

FIGURE 50. THE VARIATION OF CRYSTAL SHAPE WITH TIME 142

FIGURE 51. THE EXTENT OF CRYSTAL GROWTH DURING THE SIMULATION . . . 143

FIGURE 52. TIP OF A DENDRITE SHOWING PROGRESSIVE STEPS IN TIP MORPHOLOGY DURING THE COURSE OF ONE "PULSE CYCLE". . . . 149

FIGURE 53. PARALLEL ARRAY OF DENDRITES: LINES OF HEAT FLOW AND ISOTHERMS (SCHEMATIC). 153

FIGURE 54. INITIAL CONDITIONS FOR THE GROWTH OF DENDRITIC ARRAYS. . 155

FIGURE 55. INITIAL CRYSTAL SHAPE AND ISOTHERM DISTRIBUTION. 157

FIGURE 56. FINAL CRYSTAL SHAPE AND ISOTHERM DISTRIBUTION. 158

FIGURE 57. DEVELOPMENT OF CRYSTAL SHAPE IN THE ARRAY SIMULATIONS. . 160

FIGURE 58. SIMULATION OF A DENDRITIC ARRAY: VELOCITY-TIME RELATIONSHIP 161

FIGURE 59. THE CHANGE OF MEAN BUBBLE RADIUS WITH TIME 168

FIGURE 60. THE DECAY OF MATRIX GAS SUPERSATURATION WITH TIME. . . . 169

FIGURE 61. OSCILLATORY CONTRAST OBSERVED AS A SCREW DISLOCATION APPROACHES THE SURFACE OF A TIN DISULPHIDE CRYSTAL . . . 172

LIST OF ILLUSTRATIONS (Continued)

Page

FIGURE B-1. HEAT FLOW ACROSS A CYLINDER B-3

FIGURE E-1. FINDING THE AXIS OF ZERO TEMPERATURE GRADIENT FROM THE TEMPERATURE GRADIENTS IN TWO KNOWN DIRECTIONS . . . E-10

FIGURE E-2. THE DIRECTION OF STEEPEST DESCENT AS THE MAJOR AXIS OF AN ELLIPSE IN THE ZERO TEMPERATURE PLANE E-10

SECTION A

AN INTRODUCTION TO THE USE OF COMPUTER MODELS IN MATERIALS SCIENCE

CHAPTER 1: INTRODUCTORY IDEAS

1. The Model Concept

The idea of a model is a familiar one. In our childhood, we have models of all kinds and through them, as children, we learn a great deal about the world around us. The models we played with told us about the objects which they represented. The simplest models included only the most obvious features. For example, a model car might only simulate the shape of the full size vehicle and also its ability to move. More sophisticated models might have had speed control and features such as steering which allow the performance of the model to approximate more closely to the real object. From this we may conclude that a model simulates only some features of the real thing. More complex models might simulate a few features more closely or might include more of the properties of the article modelled. The model must neglect some aspects of the article or else it would no longer be a model but simply a copy. For example, a common feature of most toys is that they simulate the shape of an object very well but usually neglect to copy the size. Thus, a model car is more readily made and handled than a full size automobile.

A common technological use of models is for the prediction of the behavior of complex objects such as bridges, boats, airplanes, and river estuaries. These examples underline the characteristics of models which were suggested in the previous paragraph. A model used in the tank testing of a ship design, unlike a toy bears no resemblance to the real ship. Only the wetted areas of the design are reproduced and the parts of the boat above the waterline are ignored. The model can therefore be seen to be specific, that is, related to only a few properties of the ship. A number of different models may be used to study different aspects of the same object. For example, an airplane may be modelled by an airfoil used in windtunnel experiments, by a wooden mock-up used to study passenger accomodation or by a small-scale replica used by company salesman to attract prospective customers. All the models may represent different aspects of the same aircraft.

Our understanding of our environment is based upon the construction of a different sort of model. This model is a mental construction made from familiar ideas through which we can understand more novel phenomena. Such abstract models have most of the properties of the "concrete" ones which we have discussed. They may be exemplified by the models which have been developed for crystal structures. These are considered in one view as collections of incompressible spheres. In another, as an assembly of energy wells. Still another might view a crystal as a regular arrangement of points in space.

On the basis of our mental constructs or models, we are able to derive mathematical relationships which relate properties with variables. The crystal models make a good example. On the basis of mechanics, we can predict the mechanical behavior of an assembly of minute incompressible spheres. If the predictions agree with experimental results, the predictions can be generalized. The sequence of ideas is as follows:

Conceptual model
↓
Mathematical model
↓
Experimental tests
↓
Generalization

In the applied sciences (such as materials science) we are often faced with situations which cannot be treated in this way. Although we can develop simple constructs by which we can understand separate components of the problem, the property of interest results from the simultaneous operation of several separate models. Alternately, we can describe the phenomenon by means of a single model, but it then becomes too complex for the more traditional form of mathematical formulation. This is a problem area which has in the past included most of technology. At the best, the scientific approach has supplied insights which relate to terminal cases in which one or more of the simple models can be assumed to be dominant. Because of this, experimentation is very restricted in scope, generally having a narrow domain of applicability.

Since the advent of the numerical computer, we have seen many inroads into this area. The most common approach has been to develop a single, complex model to give a mathematical formulation which cannot be solved generally. Then the computer is used to solve the resulting relationships for specific conditions. The advantages of this approach lie in the universal nature of mathematics. Procedures have been evolved by which most mathematical problems can in principle be handled with facility, with little computer programming. The disadvantages are twofold. First, because the mathematical expressions are very general, the computer treatment might be extremely cumbersome. This factor may become so large that an unacceptable amount of computer time would be needed to yield a solution. For the particular model in hand, a more specific formulation might yield large increases in efficiency. Secondly, imposition of a mathematical description on the model may involve gross oversimplifications.

An alternative approach which has had much wider application in other disciplines is through the use of the computer model. Such models are well known in Operations Research and Statistics (for example, Monte Carlo modelling methods). This approach seems to be the logical line of development for the applied sciences. The physical situation is specified in terms of a number of abstract constructions. Each of these models must be simple enough to permit its behavior to be described mathematically. The computer is then used to study the interplay of the system of models.

2. The Application of Computer Models in Materials Selection

Materials science is an applied science, which exists because of the need for improved materials. Included within materials science is the basic study of materials, together with the application of the resulting basic knowledge to technology. Therefore, the science possesses an inherent dualism which is not found within the "pure" scientific disciplines. It must seek to develop an understanding of materials, and at the same time must apply this understanding in order to advance technology. This is the strength and the weakness of the science--whereas there are divisions between "Physics" and "Applied Physics", "Chemistry" and "Applied Chemistry", the materials scientist must constantly look both ways. He must study highly simplified problems, and yet be constantly prepared to extend the results into realistic (and consequently complex) applications. Herein lies the basic need for computer modelling methods.

The dual nature of materials science is reflected in two overlapping areas of application of computer models. In one area, a set of materials problems may involve an array of "sub-problems" which can be simplified and studied on a basic level. Casting solidification offers an example of such a set. Many "casting problems" can be delineated, all of which involve:

a. Nucleation of solid phases from liquid

b. Growth of the solid phase as crystals develop into the liquid

c. Diffusive transport of heat and partitioned solute from the growing surface through the liquid

d. Fluid flow,

among other processes. Each of these subdivisions has formed a specialized field of study, so that the understanding of casting solidification requires that the existing knowledge of the parts must be combined to forecast the behavior of the whole. The second area of application is within the study of a single complex phenomenon. Examples of this second area are the prediction of the advance of a phase interface through a statistical atomic attachment process(1) or the study of crystal growth. The major feature which distinguishes the two areas is the type of simplification which is made. In the first area, all the significant processes must be included in some way. The basis for the approach is the simulation of some real situation of technological significance, using basic knowledge. Approximations are permissible, but simplification (in the sense that an imaginary simple process is studied) is not permissible. The second area, on the contrary, permits complete choice of variables. The most desirable model is that for the most simple case which still retains the essence of the basic phenomenon which is being studied.

In this dissertation, an attempt has been made to illustrate both of the areas of application. Examples of the two types have been selected and studied by using computer models. The strengths and weaknesses of the computer model method can be seen in these examples. The first area is exemplified by the model of casting solidification, applied specifically to the freezing of cast iron. In this problem, fluid flow was neglected (because of the formation of a network of needle-like primary crystals at an early stage, which eliminates macroscopic fluid flow in small sectioned castings). On the other hand, several other processes besides nucleation and growth had to be included. The casting model was able to duplicate experimental results and at the same time enhance the understanding of the solidification process in castings. The interplay between theory and experiment in this way is peculiar to the model approach. It is as if the model is able to reveal the experimental results which would be obtained from a range of imaginary materials, each one faithfully following the dictates of the imposed model. The delicate "tinkering" process by which the model is altered by progressively smaller amounts until coincidence with nature has been achieved is rewarded by a deep insight into the system being modelled.

The second area (use of models in basic studies) was exemplified by the study of dendrite growth. The concept of dendritic solidification was stripped to its most simple form, a dendrite needle of isotropic material growing into a pure liquid at constant bath undercooling. The thermal conductivity of the crystal was taken to be zero, and there was assumed to be no fluid flow. The resulting problem is believed to be the simplest crystallization process which can still be termed dendritic. The model study threw a great deal of light on the "Maximum Velocity Principle" of analytic studies and again gave that insight which is peculiar to the model-building approach. The application of the model to special forms of dendrite such as spherulites and arrays of dendrites has also been illustrated. Of course, when realistic dendrites are simulated, the two areas which have been distinguished would begin to merge. The addition of the many "sub-processes" involved in the development of real dendrites merely involves their incorporation within an interactive assembly such as that developed for the casting simulation.

It might be asked whether Materials Scientists are competent to develop computer models. The answer is that they are the only people able to develop models relevant to their own area. Primarily, the reason for this is the dependence of the model upon physical understanding. The model requires an almost intuitive feeling for those processes which are important and those which are not. Furthermore, the existence of a unique solution to a model problem is hard to prove mathematically. At present, its existence must be assumed on the basis of knowledge of the tangible physical problem, known to give unique physical behavior under given sets of conditions.

Before embarking upon the main work of the dissertation, a simple example of the computer model approach will be described. The example was chosen because it formed the basis for the kinetic studies which will be described later. It is therefore outline in some detail in the next chapter.

CHAPTER 2: A COMPARISON OF THE MODEL AND ANALYTIC APPROACHES

1. Model Treatment of Diffusive Flow

Many of the phenomena which are studied in Materials Science involve diffusive transport of heat or matter. Generally, the diffusion problem is complicated by a number of additional processes which are going on simultaneously. As a consequence, the majority of these situations, particularly those of technological importance, do not lend themselves to treatment by conventional mathematical methods. This is an ideal area for the application of computer modelling techniques. The separate subsystems (which are well understood) are combined through the computer model into the macroscopic system which represents the real situation.

In many applications, it is not convenient to use the complete mathematical treatment of diffusion. The diffusion process itself, can be broken down into three separate subsystems, which represent the bulk of the diffusive medium and the two boundaries. Because many diffusion problems can be solved exactly by analytical methods, this presents a good position from which to approach computer modelling methods. The computer models and their results can be compared at each stage with analytical results. However, the additional power of the model approach will be demonstrated in the later sections of the dissertation when more complex and realistic problems are studied.

Consider, first, a simple development of the basic equat.ons governing diffusive transport. Fick's second law for one-dimensional heat flow through a conductor can be readily derived by taking a model consisting of a thin slice of the conductor parallel to the isotherms and balancing incoming heat with the heat content change and the outflow of heat. Clearly:

$$\delta t(JI - JO) = S.\delta T.\delta x \quad ,$$

where

JI = flux flowing in through the inner surface

JO = flux flowing out through the outer surface

S = specific heat of the conductor

δT = temperature change of the compartment

δt = time increment

δx = width of the slice.

Writing the flux as:

$$J = - k\, T_x \quad , \tag{2.1}$$

where

k = thermal conductivity and

$$T_x = \frac{dT}{dx} \quad .$$

Hence,

$$\delta t \left\{(-kT_x + k\,(T_x + \delta x\, T_{xx})\right\} = S.\delta T.\delta x$$

$$\frac{\delta T}{\delta t} = \frac{k}{S}\, T_{xx} \quad .$$

Taking this to the limit where $\frac{\delta T}{\delta t} \rightarrow \frac{dT}{dt}$

$$T_t = \frac{k}{S}\, T_{xx} \quad . \tag{2.2}$$

Now, imagine that we are developing a computer model. In this particular case, a computer model can be derived immediately using finite difference methods. However, it is convenient to develop the model on a more general basis. Suppose we conceive as our model a thin compartment which, as in the previous development, is constructed parallel to the isotherms. Let us choose the edges of our compartment so that no heat flows through the closures. That is, the compartment is bounded on two faces by isotherms and on the other faces by an orthogonal projection to the isotherms. Space can be subdivided into a set of such compartments, as shown in Figure 1. As before,

$$\delta t(JI - JO) = S.\delta T.\delta x \quad .$$

It is convenient to generalize this expression, i.e.,

$$\delta t(AI\ JI - AO\ JO) = S.\delta V.\delta t \quad , \tag{2.3}$$

where

AI = inner surface area of the compartment

AO = outer surface area of the compartment

δV = compartment volume.

JI and JO follow from equation 2.1. However, since the model will not be taken to the limit, $\delta t \to 0$, $\dot{T}_x$ is not known, and the equation cannot be solved.

At this stage, differences between the computer model and the analytical model emerge. Instead of considering the diffusion field in general, the computer program will approach each individual finite element as an entity in space and time. There are many consequences of this which will emerge in the later parts of this work. At this stage, it should be noted that T_x at any particular point is varying during the time increment δt which is considered in a calculation. Furthermore, because a compartment is considered individually, the variables are unspecified, since they depend upon the adjacent compartments on the two sides.

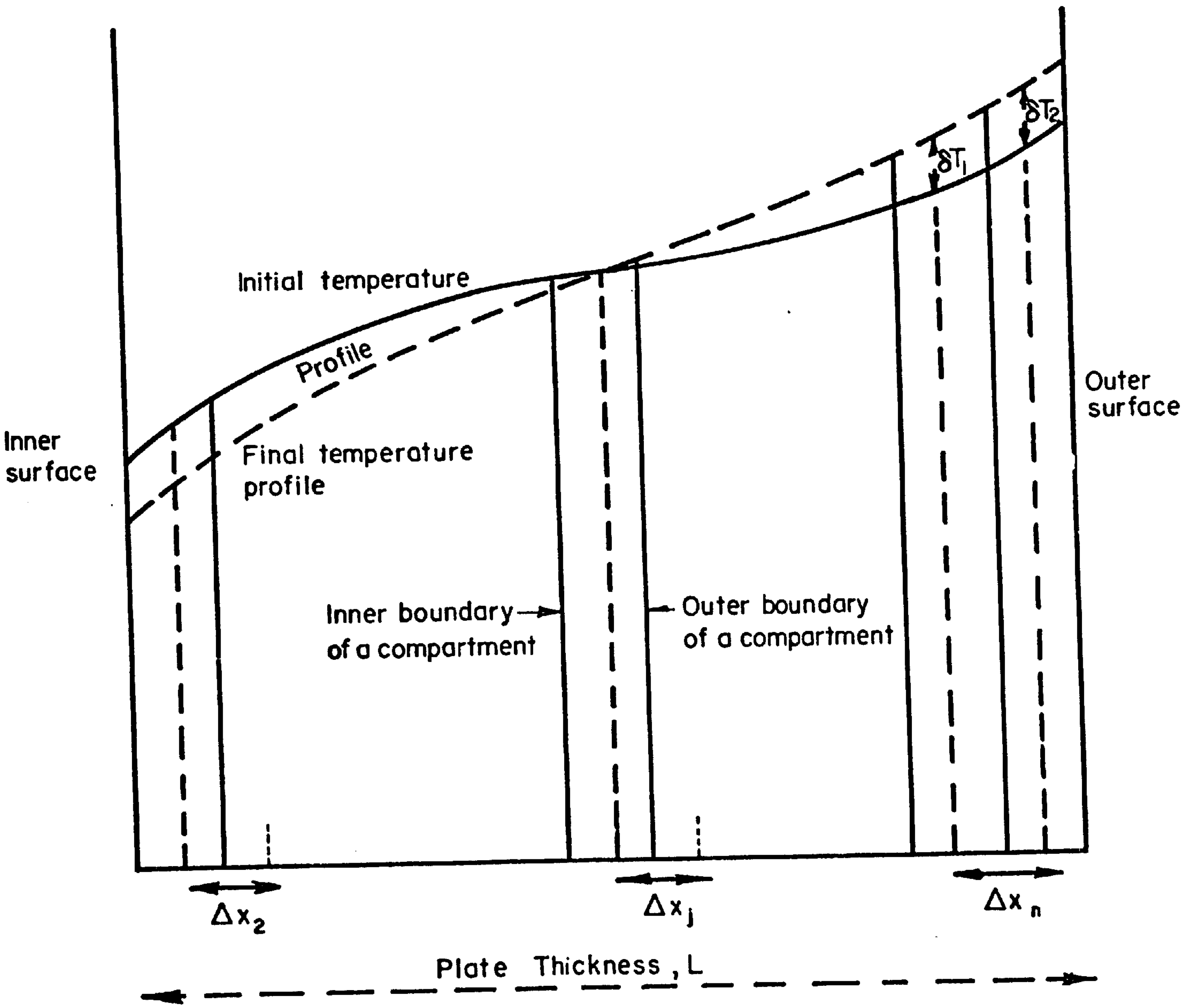

FIGURE 1 COMPARTMENTATION OF HEAT FLOW IN A PLATE: NOMENCLATURE

The time dependence of T_x will be removed from the calculation by taking the mean gradient during the time increment. This is equivalent to taking the first term of a series expansion of the integral over δt. As δt becomes very small, the mean value becomes exact. The meaning of "very small" emerges during subsequent use of the model calculation.

Suppose that we know the initial condition of the diffusion field and hence specify the temperature gradients at the inner and outer boundaries of the compartment. The mean temperature gradients during the time increment can be expressed in terms of the temperature change occurring within the compartment and its two neighbors. An appropriate means by which this can be done is to assume a linear change of gradient with distance over the dimensions of a compartment. Therefore, in the conservation equation for a compartment, there are three unknowns; the temperature change of the outer neighbor, that of the compartment itself, and that of its inner neighbor.

We are now in a position to consider the model for a boundary compartment (Figure 1). Here, there are only two unknowns because one unknown temperature has been replaced by a boundary condition. Suppose we take a boundary condition of the second kind, that the rate of heat removal is constant. Then the amount of heat removed is

$$Q = Q_t \ \delta T.A \quad , \tag{2.4}$$

where

Q = heat removed, and

Q_t = rate of heat removal.

Putting this result into equation (2.3), it then becomes:

$$\delta t(AI\ JI - AO\ Q_t) = S\delta V\ \delta T \quad , \tag{2.5}$$

placing the boundary on the outer surface of the series of compartments. This expression still cannot be solved because JI has not yet been defined.

Suppose for the sake of simplicity that both boundary conditions are of the second kind. The task remaining is to combine the model for the boundary conditions, with a model for the diffusion field based upon a number of adjacent compartments of small but finite thickness. This is essentially one of solving a series of N equations to find N unknowns (the temperature changes for each compartment). Since we can derive an equation for each, the system has a unique solution which is as precise as the assumptions allow. These assumptions (described earlier) are:

(1) That the gradients can be assumed constant during a time increment (at the mean value for a time increment)

(2) That the gradient changes linearly with distance over the width of a compartment.

Starting at one boundary, we can define the temperature change of the first (or Nth) compartment in terms of its neighbor.

$$J = -k\ T_x(\text{mean}) \tag{2.6}$$

$$T_x(\text{mean}) = T_x\ (\text{initial}) + \frac{\delta T_2 - \delta T_1}{2\Delta x}\quad . \tag{2.7}$$

T_x(initial) is known from the conditions at the beginning of the time increment. The symbols can be explained most readily by means of Figure 1.

δT_2 = temperature change at the center of the compartment being considered, at the end of the time increment;

δT_1 = temperature change at the center of the adjacent inner compartment at the end of the time increment; and

Δx = separation distance.

Then, combining (2.6) and (2.7),

$$JI = -k\ (T_x\ (\text{initial}) + \frac{\delta T_2 - \delta T_1}{2\Delta x}) \quad . \qquad (2.8)$$

From (2.5) and (2.8)

$$\delta t \left[k\ AI \left\{ -T_x\ (\text{initial}) - \frac{\delta T_2 - \delta T_1}{2\Delta x} \right\} - AO\ Q_t \right] - S\ \delta V\ \delta T_2 = 0 \quad .$$

Rearranging, we have:

$$-\delta T_2 \left(\frac{k\ AI}{2\Delta x}\ \delta t + S\delta V \right) + \delta T_1 \left(\frac{k\ AI}{2\Delta x}\ \delta t \right) = T_x\ (\text{initial})\ k\ AI\ \delta t + AO\ Q_t\ \delta t \ . \qquad (2.9)$$

Or, rewriting:

$$\delta T_2 = \frac{\alpha}{\beta}\ T_1 + \gamma \quad , \qquad (2.10)*$$

where

$$\alpha = \frac{k\ AI}{2\Delta x}\ \delta t \quad , \qquad (2.11)*$$

$$\beta = \frac{k\ AI}{2\Delta x}\ \delta t + S\Delta V = \alpha + S\Delta V \quad , \qquad (2.12)*$$

and

$$\gamma = \left\{ k\ AI\ T_x\ (\text{initial}) + AO\ Q_t \right\} \delta t/\beta \quad . \qquad (2.13)*$$

These constants (α, $\bar{\beta}$, and γ) can be evaluated numerically and their values stored in the computer memory.

The model for a central compartment can be considered in precisely the same manner. The conservation equation is:

---

* Equations for the compartment at the outer boundary.

$$\delta t\ (AI\ JI - AO\ JO) = S\delta V\ \delta T_2 \quad \text{(equation 2.3)}$$

and (analogously to equation 2.8)

$$JO = -k\left(T_x(0) + \frac{\delta T_3 - \delta T_2}{2\Delta x(0)}\right) \quad , \tag{2.14}$$

$$JI = -k\left(T_x(I) + \frac{\delta T_2 - \delta T_1}{2\Delta x(I)}\right) \quad , \tag{2.15}$$

where $T_x(0)$ is the initial temperature gradient at the outer surface of the compartment, and $T_x(I)$ is the initial temperature gradient at the inner surface. Similarly, $\Delta x(0)$ and $\Delta x(I)$ are the distances between the centers of the three compartments; the (I) and (0) indicating the side nearest the inner and outer boundary of the plate, respectively. The temperature changes, δT_3, δT_2, and δT_1 are the temperature changes at the centers of the three compartments at the end of the time increment, with the highest number indicating the compartment furthest away from the inner surface of the plate.

Consider now the set of compartments, starting with the outer boundary (equations 2.10-2.13), we have already derived a relation between the temperature change in the adjacent compartment and that in the boundary compartment (equation 2.10). This relationship can be used to eliminate δT_3 from equation (2.14) and express it in terms of δT_2. We thus have a new equation relating two temperature changes. This can be used in a conservation relationship for the next inner compartment. The process can be repeated until the inner boundary has been reached. In general:

$$\delta T_j = \delta T_{j-1}\frac{\alpha_j}{\beta_j} + \gamma_j \quad , \tag{2.16}$$

where

$$\alpha_j = \frac{AI\ k\ \delta t}{2\Delta x_j} \quad , \tag{2.17}$$

$$\beta_j = \left\{ \frac{AI}{2\Delta x_j} - \frac{\frac{\alpha_{j+1}}{\beta_{j+1}} - 1}{2\Delta x_{j+1}} \ .\ AO \right\} k\ \delta t + S\delta V \quad , \tag{2.18}$$

$$\gamma_j = \left\{ \left(T_x(O) + \frac{\gamma_{j+1}}{2\Delta x_{j+1}} \right) .\ AO - T_x(I)\ AI \right\} .\ k \frac{\delta t}{\beta_j} \quad . \tag{2.19}$$

Each of these constants is evaluated and stored for all the compartments successively. At the inner boundary, there are only two unknown temperature changes and two equations. The first of the equations from the derivation for a general central compartment:

$$\delta T_2 = \frac{\alpha_2}{\beta_2} \delta T_1 + \delta_2 \text{ (equation 2.16)} \quad ,$$

where α_2, β_2, and γ_2 have already been calculated. From the conservation condition (as for the first compartment)

$$\delta t \left[k\ AO \left\{ T_x(O) + \frac{\delta T_2 - \delta T_1}{2\Delta x_2} \right\} - AI\ Q_{t'} \right] - S\delta V\ \delta T_1 = 0 \quad .$$

Rearranging:

$$\delta T_2 \left(\frac{k\ AO\ \delta t}{2\Delta x_2}\right) = \delta T_1 \left(S\delta V + \frac{k\ AO\ \delta t}{2\Delta x_2}\right) - k\ \delta t\ AO\ T_x(O) + AI\ Q_t' \ . \tag{2.20}$$

This is the second equation that we need and from it δT_1 can be evaluated. By successive substitutions using the values of α_j, β_j, and γ_j, all the temperature changes can be calculated, in turn, and hence the temperature profile at the end of the time interval can be determined.

The results for the analytical and model treatments will now be compared using a simple example. The boundary value problem can be posed as:

$$\underline{\text{D.E.}}\quad T_t = \frac{k}{S}\, T_{xx} \qquad (T = T(x,t))$$

$$\underline{\text{B.C.}}\quad T_x(0,t) = -\frac{Q_t{}'}{k}$$

$$T_x(L,t) = -\frac{Q_t}{k}$$

$$\underline{\text{I.C.}}\quad T(x,0) = T_o \quad .$$

The solution to this problem can be readily obtained, but it is quite complex. Based on Carslaw and Jaeger[2], the results can be written as:

$$\begin{aligned} T(x,t) = {} & 2\, Q_t \frac{(K\ t)^{1/2}}{k} \sum_{n=0}^{n=\infty} \left[\text{ierfc}\, \frac{(2n+1)L-x}{2(Kt)^{1/2}} + \text{erfc}\, \frac{(2n+1)1+x}{2(Kt)^{1/2}} \right] \\ & - 2\, Q_t \frac{(K\ t)^{1/2}}{k} \sum_{n=0}^{n=\infty} \left[\text{ierfc}\, \frac{2nL+x}{2(Kt)^{1/2}} + \text{erfc}\, \frac{2(n+1)L-x}{2(Kt)^{1/2}} \right] + T_0 \ , \end{aligned} \tag{2.21}$$

where K is the thermal diffusivity, $\frac{k}{S}$, and ierfc is the integral error function. Because this equation is rather cumbersome, an equation was derived for the simple case where:

$$Q_t = Q_t{}' \quad .$$

Fourier methods lead to:

$$T(x,t) = \frac{2\ Q_t}{k} \frac{L}{\pi^2} \underset{\text{(odd values only)}}{\sum_{m=1}^{m=\infty}} \frac{1}{m^2} \left(\cos \frac{m\pi}{L} x\right) \exp\left(-\frac{k}{S} \frac{m^2\pi^2}{L^2}\right) - \frac{Q_t}{k} \left(\frac{L}{2} - x\right) + T_0 \quad . \tag{2.22}$$

The computer model can be applied directly to this problem, setting:

AI = AO = 1 for the entire field.

Thus, the dependence of temperature upon position within the plate and time could be calculated by both approaches, allowing a comparison to be made between them.

The computer program used for the model calculation is listed in Appendix A. The flow of the calculation between the different components can be better appreciated by study of the flow chart in Figure 2. This shows how the calculation passes from compartment to compartment calculating the coefficients α, β, γ, for each in turn. Then, after the inner boundary condition has been applied in the form of the model for the inner surface, the system of equations is solved. There are two parameters controlling the calculation, the size of the space increment (the value of N, the number of compartments into which the plate is subdivided) and the size of the time increment. These parameters control the accuracy of the calculation.

Table 1 lists the temperatures calculated for the surface of the plate by both analytical and computer methods. The temperatures are those which would be attained at the hotter surface after the passage of 65 seconds. Computer calculations were made with various values of the space and time parameters. The results for all cases are listed in the table. The computer drew plots of the time variation of the surface temperature. It was not possible to resolve the differences between the curves for the range of parameters studied. A typical curve is shown in Figure 3. The computer also plotted the temperature variation across the plate, for various times after the start of flow. These curves are shown in Figure 4. For all practical purposes the computer model gave the same result as the Fourier method. Furthermore, it can be seen from Table 1 that the trend is

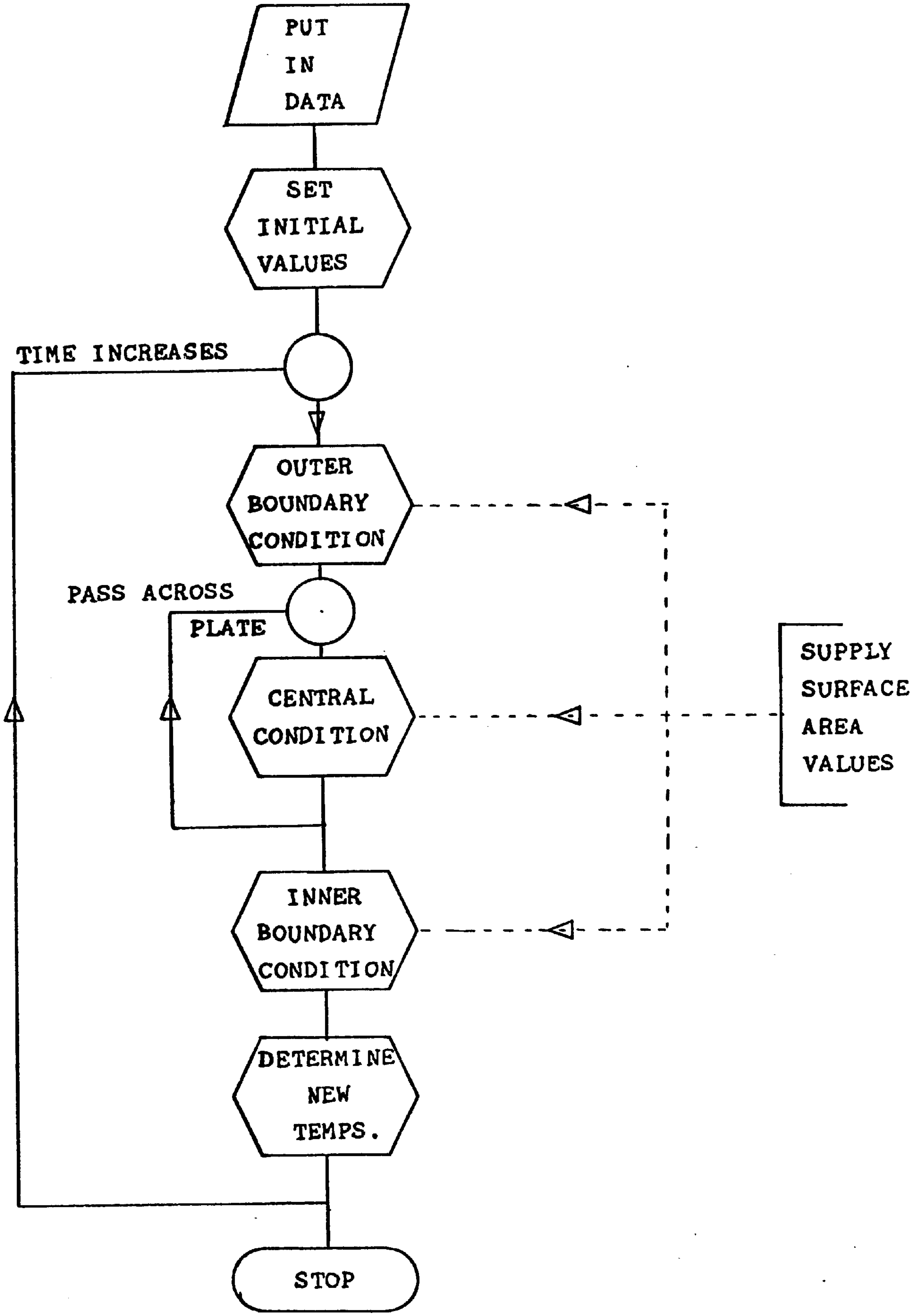

FIGURE 2. FLOW DIAGRAM FOR A SIMPLE HEAT - FLOW CALCULATION

TABLE 1. COMPUTER MODEL CALCULATION OF HEAT FLOW ACROSS A PLATE

The temperatures are those of one surface of the plate after 65 seconds have passed from the time at which the initial condition of uniform temperature prevailed. The results are for different time and space subdivision.

δt(mean)	δt(init.)	Calculated Surface Temperature j* = 15	30	45	60	loop#
1.10	0.20	196.718	196.746	196.751	196.753	58
1.01	0.15	196.675	196.722	196.726	196.728	64
0.90	0.10	196.694	196.720	196.725	196.727	72
0.76	0.05	196.685	196.712	196.716	196.718	86

Result from Fourier methods - 196.7210

* j is the number of subdivisions of the plate width

loop is the number of time increments required for the calculation.

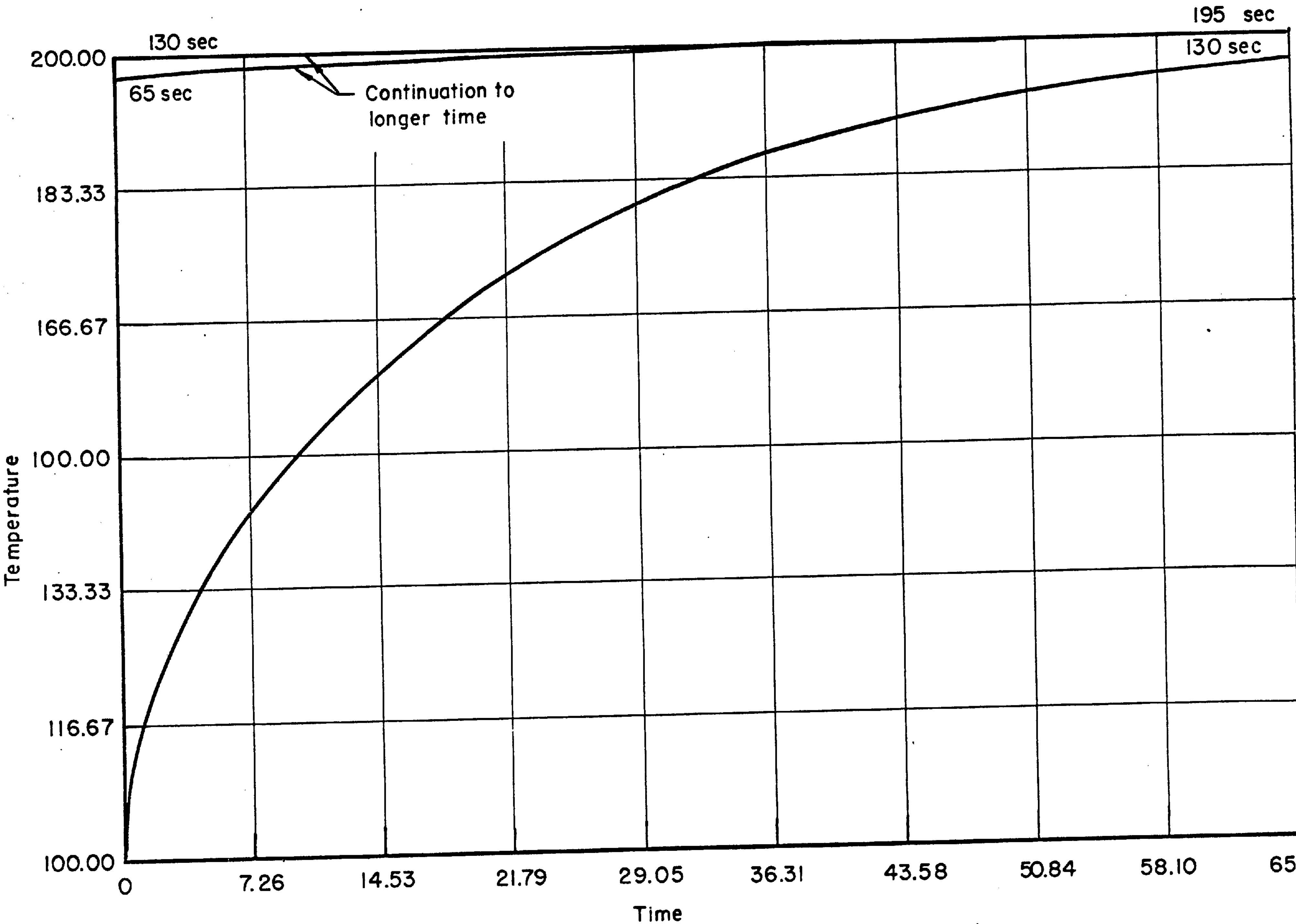

...VARIATION WITH TIME AT THE PLATE SURFACE

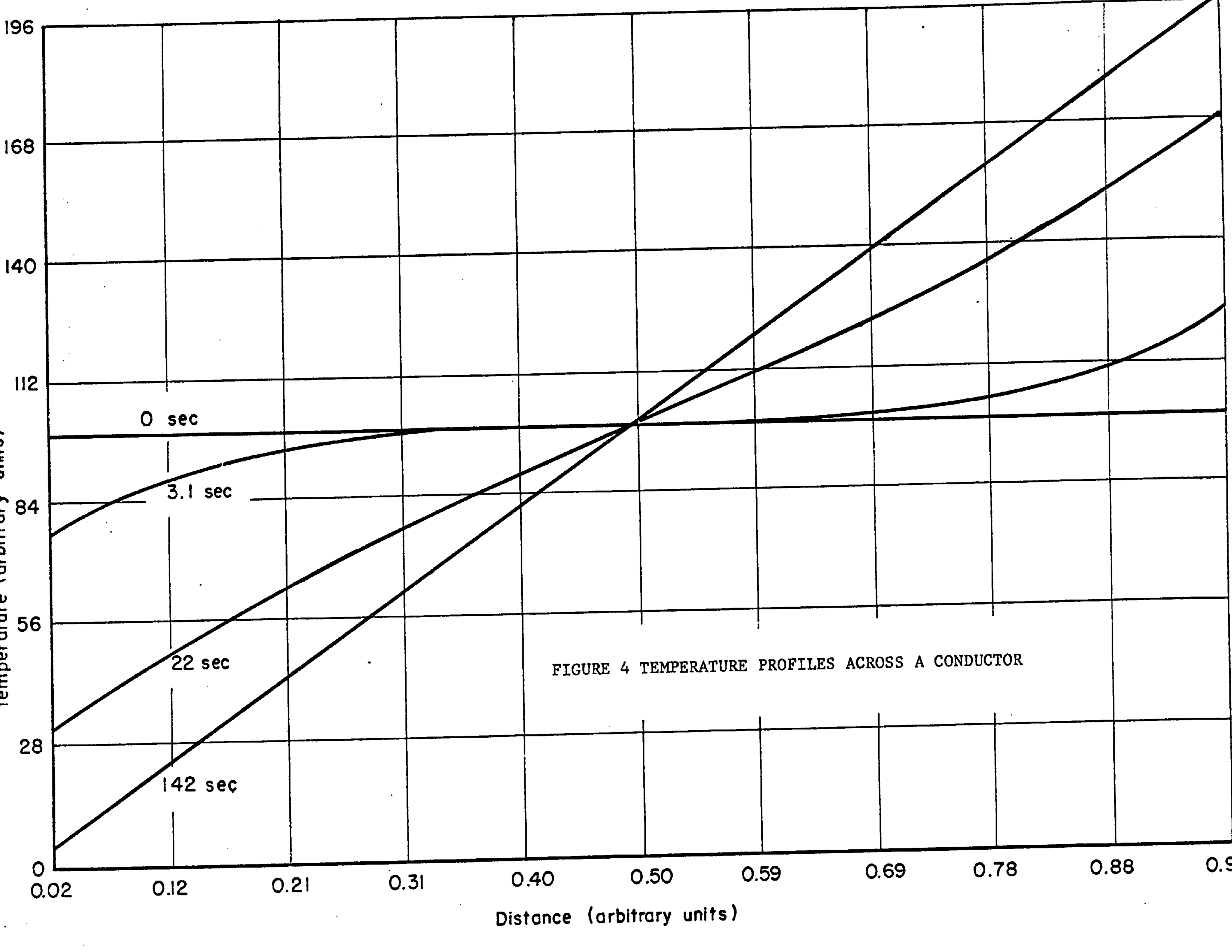

FIGURE 4 TEMPERATURE PROFILES ACROSS A CONDUCTOR

to exact agreement as the time and space subdivisions are made smaller. However, since all the results agreed within ± 0.2×10^{-2}%, the agreement is already near to the limit of the computer accuracy using single precision arithmetic.

The power of the model approach is illustrated by the fact that with very little further labor (change of the AREA function), the calculation could be immediately converted to any one-dimensional system through the insertion of appropriate values if AI and AO.

The computer model method used in this simple example can be seen to involve two main ideas.

(1) Breakdown of the problem into finite elements of space and time. In this example, three different models were used to yield N equations with N unknowns, for each time increment.

(2) The solution of the equations by a marching procedure.

The first of these ideas is present in all model treatments and is the source of the flexibility of model methods. Because there are N separate equations, they can be made up of N different models. In this particular case, this facility allows interface boundaries to be inserted, the diffusivity to be changed, or the shape of the flow path to be varied. Other examples which are described later illustrate the treatment of other combinations of models. For example, an array of bubbles of various sizes interacts with a matrix through vacancy and gas diffusion. In this case, there are many different models entering the calculation, rather than the three different types (center and two boundaries) which entered the diffusion calculation. This example could equally well have dealt with the adsorption of gas on an interface (as in the B.E.T. model of statistical thermodynamics for surface adsorption), or the transient embryo distribution in a condensation problem. It may be noted that the Fourier transform method could be regarded as an allied procedure to those described. The model in this case would be one in which a surface in potential space could be built up from a finite number of periodic functions. The limitation and strength of this procedure, of course, is that the functions are related mathematically, leaving only a relatively small number of unknowns which can be used to specify the problem. This means that the approach is far less flexible than are computer models in general, but the equations are easier to formulate and solve.

From the second idea springs the whole art and difficulty of model methods. It is not generally easy to solve N simultaneous equations with sufficient speed (even with a computer) to permit repetition of the process over a number of time increments. Fortunately, there are many approaches which alleviate this difficulty, and there are some types of model which are particularly tractable. One such case has been described in which the simultaneous equations can be solved by a marching procedure. Many models can be cast in this form, which gives an exact solution to the series of equations. In most of the examples in this dissertation, the problem has been cast in this form. When it is not possible to transform the problem in this way, resort must be made to the many computer methods which have been developed, which rely upon iterative or "trial and error" methods. Many of these are surprisingly effective, involving, for example, prediction of trends and subsequent correction of the prediction, i.e., "Predictor-Corrector" methods. These methods are illustrated in this dissertation in the complex situation of the swelling of nuclear fuel, and more simply in the treatment of the boundary conditions in the study of dendrite growth.

SECTION B

A COMPUTER SIMULATION OF THE FREEZING OF A CYLINDRICAL CAST IRON BAR

CHAPTER III: CONCEPTUAL BASIS FOR THE MODEL

1. The Freezing of Cast Iron

Cast iron was chosen as an example of a material of great technological importance, which made a suitable subject for a model study. The objectives were to combine the results of basic studies within a model, in order to predict the behavior of the whole casting.

When this model was first conceived, a large body of experimental data had been accumulated in a study of graphite formation in grey cast iron.[3,4,5] The separate processes which together determined the properties and structure of the material had been studied in controlled experiments, designed to clarify the manner in which the microstructure of the material developed. In particular, the search for an understanding of the processes controlling the graphite structure formed a prime motive for the original work. However, although the nucleation and growth models for the material were quite well developed, it was not possible to relate them to the system represented by the complete casting in anything but a very qualitative manner. Before describing the models for the processes, the phenomena associated with the freezing of cast iron will be described.

Many descriptions of the freezing of cast iron have been published.[3,6] The alloys of interest are all of eutectic or hypoeutectic composition. The equilibrium diagram as it applies to eutectic solidification is shown in Figure 5. A description of solidification can be based upon Figures 6 and 7 (a,b, and c) taken from Reference 3. Figure 6 shows sections of bars which were poured from liquid metal at the same time but quenched successively during solidification. The dark areas (ignoring cracks)

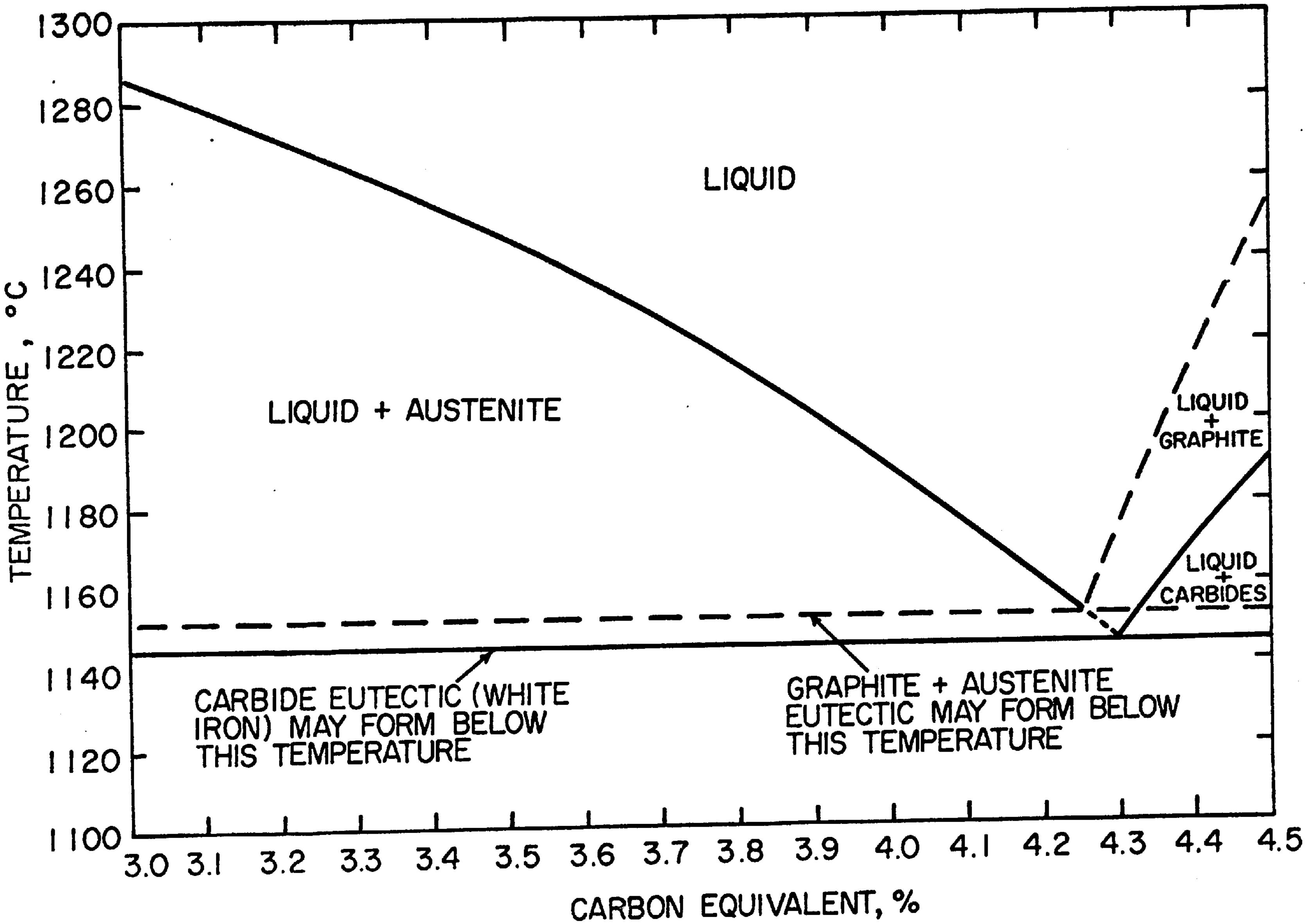

FIGURE 5. THE EQUILIBRIUM DIAGRAM FOR THE CAST IRON EUTECTIC

(a) The start of eutectic solidification

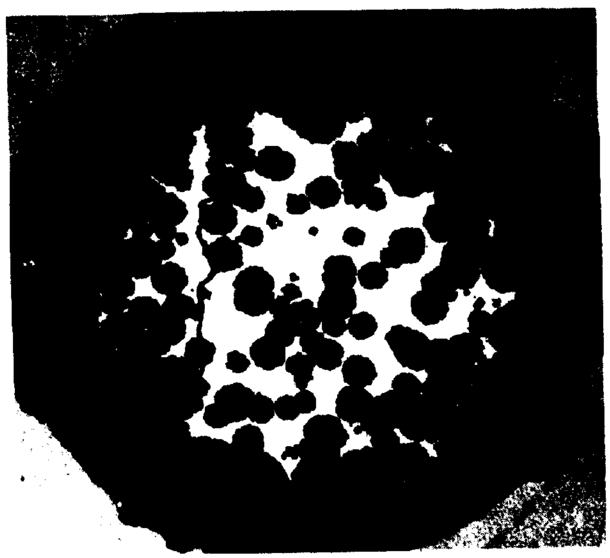

(b) During solidification

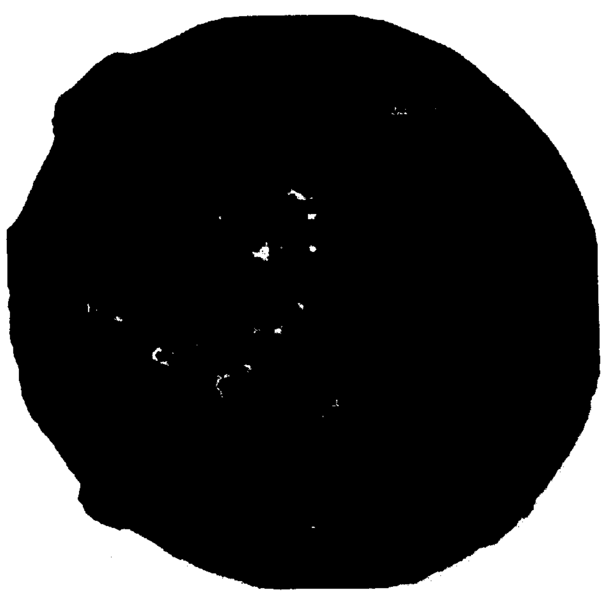

(c) Solidification almost complete

FIGURE 6. THE APPEARANCE OF BARS QUENCHED DURING SOLIDIFICATION (from Ref. 3)

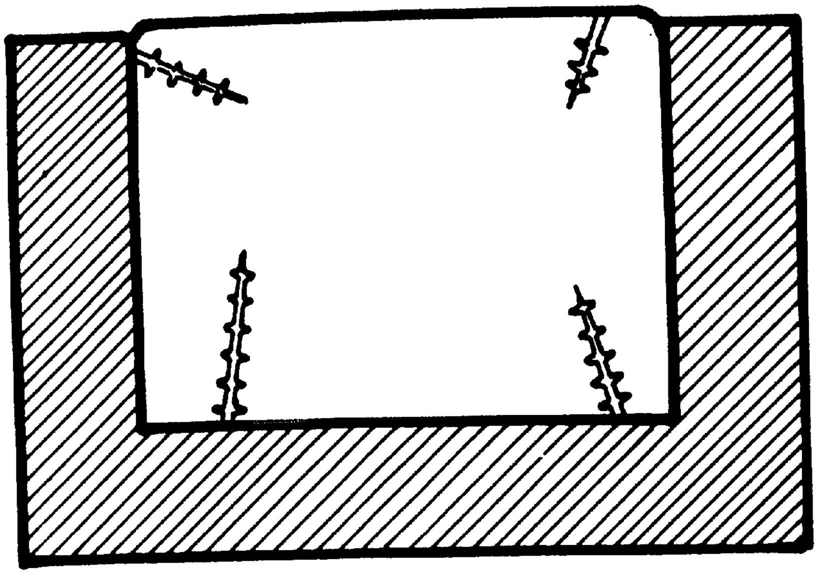

(a) Austenite dendrites form

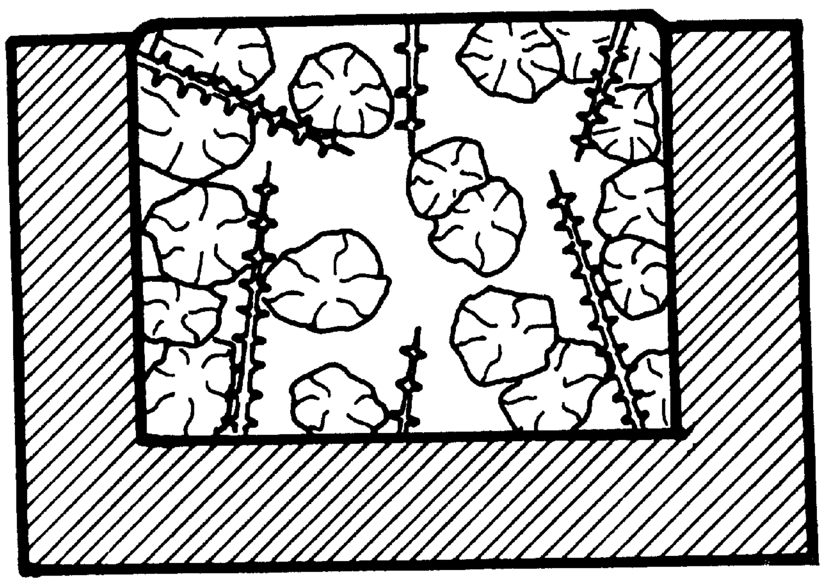

(b) Eutectic cells grow from nuclei

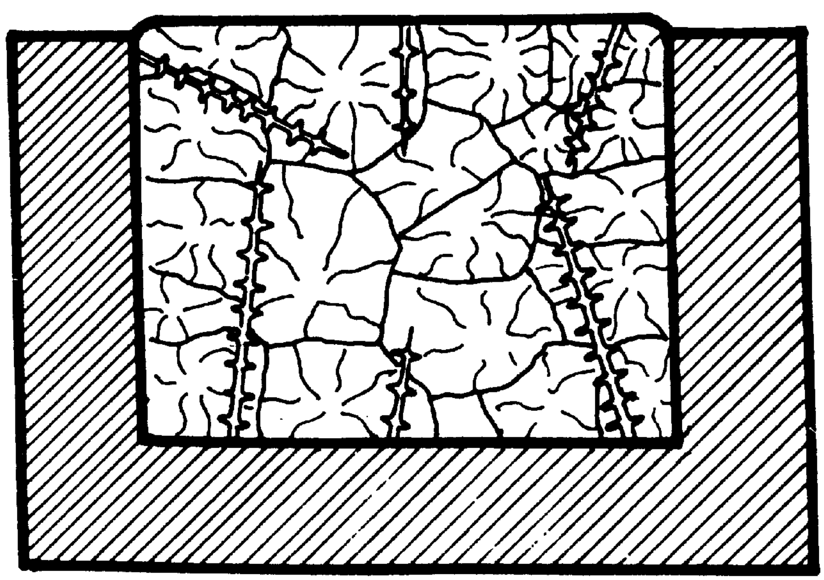

(c) Interlocked eutectic cells after solidification is complete.

FIGURE 7. THE PROGRESS OF SOLIDIFICATION (Schematic)

were solid at the time of the quench and consist of graphite-austenite eutectic. The illustrations show that eutectic cells were nucleated throughout the melt and grew in a radial fashion until all the liquid had frozen and the cells were in contact. Figure 7 shows the process in a schematic manner; primary austenite dendrites are shown growing into the liquid metal both before and during eutectic solidification. The study of cast iron solidification in a general way, such as by means of quenching experiments, generates a vivid impression of the interplay of growing surface area, growth rate, and cell-cell contact controlling the freezing temperature of the melt at any instant. In order to simulate the processes in a calculation, each of these must be specified in a rigorous manner.

The solidification system can be subdivided into a number of separate processes as follows:

a. Heat flow - latent heat released by the separation of solid throughout the casting must flow out through the free surface.

b. Nucleation - centers of eutectic growth originate throughout the casting. The nucleation frequency is not constant, depending, for example, on the temperature of the liquid.

c. Growth - eutectic solidification takes place on the nuclei, liberating latent heat. The growth rate is not constant.

d. Primary phase solidification - the liquid composition varies as the temperature of the casting changes, in accordance with the equilibrium diagram. The composition change is accomplished by the formation of primary phase dendrites of austenite. The formation and dissolution of these crystals as the casting temperature changes liberates or absorbs latent heat.

e. Mechanical effects - the growing eutectic cells touch each other and the casting surface, and the free surface in contact with liquid is reduced.

These subsystems can be described by models. The models can then be combined to give a description of the whole casting.

The treatment which has been developed can be approached from the viewpoint of the model treatment for heat flow described in the previous chapter. Considering the casting to be a long round bar, the heat flow is one dimensional. Subdividing it into compartments (radial annuli), each subdivision can have its own thermal properties and the conservation equation can include a term for heat liberation resulting from any solidification taking place within it. Within each subdivision, the nucleation and growth rates can be assumed to be sensibly uniform for small subdivisions. Again, the meaning of "small" follows from trial calculations with different subdivisions (as in Table 1), which show the effect of changing the size of the calculation parameters. Clearly, at the limit when the size is infinitesimal, the approximation disappears. The effect of the approximation is demonstrated by the trial calculations.

Since the nucleation and growth rates are dependent upon the temperature, the problem becomes one of determining the temperature of each subvolume throughout the casting for the whole period of solidification, and integrating the growth of the solid throughout the casting and over the whole time period. The total rate of heat generation in the casting is the sum of latent heat liberated in each small subdivision of the material together with the heat absorbed or liberated as a result of the temperature changes. The latent heat liberation as a result of eutectic growth is evaluated by multiplying the surface area growing into the liquid by its rate of advance (thus giving the rate of formation of eutectic solid), multiplied by a latent heat constant. The heat content change derives from the product of the mean specific heat constant for the mixture of solid and liquid and the rate of change of temperature. The processes determining the temperature of any volume increment can be summarized:

$$\frac{dQ}{dt} = \sum_V \left[(SA)\ L\ \frac{\partial R}{\partial t} + \left\{ Cp_l + (FVS)\ (Cp_s - Cp_l) \right\} \frac{\partial T}{\partial t} \right] \delta V \quad , \qquad (3.1)$$

where $\frac{dQ}{dt}$ is the rate of heat removal from the whole metal mass, L is the number of calories liberated during the formation of unit volume of the solid, $\frac{\partial R}{\partial t}$ is the rate of growth of cells of radius R_i, $\frac{\partial T}{\partial t}$ is the rate of change of temperature, Cp_s is the specific heat per unit volume of solid, Cp_l is the specific heat per unit volume of liquid, SA is the surface area of solid eutectic in contact with the liquid, FVS is the fraction of the casting volume which is solid, and δV is a small volume of the casting which can for some purposes be considered to be isothermal. Summation is carried out for all the subvolumes of the casting.

This equation highlights details of the solidification process which must be understood prior to calculation of the temperature-time relation for each part of the casting. Separating, first, the less important features: the physical constants are available in the literature, although, because of the various types and compositions of cast iron, they are to some extent unsatisfactory; FVS follows from prior calculation of latent heat liberation; $\frac{dQ}{dt}$ has been assumed to be constant in this work, but it would of course be replaced by a function appropriate to each particular form of mold; i.e., each specific freezing situation. The remaining terms are then brought into prominence; SA is a complicated variable relating to the nucleation rate of the eutectic cells and their growth, and the impingement of the cells upon each other and the mold wall; $\frac{dR}{dt}$

is an expression for growth rate, which is readily available from both theoretical study and from controlled experiments.

2. Treatment of Heat Flow in the Casting

The treatment of diffusive flow which has been described in Chapter II formed the basis for the model of the casting. Because the nucleation and growth processes were less sensitive to temperature changes than the thermal diffusion processes, it was possible to assume that the nucleation and growth rates were constant throughout a time increment, and within each volume subdivision. Furthermore, it proved to be reasonable to assume also that the surface area of eutectic growing into the liquid was constant within a space and time subdivision. Hence, the latent heat liberation was calculated from the growth rate and surface area of solid for each subvolume. This quantity was then included in the conservation equations. Furthermore, appropriate values of S and k were derived from the fraction of the volume solid.

Equations were developed in essentially the same manner as those in Chapter II. Three differences exist between the treatments. First, the width of the compartments varied across the cylinder. The spacing was selected to give equal metal volumes within each annulus. Secondly, in the program shown in Figure 2 and listed in Appendix I, the initial temperature gradients (T_x(initial)) were calculated by fitting a quadratic expression between each set of three temperature points, and taking the differential. In the present instance, this was not considered to be necessary, and a simple linear approximation was made. (This is the approximation generally made in finite difference arithmetic). Finally the areas of the interfaces between compartments were previously calculated by a separate computer subprogram. This was done for generality; in the present instance the areas were readily calculable and were included within the main program. The development of the equations was similar to the one described in Chapter II. It has therefore been described in Appendix B.

3. Nucleation Processes

There is a considerable literature relating to the nucleation of cast iron.[3,4,7,8] The salient features can be fitted with the following scheme. Nucleation of eutectic depends upon the initiation of the graphite phase. The embryos for nucleation form an unstable population, being generated by metal treatments such as innoculation (solid additions made to the melt) with impure ferro-silicon or graphite or by initial freezing and subsequent remelting of the graphite eutectic to liberate freshly formed particles of graphite.[9] The number of embryos in the liquid metal is continually decreasing, the rate at which they are being destroyed depending upon the holding temperature and somewhat on the composition of the liquid metal.[6] Because of the wide undercooling range generally encountered for this material plus the fact that the process is, in no sense, an equilibrium situation; i.e., embryos used up are not replaceable, the nucleation process can be approximated to a time-independent model, in which all available embryos which can become nuclei with appreciable probability within the undercooling range, are assumed to grow. The number of nuclei which grow can be measured by counting the number of eutectic cells lying on the plane surface of a microspecimen taken from the ingot. Some experimental relationships between nucleation and undercooling taken from

References 3 and 6 are listed in Table 2. Increased undercooling despite increased nucleation had been achieved by modifying cell growth rate via the means of sulphur additions. Nucleation data have been recalculated to estimate the number of cells/cc from the quoted cells/in. The data can be approximated to an equation of form:

$$N = A.\Delta T^2 \quad , \tag{3.2}$$

where A is independent of ΔT and varies between 0.91 and 7.12. The relationships are shown graphically in Figures 8 and 9. Commercial cast irons probably obey similar nucleation laws, where A might attain values as high as 300. If this simple relationship holds generally, it means that one measurement of nucleation and undercooling enables A to be calculated.

Differentiating, we find that:

$$dN = 2\ A\ \Delta T\ dT \quad . \tag{3.3}$$

Alternatively, for small but not infinitesimal increments of ΔT:

$$\delta N = A\ (2\ \Delta T\ \delta T + \delta T^2) \quad , \tag{3.4}$$

where δT is the small but finite change in ΔT which occurs in a time interval.

Physically, this represents a system in which the embryo population contains a number of particles of a size capable of growing at each level of ΔT, the increase in the number capable of growing at each level being directly proportional to the undercooling.

TABLE 2. RELATION BETWEEN THE NUMBER OF NUCLEI AND THE UNDERCOOLING

The number of nuclei was measured from the number of eutectic cells in the final casting and the undercooling from the difference between the minimum eutectic arrest temperature and the equilibrium freezing temperature.

Metal Treatment	Bar Diameter+	Cooling Rate*	Number of Nuclei#	Undercooling
Low Sulphur Content	0.6	311	510	29.5
	0.875	148	615	21
	1.2	70	202	11.5
	1.6	48.5	214	9.5
High Sulphur Content	0.6	266	14,190	40
	0.875	168	5,780	27.5
	1.2	77	2,800	22
	1.6	50.3	1,400	13
Medium Sulphur Content	0.6	311	2,640	33
	0.875	185	1,890	23
	1.2	77	875	17.5
	1.6	43.4	649	12.5

* Cooling rates were taken as the slop of the cooling curve at 1158°C, in degrees C second^{-1}.

The number of nuclei was taken as the number of eutectic cells cm^{-3}.

+ Bar diameters are expressed in inches.

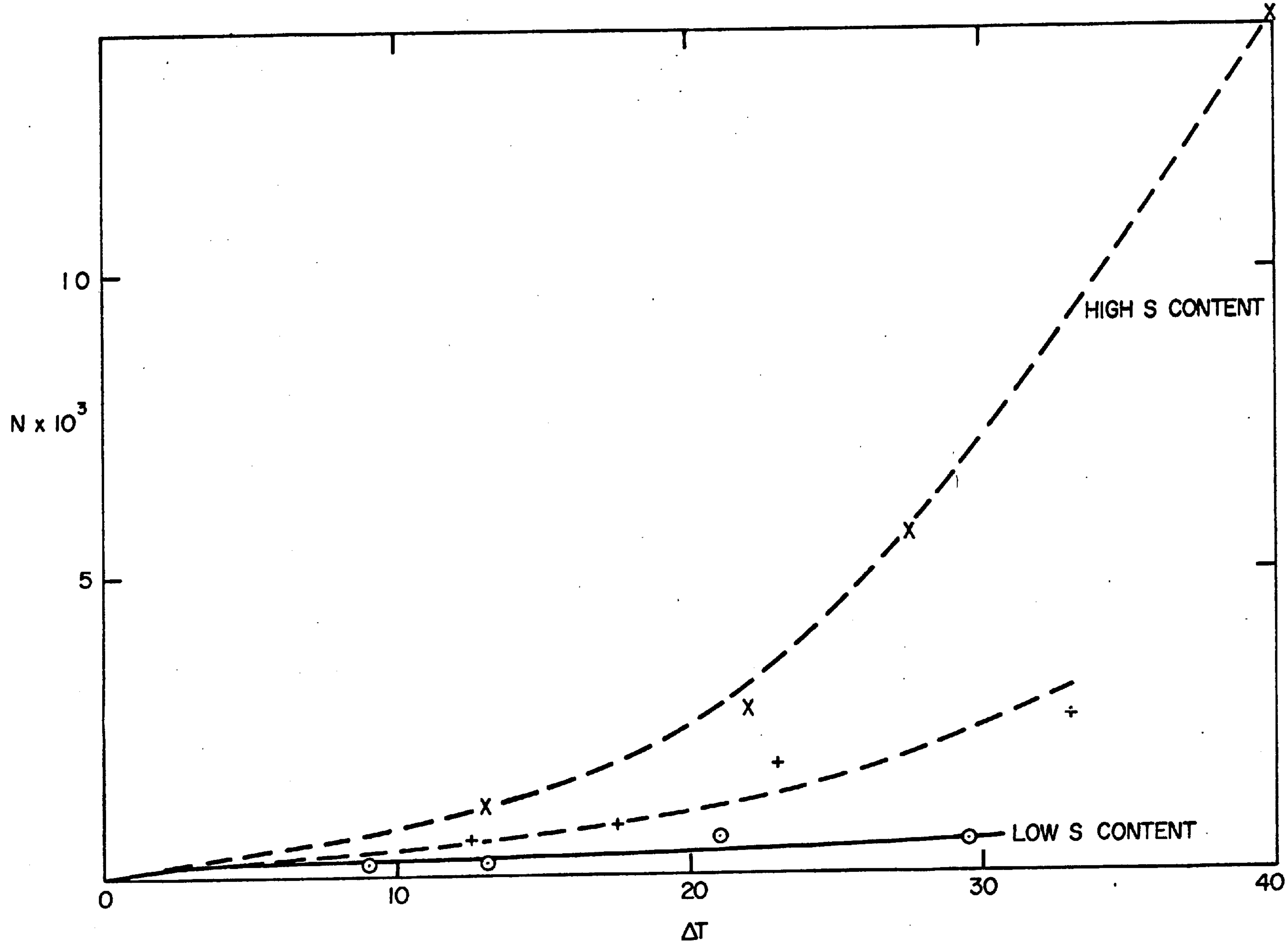

FIGURE 8 THE RELATIONSHIP BETWEEN CELL NUMBER AND UNDERCOOLING

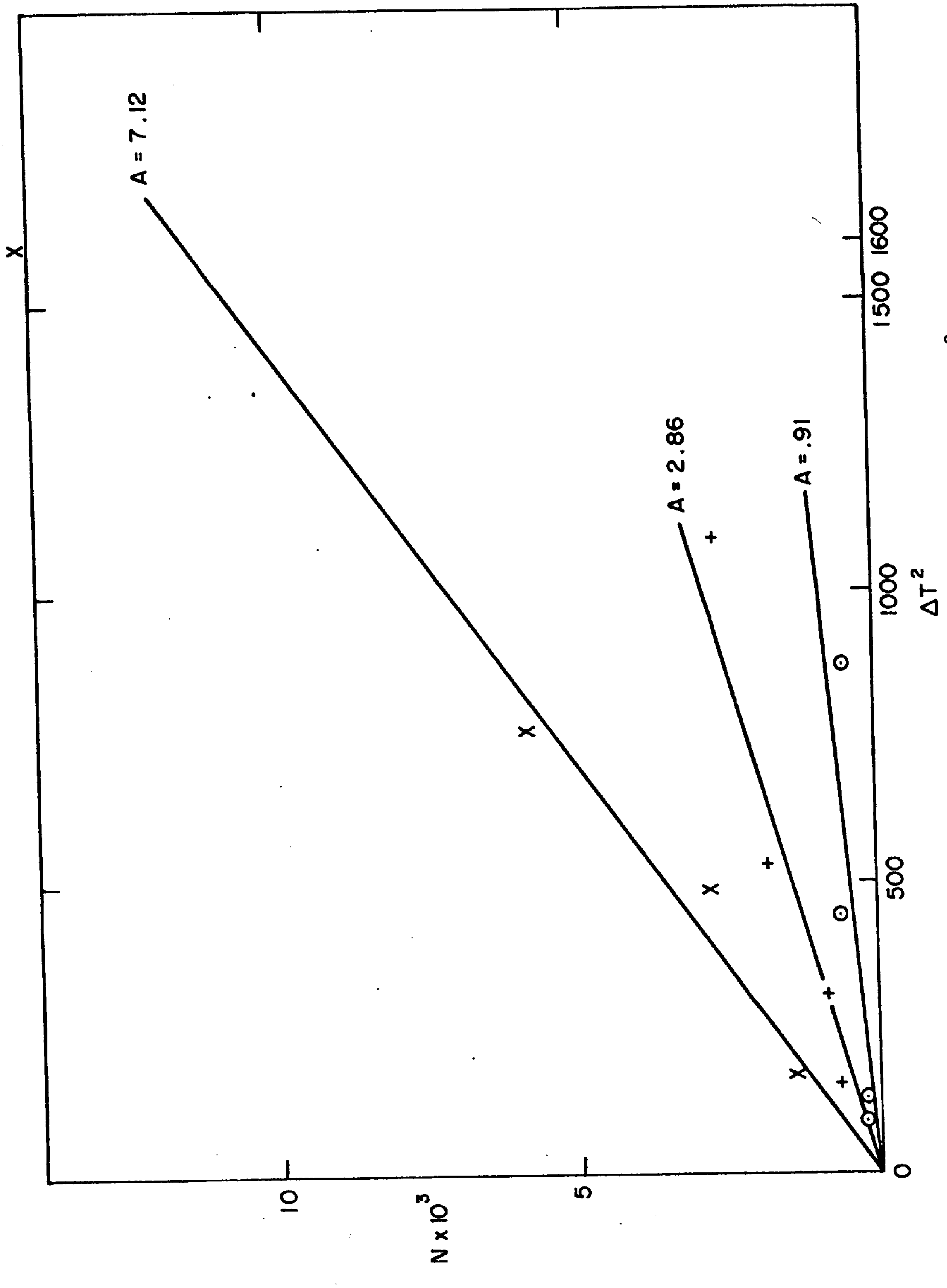

FIGURE 9. NUCLEATION PLOTTED AGAINST (UNDERCOOLING)^2

4. Eutectic Solidification

The growth process is very complex, because a range of growth regimes are possible (for example, the formation of fine as opposed to coarse graphite flake structures), and the graphite eutectic may occur in a variety of growth habits (for example, flake or spheroidal forms). Furthermore, the alloys which are classified as commercial cast irons are multicomponent, containing not only graphite and iron, but silicon, manganese, phosphorus, and sulphur to name the more common constituents.

Flake graphite eutectic crystallization has been studied by Tiller.[10] Conveniently subdividing the total driving force for the eutectic reaction into the undercooling required to overcome the separate limiting processes, he considered the following factors.

1. For two phases to grow cooperatively in a side-by-side fashion, the constituent rejected by one phase must diffuse and be incorporated into the second phase. To drive this process, a concentration difference is built up between the two phases. This is effectively an undercooling of the two interfaces, the change in liquidus temperature from the eutectic temperature associated with the concentration difference. This undercooling is termed $\Delta T_s^{\alpha\beta}$.

2. The growth of two phases leads to the incorporation of phase boundaries into the solid. This excess free energy lowers the liquidus for the eutectic by an amount ΔT_B.

3. Tiller[10] considered the overall curvature of the eutectic interface. However, the spherical eutectic cells are quite large for the greater part of their life, this term will be neglected.

4. The elements other than iron and carbon are also partitioned at the solid-liquid interface. This consumes an additional part of the available driving force, termed ΔT_s^I .

5. Some driving force is required to cause the atoms to attach to the solid. This is the energy consumed by the development of screw dislocations and the growth of reentrant corners produced by rotation twins.[11] This may again be expressed conveniently as an undercooling, term δT. These ideas can be summarized for the case where the bath is isothermal, as

$$\Delta T(\text{total}) = \Delta T_s^{\alpha\beta} + \Delta T_B + \Delta T_s^I + \delta T \quad . \tag{3.5}$$

By an optimization procedure, i.e., finding the maximum velocity with respect to the fineness of the eutectic dispersion as the controlling variable, the result obtained by Tiller[10] was:

$$\frac{dR}{dt} = C\,(\Delta_s^{\alpha\beta} + \Delta T_B)^2 \quad . \tag{3.6}$$

If the other components of the total undercooling are small, or alternatively a constant proportion of the whole, this equation can be approximated to:

$$\frac{dR}{dt} = C' \left\{\Delta T(\text{total})\right\}^2 \; . \tag{3.7}$$

However, if (as is probable) the driving force for attachment and that for the partitioning change disproportionately, the exponent would differ from 2, and this expression might become a severe oversimplification.

5. Mechanical Effects: Cell-Cell and Cell-Mold Wall Interactions

The rate of growth of the eutectic, calculated in accordance with equation (3.7) permits the increase in radius of the eutectic cells in a time increment, δt, to be calculated, i.e.,

$$\delta R = \frac{dR}{dt}\,\delta t \quad . \tag{3.8}$$

The volume of solid formed, and hence the amount of latent heat liberated, follow directly from the knowledge of the increase in radius, and the free (growing) area of the eutectic cells.

The surface area of the cells, assuming that they do not interact with each other or with the mold wall, can be calculated from their radii and the number of cells of each size (the number nucleated in each particular time increment). Both of these quantities are stored in the computer memory. The area lost as a result of cell-cell interactions can be calculated for each subvolume of the casting from the relation between the fraction of the volume solid (stored in computer memory) and the area lost. This relation has been derived by Johnson and Mehl[12] and later using a different approach by Evans[13].

The surface area of the cells, assuming no contact is:

$$(SA) = \frac{4}{3}\,\pi\Sigma N_i R_i^{\,3} \quad , \tag{3.9}$$

where N_i is the probable number of cells nucleated in the ith intervals and R_i is their size. The surface area still growing at any time is calculated by correcting for the area lost by cell-cell impingement:

$$(SA)' \approx (1 - FVS)\,(SA) \quad , \tag{3.10}$$

where $(SA)'$ is the surface area still growing and FVS is the fraction of the volume solid.

A second correction must be made to account for the interaction between the cells and the mold wall. This correction is of particular importance in the annuli near the outer surface of the bar, and it must be applied before the correction for cell-cell interactions.

Consider a eutectic cell growing within an annular subdivision. Referring to Figure 10, β and γ are the radii of the outer and inner limits of the annulus within which the cell is growing. Using the definitions: x is the distance of the center of the cell from the center of the cylinder, D is the radius of the cylinder, R is the radius of the eutectic cell, and Δ is the portion of the sphere projecting beyond the limits of the mold wall. The fraction of the surface area lost, F, is given by

$$F = \frac{\Delta}{2R}$$

$$= \frac{R + x - D}{2R} \quad . \tag{3.11}$$

Consider, now, a volume (δV) formed by a smaller annulus of unit length, radius A, and width δA, lying between the radii β and γ, i.e.,

$$\delta V = 2\pi A \delta A \quad . \tag{3.12}$$

Let N be the total number of cells in volume V, the total volume of the annulus between β and γ. Assume that the N cells are uniformly distributed within the volume, and that n cells lie between x and β. At the limit $\delta A \rightarrow 0$,

$$n = \frac{N}{V} \int_{A=x}^{A=\beta} dV$$

$$= \frac{N}{V} \int_{x}^{\beta} 2\pi A dA$$

$$= \pi \frac{N}{V} (\beta^2 - x^2) \quad . \tag{3.13}$$

Now x can be related to N, V and n as

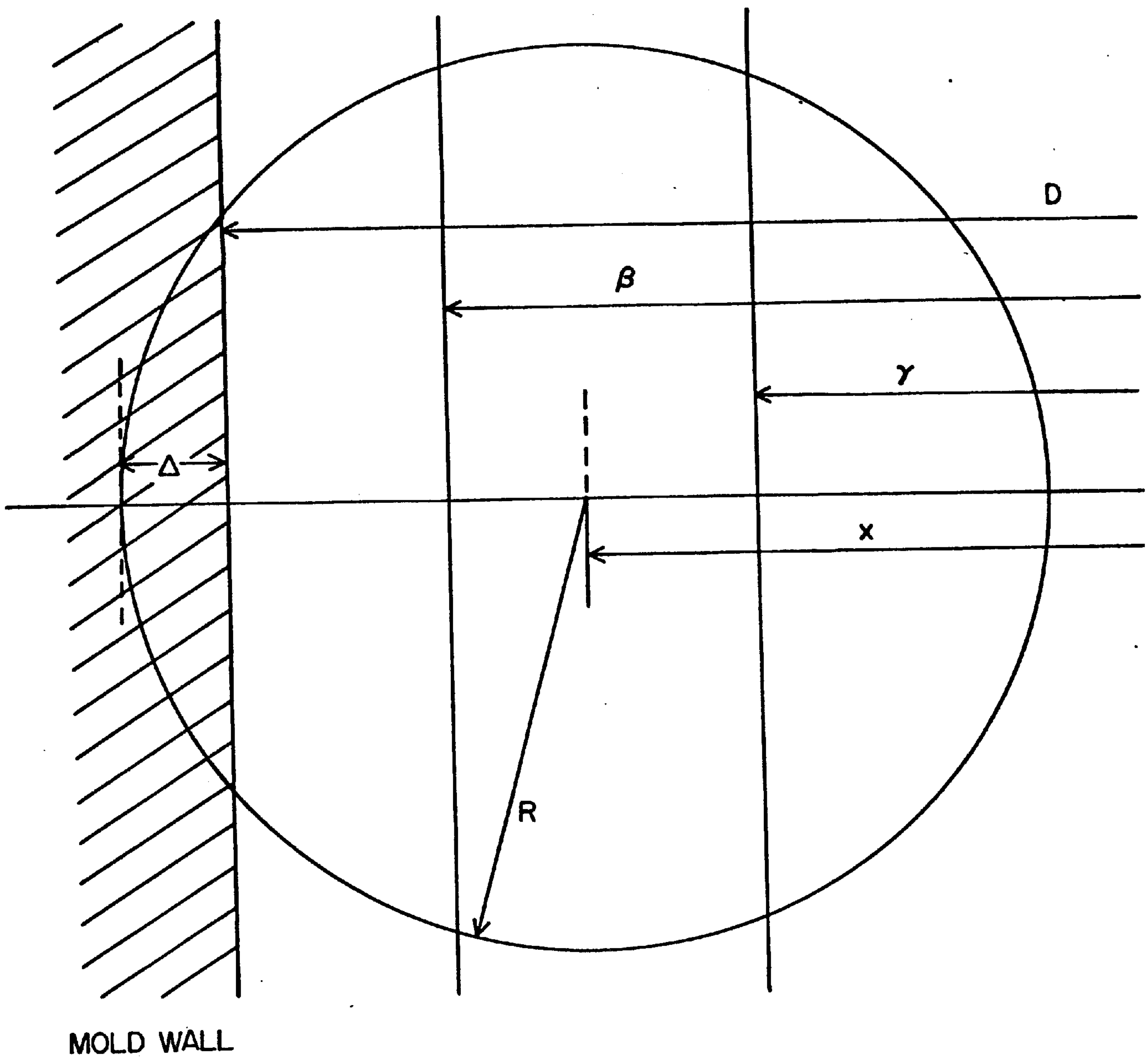

FIGURE 10 SURFACE AREA LOST BY WALL CONTACT

$$x = (\beta^2 - \frac{nV}{\pi N})^{1/2} \quad . \tag{3.14}$$

But since

$$V = \pi(\beta^2 - \gamma^2) \quad ,$$

$$x = \left\{\beta^2 - \frac{n}{N}(\beta^2 - \gamma^2)\right\}^{1/2} \quad . \tag{3.15}$$

For a given size group (i.e., the same radius), the fraction lost can be averaged over the whole subvolume; i.e.,

$$\text{Mean F} = \overline{F} = \int_0^N (\frac{R + x - D}{2RN})\, dn \quad . \tag{3.16}$$

Substituting for x we find

$$\overline{F} = \frac{1}{2RN}\int_0^N \left[R - D + \left\{\beta^2 - \frac{n}{N}(\beta^2 - \frac{n}{N}(\beta^2 - \gamma^2)\right\}^{1/2}\right] dn$$

$$= \frac{1}{2\ R}\left[R - D + \frac{2}{3}\left(\frac{\beta^2 - \gamma^2}{\beta^2 - \gamma^2}\right)\right] . \tag{3.17}$$

CHAPTER IV: COMBINATION OF THE SEPARATE MODELS INTO A SYSTEM, TRIAL CALCULATIONS

Models have been described for all the main processes which operate in the freezing of cast iron with the exception of primary austenite precipitation. This is omitted from most descriptions of eutectic solidification, and it was considered to be a second order process which could well be ignored. Furthermore, because temperature gradients are usually small, in the first model, the casting will be considered to be isothermal. This will highlight the assembly of the system, and illustrate the manner in which a model can be developed as further components of the system are added.

1. Simulation of the Freezing of an Isothermal Cylinder

Having derived expressions for $\frac{dN}{dt}$ and $\frac{dR}{dt}$ in equations (3.4) and (3.7), the various processes can now be linked together in a calculation of the "cooling curve" for a casting. To provide an introduction to the more involved calculations which take temperature gradients into consideration, an isothermal system will be first considered in detail. A volume of liquid metal is assumed to develop no temperature gradients, and to have a constant rate of heat removal. The flow diagram for a simple program is shown in Figure 11.

After preparing computer storage, calculating constants, writing headings and so on, the program moves into a section (named COOL) in which the calculated amount of heat is taken from the metal, and the temperature drop is determined from the metal volume and specific heat. The temperature is lowered by this amount, and the time is advanced.

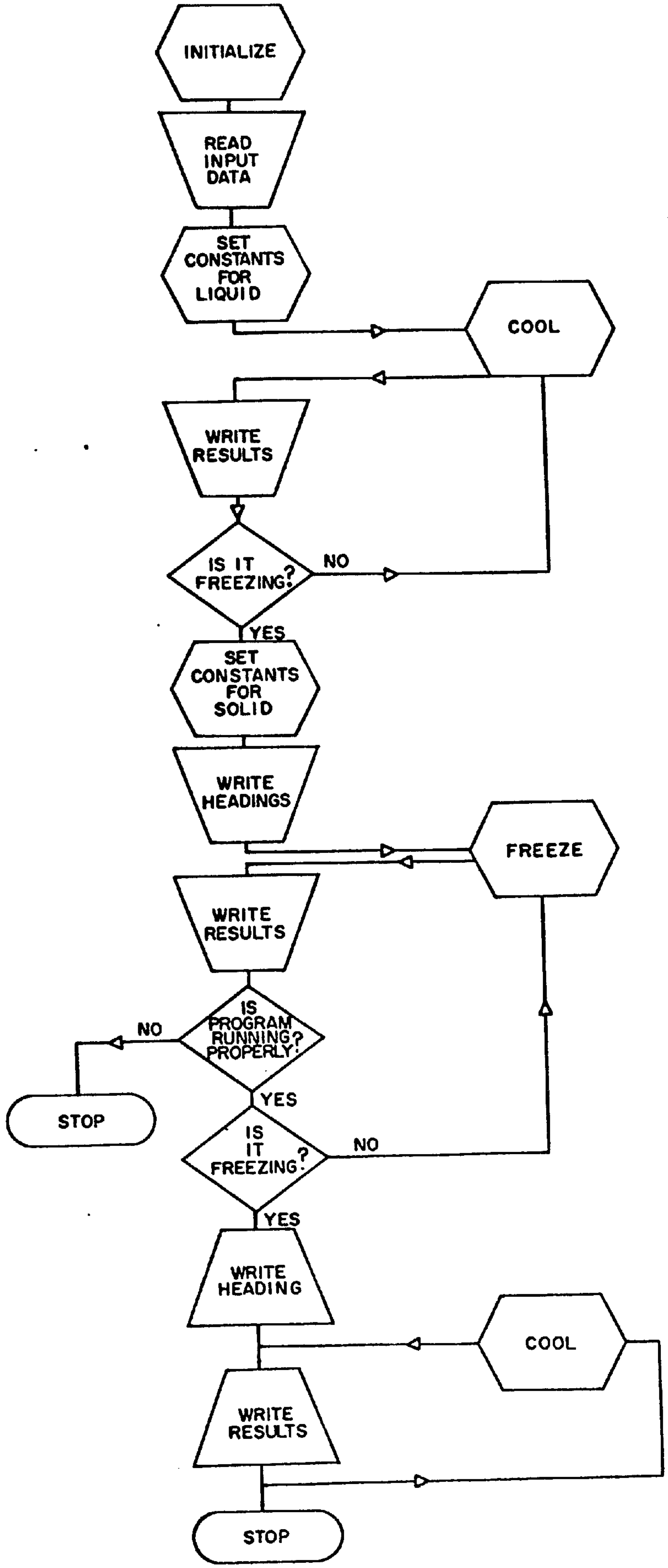

FIGURE 11 FLOW CHART FOR THE SIMULATION OF AN ISOTHERMAL CASTING

Time intervals appropriate to the casting size and cooling rate are calculated during the preliminary stages of the computation (termed initiation in the flow diagrams). Hence, the first point in the temperature-time relationship (cooling curve) has been obtained. The result is written and stored on magnetic tape for plotting. The temperature is then compared to the eutectic temperature. The cycle is repeated until the liquid has cooled below the equilibrium freezing temperature. The calculation then enters the FREEZE section of the calculation, after changing various constants so that when solidification is complete and COOL is reentered, it will simulate cooling of the solid. In this calculation, the probable number of nuclei starting to grow in the time interval δt is calculated. As derived earlier,

$$\delta N = A(2\ \Delta T\ \delta T + \delta T^2) \quad \text{(equation 3.4)} ,$$

where ΔT is the temperature difference between the metal temperature and equilibrium. δT is the fall in temperature which has occurred during the previous interval.

The increase in radius of the cells is then calculated:

$$\delta R = \frac{dR}{dt}\,\delta t \quad , \tag{4.1}$$

where δt is the time increment of the calculation. The surface area of the cells is then calculated from information stored in the computer memory as:

$$SA = \frac{4}{3}\,\pi \Sigma N_i R_i^{\,3} \quad , \tag{4.2}$$

where N_i is the probable number of cells nucleated in the time interval i and R_i is their radius.

In this calculation, the cell-mold interactions will be neglected. A correction is applied for cell-cell interactions as discussed earlier. Thus, the area of growing surface can be derived, and therefore, the volume of solid formed during the time increment follows simply as the product of the growing area with the radius increment, δR. The sum of the volumes of solid formed in each of the previous time increments is also stored in the computer memory and is increased at each increment of growth.

The radii of all the cell size groups are increased by δR, and various quantities are calculated such as the mean specific heat, volume fraction solid, and so on. Finally, from knowledge of the specific heat, latent heat liberated, and heat removed, the new temperature of the liquid metal is derived. The calculation cycles through the FREEZE calculation until all the volume has become solid. The program then simulates the cooling of a solid casting for a short period and then the calculation stops.

2. Freezing of a Nonisothermal Cylinder

The simple description of the solidification system can now be developed to approximate more closely to reality, by taking account of the temperature gradients and the interaction between the growing cells and the mold wall.

These processes were treated by subdividing the cylinder into a number of annular volumes as was described in Appendix B. When the volumes are small, each subvolume of the casting can be treated as being isothermal and passed through a series of calculations similar to those described above. The flow chart is described in Figure 12. Careful study will show the basic similarity between this calculation and the isothermal

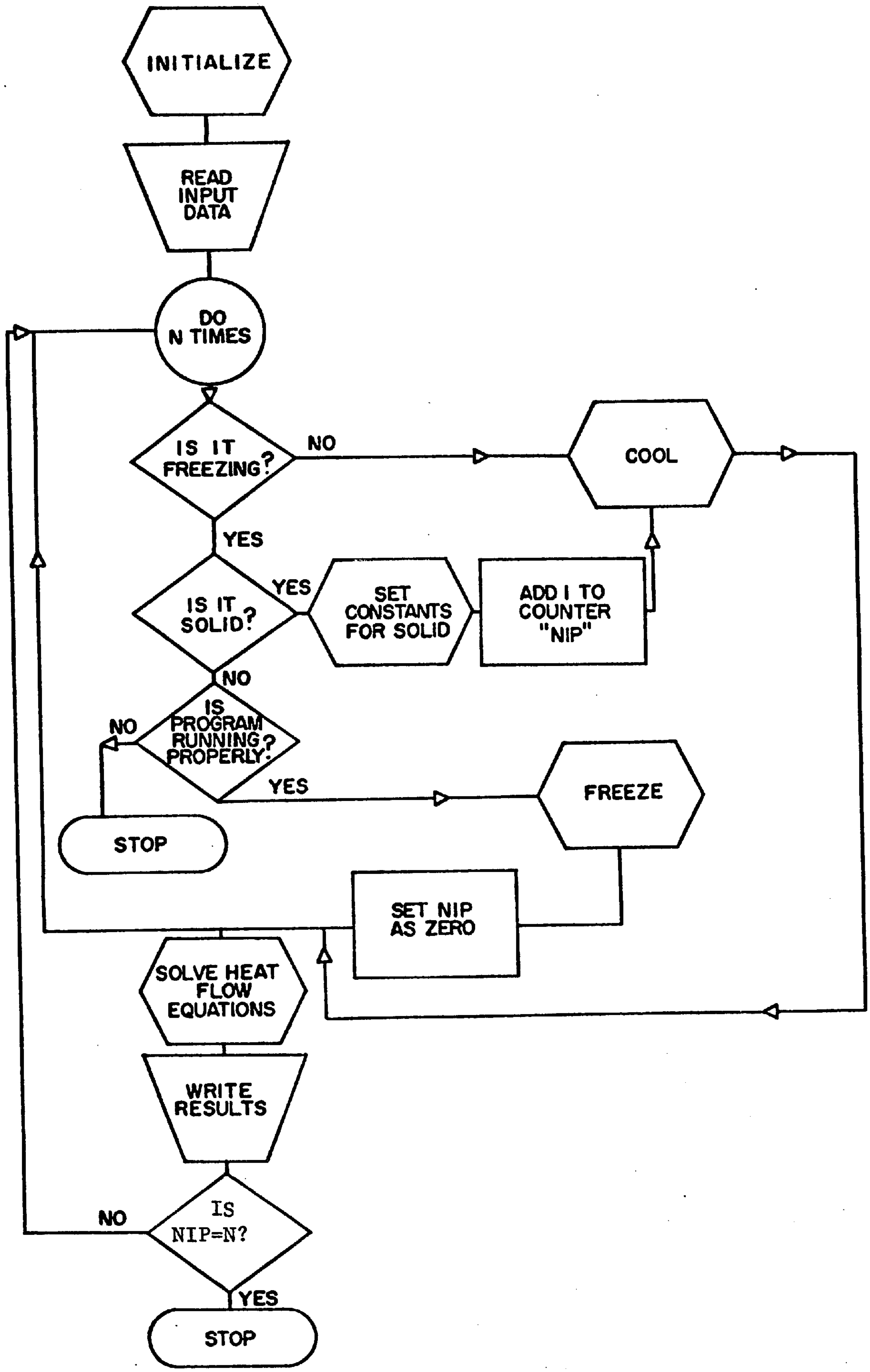

FIGURE 12. FLOW CHART FOR A COMPUTER SIMULATION OF THE FREEZING OF A ROUND BAR SUBDIVIDED INTO N ANNULI

treatment shown in Figure 11. The program was designed to scan each subvolume of the cylinder in turn, keeping score of the number and size of the cells in each subdivision and evaluating the latent heat liberation. After all the subvolumes have been scanned, the program moves into the SOLVE section of the calculation. In this routine, the heat flow equations are solved. These have been described in Chapter III and in Appendix B.

The calculation cycles through either the COOL or the FREEZE routines, and the SOLVE routines, until each of the volume subdivisions is solid, and then stops. It may be noted that the function of the COOL calculation is now reduced compared to the "isothermal" calculation. The cooling of solid or liquid is now automatically treated by the heat flow calculation SOLVE so that, in COOL, the program merely sets latent heat liberation for the particular subdivision at zero and specifies the appropriate thermal conductivity.

3. The Effect of Sulphur on Solidification

Sulphur has many interesting effects upon the structure of cast iron. It changes the nucleation[3] as shown by the typical experimental results contained in Table 2. Further, at low sulphur contents the graphite structure is very fine flake graphite eutectic. At higher levels, the structure becomes coarser and typical of most commercial cast irons. With still higherlevels, the formation of graphite is suppressed, and iron carbide eutectic is formed in its place. At very low sulphur levels, achieved by treatment with magnesium or by vacuum melting at better than 10^{-6} Torr for long periods, the structure changes from a-direction flakes to c-direction spherulites. In previous papers[14,15] these phenomena had been explained as the effect of sulphur adsorbed on the graphite particles which are the nuclei in this system. The adsorbed layer was presumed to reduce the graphite-liquid iron interfacial surface energy, thus allowing particles to grow at reduced undercooling levels. In a similar way, the adsorbed layer was supposed to slow down the attachment of carbon atoms on the graphite interface. In doing this, the overall growth rate of the graphite-austenite eutectic is slowed. Since the interlamellar spacing is related to the growth velocity, sulphur would, on this basis, be expected to first coarsen the flake structure, and finally, when attachment became severely impeded, prevent graphite growth completely. This picture is greatly simplified, because many interacting variables effect the result. For example, increased nucleation, by increasing surface area of eutectic growing into the liquid, would tend to reduce undercooling and thus coarsen the graphite structure. On the other hand, by slowing the growth rate, sulphur would tend to increase undercooling, and increase the driving force available to cause growth.

There are not only structural changes resulting from sulphur content changes. The soundness of castings is altered. Regions of iron carbide are produced (inverse chill) which reduce the machineability of the material. Despite the importance of these effects, it has only been possible to discuss the phenomenon in the very qualitative way outlined in the opening paragraph of this section.

In contrast to the poor theoretical state of the art, there have been a number of experimental studies of the problem, producing cooling curves and nucleation data which described the effect of sulphur on the freezing of cast iron. Because the author had developed the conceptual model for the effect of sulphur on graphite structures, it was of some interest to determine whether the experimental results could be explained quantitatively by the model.

The published cooling curves summarized in Table 2 were well suited for comparison with the computer model which has been described, because the cooling curves were obtained from thermocouples placed at the centers of 10-in. long bars, cast into dry sand molds (see Figure 13). In this situation, for the diameters studied, the results can be considered to be those for infinite cylinders. Although the cooling rate changes during cooling, the change is believed to be sufficiently small during the early part of the freezing arrest to permit the assumption of a constant rate of heat removal. The material used in the published work was an iron-carbon-silicon alloy of 4.1% carbon equivalent containing 0.14% Mn, 2.5% Si, and less than 0.1% total of all other elements. This composition ensured the absence of iron carbide eutectic at the cooling rates studied.

A series of 16 calculations were performed using the three nucleation constants derived earlier and a series of growth constants which were chosen to cover the range of freezing temperatures of interest. From the results, the maximum and minimum temperatures of the eutectic arrest at the center of each "bar" was determined, and hence the response of these characteristics to changes in the nucleation and growth constants were observed. For these calculations, the growth law:

$$\frac{dR}{dt} = B\Delta T^2 , \quad \text{(equation 3.7)}$$

was assumed (using the cooling rate and bar size for a 1.2-in. bar to evaluate B). The results are shown in Figure 14 where ΔT in each case is the temperature difference between the arrest temperature and the equilibrium freezing temperature.

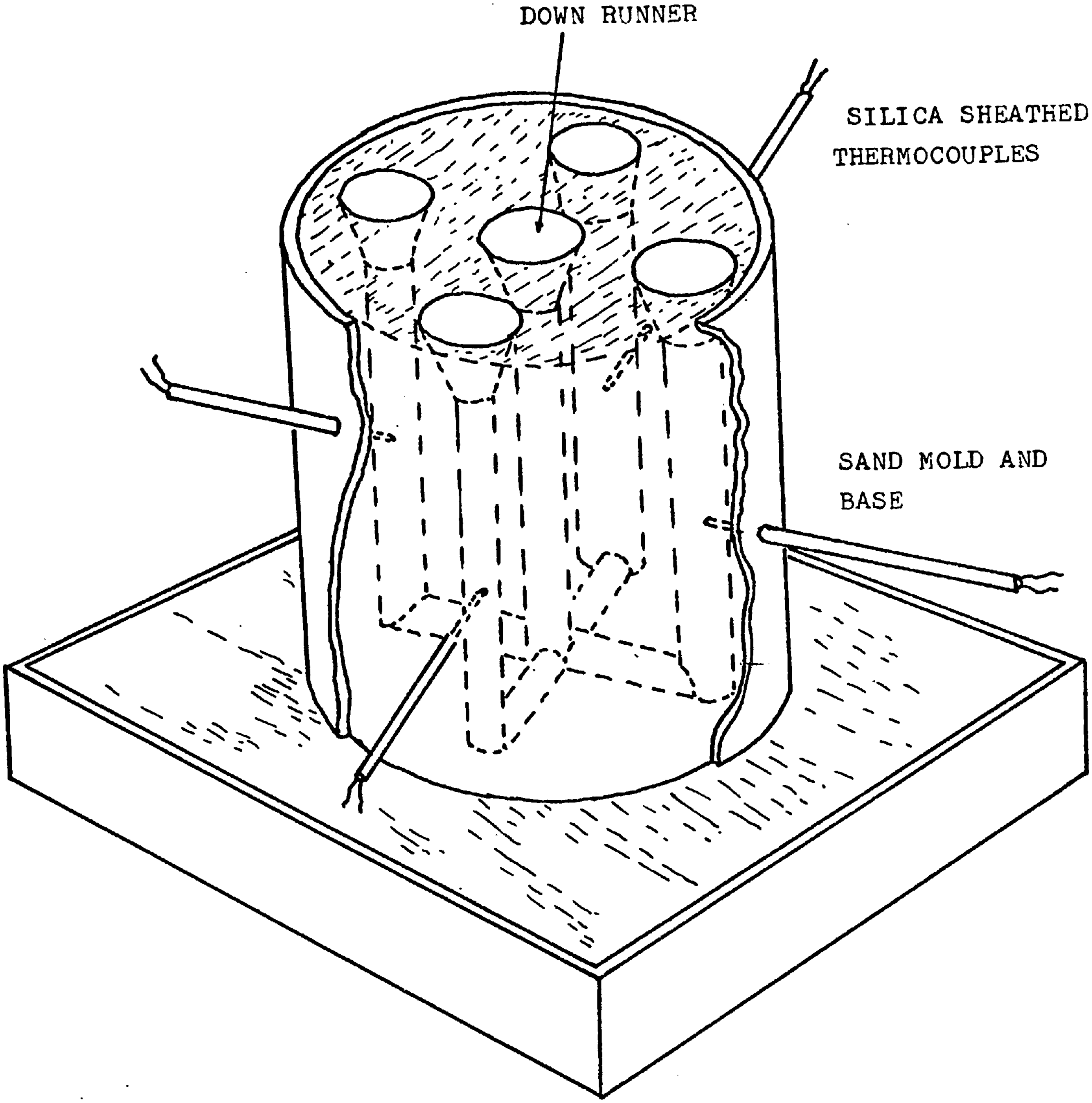

FIGURE 13: APPARATUS FOR FREEZING POINT DETERMINATIONS (SCHEMATIC)

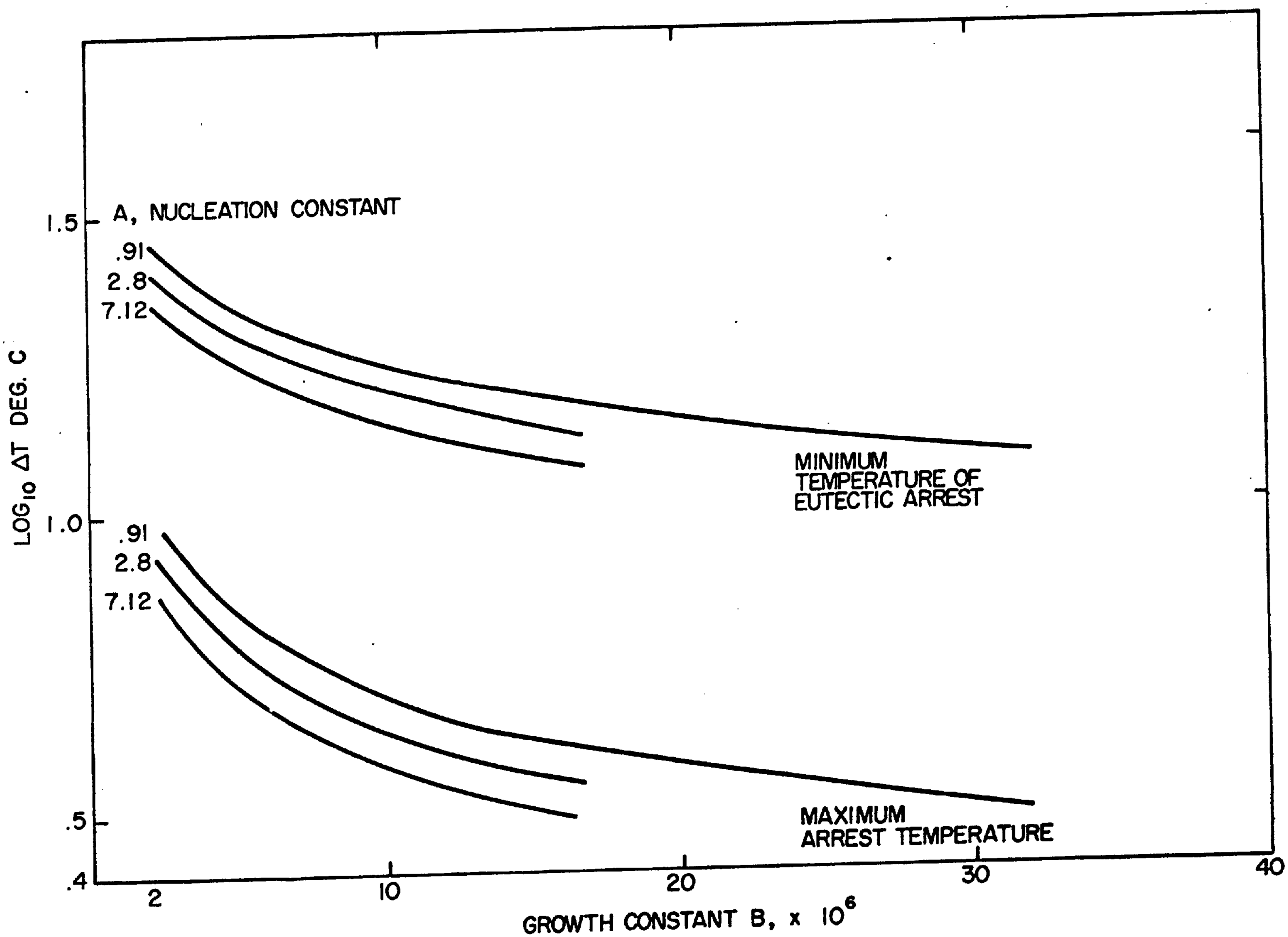

FIGURE 14 MAXIMUM AND MINIMUM SOLIDIFICATION TEMPERATURES RELATED TO KINETIC CONSTANTS

From Figure 14, growth constants were derived which were appropriate to the irons of the three sulphur contents. They were chosen to yield the same maximum ΔT as the experimental results for the 1.2-in. bar. The constants were:

	value of B
low sulphur	34.5×10^{-6}
intermediate sulphur	7.2×10^{-6}
high sulphur	2.5×10^{-6}

The same constants were used to simulate the freezing of 0.6 and 1.2 in. bars and the fit between the curves and those experimentally observed was poor. This was taken to indicate that the growth rate did not obey a square power relation with ΔT. In fact, the maximum undercooling of the 1.6-in. bar was overestimated and that for the 0.6-in. bar grossly underestimated. The work was taken a stage further and the relationship:

$$\frac{dR}{dt} = B\Delta T^{1.7} \quad , \tag{4.3}$$

was assumed. Again the cooling of 1.6, 1.2, and 0.6 in. bars was modelled, but now a reasonable approximation to the cooling of all the bars was possible. The undercooling of the large cylinders was still slightly overestimated and that for the small bars underestimated suggesting that a slightly smaller exponent than 1.7 was required. Figure 15 shows a comparison between the cooling curves and those predicted by the computer for the 1.2 and 0.6 in. bars of high sulphur cast iron. The growth constant had to be altered from 2.5 to 4.5×10^{-6} to yield the correct results when using the changed growth law. Discrepancies between the shapes of the curves are considered to be important and will be discussed in the next chapter.

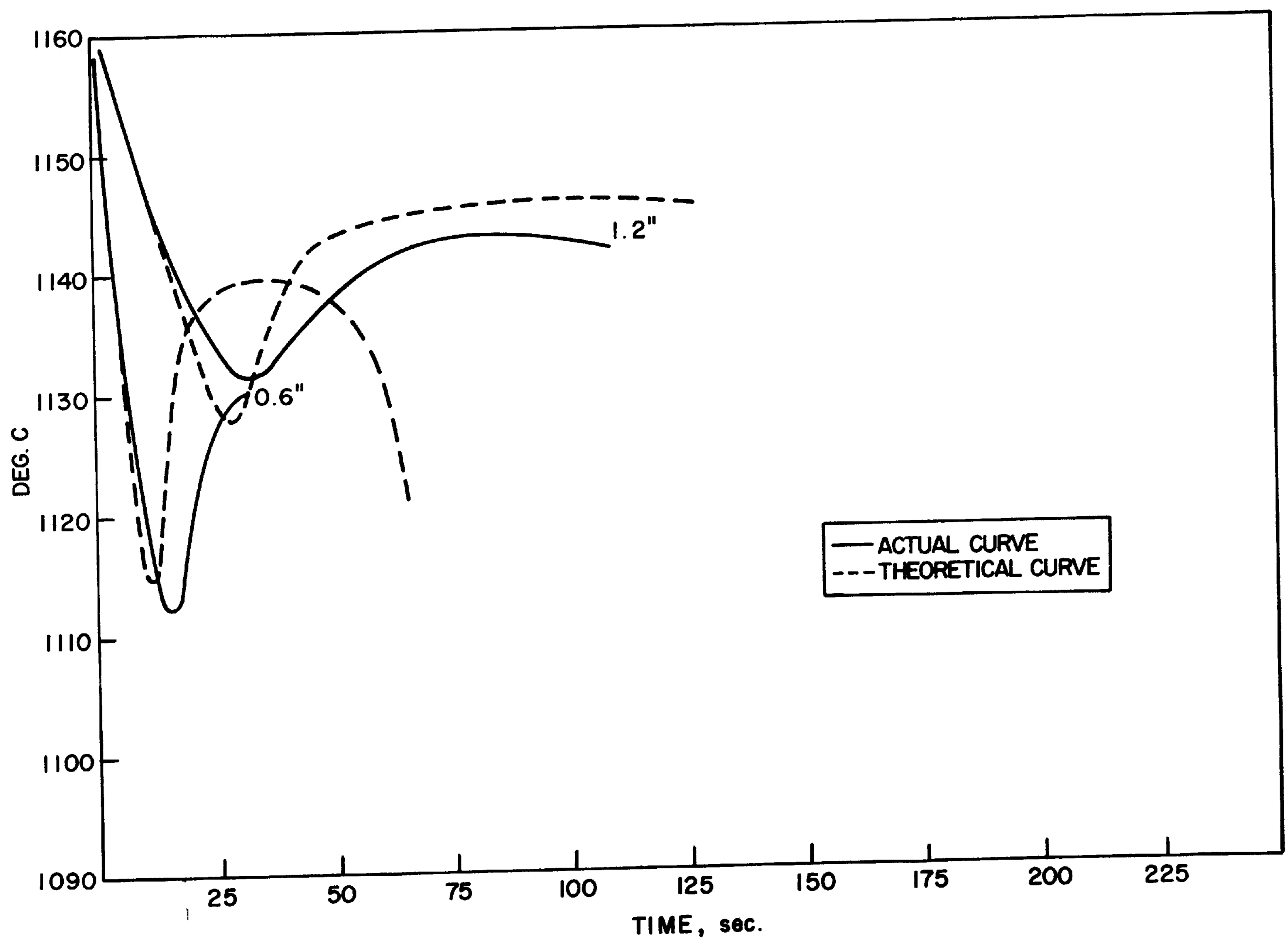

FIGURE 15. COMPARISON OF EXPERIMENTAL AND PREDICTED COOLING CURVES

CHAPTER V: STUDY OF PRIMARY PHASE SOLIDIFICATION AND THE REFINEMENT OF THE MODEL

1. Primary Phase Solidification

The influence of primary austenite crystallization on the eutectic solidification is generally minimized in descriptions of the freezing process. Treating the phenomenon qualitatively, it will be readily seen that not only could it account for the major discrepancies between theoretical and experimental cooling curves, but more important it could have a major influence upon the properties of the casting.

Normally, a casting undergoes a primary arrest at a higher temperature than the eutectic temperature. Hence, the primary phase is growing in equilibrium with the melt by the time the liquid metal has cooled to the eutectic temperature. From this, the first conclusion follows: since primary phase solidification liberates latent heat, the apparent rate of cooling will be slower than expected while the temperature is falling and γ-iron is being precipitated.

After recalescence, the composition does not change along the extension of the γ-iron liquidus line in a simple way. Eutectic solid forms at the composition of the bulk liquid. When the temperature rises, austenite dissolves where it is in contact with the liquid, and the carbon content of the liquid as changed in accord with the extension of the liquidus line. Hence, when there is recalescence there is absorption of heat as a result of the dissolution of the primary austenite phase.

We may therefore develop a model for the precipitation and solution of primary austenite during the freezing of a casting which qualitatively accounts for the observed discrepancies between the experimental and computer drawn cooling curves. Assume that

a. Nucleation of primary phase occurs well before the temperature range of interest.

b. There is a fine dispersion of primary phase dendrites so that the bulk liquid is maintained at the liquidus level by precipitation and dissolution of austenite.

From this assumption it is possible to compute the composition of the liquid at any temperature:

$$C = C_{eu} + (T - T_{eu})/(\text{slope of the liquidus line}) \quad , \tag{5.1}$$

where C is the liquid composition, C_{eu} and T_{eu} are the eutectic carbon content and eutectic temperature, respectively, and T is the liquid temperature. The amount of austenite formed in a time increment follows from the temperature change:

$$\delta = 1.0 - \left\{\frac{C_T}{C_T + \delta T}\right\}^{\frac{1}{1-m}} \quad , \tag{5.2}$$

where δ is the volume of austenite formed in unit volume of liquid, m is the equilibrium solute distribution coefficient, and δT is the temperature change in the time increment δt. Hence, from the fraction volume solid, the actual amount of austenite formed or dissolved can be determined as:

$$\delta' \approx V_i \ \delta(1.0 - FVS_i) \quad , \tag{5.3}$$

where the subscripts i indicate that the calculation is performed separately for each of the subvolumes.

The model makes the rather surprising prediction that recalescence causes a fragmentation of the primary austenite crystals. Because the eutectic cells grow in the casting containing primary crystals, the primary dendrites become partly embedded in the eutectic. Thus, only the regions of austenite dendrites between the eutectic cells are exposed to liquid, and free to dissolve. This prediction was examined experimentally. Ingots of cast iron were induction melted in an inert atmosphere furnace in which they could be rapidly quenched. The ingots weighed 50 gm, and they were contained in alumina crucibles supported below a graphite tube connected through a tap to the main water supply. The crucibles were mounted inside a graphite susceptor, the size of which was adjusted to give a cooling rate of about 150°C/min. The temperature was continuously recorded by a platinum/platinum 13% rhodium thermocouple mounted inside a 1 mm O.D. sheath at the center of the ingots. A cooling curve was drawn for the first ingot. Then, the other ingots were melted and cooled under precisely the same conditions but the cooling was interrupted at different stages through the freezing arrest. The structure at the center of each ingot was studied metallographically. Figure 16 shows the structure at the center of an ingot quenched during recalescence. It is possible to trace the outline of the primary phase dendrites through the eutectic cells. However, at the periphery of the cells (indicated by quenched liquid) the dendrites can be seen to have dissolved, many of them disappearing completely. This phenomenon must have an effect upon many properties of castings. In particular, since the primary phase is much stronger in tension than the flake graphite eutectic, the fragmentation must cause a weakening of the material. This prediction is in agreement with the hitherto unexplained

FIGURE 16. THE STRUCTURE OF AN INGOT QUENCHED DURING RECALESCENCE

Note partially dissolved dendrites in the quenched liquid at the cell boundaries.

unexplained effects of eutectic nucleation upon the modulus and upon the ultimate tensile strength of the material. The changes are in accord with a fibre strengthening model, with the length of the fibres being reduced by reduced nucleation (increased recalescence).

2. The Computer Model With Primary Phase Solidification Included

The computer model was modified to include primary phase solidification. The program is listed in Appendix C.

The two variables in the growth law, B (the pre-exponential factor) and the exponent were used as "curve fitting" parameters, and used to give the best possible agreement between the predicted and actual values of undercooling for the 0.6 and 1.6 inch bars of each composition. The calculated and actual values of the undercooling levels for all the bar sizes are compared in Table 3, where the revised growth law constants are also shown. For the medium and low sulphur content irons, the agreement between the theoretical and actual cooling curves were quite good. However, recalescence was still too rapid, although the peak temperatures were achieved at almost the same time in the solidification arrest in both the model and the experimental curves. The difference may be due to errors in the experiment result; a thermocouple in a cooling bar does not record the temperature at a point in space and time, but an average for a small range of coordinate values. This results in a "smearing" of the curves when the temperature is changing rapidly, and when there is a large temperature gradient across the bar. Figures 17 and 18 summarize the theoretical cooling curves plotted by the computer for the low sulphur and medium sulphur alloys, respectively. The curves for each of the four bar sizes (Table 3) for the same composition are superposed on the same graph. Figure 19

TABLE 3. CALCULATED AND EXPERIMENTAL VALUES OF UNDERCOOLING

Treatment	Bar Size (inches)	Growth Constants		Undercooling	
		Pre-exp.	Exponent	Model	Measured
Low Sulphur	0.6	52×10^{-5}	0.78	29.5	29.5
	0.875			20	21
	1.2			13.5	11.5
	1.6			11	9.5
High Sulphur	0.6	42×10^{-5}	0.44	39.5	40
	0.875			29	27.5
	1.2			18	22
	1.6			13.5	13
Medium Sulphur	0.6	29×10^{-5}	0.78	33	33
	0.875			24.5	23
	1.2			16	17.5
	1.6			11.5	12.5

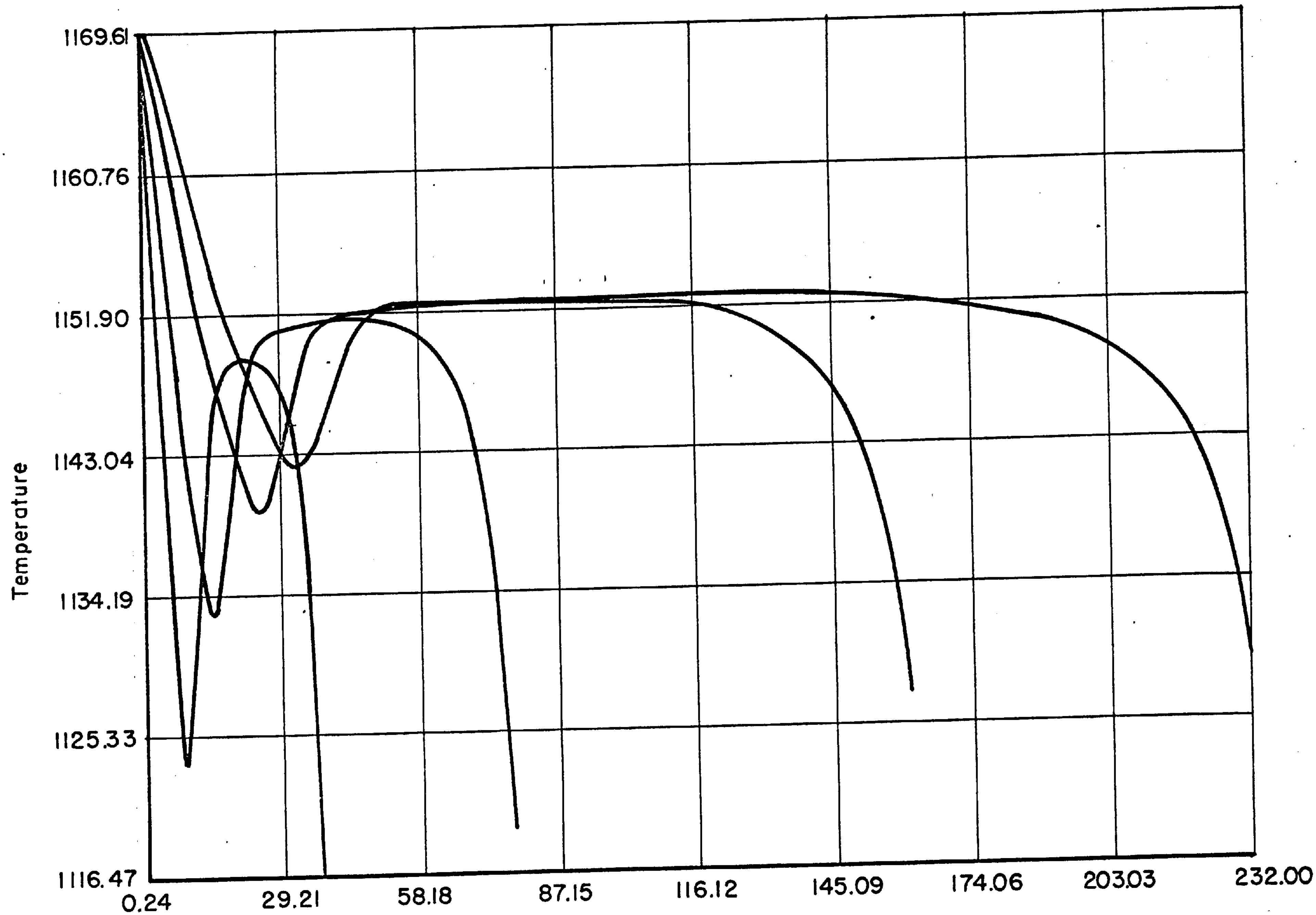

FIGURE 17. THEORETICAL COOLING CURVES FOR LOW SULPHUR ALLOY

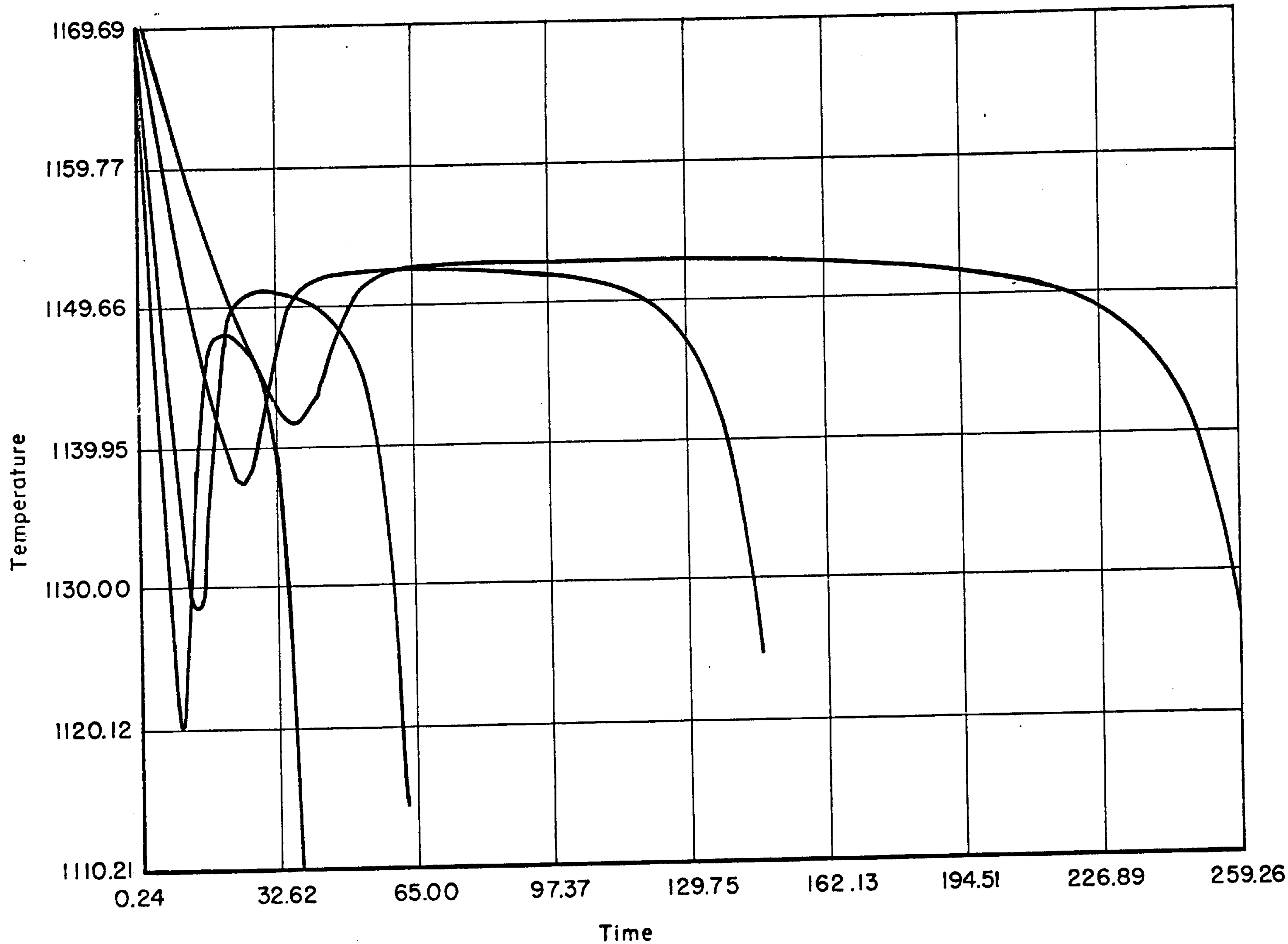

FIGURE 18. THEORETICAL COOLING CURVES FOR HIGH SULPHUR ALLOY

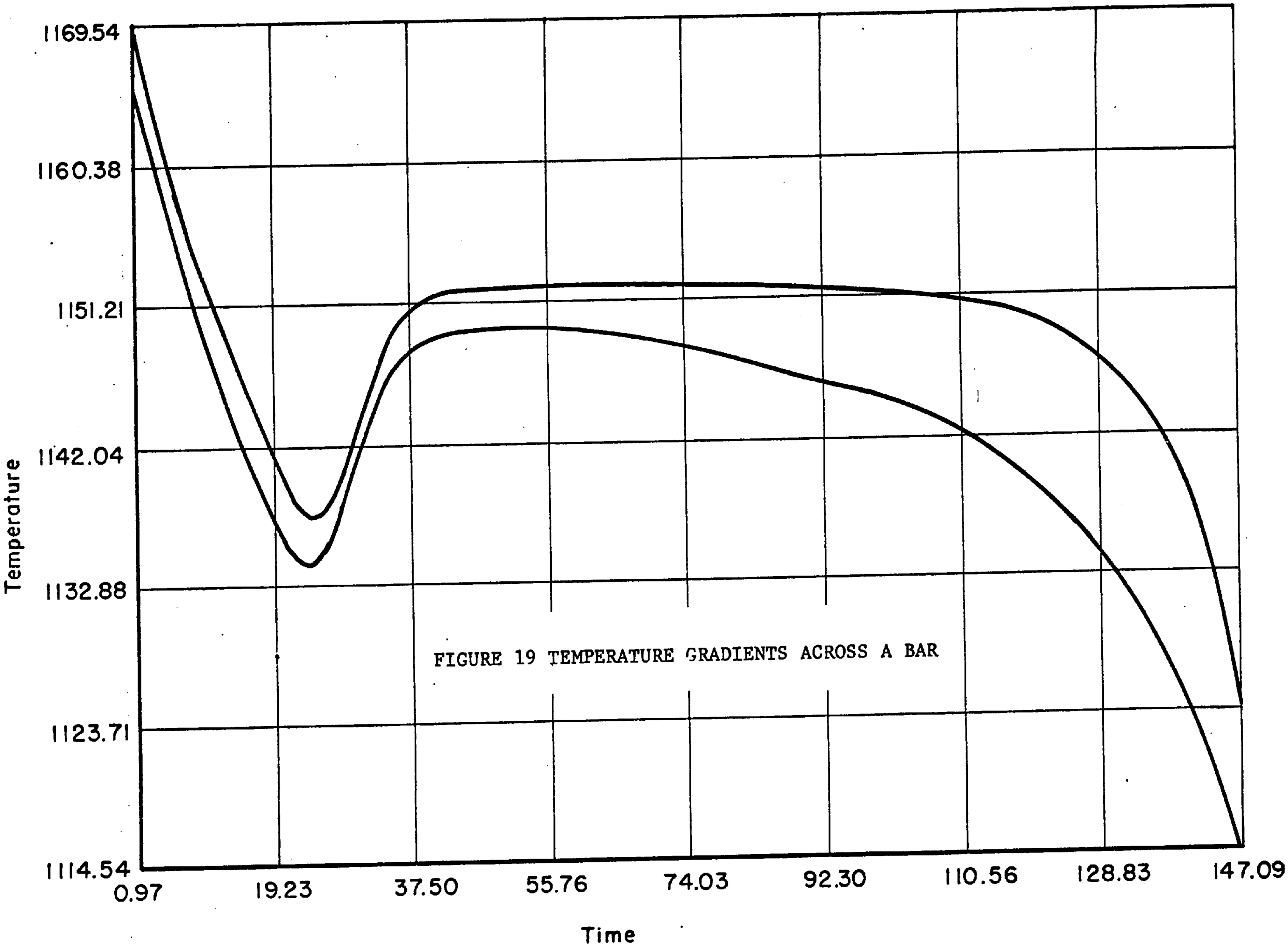

FIGURE 19 TEMPERATURE GRADIENTS ACROSS A BAR

illustrates the temperature gradients across a typical bar casting, in this case the 1.2-in. bar of medium sulphur content alloy. In this graph, the cooling curve for the outer section and the curve for the central portion are shown on the same axes. For the high sulphur content alloy, the agreement between the predicted and actual curves was not so good. Of course, the predicted and observed values of undercooling could be brought into close agreement. However, the growth constants which gave this result caused very large amounts of recalescence, whereas the observed recalescence was very sluggish, to a final maximum well below the eutectic equilibrium temperature. Expressing this observation more explicitly, the maximum temperature of the eutectic arrest was actually much lower than the forecast made by the model. For a 1.2-in. bar, the maximum temperature observed was 1145°C. The simulation for the same casting showed that it recalesced to the eutectic equilibrium temperature, 1153°C. The explanation for this phenomenon could well lie in the segregation of sulphur during freezing. Sulphur has been shown to segregate at the surface of the growing eutectic cells. Since it also adsorbs strongly on the graphite flakes, we would expect δT would increase strongly with the rejection of solute. This is brought out by the change in value of the pre-exponent with the change from low to medium sulphur content and by the more marked change upon increasing the sulphur content still further. The rejection of dissolved sulphur would cause a progressive change in the values of the constants in the growth law. Hence, a more complicated growth law is needed to provide a more precise model for the behavior of high sulphur content cast irons.

The eutectic nucleation law operated quite well. The eutectic nucleation was generally underestimated, particularly in the cases where a undercooling took place. This resulted from the reduction in volume of liquid as a consequence of primary austenite liberation. Since the number of centers initiating growth was based upon the product of the probability of a cell forming in unit volume of liquid and the volume of liquid, the final nucleation was underestimated when an appreciable fraction of the casting had solidified prior to the minimum arrest temperature. This error can be neglected, since it was much smaller than the experimental error of the original nucleation measurements.

The model was able to show all relevant features of casting solidification. Space does not permit a full discussion of all the data generated, but a sample of the computer output is given in Appendix D. This relates to the freezing of an 0.6-in., medium sulphur alloy bar. The listing shows the time in seconds after the temperature fell below 1170°C, the radius of the outer boundary of the annulus to which the data refers, the temperature at the center of the annulus, the number of cells cm^{-3} in the annulus, the volume of metal within the annulus, the fraction of the volume already solid as gamma austenite, the fraction solid including both austenite and eutectic and the surface area of the growing eutectic cells. Any other pertinent data could also be listed, including for example the eutectic growth rate and perhaps the predicted graphite dispersion.

CHAPTER VI: MODEL STUDY OF CASTING SOLIDIFICATION

1. Aims of the Study

In this dissertation, the object is to illustrate the application of the computer model, rather than to solve some particular casting problem. Therefore, an attempt will be made to illustrate some of the appeal which model methods should have in technology, where the systems are too complicated to be studied by conventional methods.

The first impetus towards model methods is given by economic considerations. The cost of experimental studies of casting solidification is very high. For example, the study of the effect of sulphur on cast iron which has formed the experimental basis for much of this work would cost more than $10,000 to repeat under present conditions. Because of the many interacting variables, the ability to predict in a meaningful way the solidification of castings under slightly different conditions is a valuable contribution. A computer model permits such an extension, allowing any particular combination of conditions to be simulated for about $35, a marked saving in time and money. Even more important, the simulation opens new avenues which are not amenable to experimental study in castings. Temperatures can be measured with some ease. However, the extent of solidification at various stations across a casting is much more difficult to study. Generally, quenching experiments are used in which freezing is stopped by rapid cooling. Liquid present at the time of the quench is precipitated as a fine iron carbide-austenite mixture, which can be readily distinguished from the graphite-austenite eutectic. The casting is then sectioned, and the volume of solid at the time of the quench is determined by tedious metallographic methods. Primary austenite precipitation is almost impossible to study. Except under the most favorable circumstances, quench studies are unsuccessful because of the slow rates of quench which can be attained in practice when compared to the rapid crystallization of austenite dendrites. Therefore, the use of a computer model which can be related to the real casting system through the time variation of some accessible property of the casting, such as its temperature, offers both economic and scientific advances. The model permits one experimental study to be extended throughout a host of practical variables: casting shape, rate of heat removal, nucleation, and carbon content to name a few of the many parameters. It permits the calculation of the progress of solidification and therefore the study of many features of the process which are not easily studied experimentally.

In the following two sections, studies of casting soundness and the graphite structure of cast irons will be used to illustrate these comments.

2. The Soundess of Cast Iron

Cast iron suffers very little volume change on freezing. Therefore, unsoundness would be expected only as a result of two types of situation. First, if a casting has a low carbon content and is improperly fed, the liberation of primary phase (austenite), which has a lower density than the liquid, can cause a net volume change and minor porosity. Secondly, and of much greater importance, is the expansion of the mold cavity under the pressure of liquid metal. Since the feeding of the casting from excess metal in a "header" above the main part of the casting is progressively impeded, mold expansion can cause large cavities in the casting. This becomes increasingly severe as the mold movement takes place at later stages of solidification. Mold movement becomes generally more severe with time after casting because the sand mold becomes hotter and moisture driven off from the sand near the casting surface accumulates as a weak, wet layer just behind the sand-metal interface.

Taking a simple view of the problem, the dispersion of solidification across the section of the casting can be considered as an index of its tendency to be unsound. When solidification is dispersed (taking place uniformly across the section), there is a considerable time lag after the metal has been poured before there is a solid shell of metal in contact with the mold. This is shown schematically in Figure 20a. By contrast, when solidification is progressive (Figure 20b) it takes place through the development of a shell at the mold surface which thickens progressively. Since the dilation of the mold wall can only take place while the metal is free to follow the mold, it ceases when a casting skin has formed. Therefore, the most obvious effect of dispersed solidification is that the formation of a rigid metal shell around the casting is delayed.

The computer model was used to study the pattern of solidification across the bar castings. The effects of eutectic growth rate (caused by changed sulphur content) was studied, together with its interaction with the degree of eutectic nucleation. Table 4 shows the time taken for the outer layers of the 1.6-in. bars of high and low sulphur content iron to become completely solid. Two nucleation levels are studied; the low level is the nucleation given by the constants in Table 2. The high level employs a nucleation constant of 200 in all cases, representing "innoculated" alloy, in which a late addition of a nucleating agent had been made just prior to casting.

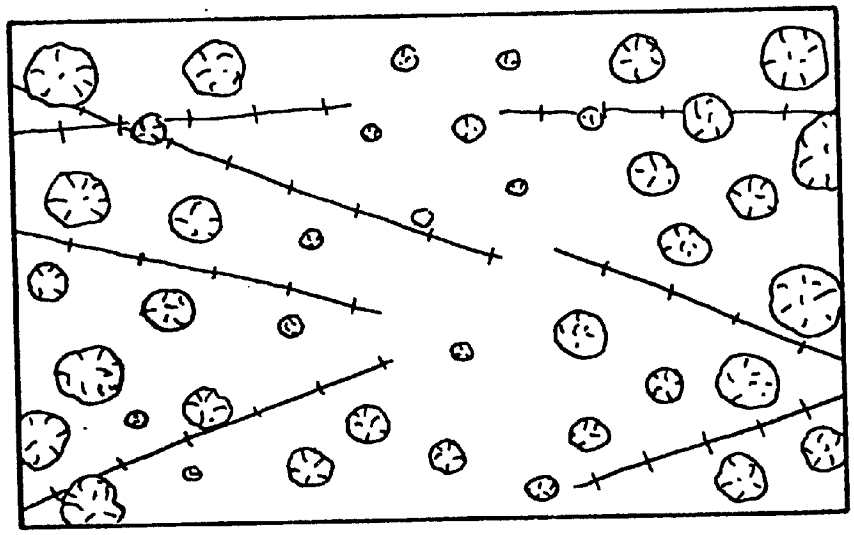

(a) DISPERSED

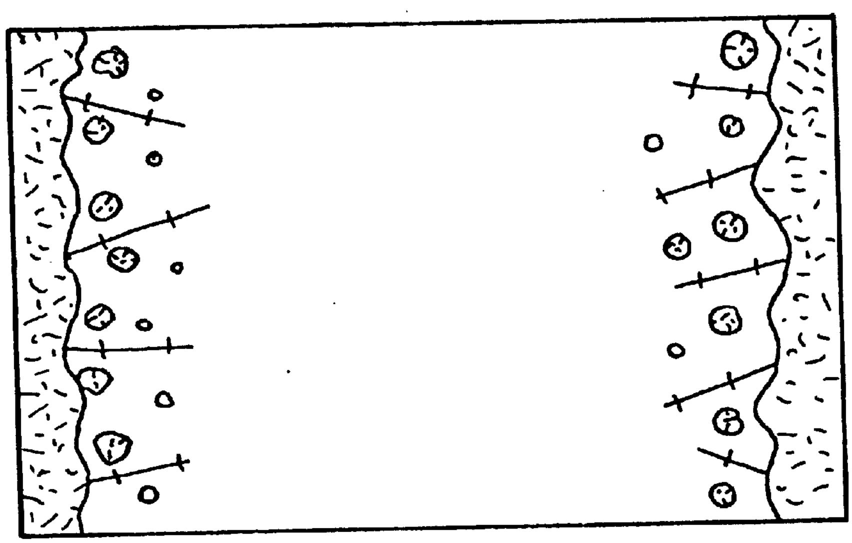

(b) PROGRESSIVE

FIGURE 20: DISPERSED AND PROGRESSIVE SOLIDIFICATION (SCHEMATIC)

TABLE 4. EFFECT OF NUCLEATION AND SULPHUR CONTENT ON THE TIME FOR THE OUTER LAYER OF THE CASTING TO BECOME SOLID

Nucleation Constant	Time to Form a Solid Skin (sec)	Alloy
0.91	163	Low Sulphur
200	92	
7.12	135	High Sulphur
200	100	

The results are in accord with the general trend which might be expected. When the kinetic factors are large, that is, growth and nucleation rates are high, eutectic solidification appears to be progressive. On the other hand, when kinetic factors severely impede solidification, eutectic solidification is dispersed. This result is in close agreement with experiment. Figures 21 and 22 show the computer results for the high sulphur alloy of low and high nucleation respectively. Each line on the graphs represents a station across the casting given by the inner and outer radii tabulated in Appendix D. With the low nucleation constant casting, the lines are bunched together, indicating that solidification is more dispersed than for the high nucleation constant casting (Figure 22), where the lines are spaced more widely. The same general observation can be made for the low sulphur alloy castings. The computer-drawn curves are shown in Figures 23 and 24, again for the high and low nucleation constant castings, respectively. The results show a close agreement with experiment. Figures 25 and 26 show similar curves drawn from the work of Merchant and Wallace(16). The same trend is apparent, the low nucleation constant casting having the curves much closer together than the high nucleation constant

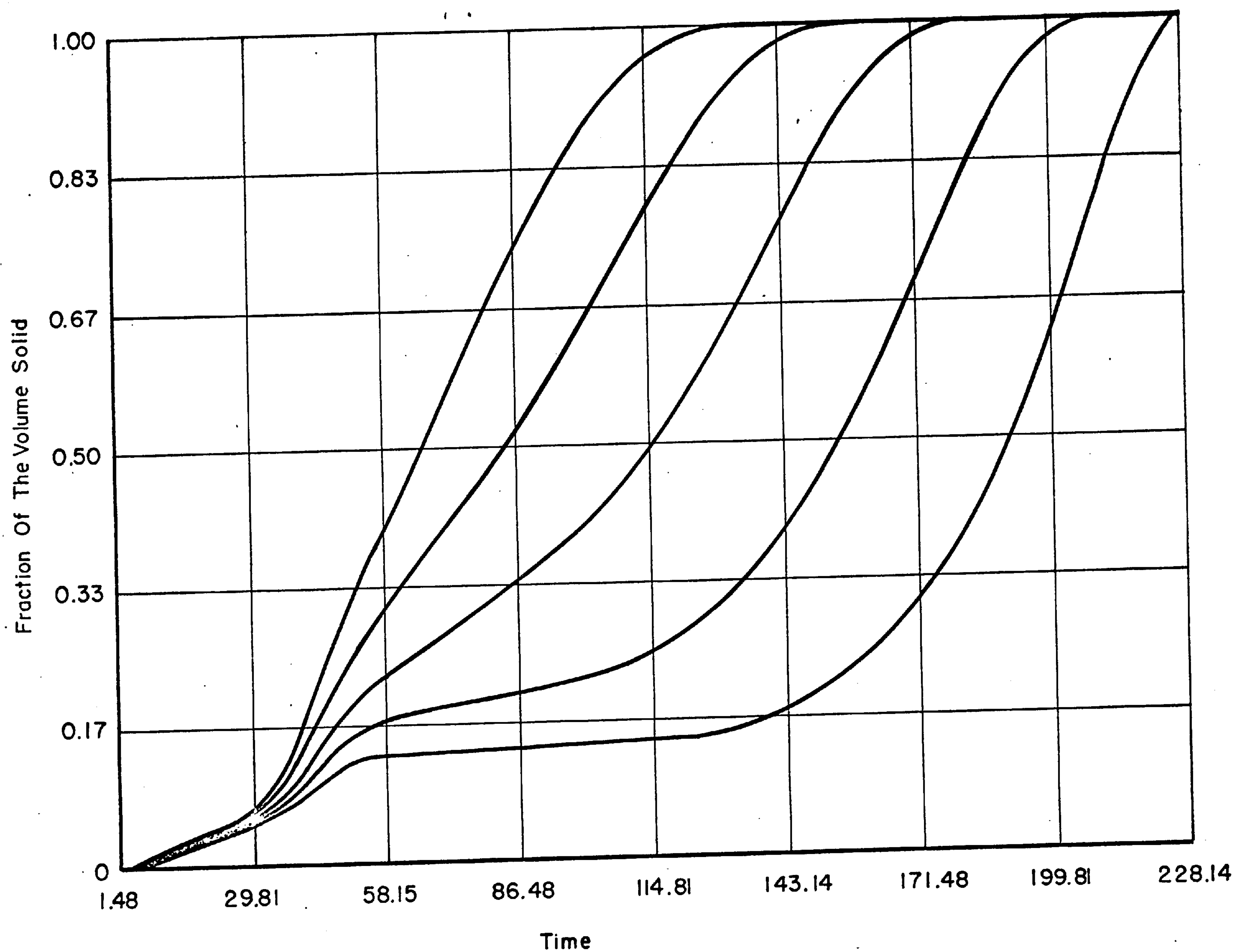

FIGURE 21 PROGRESS OF SOLIDIFICATION: HIGH SULPHUR ALLOY OF LOW NUCLEATION

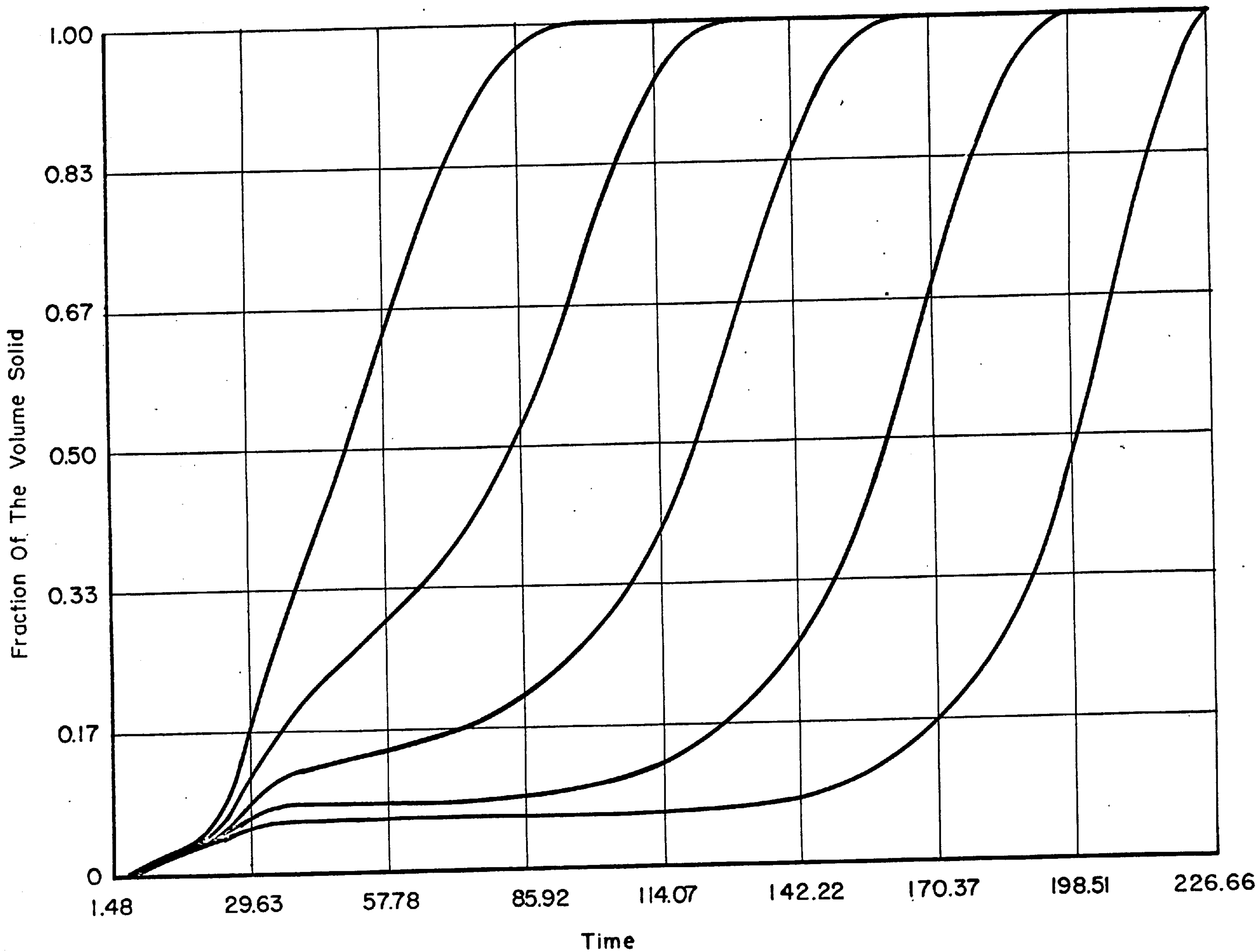

FIGURE 22 PROGRESS OF SOLIDIFICATION: HIGH SULPHUR ALLOY OF HIGH NUCLEATION

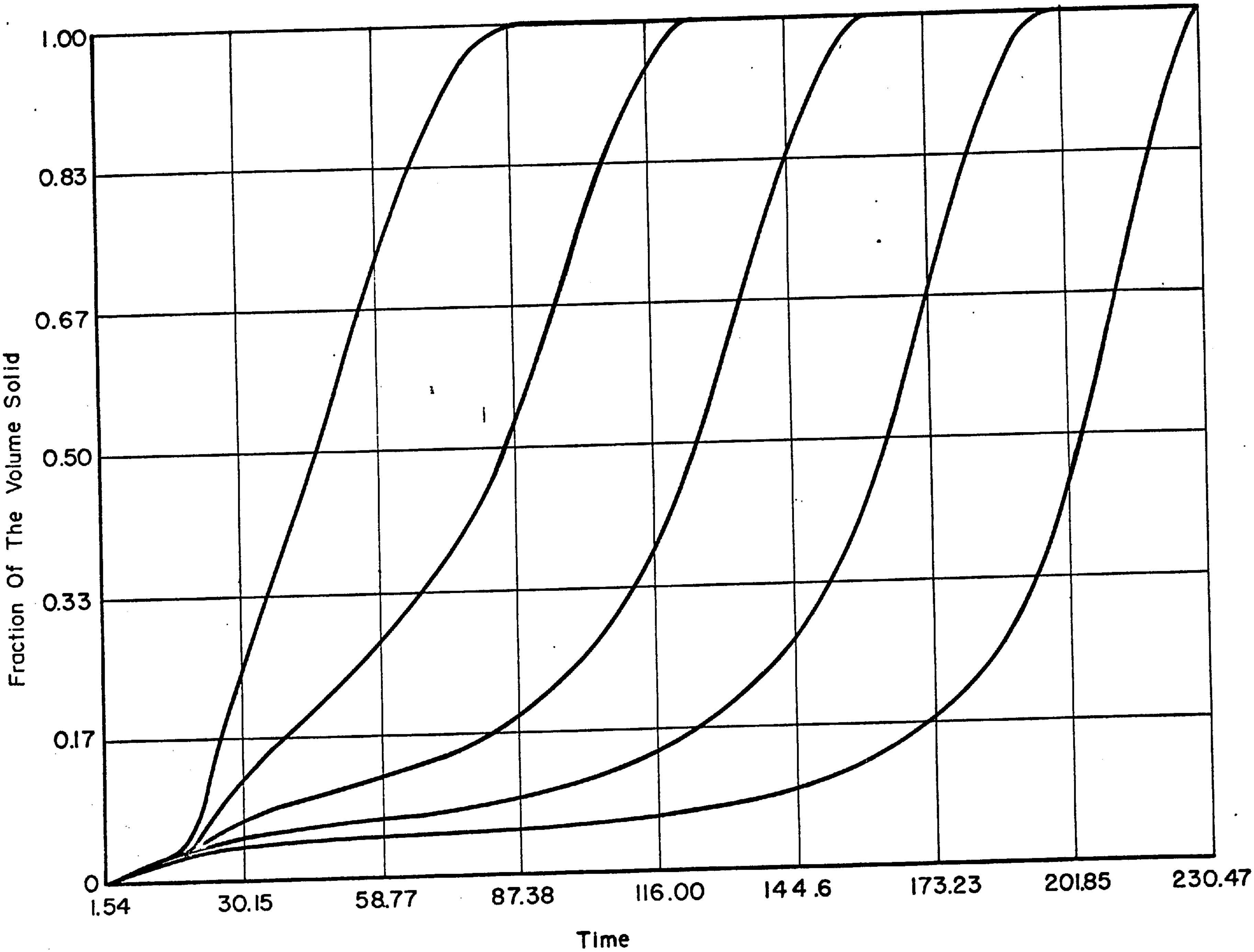

ALLOY OF HIGH NUCLEATION

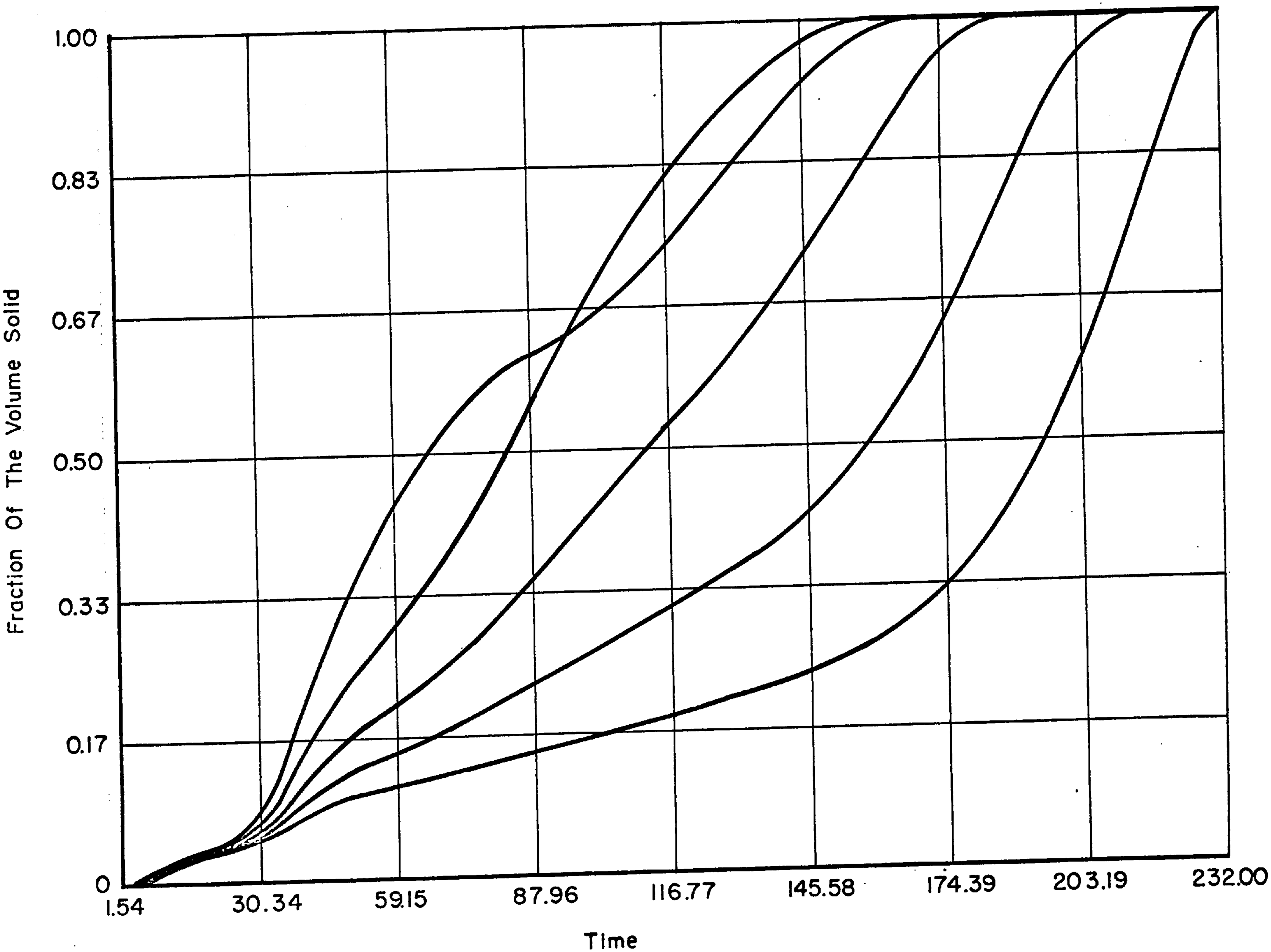

FIGURE 24. PROGRESS OF SOLIDIFICATION: HIGH SULPHUR ALLOY

FIGURE 25 MEASURED PROGRESS OF SOLIDIFICATION AT LOW NUCLEATION

(re-drawn from the data of Merchant and Wallace, 1961)

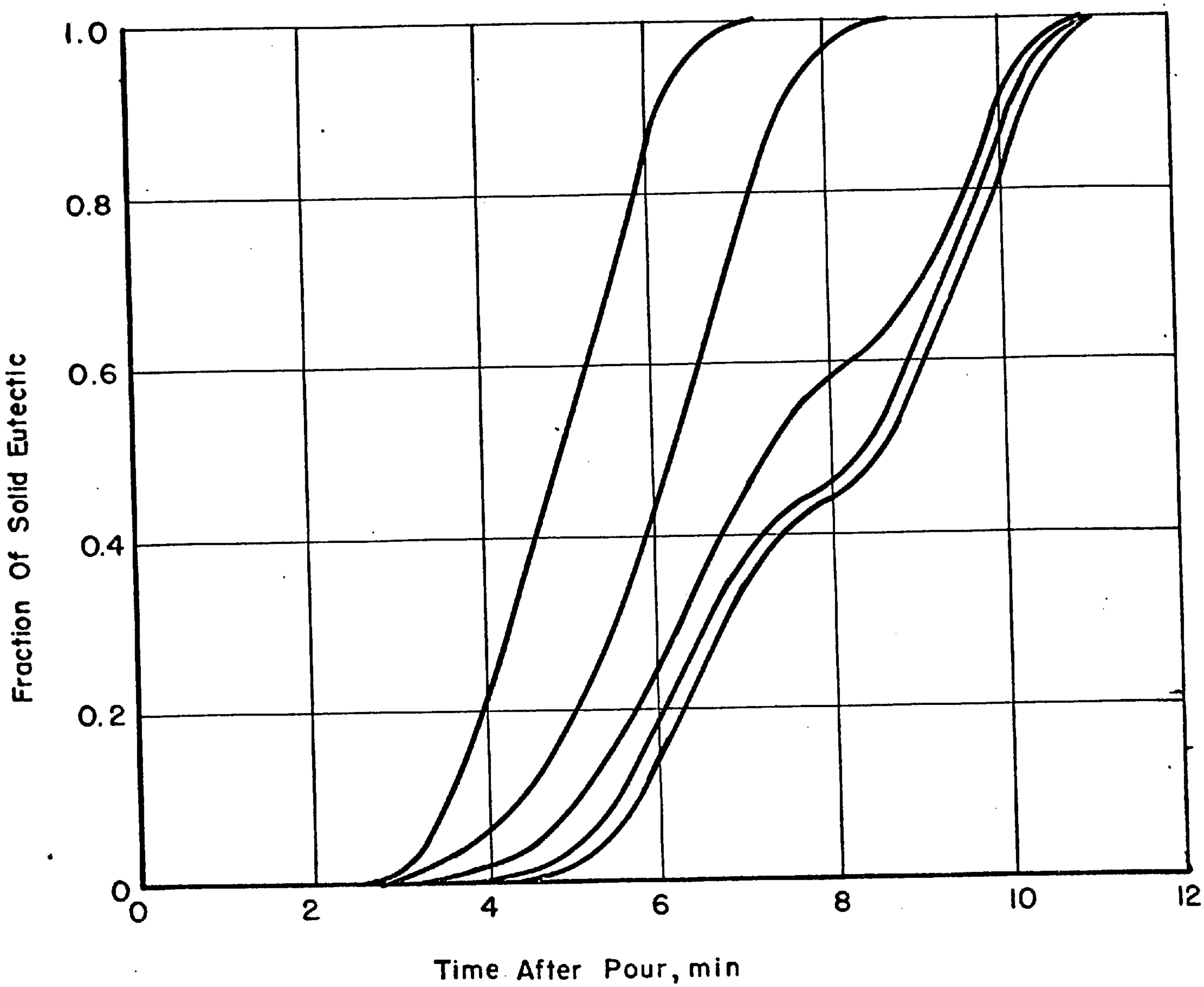

FIGURE 26 MEASURED PROGRESS OF SOLIDIFICATION AT HIGH NUCLEATION

(re-drawn from the data of Merchant and Wallace, 1961)

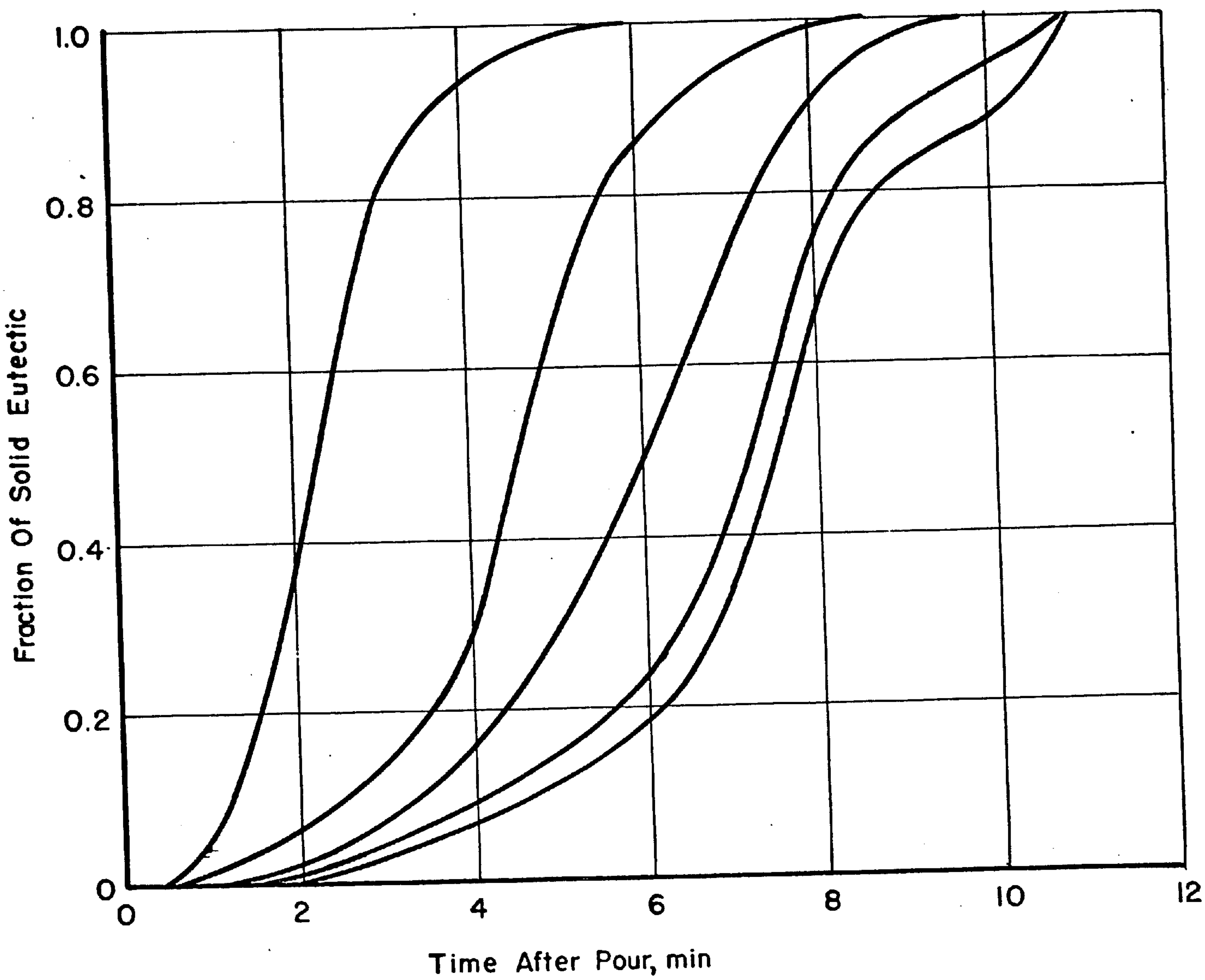

casting. This agreement occurs despite the wide disparity in casting size, suggesting that the effect is a general one. In fact, in research lasting for about 2 years, the effect of nucleation constant was determined to be a reduction in the soundness. This effect was found to be quite general.[17,18,19]

From our review of the soundness phenomenon, this seems to be a trifle strange. In the earlier discussion, it was concluded that the earlier development of a casting skin should be promoted by less dispersed freezing and that this should in turn increase soundness. The computer and experimental results seem to conflict with this view. Additional conflict is provided by the unpublished work of Oldfield, and the experiments of Merchant and Wallace[16]. For the same castings for which Figures 25 and 26 were produced, they found that a casting skin formed earlier for the low nucleation constant alloys. Oldfield showed the same result by a "slush casting" method, in which the molten metal is poured from partially solid castings.

The apparent conflict can be resolved by again considering the effect of primary phase solidification. At an early stage of development, eutectic cells are small, separate spheres. Thus, eutectic solidification confers no mechanical strength to the casting until solidification is well advanced. Such eutectic solid would be flushed in a slush casting experiment, and would play no part in preventing mold wall movement. The role of primary austenite in linking the eutectic cells has already been described (Chapter V). If we consider the effect of austenite solidification, we find surprising differences between the castings of high and low nucleation. Figures 27 and 28 show the fraction of the outer layer of the

FIGURE 27 EFFECT OF NUCLEATION ON THE AUSTENITE SOLIDIFICATION AT THE EDGE OF A BAR; LOW SULPHUR ALLOY

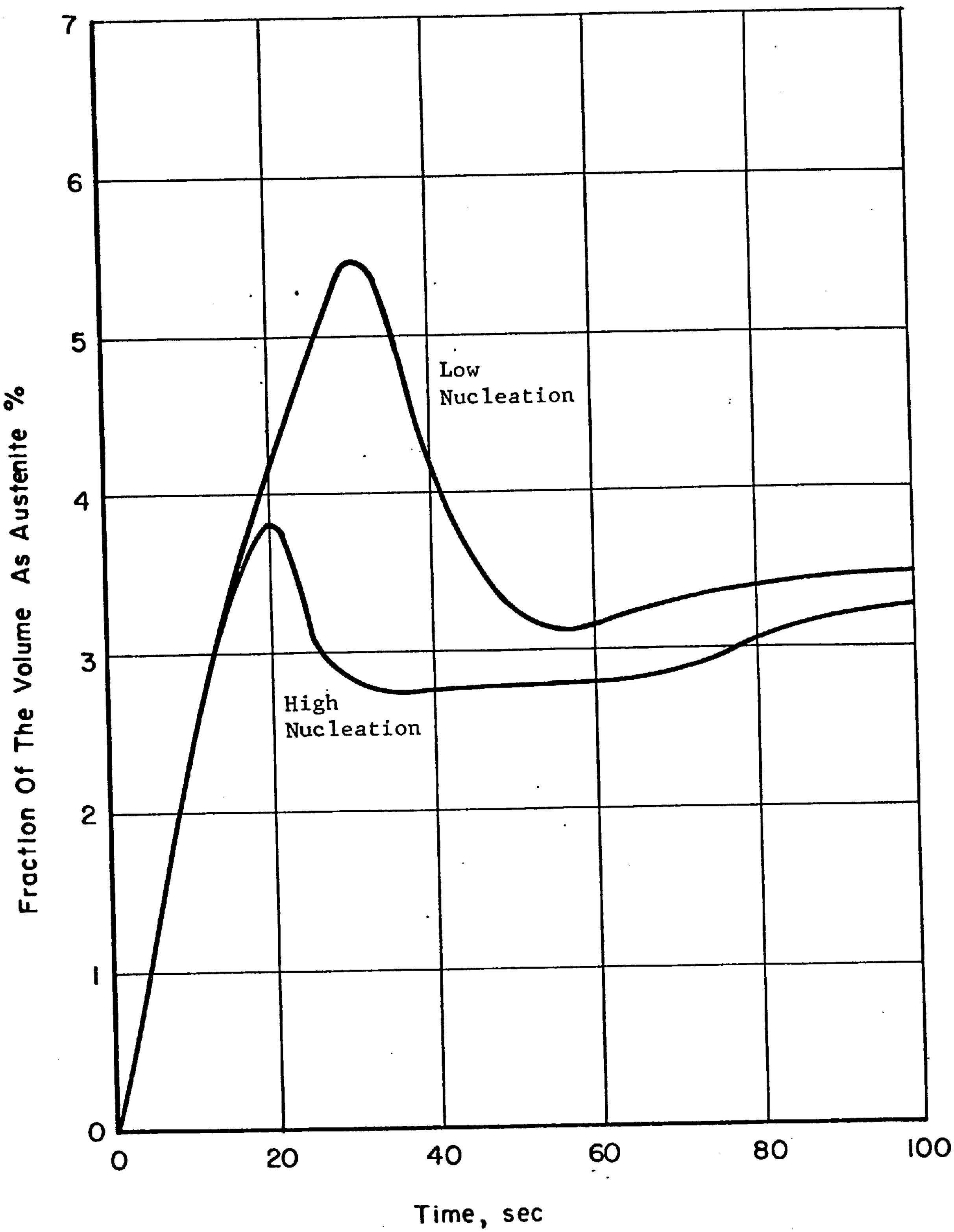

FIGURE 28 THE EFFECT OF NUCLEATION ON THE AUSTENITE SOLIDIFICATION AT THE EDGE OF A BAR; HIGH SULPHUR ALLOY

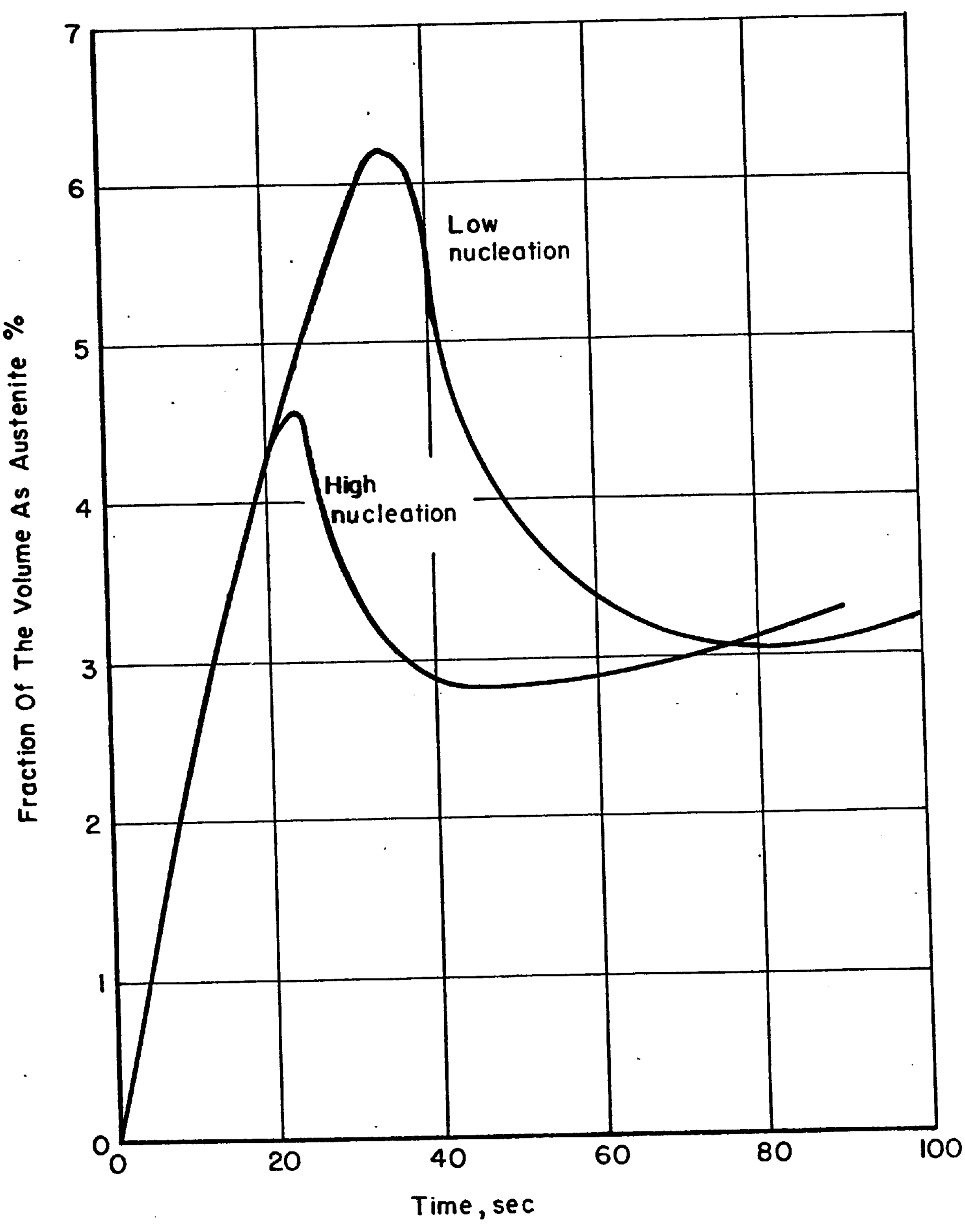

1.6-in. bar casting which has formed austenite plotted as a function of time. Each graph shows the curves for the high and low nucleation bars of a single composition. Figure 27 shows the low sulphur alloy, and Figure 28 the high sulphur. The results show marked differences in the amount of primary phase formed with time, showing that the precipitation is more pronounced for the poorly nucleated material. It is therefore suggested that this is the cause of the difference in soundness. Certainly, the result suggests further experiments are needed to clarify this phenomenon.

3. Flake Graphite Structure

The variation in flake graphite structure which is found in commercial cast iron has been a source of interest to researchers in the area for many years. Fine graphite has long been associated with large amounts of undercooling, and this formed the basis for the original nomenclature. Fine graphite was termed "undercooled" graphite. Morrogh pointed out that the graphite structure might be related to the rate of eutectic growth.[20] This is in accord with the more recent understanding of eutectic growth, in which the interlaminar spacing, λ, relates directly with the growth velocity:[10][21,22]

$$\lambda = \frac{1.0}{\sqrt{(\text{velocity})}} \times (\text{constant term}) \quad . \tag{6.1}$$

The effect of certain elements which are commonly found in cast iron formed an impediment to this simple view of cast iron solidification. Sulphur had been found to coarsen the graphite structure, together with hydrogen.[23,24] Titanium, cerium, and magnesium additions refined the structure. On the basis of cooling curve data, Oldfield[25] showed that sulphur and hydrogen slowed the rate of eutectic growth, but the arguments which were used were qualitative only. The computer model allows the cooling curve data to be interpreted in a quantitative manner.

The model calculation was arranged to plot the variation of λ with time for low and high sulphur content alloys. The calculation underestimated λ for the later stages of solidification of the high sulphur alloys, as was discussed earlier. This portion of the plot is drawn as a dotted line. The result is shown in Figure 29. The curves illustrate the effect of sulphur on flake size. The flake separation, λ is increased by more than an order of magnitude by the addition of sulphur. The curves also illustrate the so-called "rosette" structure, in which the flake separation is small at the center of the cells, then coarse, and fine at the periphery. This phenomenon is shown clearly by the high sulphur-content cast-iron model.

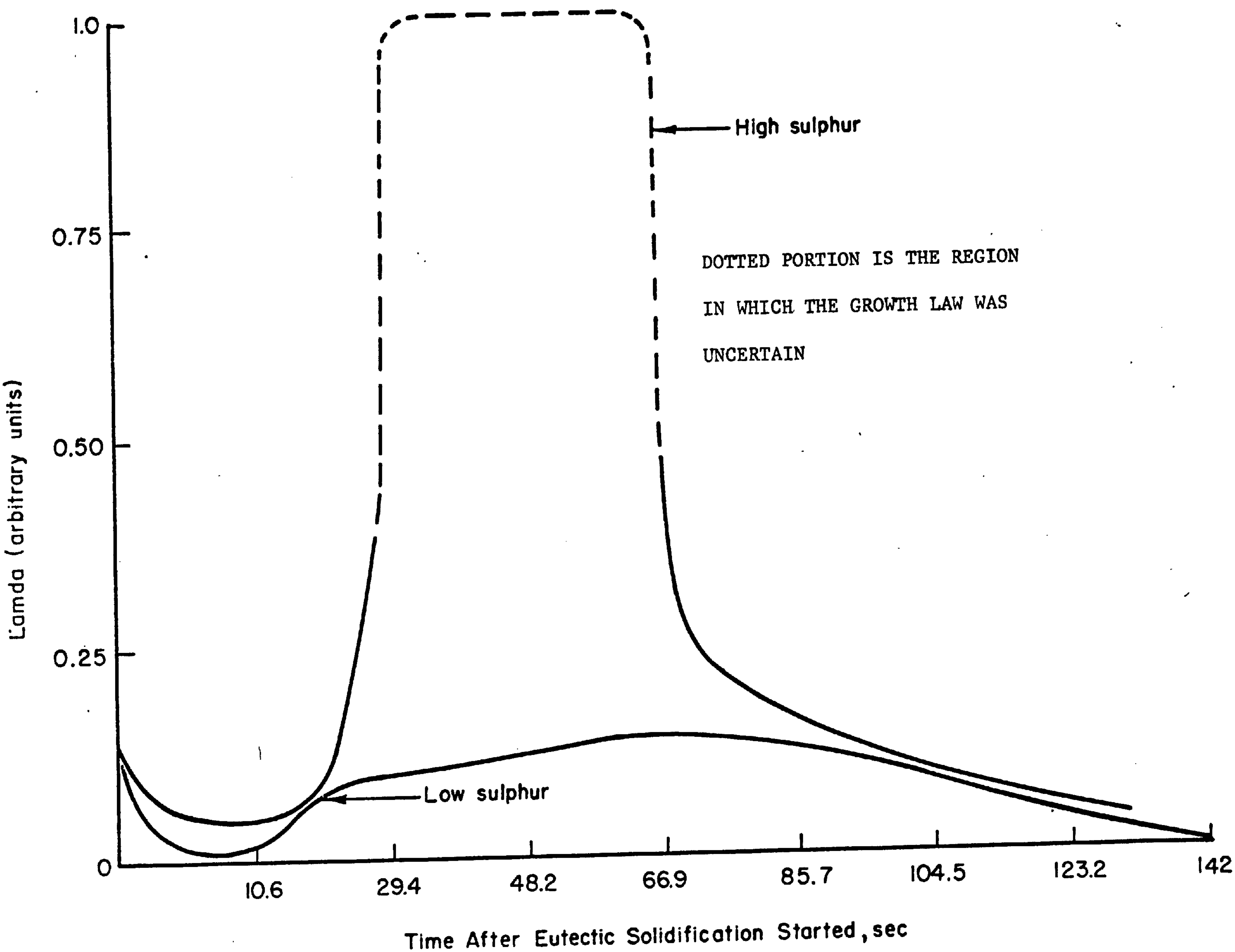

FIGURE 29 THE VARIATION OF FLAKE GRAPHITE SIZE WITH TIME; COMPARISON OF HIGH AND LOW SULPHUR ALLOYS

SECTION C

A STUDY OF DENDRITE GROWTH BY MEANS OF A COMPUTER MODEL

CHAPTER VII: DENDRITE GROWTH

1. A Description of a Growing Dendrite

Dendrites are a familiar crystal form which can be observed in such diverse circumstances as metallographic specimens taken from castings, within plastics, or in snowflakes. A dendrite can be described as an assembly of branched rods or needles. The crystal can be considered to originate from a single stem, which forms side-branches, which themselves act as stems from which further branches arise. It has become conventional to idealize the crystal shape and consider one single needle to be characteristic of the whole crystal. The characteristic features of dendrite growth are then seen to be even more common than a more casual classification of crystalline morphology would suggest. The same basic growth process is found, for example, in spherulitic growth (as in polymer crystallization[26])and in whisker growth.

The feature common to all these growth situations is that the growth of the crystal surface is substantially hindered by the accumulation of heat or matter at the freezing interface. Furthermore, the growing crystal has developed a needlelike shape which penetrates and leaves behind the accumulation of growth products. An analogy can be made with the passage of a ship through water. The bow always sees the clear water with a minimal thickness of disturbed water at the stem, but an increasing width of disturbed water surrounds the ship as one moves towards the stern. In the same way, the tip of a growing dendrite has tightly-wrapped heat and solute fields. The fields widen towards the root, and consequently the solute and heat gradients are reduced. There is an important flaw in this analogy, which must be considered if a deeper insight into the growth process is to be obtained. Whereas a ship has a rigid envelope, a growing crystal must be considered to have a variable shape, which can change freely to accommodate any change in its environment. In fact, a dendrite's shape will be seen to be in a constant state of transition during growth.

2. The Study of Dendrite Growth

When a liquid transforms to a solid, latent heat is given off at the liquid/solid interface and must be carried away if solidification is to continue. If the liquid is multicomponent and the solubility of some of the components differs between liquid and solid, diffusion must occur as an analogue to heat removal. The solid which forms may have curved surfaces and may contain defects and consequently have a melting point which differs from that of an annealed crystal with a planar surface. Since solidification is a nonequilibrium process, a free energy driving force for atomic or molecular attachment is also necessary. All four of these requirements (a) heat flow, (b) solute flow, (c) melting point changes due to the formation of solid with a large surface curvature or defect structure and (d) kinetic driving force at the interface must be met simultaneously[27] and they may interact. A moving solid/liquid interface and its heat and solute field is illustrated in Figure 30.

Each one of the four requirements can be assigned a driving force in terms of a temperature difference, since $\Delta T = \Delta G/\Delta S$, where ΔG is the free energy change for the particular process and ΔS is the entropy change. The sum of these forces must equal the total driving force, which is related to the amount of supercooling of the liquid with respect to the

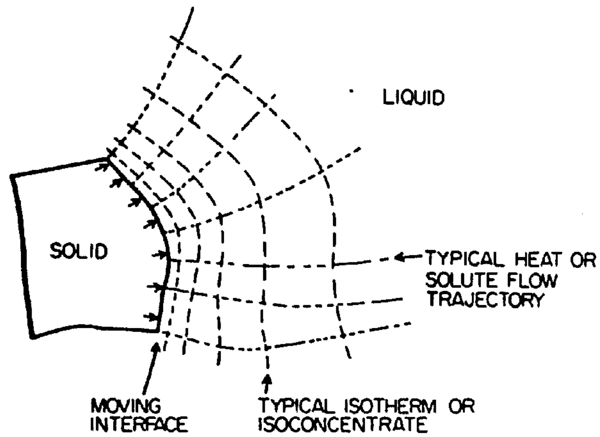

FIGURE 30. HEAT FLOW AT A MOVING SOLID/LIQUID INTERFACE

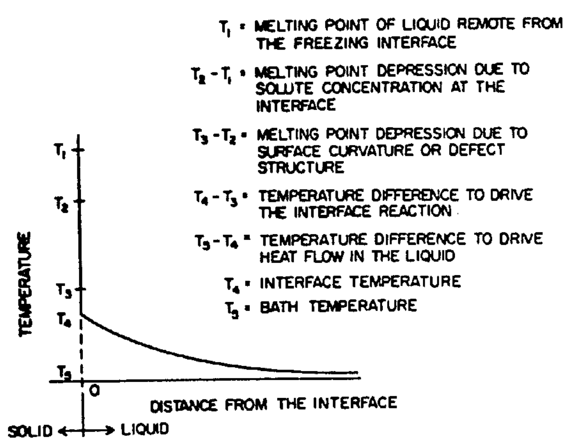

FIGURE 31. GRAPHICAL REPRESENTATION OF THE COUPLING EQUATION

the melting point of the solution.[27] In analytical work, this summation becomes a coupling equation. The driving forces are indicated relative to the temperature field ahead of the interface in Figure 31.

Most of our knowledge of dendrite growth has been obtained experimentally. Dendrites have been studied in transparent systems[28], growing from the vapor phase[29], growing upon the surface of liquid metals[30], and other freezing systems. Because of the basic unity between so many crystal forms, there is an urgent need to understand the underlying principles. To gain such an understanding, theoretical models of the growing dendrite have been constructed. Such models are greatly simplified approximations to an observed crystal. In general, a dendrite has been assumed to have attained a steady state and to conform to some geometric shape such as a parabola of revolution.

One of the earliest treatments was that of Ivantsov[31]. In this treatment the model for dendrite growth was chosen to be a single stalk of solid in the form of a paraboloid of revolution, with growth controlled solely by the transport of heat away from the growing crystal surface. The crystal was shown to maintain its shape during growth; the axial component of growth velocity was uniform over the whole crystal surface. The growth velocity was calculated as:

$$V = \frac{2\alpha\Omega}{\rho} \quad , \tag{7.1}$$

where

V = axial growth velocity

α = thermal diffusivity

Ω = a constant depending upon bath supercooling and the thermal properties of solid and liquid

ρ = radius of curvature of the dendrite tip.

Ivantsov's model for a dendrite is not very realistic because it suggests that any tip shape could exist in a given situation, and therefore a range of dendrite velocities might be observed. In nature, very fine crystals are penalized by surface energy effects. The equilibrium melting temperature of a curved surface is reduced (Gibbs-Thompson effect).

$$\delta T = \frac{\gamma T_m}{Hd}\left(\frac{1}{R_1} + \frac{1}{R_2}\right) \quad . \tag{7.2}$$

where

δT = depression of melting temperature due to capillarity

γ = interfacial surface energy between solid and liquid

T_m = equilibrium melting temperature of the solid

H = enthalpy of fusion

d = density of the solid, and

R_1 and R_2 are the radii of curvature of the surface in two directions at right angles.

Temkin[32] developed a new treatment which included not only the transport of heat in the liquid but also curvature effects. To enable comparison with the experiment, he included an attachment law to account for the driving force required to cause an atom to attach to the surface. Heat flow in the crystal was also taken into account. By suitable choice of γ (about 80% of the value reported by Turnbull[33]), he was able to calculate the tip radius and growth velocity of that crystal which would grow at the fastest rate in a given environment. His calculated growth velocities were in close agreement with those which had been determined experimentally.

3. The Need for a Model Study

There are a number of objections to the treatments of Ivantsov, Temkin, and others[34]. The calculations are very complex and it is difficult to incorporate many interesting features of dendrite growth such as anisotropic attachment processes. Similarly, because of the extreme mathematical complexity, it is not possible to study crystals of general shape. Furthermore, it has proved impossible to follow the development of the crystal shape in a time-dependent manner. The closest approach to a time-dependent study has been through first-order perturbation analysis.[35]

Model methods employing computers are in principle ideally suited to the treatment of this type of problem. The growth processes can be broken down into a number of distinct components, each of which can be properly treated. Then, after a model has been prepared, it can be developed to include additional complexities as desired.

CHAPTER VIII: A GENERAL TREATMENT OF HEAT TRANSFER BY NUMERICAL TRANSFORMATION OF COORDINATES

1. The Simulation of Dendrite Growth

Model methods are potentially capable of showing the time-dependent growth of dendrites and allow the study of needle arrays, an isotropic crystal growth and the inclusion of surface kinetic factors in the growth calculation. In this work, an attempt has been made to demonstrate that a model for dendrite growth is feasible and that it can, in fact, perform the above-mentioned tasks. The model has not been fully developed; the computer costs prohibit such a complete work. However, the relatively simple study which has been made is believed to contribute a great deal to the understanding of dendrite growth and to indicate the paths that future studies will take.

The basis for the method was similar to that of the casting study. Calculations of surface growth were made for a sequence of time-intervals and the full sequence of time intervals modelled the growth in a similar manner to the way a movie film takes a pictorial model of a changing scene. Within each time-interval, certain assumptions were made concerning the change of the parameters. In the first portion of this work, it was assumed that the surface positions, and the form of the thermal field, remained unchanged during the time pulse. In later calculations, the changes were assumed to take place smoothly during the time interval. It was clear at the outset that a conventional numerical treatment of the problem would be an immense task. Considering only heat flow subject to the complicated surface boundary conditions, the heat transfer problem would have been very difficult to solve when the thermal field and the crystal shape diverged appreciably from a form which could be described by a simple mathematical expression. The model of the crystal could not impose any shape constraints, so that some other, more tractable, approach was sought.

2. One-Dimensional Heat Transfer

The examples of Chapter II, and the subsequent study of casting solidification, employed the idea of one-dimensional heat transfer in simple situations. The flow problem described in Chapter II was concerned with an "infinite" plate. In the context of the problem, this meant that the isotherms were parallel to the two surfaces of the plate. Hence, no heat flowed out of the sides of the compartments and it was possible to write conservation equations for each compartment. The models of Chapter III and the subsequent chapters included a treatment of radial heat flow in a cylinder. The cylinder was assumed to be "infinitely" long, so that again conservation equations could be derived, because no heat was lost through the sides or ends of compartments. Clearly, the general requirement is that side-closures must be orthogonal to the isotherms. For a model calculation, the compartments must be formed by the isotherms (the surfaces across which heat flows) and the orthogonal projection to the isotherms (the side-closures across which no heat flows). Any heat flow situation can be represented by a set of one-dimensional flow models. A single set of compartments for a one-dimensional calculation is defined by a grouping of orthogonal surfaces. Such a grouping is shown in Figure 32. Within each channel produced by the surfaces orthogonal to the isotherms, a set of

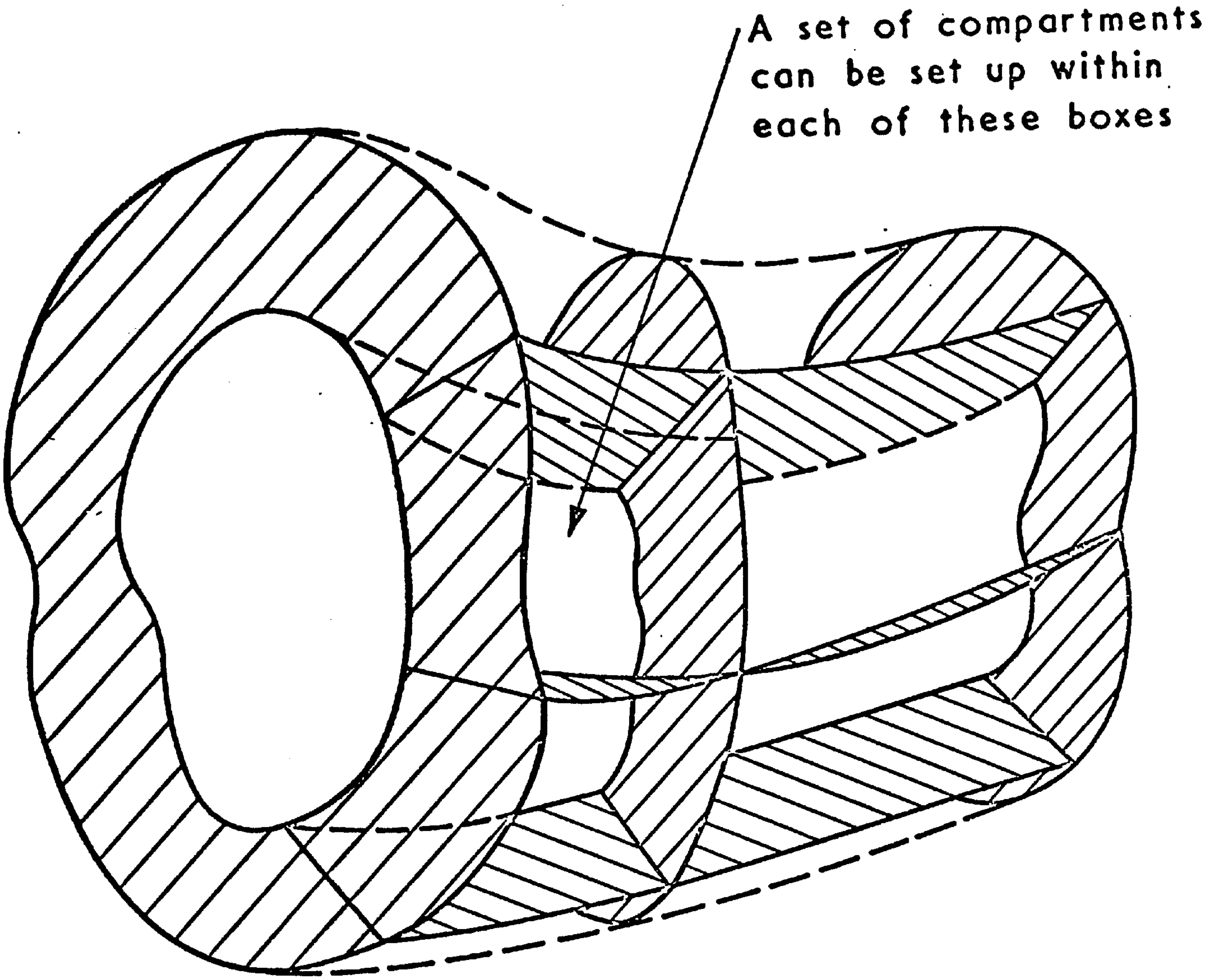

Figure 32. Subdivision of Space
Into One-Dimensional
Flow Channels

compartments is formed in a similar manner to those formed in the preceding chapters. For the complete solution of the three-dimensional heat transfer problem, the one-dimensional flow channels must fit together, so that the sum of the solutions for the individual channels is the solution for the entire field. This technique resembles the conventional approach to these problems in which the coordinates are transformed. Such a transformation relies upon a comprehensive relationship between temperature and position and upon the existence of a tractable mathematical formalism. In the model approach, a numerical transformation has been developed which does not require a more general relationship between temperature and position.

3. Model Calculation

The model was designed to simulate the most simple growth situation which could still be termed dendritic. A crystal was imagined to be growing from a pure melt (only heat flow involved), with no heat flow down the solid crystal and with rotational symmetry.

A flow chart for the calculation is shown in Figure 33. The first step in the sequence is the development of the initial conditions. This involves the definition of the thermal field and dendrite shape and subdivision of space into one-dimensional flow channels. Heat flow and dendrite growth calculations can now commence. Heat flow for each channel is considered in turn; the amount of heat flow which takes place determines the surface growth at the base of the channel. When the whole set of channels has been treated, the network points no longer represent an orthogonal network of flow-lines and isotherms, but instead we have a series of points which define the temperature at the position of the point. The

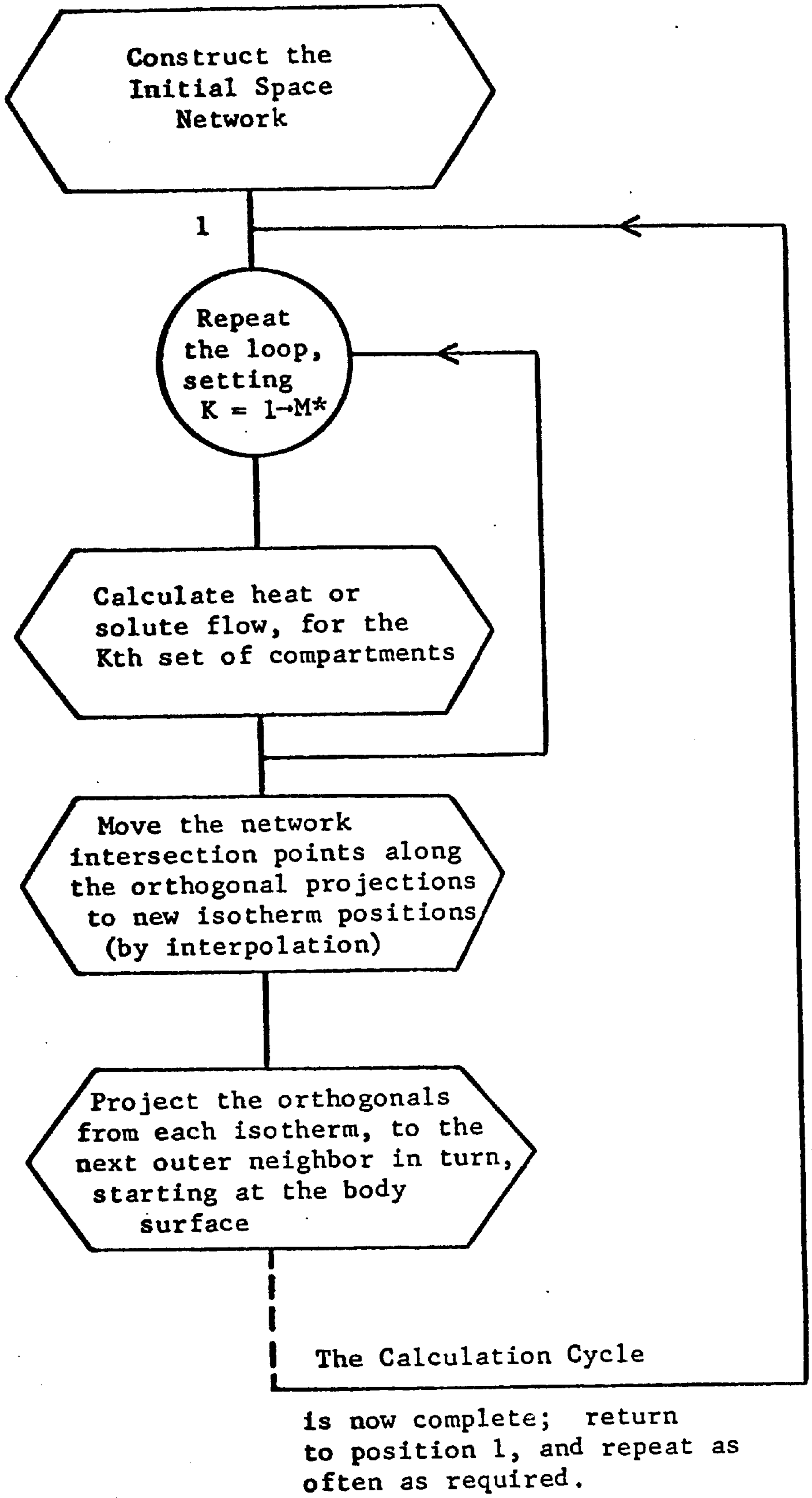

*No. of orthogonals

FIGURE 33. FLOW CHART FOR SIMULATION OF DENDRITE GROWTH

positions of the points are now changed in two stages, to provide a new orthogonal network ready for a fresh calculation. First, new points which lie upon the isotherms are found by interpolation. Secondly, projections are made from the dendrite surface, through the isotherms defined by the new points, to give a new orthogonal network. At this stage, the crystal shape and the thermal field have changed slightly from the initial condition and the network is ready for a new calculation (representing an additional advance in time). The sequence can be repeated as often as needed, giving the time-dependent development of the crystal shape and the thermal field.

4. Initial Conditions

At the start of the calculation, an initial set of points is required to describe the crystal shape and the initial thermal field. A modification of Ivantsov's result[31] was used because of its convenient form. Ivantsov showed that an isothermal crystal and the surrounding isotherms could be described by a family of confocal paraboloids. The focal length of the parabola are fixed conveniently by the temperature profile along the crystal axis. The Ivantsov result was modified to fit a non-isothermal crystal. The axial temperature profile was based upon the correct tip temperature (depressed below the equilibrium melting point because of its curvature). This moved the isothermal parabolic surfaces closer to the crystal surface than they would have been if the temperature profile had been based upon the equilibrium melting temperature as it was in the Ivantsov result.

The tip temperature profile follows the E1 function.[36]

$$T(F) = T_\infty + (T_t - T_\infty)\,\frac{E1(\frac{\Omega F}{F_o})}{E1(\Omega)} \quad , \tag{8.1}$$

where F is the focal length of the isothermal parabolic surface, F_o is that of the crystal surface, T_t is the tip temperature, and T_∞ that of the liquid bath remote from the crystal surface. The parameter Ω which has already been mentioned in an earlier section relates to the thermal diffusivity of the liquid, α, the crystal tip radius, ρ, and the growth velocity V:

$$\Omega = \frac{V\rho}{2\alpha} \quad . \tag{8.2}$$

This is not a convenient relationship, because V is not known. An alternative form is:

$$(T_{eq} - T_\infty)\ Cp_1/L = \Omega \exp(\Omega)\ E1(\Omega) \quad . \tag{8.3}$$

Equations (8.3) and (8.1) were solved by iterative methods based upon Newton's method.[38] A set of F values was found, describing the family of isothermal parabolae.

The positions of the orthogonal lines on the crystal surface was set arbitrarily. Two considerations were used to determine the origin of these surfaces. The isotherms have their greatest curvature near the dendrite tip, so that the one-dimensional approximation requires that the heat flow channels are narrow. Farther from the tip, the curvature is less and the orthogonal surfaces can be more widely spaced. On the other hand, the orthogonals were represented by straight lines (viewing the body of revolution in a two-dimensional section) between the isotherms. This approximation required that "compartments" formed by orthogonals and isotherms had to be wide and thin, that is, with smaller isotherm spacing than orthogonal spacing. A ratio which was found convenient was 5:1 for the compartment adjacent to the crystal surface. Using this criterion to fix the position of the first isotherm relative to the crystal tip and fixing the length of crystal to be studied and the number of orthogonals to be used, the remaining portions were uniformly spaced along the crystal as follows:

$$Z(1,k) = Z(1,2) - \delta\,(k-2)^{p} \quad , \tag{8.4}$$

where k is the index of the orthogonal (see Figure 35) taking the index of the axis as 2,

$$\delta = 5\left\{Z(2,2) - Z(1,2)\right\} \quad , \tag{8.5}$$

(the first of the two indices represents the isotherm. The index 1 represents the crystal surface, 2 the nearest isotherm, and so on).

$$p = \frac{\ln z(1,2) - \ln \delta}{\ln(N_o - 2)} \quad , \tag{8.6}$$

where N_o is the total number of orthogonals. The X ordinates followed from the equation for the crystal surface:

$$X(1,k) = F_o\left[1.0 - \frac{\left\{Z(1,k)\right\} - Z_o}{F_o}\right]^{1/2} \quad , \tag{8.7}$$

where Z_o is the Z ordinate of the focal point of the crystal.

The intersections between the orthogonal lines and the isothermal parabolae were found by a shooting method, starting from the points just found on the crystal surface. The intersection point was calculated for a line projected at right angles from the parabola representing the crystal surface, with the parabola of known focal length and focal point representing the adjacent isotherm. The normal to the isotherm was then found:

$$T2 = -\frac{1}{\frac{dz}{dx}} \quad , \tag{8.8}$$

where T2 is the slope of the normal, and $\frac{dz}{dx}$ is the slope of the isotherm at the point of intersection. T2 was taken as a good approximation to the gradient of the orthogonal at the correct intersection position, whereas T1 (the slope of the projection from the crystal) was the gradient of the orthogonal at the surface. The difference between the two gradients represents the curvature of the orthogonal, which is to be represented by a straight line. A new projection was therefore taken at the mean angle of the two intersections. The tangent, Tm is given by:

$$Tm = \left\{T1 + \frac{(T2 - T1)}{2(1+T1.T2)}\right\} \Big/ \left\{1 - \frac{T1(T2 - T1)}{2(1+T1.T2)}\right\} \quad . \tag{8.9}$$

The intersection of the new projection and the isotherm was taken as the network point. This formed the basis for a projection to the next isotherm, and the process was carried out through the whole set of parabolae and for each orthogonal.

Having formed a network of points representing the orthogonal system, a distance vector R(j,k) was calculated. This was the separation of the point on the jth. isotherm and the kth. orthogonal line from the point on the same orthogonal and the (j-1)th isotherm. Each network point could then be defined in the new coordinate system by a k-index represeseNting the orthogonal line, and a distance vector R(j,k).

5. One-Dimensional Flow Channels

Consider Figure 34 which shows a set of compartments produced by the intersection of isothermal surfaces and orthogonal trajectories. The

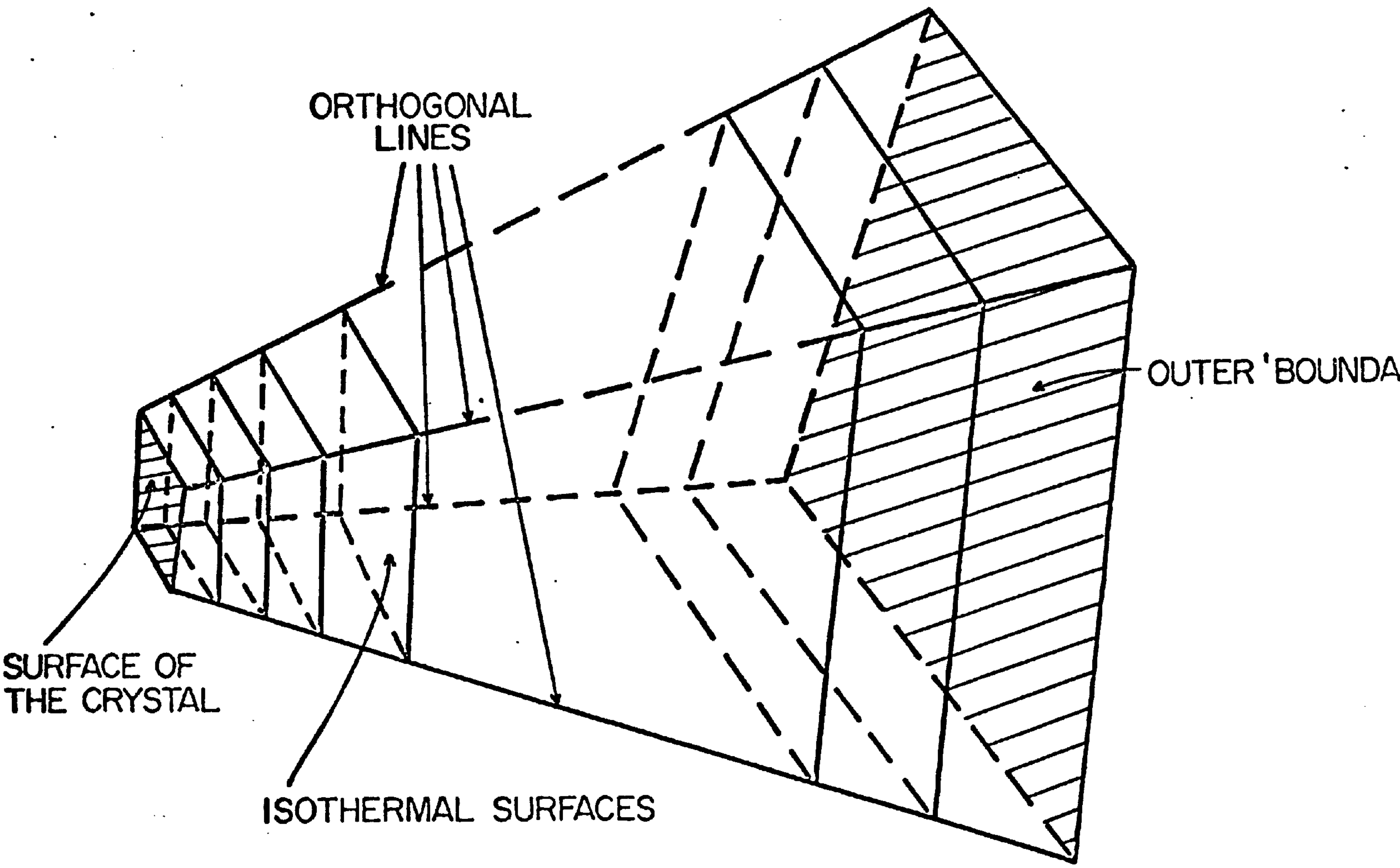

FIGURE 34. COMPARTMENTATION OF SPACE FOR ONE-DIMENSIONAL FLOW

coordinates of the points of intersection of the surfaces are stored in the computer memory. Within this set of compartments, all heat flow takes place across the isothermal planes. There is no flow through the side walls of the compartments since they are orthogonal surfaces. Therefore, heat conservation in any particular compartment in the set is dependent only upon the heat flow through the two isothermal walls. Terming the intersections of two orthogonal planes an orthogonal line, the corners of the compartments have been indexed. That is, a particular corner of a compartment would refer to the J^{th} isothermal plane and the K^{th} orthogonal line. In the present study, a body of rotational symmetry was considered, so that only one orthogonal plane is used. This is illustrated in Figure 35.

Such a set of compartments has been found inconvenient for calculation purposes. An equivalent set of boundaries can be constructed around each orthogonal trajectory. The boundaries are the surfaces midway between adjacent orthogonal surfaces and midway between isothermal surfaces. A section through the center of a set of compartments is shown in Figure 36a. This figure shows that each network point stored in the computer memory lies at the center of a compartment. A curvilinear coordinate R is defined as the distance along an orthogonal line from the liquid/solid interface to the point in question. Figure 36b illustrates the temperature distribution along this R coordinate and the arrangement of three typical compartments; those at the inner and outer boundaries, and the intermediate ones.

Let us evaluate the temperature changes in these compartments as in the previous sections, when heat is allowed to flow according to Fourier's Law for a time interval δt. We shall use c.g.s. units and the same definitions of the compartments and their physical properties.

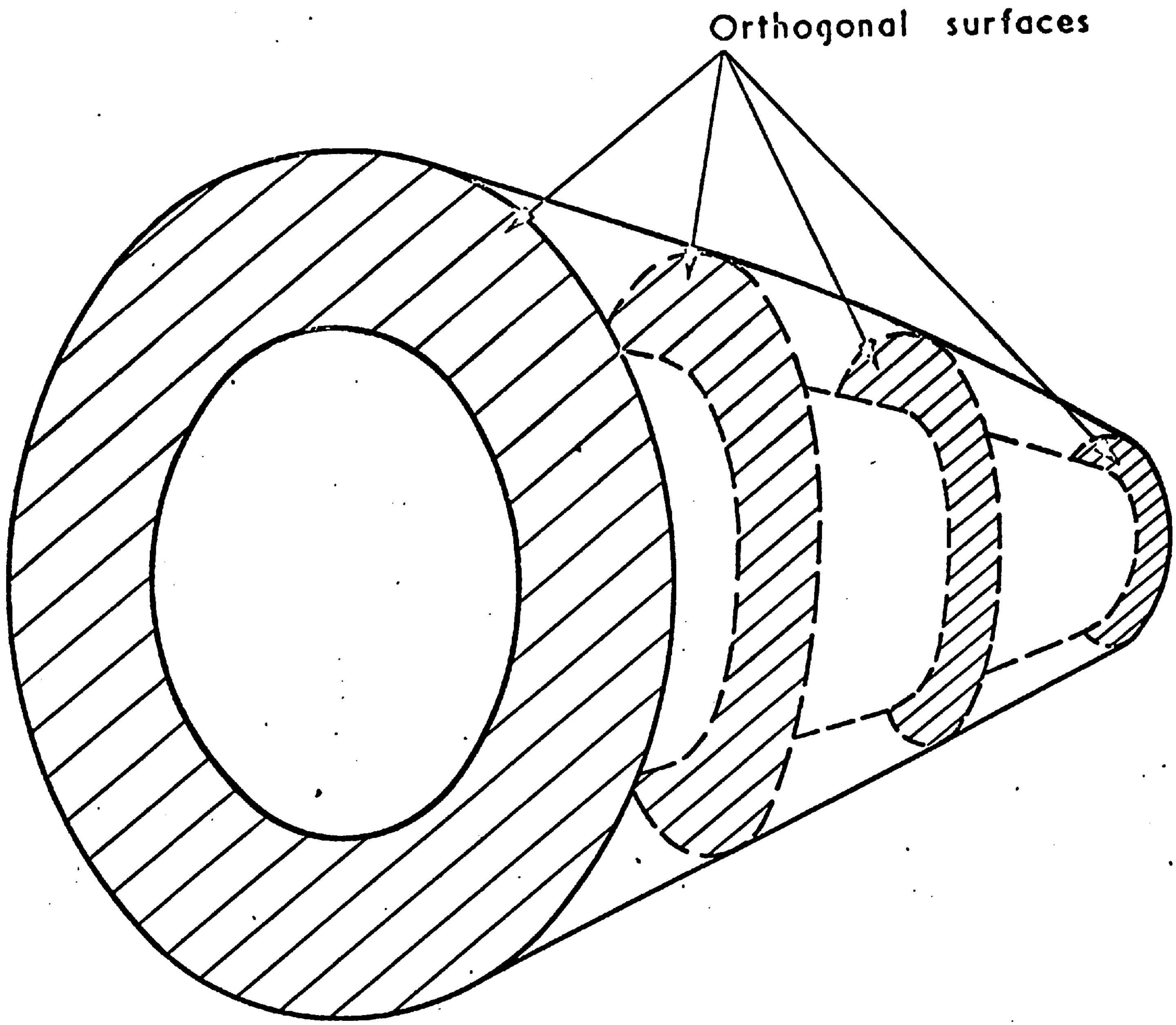

FIGURE 35. ORTHOGONAL PLANES FOR A BODY WITH ROTATIONAL SYMMETRY

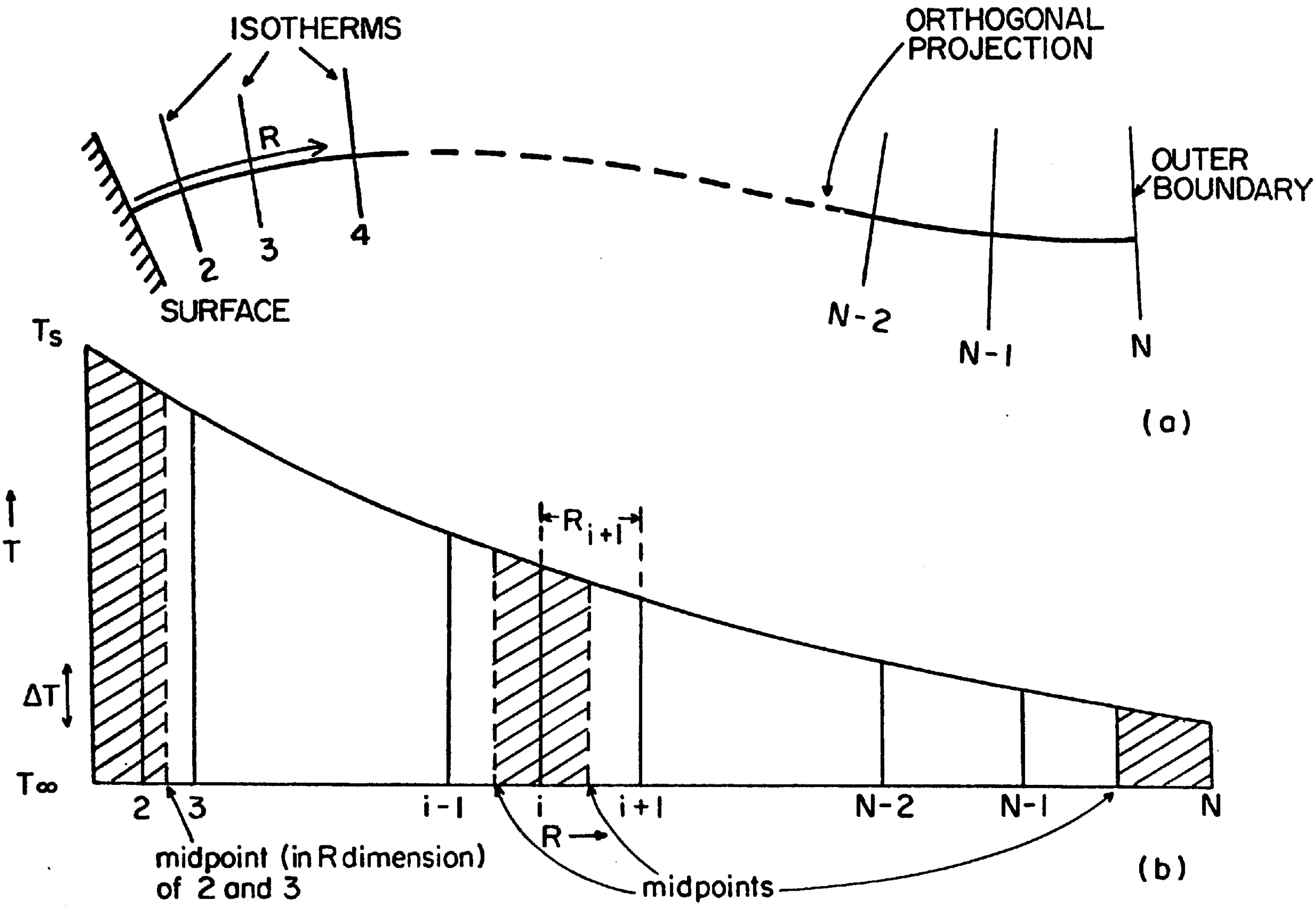

FIGURE 36. TEMPERATURE PROFILE ALONG A RADIAL COORDINATE

6. Outermost Compartment

The computation is very similar to those already described. Let the temperature gradient at the outermost surface (outer boundary of the set) be $(dT/dR)_0$ and the gradient at the midpoint between the N and N-1 isotherms be $(dT/dR)_I$. These gradients are computed by fitting a quadratic function through three adjacent points on the temperature profile. For the outermost compartment, the three temperatures are those at the N-1, and N isotherms, where N is the last isotherm and the far-field bath temperature at some remote point which is considered to be at infinity for the purpose of calculation. The mean temperature gradient at the inner surface during a time pulse is

$$\frac{dT}{dR_I} + \frac{\delta T_2 - \delta T_1}{2R_N} \quad .$$

Let us assume at this stage, (i) that the temperature gradient change at the outer boundary is negligible during a time pulse δt (although it may change from one pulse to the next) and (ii) that the change in temperature can be taken as a linear function of R over the width of a compartment. Also make the assumption (except in the surface compartment) that the change in central temperature of a compartment is the mean temperature change. This assumption reduces computations and is a close approximation to reality. The mean temperature change of the outer compartment is $(3\delta T_2 + \delta T_1 0/4)$ and the heat balance within the compartment is given by:

$$\left\{\left(\frac{dT}{dR}\right)_I + \frac{\delta T_2 - \delta T_1}{2R_N}\right\} AI\ k\delta t - \left(\frac{dT}{dR}\right)_0 AO\ k\delta T + \frac{VS}{4}(3\delta T_2 + \delta T_1) = 0 \quad .$$

$$\delta T_2 = \frac{\alpha_N}{\beta_N} \delta T_1 + \gamma_N \quad . \tag{8 10}$$

This expression is very familiar, having been derived in both the heat flow treatments which have been described in the earlier sections. For this expression,

$$\left.\begin{aligned} \alpha_N &= \frac{AI\ k\delta t}{2R_N} - \frac{V\ S}{4} \quad , \\ \beta_N &= \frac{AI\ k\delta t}{2R_N} + \frac{3VS}{4} \quad , \\ \text{and} \quad \gamma_N &= \frac{k\delta t}{\beta_N}\left\{AO\left(\frac{dT}{dR}\right)_O - AI\left(\frac{dT}{dR}\right)_I\right\} \quad . \end{aligned}\right\} \tag{8 11}$$

7. Central Compartments

Using the same nomenclature and assumptions (where appropriate) and proceeding in precisely the same way as in the previously described heat flow calculations (Chapters II and III), an equation having the same form as (8 10) can be derived for each of the central compartments. For the ith compartment, the three constants of the equation become:

$$\left.\begin{aligned} \alpha_i &= AI\ \frac{k\delta t}{2R_i} \quad , \\ \beta_i &= \left\{\frac{AI}{2R_i} - \frac{\frac{\alpha_{i+1}}{\beta_{i+1}} - 1}{2R_{i+1}} AO\right\} k\delta t + VS \ , \\ \text{and} \quad \gamma_i &= \left[\left\{\left(\frac{dT}{dR}\right)_O + \frac{\gamma_{i+1}}{2R_{i+1}}\right\} AO - \left(\frac{dT}{dR}\right)_I AI\right] \frac{k\delta t}{\beta_i} \quad . \end{aligned}\right\} \tag{8-12}$$

8. Surface Compartment

When we have reached a compartment near the surface, we have an equation whose constants, α, β, and γ, contain information about every preceding compartment of the set. This equation (equation 8-10) contains only two unknowns, δT_1 and δT_2. The growth process which occurs at the liquid/solid interface is a constraint on δT_1. Hence, the equation can be solved. Because every pair of adjacent temperatures has been related, and the constants α_i, β_i, and γ_i stored in the computer memory, the heat flow, new temperature field, and extent of surface growth can be calculated. The sequence of calculation was ended at the compartment next to the one which adjoins the surface. Referring to Figure 36, this is the compartment centered on isotherm 3.

To satisfy the solid/liquid interface boundary conditions, all the aspects of the growth process must be accounted for. Hence, the calculation for the surface compartment is more complex than those which have been described. It was found convenient to satisfy these boundary conditions using an iterative procedure.

For a given amount of surface growth, the temperature profile after a time pulse can be determined. Using the assumption that the change in temperature during a time pulse is a linear function of R over short distances,

$$\delta T(R) = KR + C \quad ,$$

where K and C are constants and R is measured from the initial liquid/solid interface. Taking $D = R_2 + R_3$ and δT_3 as the rise in temperature at the third isotherm, we find

$$\delta T_3 = KD + C \quad . \tag{8 13}$$

Representing the initial temperature profile by a quadratic expression

$$T - T_S = AR^2 + BR \quad , \tag{8.14}$$

where T_S is the initial surface temperature and A and B are constants, let δT_1 be the change in surface temperature which occurs during the time pulse and let g be the growth normal to the surface. Then

$$T_f = T + \delta T(R) \; , \tag{8.15}$$

where T_f is the resulting temperature profile. This can be written

$$T_f = AR^2 + BR + T_S + KR + C$$

or

$$T_f = AR^2 + (B + K)R + T_S + C \quad . \tag{8.16}$$

Setting R = g

$$T_f = T_S + \delta T_1 \quad ,$$

and

$$C = \delta T_1 - \left\{ Ag^2 + (B + K)g \right\} \quad . \tag{8.17}$$

Then from equations (8-13) and (8-17)

$$\delta T_3 = KD + \delta T_1 - \left\{ Ag^2 + (B + K)g \right\} \quad ,$$

and

$$K = \frac{\delta T_3 + Ag^2 + Bg - \delta T_1}{D - g} \quad . \tag{8.18}$$

The temperature gradient at the inner boundary of this compartment is

$$\left\{ \left(\frac{dT}{dR} \right)_I \right\}_f = 2A(R + \frac{R_3}{2}) + B + K$$

$$= \left(\frac{dT}{dR} \right)_I + K \quad .$$

The mean gradient during the time pulse is

$$\left\{\left(\frac{dT}{dR}\right)_I\right\}_{mean} = \left(\frac{dT}{dR}\right)_I + K/2 \quad ,$$

or

$$\left\{\left(\frac{dT}{dR}\right)_I\right\}_{mean} = \left(\frac{dT}{dR}\right)_I + \frac{-\,\delta T_1 + \delta T_3 + Ag^2 + Bg}{2(D - g)} \quad . \tag{8.19}$$

Using this relationship for the mean gradient at the inner surface, we obtain the conservation equation

$$AO.k\delta t\left\{\left(\frac{dT}{dR}\right)_0 + \frac{\delta T_3\left(\frac{\alpha_4}{\beta 4} - 1\right) + CZ_4}{2R_4}\right\}$$

$$- AI.k\delta t\left\{\left(\frac{dT}{dR}\right)_I + \frac{-\delta T_1 + \delta T_3 + Ag^2 + B}{2(D - g)}\right\}$$

$$- VS\delta T_3 = 0 \quad . \tag{8.20}$$

In this equation, only δT_3 is unknown (for an assumed value of g and subject to certain reservations concerning δT_1). Hence, δT_3 can be calculated.

All the information is now available to make a heat conservation calculation in the surface compartment. Such a calculation will not yield a proper heat balance, in general, since our choice of g is arbitrary. The calculation can be easily repeated with new values of g in a computer iteration until a heat balance is achieved and the inner boundary conditions are satisfied.

A simplified flow chart for the entire heat or solute flow calculation is shown in Figure 37. The iteration procedure to satisfy the inner boundary conditions is described in the next section.

9. Application of the Solid/Liquid Interface Boundary Condition

The boundary conditions at the solid/liquid interface are those demanded by the interface reaction (kinetic mechanism), the continuity of the heat and solute diffusion fields, the heat conduction in the solid and the Gibbs-Thompson effect due to surface curvature. In this study, we are considering only heat flow from an isothermal solid surface, although the computer program is written to accommodate the other boundary conditions if necessary.

For a given amount of surface growth, all the interface boundary conditions are fixed. If the surface growth is known, the amount of heat or solute carried into the liquid is fixed and, thus, the temperature and solute profiles are fixed. The depression of the melting point by the Gibbs-Thompson effect is also known since surface curvature can be calculated. The depression of the melting point due to changing solute concentration follows from the value of g and from the equilibrium partition coefficient. The temperature difference needed for the interface reaction also follows from the kinetic relationship between temperature difference and the growth velocity. Thus, all of the factors in δT_1, the change in surface temperatures, are defined.

If an arbitrary value of g is selected, a proper heat balance will not be obtained, in general. The amount by which it does not balance is called BAL, and an iterative calculation can be used to obtain the value of g which gives a balance. A flow chart of the balancing procedure is shown in Figure 38.

To make the description as simple as possible, the procedure will be restricted here to the case of heat flow only. In this case, δT_1 is zero,

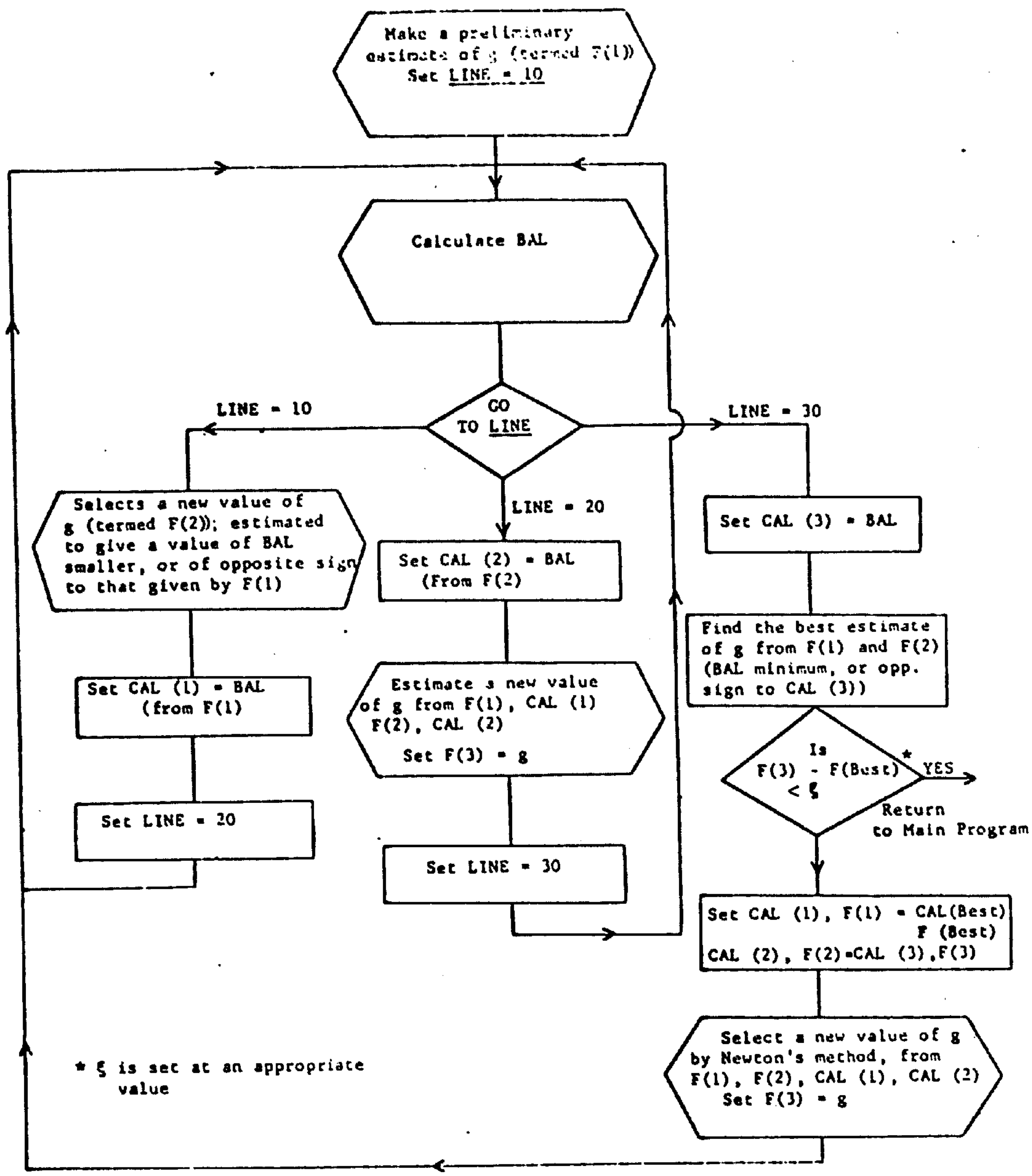

FIGURE 38 SOLUTION OF THE INTERFACE BOUNDARY CONDITIONS

whereas in a more physically satisfactory treatment the other factors mentioned earlier would enter the calculation here. For example, a part of δT_1 would be determined by the interface reaction kinetics and the solute effect.

Consider the surface compartment shown in Figure 39. For this compartment we have

BAL = latent heat liberated - heat flowing out + specific heat change.

Assume that the sides of the compartment are built up of planes, rather than curved surfaces, as shown in Figure 39. Note that this assumption affects the accuracy of the specific heat calculation but that the loss in volume on one side is made up by a gain on the other. This assumption ensures overall conservation of energy between neighboring sets of compartments.

In Figure 39 the various features of the surface compartment are illustrated. For computational purposes we shall let AI be the area of the crystal surface bounding the compartment, AO be the outer surface area, AC be the surface area of the isothermal plane 2 included in the box, g be the assumed value of normal surface growth, V_S be the volume of solid formed during the time pulse, Q_S the amount of heat needed to increase the internal energy of the liquid in the compartment, Q be the amount of heat conducted away into the liquid, δT_1 be the change in surface temperature and L be the heat liberated by a unit volume of liquid upon freezing.

Then our BAL equation becomes

$$V_S L + Q - Q_S + \left(\frac{dT}{dR}\right)_0 k\delta t.AO = BAL \quad . \tag{8 21}$$

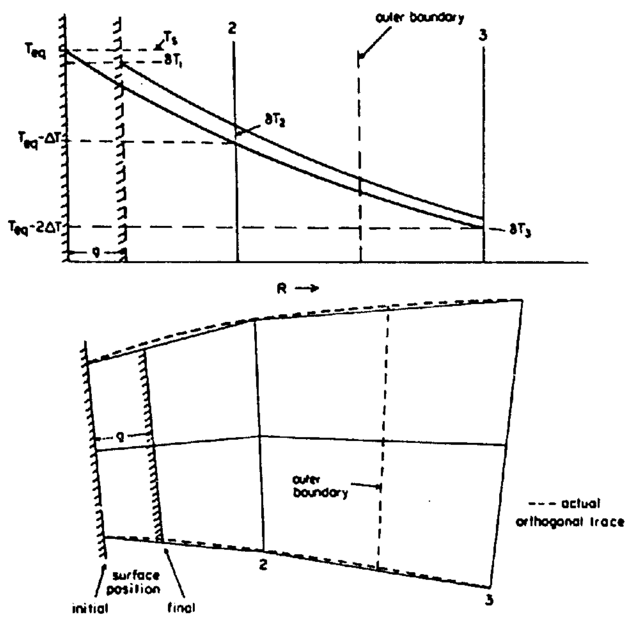

FIGURE 39. SURFACE COMPARTMENT

When the boundary conditions are satisfied, BAL = 0. The terms of this equation will now be derived.

(i) Change in Internal Energy of the Liquid

Let the area of a travelling surface located a distance R from the solid/liquid interface be

$$A(R) = MR + N \quad , \tag{8.22}$$

where we recognize two volumes of differing dimensions so that the constants M and N have the values

$$\left.\begin{aligned} N &= AI \\ M &= \frac{AC - AI}{2} \end{aligned}\right\} \text{ between the surface and isotherm 2} \tag{8.23}$$

$$\left.\begin{aligned} N' &= AC \\ M' &= \frac{2(AO - AC)}{R_3} \end{aligned}\right\} \text{ between isotherm 2 and the outer boundary of the compartment} \quad . \tag{8.24}$$

As before, the temperature profile before and after the heat pulse is represented by quadratic expressions. Let T and T_f represent the initial and final temperatures respectively at some position R; i.e.,

$$T - T_S = AR^2 + BR$$

$$T_f - (T_S + C) = AR^2 + (B + K)R \quad ,$$

where C and K are the constants used in (8-23). Let us write

$$T_F = T_S + \delta T_1$$

and

$$B + K = B' \quad .$$

Let the distance along R from the interface to the outer boundary be R_o. Then

$$Q_S = S\left\{\int_g^{R_2} A(R)T_f dR + \int_{R_2}^{R_o} A(R)T_f dR + \int_o^g A(R)T_F dR - \int_o^{R_2} A(R)TdR + \int_{R_2}^{R_o} A(R)TdR\right\}$$

$$= S\left\{\int_o^{R_2} A(R)(T_f - T)dR + \int_{R_2}^{R_o} A(R)(T_f - T)dR - \int_o^g A(R)T_f - T_F)dR\right\} \qquad (8.25a)$$

In this expression, the first two integrals are equal to the products of the initial volumes and a mean increase in internal energy. The last integral accounts for the intrusion of solid into the liquid and the resulting heat needed to raise this volume to the freezing temperature. Substituting (8.22) into (8.23-4), we obtain the following expression:

$$Q_S = S\left[\int_o^{R_2} (MR + N)(KR + C)dR + \int_{R_2}^{R_o} (M'R + N')(KR + C)dR\right.$$

$$\left. - \int_o^g (MR + N)\left\{AR^2 + (B + K)R + (C - \delta T_1)\right\} dR\right] \quad , \qquad (8.25b)$$

and integrating, we obtain

$$Q_S = S\left[\frac{MKR_2^3}{3} + \frac{(MC + KN)}{2} . R_2^2 + NCR_2\right.$$

$$+ \frac{M'K(R_o^3 - R_2^3}{3} + \left(\frac{M'C + KN'}{2}\right)\left(R_o^2 - R_2^2\right)$$

$$+ N'C(R_o - R_2) - \frac{MA\text{-}g^4}{4} + \frac{g^3}{3}\left\{M(B + K) + NA\right\}$$

$$\left. + \frac{g^2}{2}\left\{M(C - \delta T_1 + N(B + K)\right\} + Ng(C - \delta T_1)\right] \quad . \qquad (8.25c)$$

(ii) Latent Heat Liberation

$$V_S L = L \int_0^g A(R)dR$$

$$= L \left(\frac{Mg^2}{2} + Ng \right) \quad . \qquad (8\cdot 26)$$

(iii) Mean Temperature Gradient at the Outer Boundary

$$\left[\frac{dT}{dR_0}\right]_{mean} = \left(\frac{dT}{dR}\right)_0 + \frac{K}{2} \quad ,$$

as given in (8·19).

All the quantities in the equations above are available, and now BAL can be calculated. The calculation can now be iterated until repeated estimates of the velocity to give BAL = 0 agree within a very small value.

In the case we defined in this paper, the relationship between g and BAL is smooth and monotonic. The iteration procedure we choose is a modified Newton's Method. Only two iterations were generally needed to obtain the correct g within 0.5%.

10. Preparation of a New Orthogonal Network

After each time pulse, a set of temperature changes is defined on the existing network points. To continue the process of solidification in the next time frame, a new solid/liquid interface and a new heat field must be set up. In the model, this is done by first fitting new isotherms to the field by means of a quadratic interpolation and then generating a new set of orthogonal trajectories. The subroutines entitled MOVER and HUNT perform these two operations.

In MOVER, a quadratic expression is first fitted through the surface temperature and the next two temperatures outward. In this way, a temperature profile is generated and the position of the first isothermal plane can be found. This process is repeated in sequence so that a whole new series of isotherms are generated as shown in Figure 40. The last quadratic fit is made through a point which is sufficiently remote from the solid/liquid interface to be regarded as at infinity. A simplified flow diagram for MOVER is shown in Figure 41.

At this point in the calculation, the dendrite surface has advanced, the heat pulse generated at the surface has run through the boxes out toward the far-field, and a new temperature field has been generated. To conform to our requirements for a one-dimensional analysis, a new set of orthogonal trajectories must be generated. This is the purpose of the subroutine HUNT. The routine which will be described here has been developed for a "two-dimensional" problem; that is, where the crystal is a body of revolution.

The computer had first to find the index of the isotherm nearest to the non-isothermal surface by comparing the surface temperature depression with the temperature step between the isotherms. Then, the angle of the line of steepest descent through the temperature field was found from a selected point on the crystal surface. To determine the angle of this line, four quantities had to be calculated.

(a) The angle α made by the tangent to the crystal surface at the point

(b) The gradient (at the surface) of a curve passing through the points of the same k-index on the next

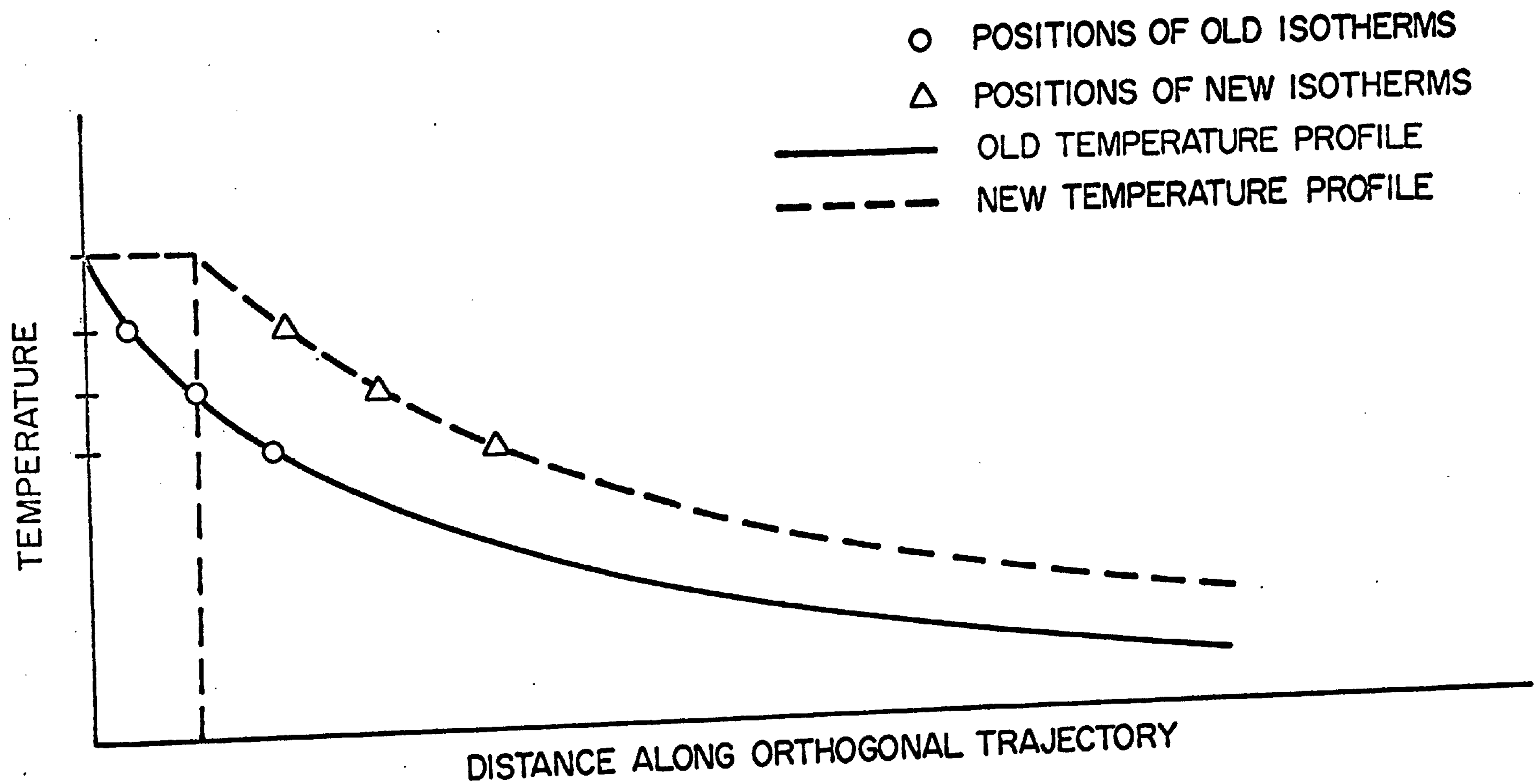

FIGURE 40. ISOTHERM MOVEMENT

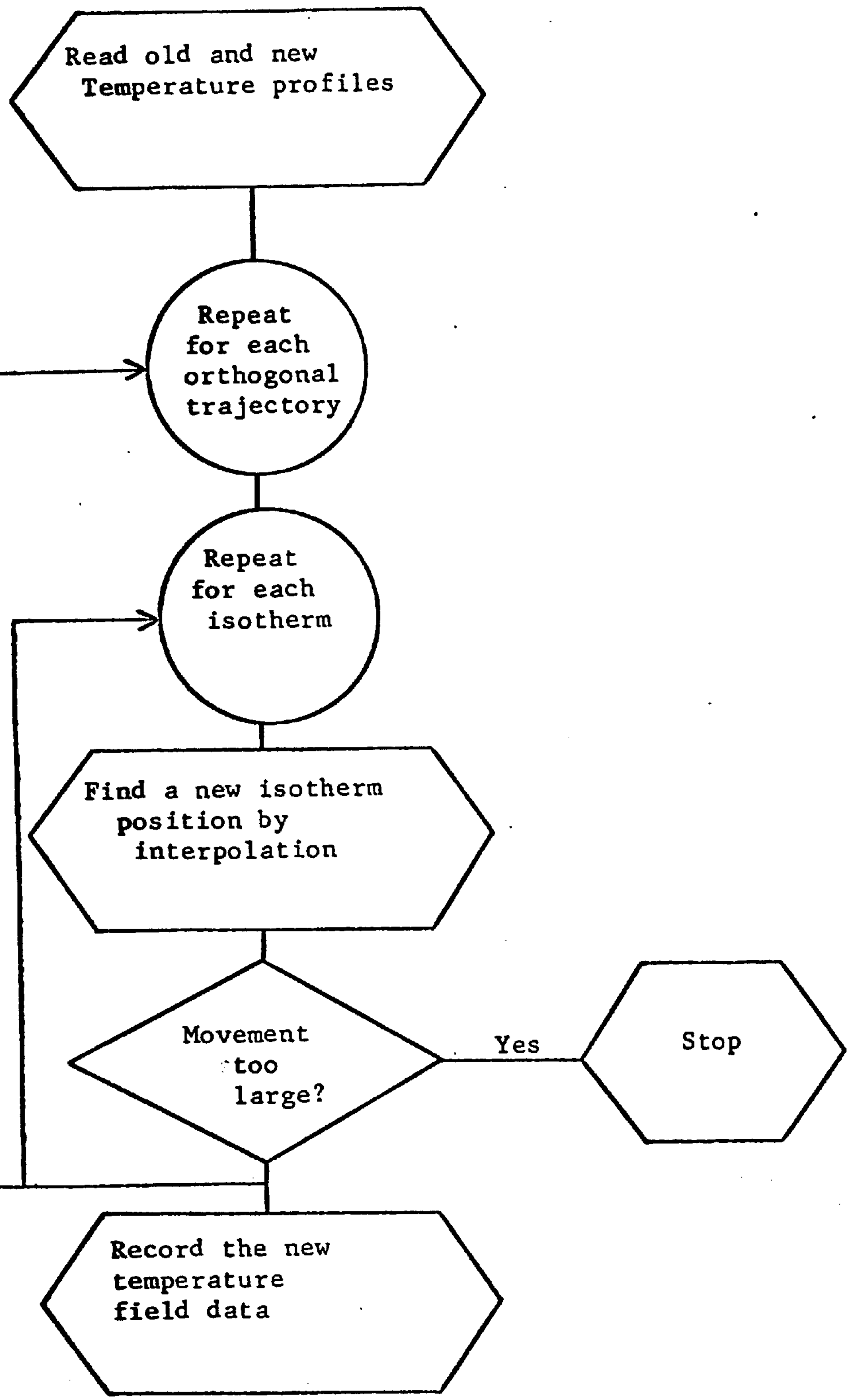

FIGURE 41. FLOW CHART FOR "MOVER"

two isotherms. This gradient made an angle β with the X-axis

(c) The temperature gradient along the crystal surface at the selected point, $T'\alpha$

(d) The temperature gradient at the surface along the curve found in (b), $T'\beta$.

These quantities were found by differentiating quadratic expressions fitted through each set of three points using the appropriate parameters. For the temperature curves, for example, the parameters were the isotherm temperatures and a radial distance between the points. Then:

$$\text{Gradient} = \left(\frac{\cos\alpha}{\cos\beta\ Am} - 1\right) \Big/ \left(\tan\beta - \frac{\sin\alpha}{\cos\beta\ Am}\right) , \tag{8.27}$$

where $Am = \frac{T'\alpha}{T'\beta}$. This expression is developed in Appendix E.

The orthogonal network was then developed in a manner similar to the method used in preparing the initial network, described in Part 5 of this chapter. There was a major difference. Because long-range mathematical descriptions of the temperature field cannot be imposed, a short-range description had to be found near each point from which a projection was desired. Considering the development from a surface point. The gradient of the orthogonal line has already been found by the procedure described in the previous paragraph. The projection of this line is used to find the three network points on the first isotherm which lie about the line. These are then used to derive a quadratic expression through the points and the intersection of the orthogonal line with the curve is then found by a root finding procedure. Hence, the angle made by the orthogonal line with the

the curve at the point of intersection is derived. This is a first approximation to the orthogonal curve; a new projection is then made from the surface at the mean angle, and a new intersection point derived. This is taken as the new network point, and the projection is continued through the whole set of isotherms and repeated for each orthogonal. The flow diagram for this calculation is shown in Figure 42.

At this juncture, a new orthogonal network is available for a new heat flow calculation, and a new increment of crystal growth can be calculated.

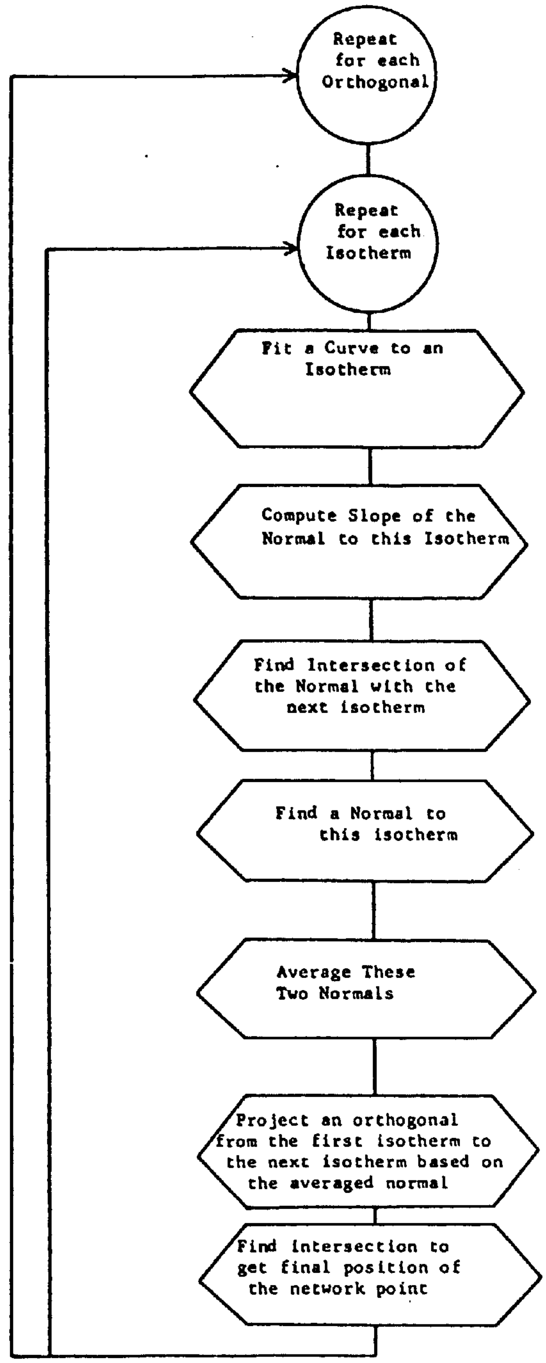

FIGURE 42. SIMPLIFIED FLOW CHART FOR THE CONSTRUCTION OF NEW ORTHOGONAL TRAJECTORIES

CHAPTER IX: SIMULATION OF ICE AND TIN DENDRITES

1. Comparison With Ivantsov's Results

Ivantsov's calculation has already been mentioned in Chapter VII. It was possible to simulate his model dendrite by setting the value of surface energy as zero, which eliminated the curvature effect which is incorporated within the computer model. The initial conditions are then exactly those derived for the thermal field of a dendrite growing (according to this model) at steady state. Therefore, the computer calculation for dendrite growth should yield a calculated growth velocity in close agreement with Ivantsov's analytical result. This result is summarized in the expression for Ω described in Chapters VII and VIII. This may be recast as:

$$V = \frac{(\text{constant})}{(\text{tip radius})} \quad .$$

However, the Ivantsov dendrite cannot be meaningfully simulated for any long period of growth, since it cannot be optimized. The crystal can grow at any velocity without any of the penalty incurred in real crystal when at high velocities the tip of the crystal becomes very pointed. Therefore, an appropriate test for the computer model comprises a check on the velocity at the first loop around the calculation, and a few repeat loops to ascertain the utility of the routines for rearranging the network. In calculations for the ice crystal, the time increment was varied in the range 0.1-1.0 sec, a tip radius ρ of 0.01 cm and a length Z_o of 0.50 cm were combined with varying network subdivisions in a comparison with the calculated tip velocity. The results are shown in Table 5. It was found in practice that

TABLE 5. AXIAL GROWTH VELOCITIES NEAR THE TIP

K Index	Velocity x (10^{-3}) for Various Matrix Dimensions (cm/sec)			
	10 x 11	10 x 21	20 x 21	40 x 41
2	1.424	1.485	1.498	1.523
3	1.466	1.469	1.490	1.515
4	1.525	1.525	1.513	1.520

Theoretical result: 1.536×10^{-3} cm sec^{-1}

the time increment was not a free variable. It had to be related to the network size so that the amount of surface growth never exceeded the distance from the surface to the first isotherm. It was therefore set automatically by the model to give a growth of one-half (isotherm spacing). The results are in close agreement with the theoretical value, the agreement becoming better with successive loops through the calculation in most cases. For the finest matrix studied, the growth velocity was

$$V(\text{computer}) = 1.523 \times 10^{-4} \text{ cm sec}^{-1} \quad (40 \times 41 \text{ matrix}) \ .$$

This result can be compared to

$$V(\text{theoretical}) = 1.536 \times 10^{-3} \text{ cm sec}^{-1} \ .$$

It was not possible to meaningfully separate the effects of the individual variables, number of isotherms and number of orthogonals. The overall relationship is therefore shown schematically in Figure 43. This shows the effectiveness of the various matrices on the tip velocity in comparison with the theoretical value.

The axial component of surface growth was calculated at a number of different stations (values of k) along the crystal. There was very good agreement between the results, indicating that the crystal shape was being maintained. The results for a crystal simulated by a 40 x 41 matrix are shown in Table 5. All of the stations along the crystal were within 0.5% of the theoretical velocity required to maintain the parabolic shape. A cross section through the network is shown in Figure 44. This network has the orthogonal lines spaced by a slightly different method from that described in the last chapter, so that the orthogonal lines are not clustered quite as closely around the tip region as in later calculations.

Equally good agreement was obtained when the growth of a tin dendrite was simulated. Table 6 lists the axial velocities calculated at the stations along the crystal. A tin dendrite was modelled, growing in a liquid bath supercooled 5°C below the freezing temperature. The tip of the dendrite had a radius of curvature of 2.5×10^{-4} cm. The physical constants for tin used in this and subsequent calculations are listed in Table 7. It can be seen that again all the velocities calculated are within 0.5% of the theoretical value. The tip and theoretical velocities are:

$$\text{Tip velocity} = 6.556$$

$$\text{Theoretical velocity (Ivantsov)} = 6.560 \quad .$$

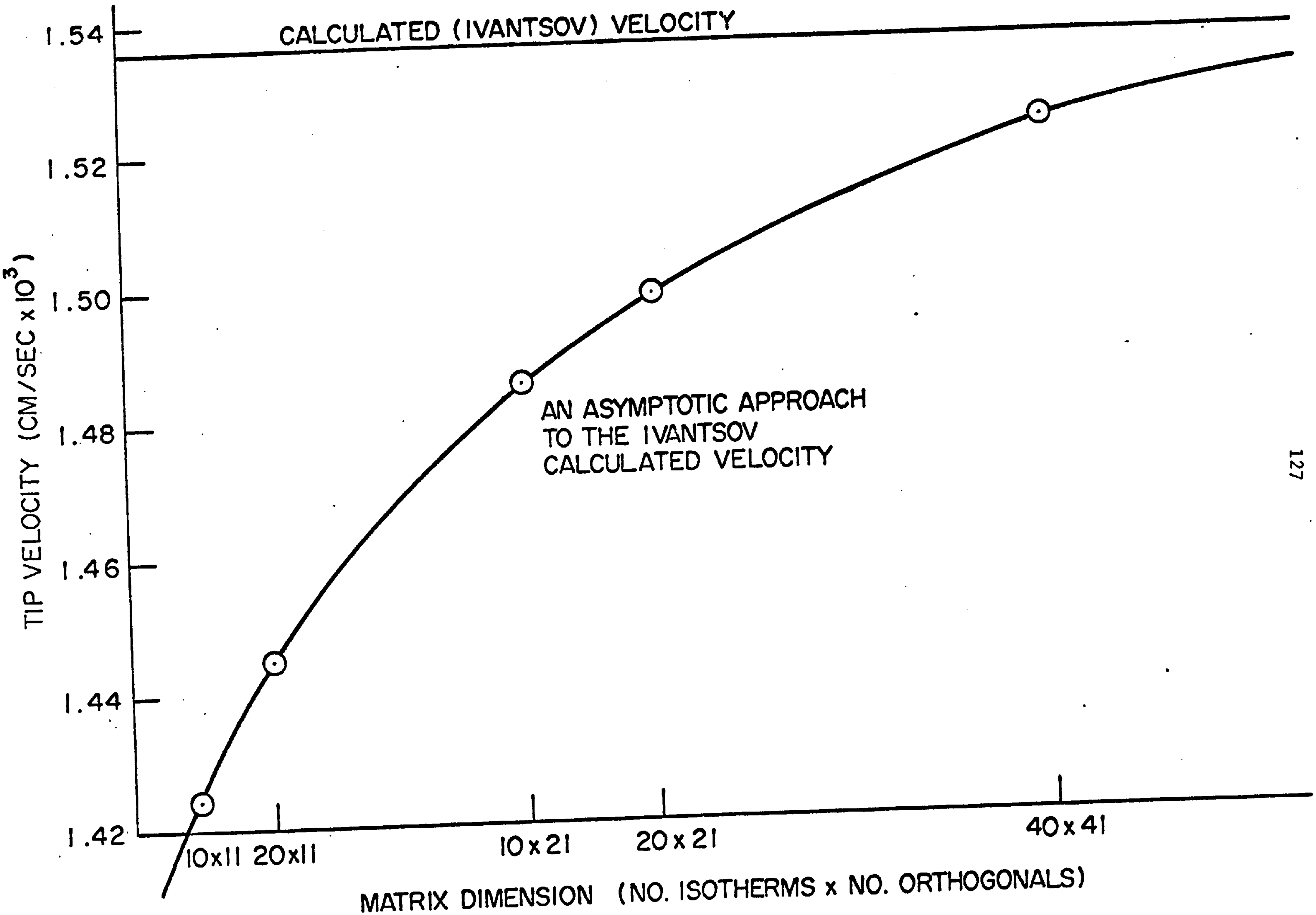

FIGURE 43. EFFECT OF NETWORK SIZE UPON THE CALCULATED DENDRITE GROWTH VELOCITY

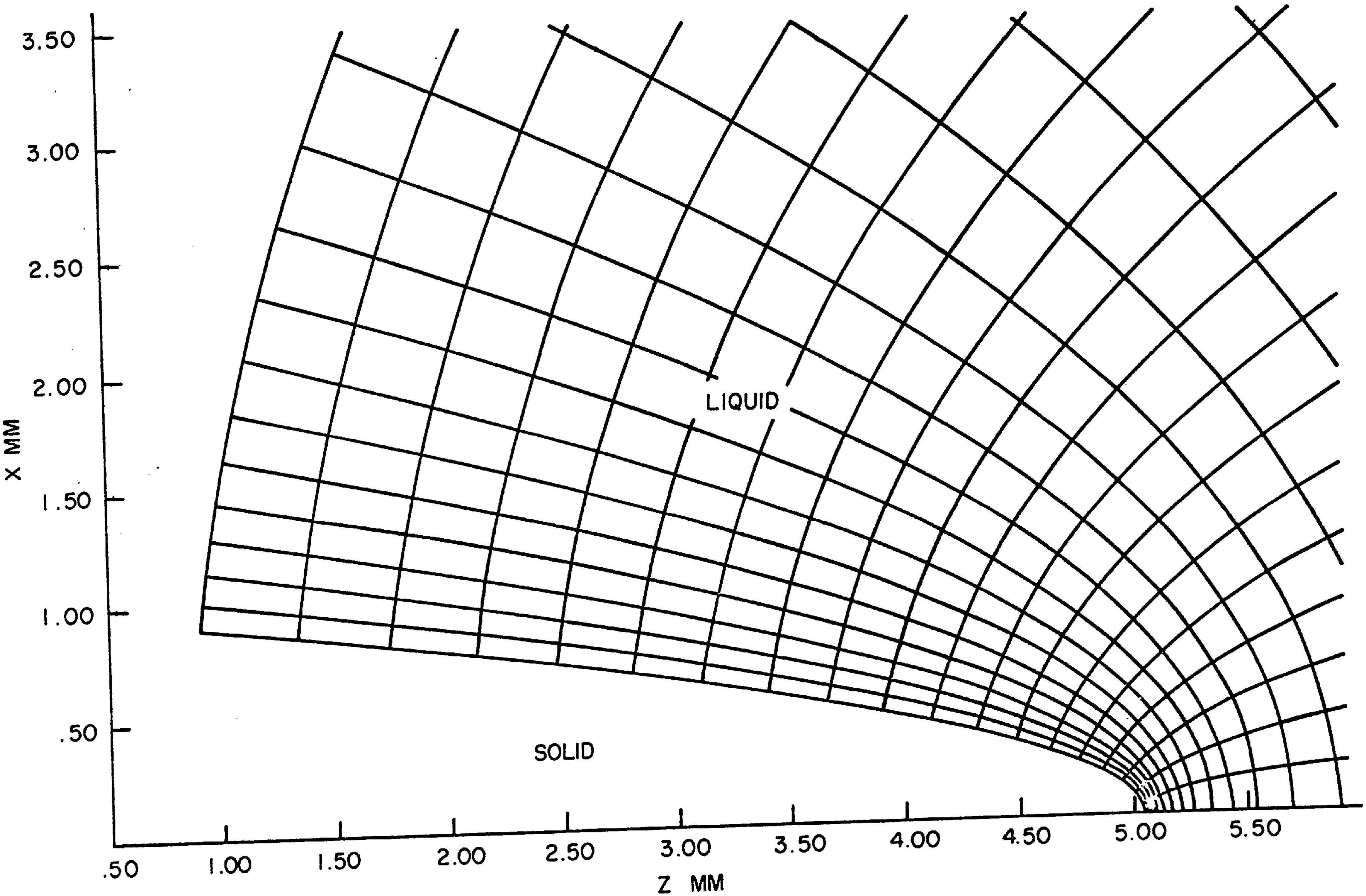

FIGURE 44. CROSS SECTION THROUGH THE ORTHOGONAL NETWORK

TABLE 6. AXIAL COMPONENT OF VELOCITY OF AN ISOTHERMAL TIN DENDRITE

k	V (axial comp.)	Z	Theoretical Value for Axial Velocity
2	6.556	1.51250×10^{-2}	
3	6.568	1.51213×10^{-2}	
4	6.548	1.511767×10^{-2}	
5	6.540	1.51103×10^{-2}	
6	6.530	1.50957×10^{-2}	
7	6.519	1.50664×10^{-2}	6.56
8	6.516	1.50078×10^{-2}	
9	6.525	1.48906×10^{-2}	
10	6.541	1.4656×10^{-2}	
11	6.555	1.4187×10^{-2}	
12	6.563	1.3255×10^{-2}	
13	6.569	1.139×10^{-2}	
14	6.573	0.756×10^{-2}	
15		0.0	

k is the number of the station along the crystal

Dimensions are cm sec^{-1} and cm

Theoretical velocity calculated following Ivantsov[31].

TABLE 7. PHYSICAL CONSTANTS FOR TIN USED IN THE CALCULATIONS*

Equilibrium melting temperature	505°K
Heat of crystallization	13.96 cal gm^{-1}
Density of solid	7.3 gm cm^{3}
Density of liquid	6.98 gm cm^{3}
Thermal conducitivity of liquid	0.082 cal cm^{-1} sec °C
Specific heat of liquid	0.060 cal gm^{-1} °C
Interfacial surface	36 erg cm^{-2}

* Taken from Reference 32

2. Simulation of a Non-Isothermal Dendrite

Calculations were next performed on a non-isothermal dendrite following the Temkin model. The attachment of atoms at the crystal surface was assumed to be easy, requiring no driving force. A bath supercooling of 3°C was assumed, and the physical constants for tin (Table 7) were employed. Because the initial conditions did not correspond to the steady state solution for the non-isothermal dendrite, the growth velocity was calculated by allowing the calculation to pass through several time increments. This gave the temperature field opportunity to develop the correct form from the approximate distribution used to start the calculation. A range of tip shapes were used in the calculations, in an attempt to determine a maximum velocity for the dendrite growth.

The results are summarized in Figure 45, where the results predicted by Ivantsov's equation are shown for comparison. A peak velocity of about 6.5 cm sec^{-1} occurs for a tip radius of about 1.0×10^{-4} cm. This is rather slower than predicted by Temkin's equations* (11.1 cm sec^{-1}) and less curved (Temkin's equations predict a tip curvature of 0.39×10^{-4} cm). For all the cases studied, the tip velocity was slowly falling and the curvature of the tip became flatter as the growth simulation proceeded.

Long term calculations were next attempted, in an attempt to study the development of the crystal shape with time. It was possible to model growth to the extent of 10 - 15 tip radii, which took 200 microseconds of "real" time, and about 200 seconds of computer time. After this period,

---

* This calculation was performed by G. Kotler, using a computer solution to the Temkin equations[34].

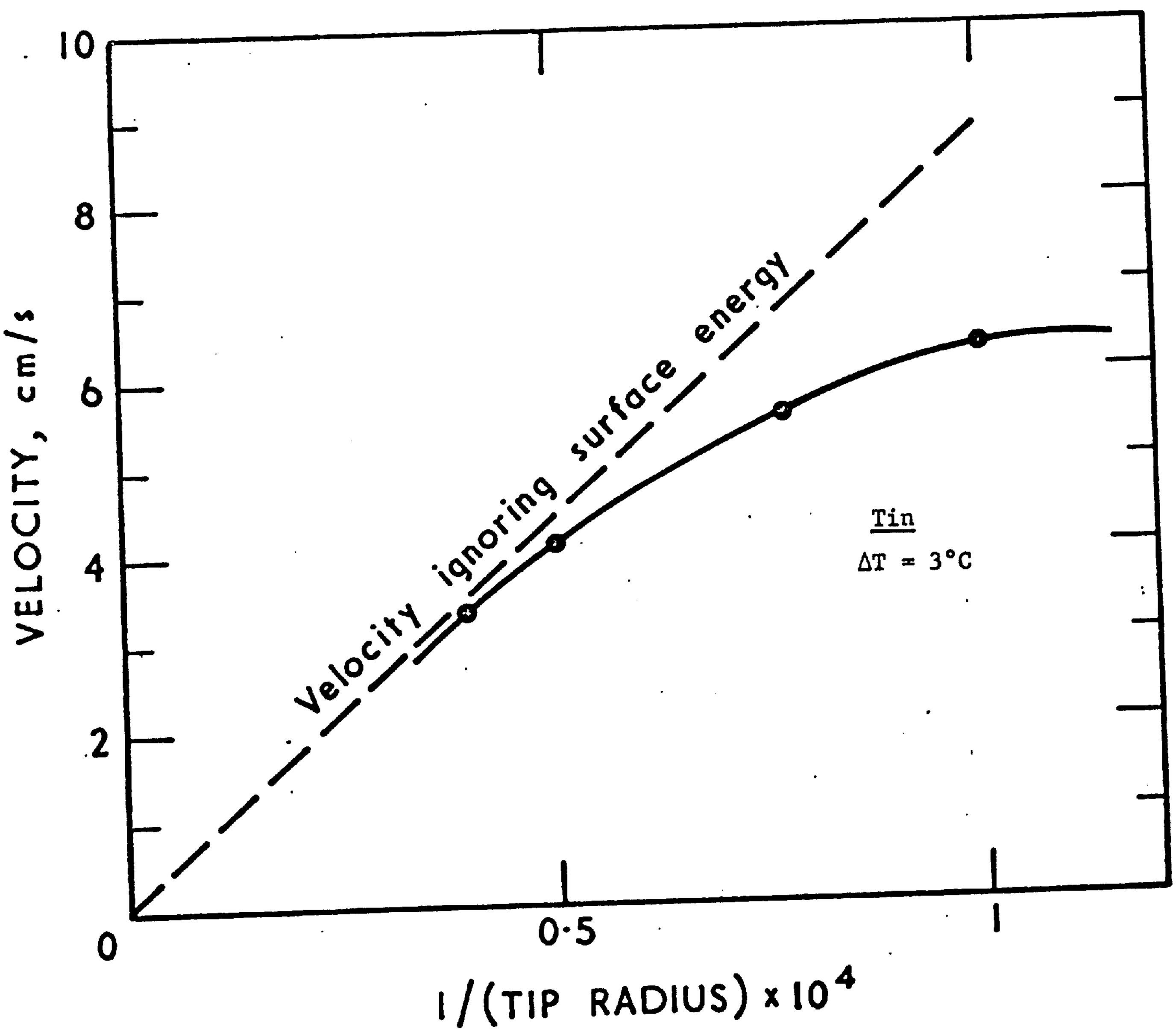

FIGURE 45. VARIATION OF PREDICTED VELOCITY WITH TIP RADIUS

the program gradually developed an instability, and the calculation had to be terminated. An example of the result given by this procedure is shown in Figure 46. For this particular instance, a bath supercooling of 5°C for tin was assumed; the computer crystal tip radius did not become as small as that predicted for optimum velocity, and consequently the velocity was much less than the optimum for a tin crystal growing under these conditions.

3. Modification to Increase Stability

A full discussion of the stability of computer calculations exceeds the scope of this dissertation. However, a brief discussion is germane to the dendrite model development and to other work described in subsequent chapters.

One viewpoint of the stability of computer models originates with the idea of "open" and "closed" form calculations. In the present context, a closed form calculation is one in which there is only one unknown and which therefore can be solved exactly. An expression in open form contains more than one unknown which must be guessed. This idea can be illustrated by the models which have already been described. In the heat flow calculations the expressions were in closed form. The solution was exact subject to the approximations of the models. The simulation of the casting was in open form, and hence liable to become unstable. The number of nuclei forming in a time increment or the instantaneous rate of eutectic growth were both unknown and dependent upon the change in degree of undercooling. The stability of the model resulted from the short time increments used in the computation, so that the unknowns in the calculation were guessed with only slight error. It was possible to induce instability by using very long time

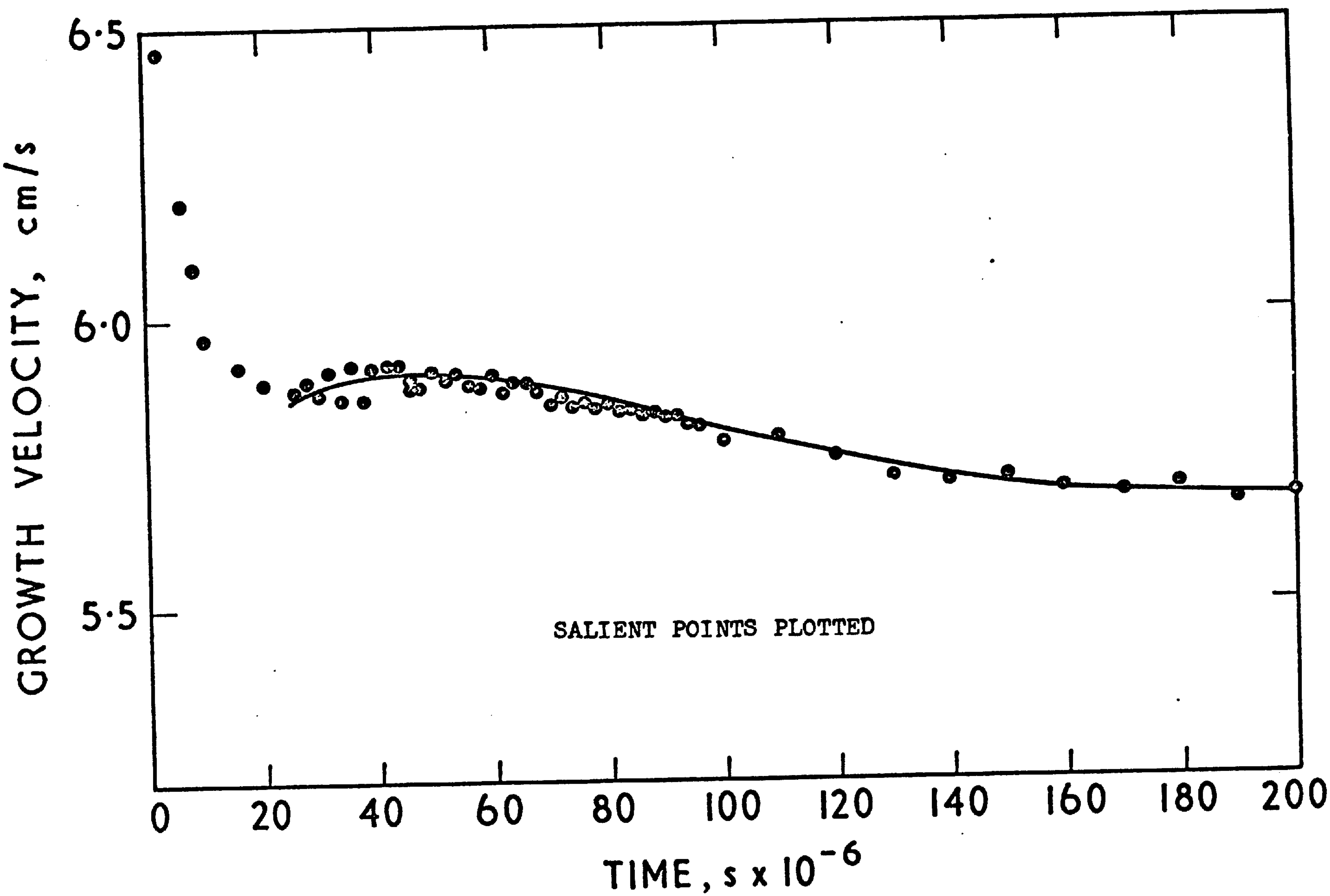

FIGURE 46. GROWTH VELOCITY CHANGE WITH TIME

intervals, with the characteristic result that the results for each time increment varied widely about the mean, and the variation increased with each calculation loop (time increment). The mathematical theory of stability for computer models is still in an embryo state of development.[37] Fortunately, it was preceded, by many years, by the study of techniques to control stability.

Although the dendrite model could be operated stably when it was used with great care, it was potentially unstable. This arose from the assumption that the orthogonal network was unchanged throughout the time increment. Clearly, the flow channel must move to some extent, and a zero estimate could only be correct for short intervals. To make the model more tractable, a form of the Runge-Kutta method[38] was employed. The objective was to make a better estimate of the position of the heat flow channels. The position of the isotherms was already relaxed in the one-dimensional heat flow calculation. The sequence of calculations was as follows:

(a) Dendrite growth was computed as before, assuming that the orthogonal curves remained fixed.

(b) The amount of surface growth and the temperature changes throughout the field were stored in the computer memory.

(c) The network was then moved to find a new set of orthogonal heat flow channels.

(d) The isotherms were then moved back up the new channels so that the original temperature field was restored, but with altered flow channels.

(e) A second calculation of dendrite growth was made.

(f) The mean surface growth and the mean temperature changes were then found.

(g) The network was moved on the basis of the mean changes in preparation for a new loop through the calculation. This procedure is equivalent to the assumption of a mean position for the heat flow channels during each time pulse.

The additional computer time involved in this more complex procedure was more than balanced by the longer time increments which could be used.

4. Tin Dendrites Simulated by the Runge-Kutta Model

The variation of tip velocity and tip radius with time for a simulation using the Runge-Kutta routines is shown in Figure 47. The crystal model was growing into a bath undercooled 3°C and initially had the optimum (Temkin) tip radius. The optimum (Temkin) tip velocity was 6.5 cm sec^{-1}. It can be seen that the computation had almost completely "settled down" by the fourth loop through the calculation and that subsequently the velocity changed smoothly with time. All the early points on the velocity-time curve are shown. Later points, which lay on the smooth curve are not all shown. The dendrite tip velocity fell gradually, and at the same time, the tip curvature increased slowly (that is, the needle became blunter). The axial velocities at the other stations along the crystal (moving back from the tip) remained fairly constant at the Ivantsov velocity.

The slowing of the crystal growth is not surprising. The initial conditions postulate a parabola of revolution, which according to Ivantsov's

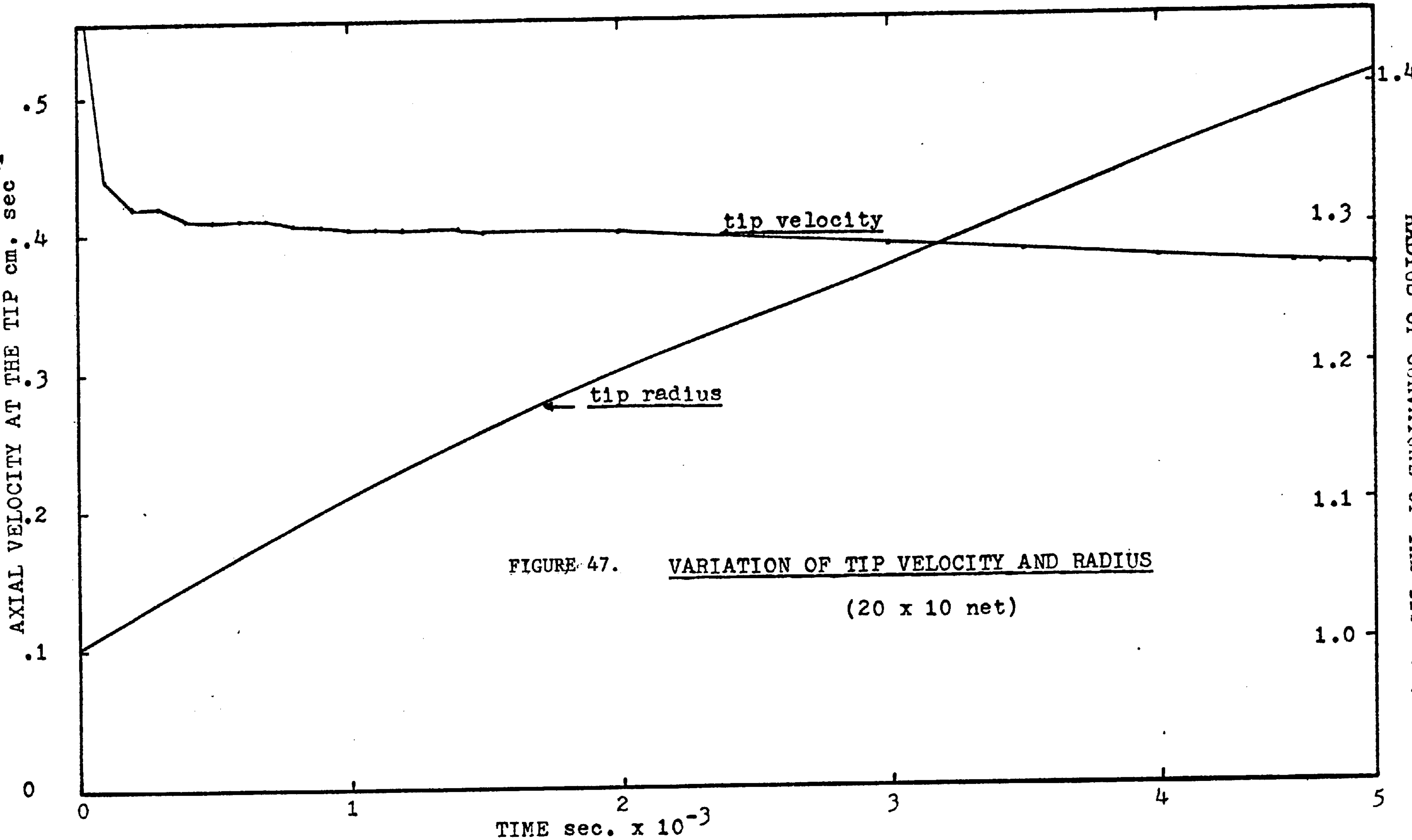

FIGURE 47. VARIATION OF TIP VELOCITY AND RADIUS

(20 x 10 net)

result, maintains it shape if curvature effects are ignored. When curvature is included in the computation, it has a negligible effect on the axial growth velocity of the crystal away from the extreme tip. These parts of the crystal therefore continue to grow with the "Ivantsov" velocity. The tip, on the other hand, is drastically slowed. The difference in velocity between the tip and adjacent regions of the crystal can be seen in Figure 45. Whereas the tip velocity is related to the tip curvature by the lower (solid) curve, the axial velocity of the remainder of the crystal follows the upper (dashed) line. Clearly a crystal growing in a pure melt in a temperature field resembling the Ivantsov solution cannot have a parabolic form; if it is given this shape, it progressively becomes blunter.

At this stage, it seemed appropriate to change the profile of temperature field, in an attempt to force the crystal to accelerate. The boundary conditions remain those described in Section 2 of this chapter. A crystal of the optimum tip curvature was forced to grow with a faster tip velocity than the Temkin or Ivantsov velocities. As a result, the tip radius became sharper. The results are shown in Figure 48(a) and (b). The tip radius fell initially because of the perturbation but rapidly increased, leveling off at the optimum tip radius of 1.0×10^{-4} cm. The tip velocity also leveled off at about the same stage of growth and then began to fall gradually. This result would seem to indicate some independence from the initial temperature field and illustrates how excessive tip curvature is rapidly lost.

5. Long-Term Growth of Tin Dendrites

A streamlined version of the calculation was next developed, to

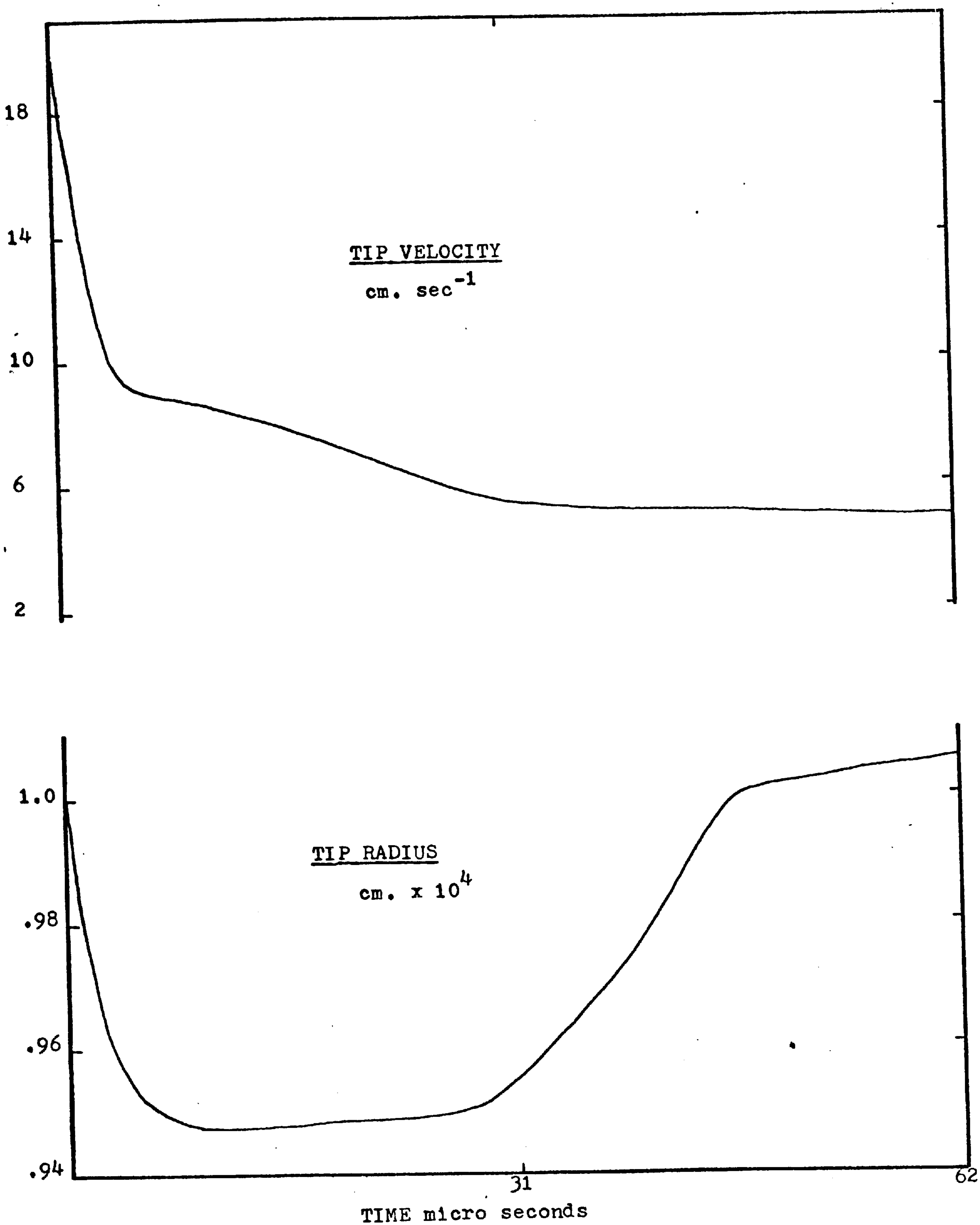

FIGURE 48. SLOWING OF A DENDRITE INITIATED AT FASTER

permit simulation of crystal growth for longer periods. Part of the speeding process was the removal of most of the data output, and concentrating output on only the most significant results. Unfortunately, this "streamlining" process introduced a bookkeeping error into the calculation, which perturbed the initial calculation of the Runge-Kutta sequence by about 15% on alternate loops through the calculation. The absence of data output made the error impossible to find and since the mean results were in close agreement with those obtained previously, they will be described for their qualitative importance.

Figure 49 shows the smoothed velocity of the crystal tip plotted against the real time after the initial conditions had been applied. The growth of the crystal was accompanied by changes in the crystal shape and a fall in growth velocity. Figure 50 shows the shape of the crystal at intervals during the period of growth. Figure 51 shows the increase in crystal size during the growth simulation. The amount of growth is shown by the blacked area, which is the difference in the crystal shape at the beginning and the end of the computation. The figure also shows some of the isotherms near the crystal surface.

The development of "branches" in the neighborhood of the tip is noteworthy. These projections were accelerating during the whole period of growth. Their behavior can be contrasted to the manner in which the tip fell back when it was perturbed beyond its optimum curvature. One of the major reasons for the difference in behavior can be found in the temperature depression due to curvature. The side projections are inadequately penalized for their curvature because of the shortage of points of the network. The growth of the surface has separated the points which describe the surface

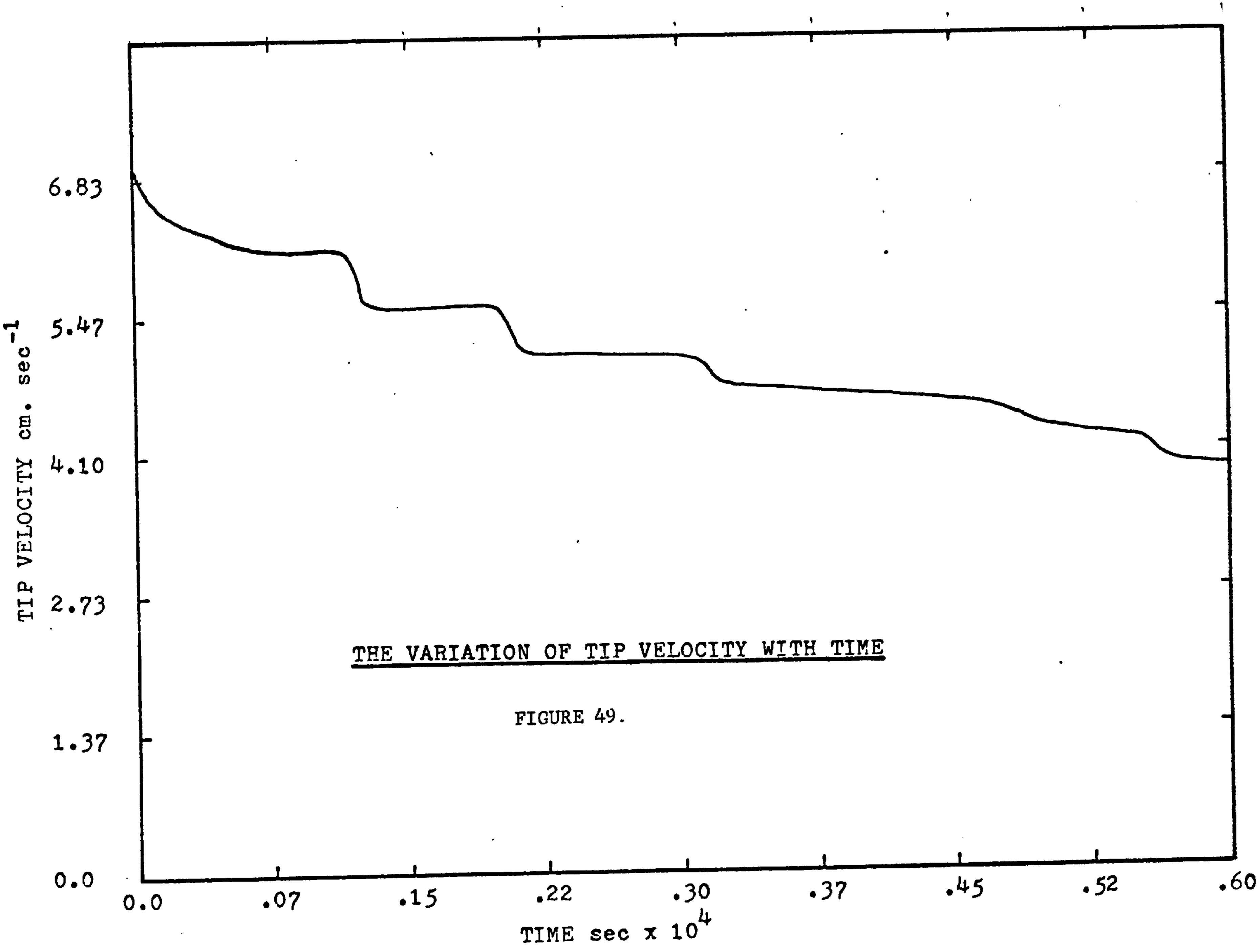
6.83
5.47
4.10
2.73
1.37
0.0
TIP VELOCITY cm. sec^{-1}
0.0
.07
.15
.22
.30
.37
.45
.52
.60
TIME sec x 10^4
THE VARIATION OF TIP VELOCITY WITH TIME

FIGURE 49.

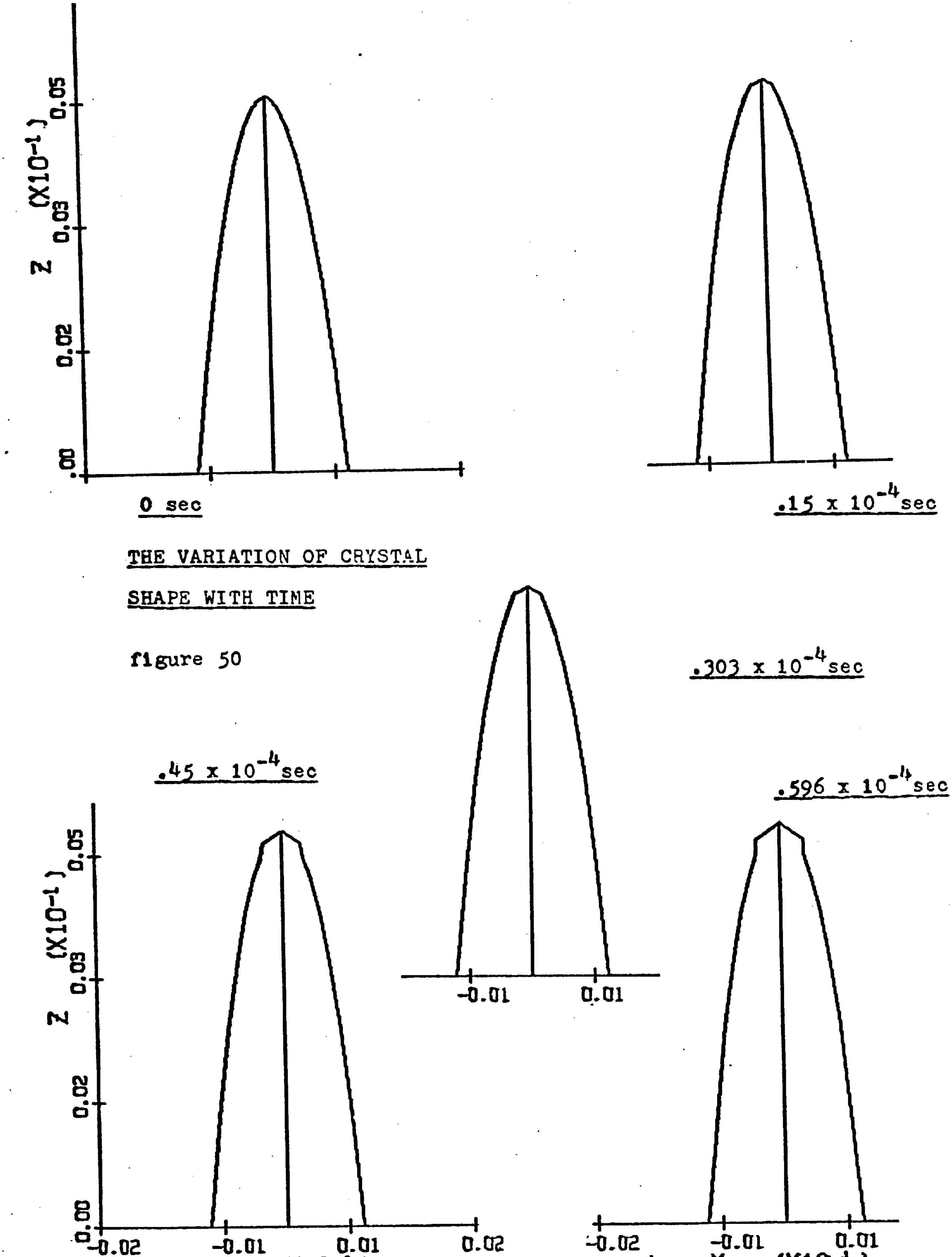

THE VARIATION OF CRYSTAL SHAPE WITH TIME

figure 50

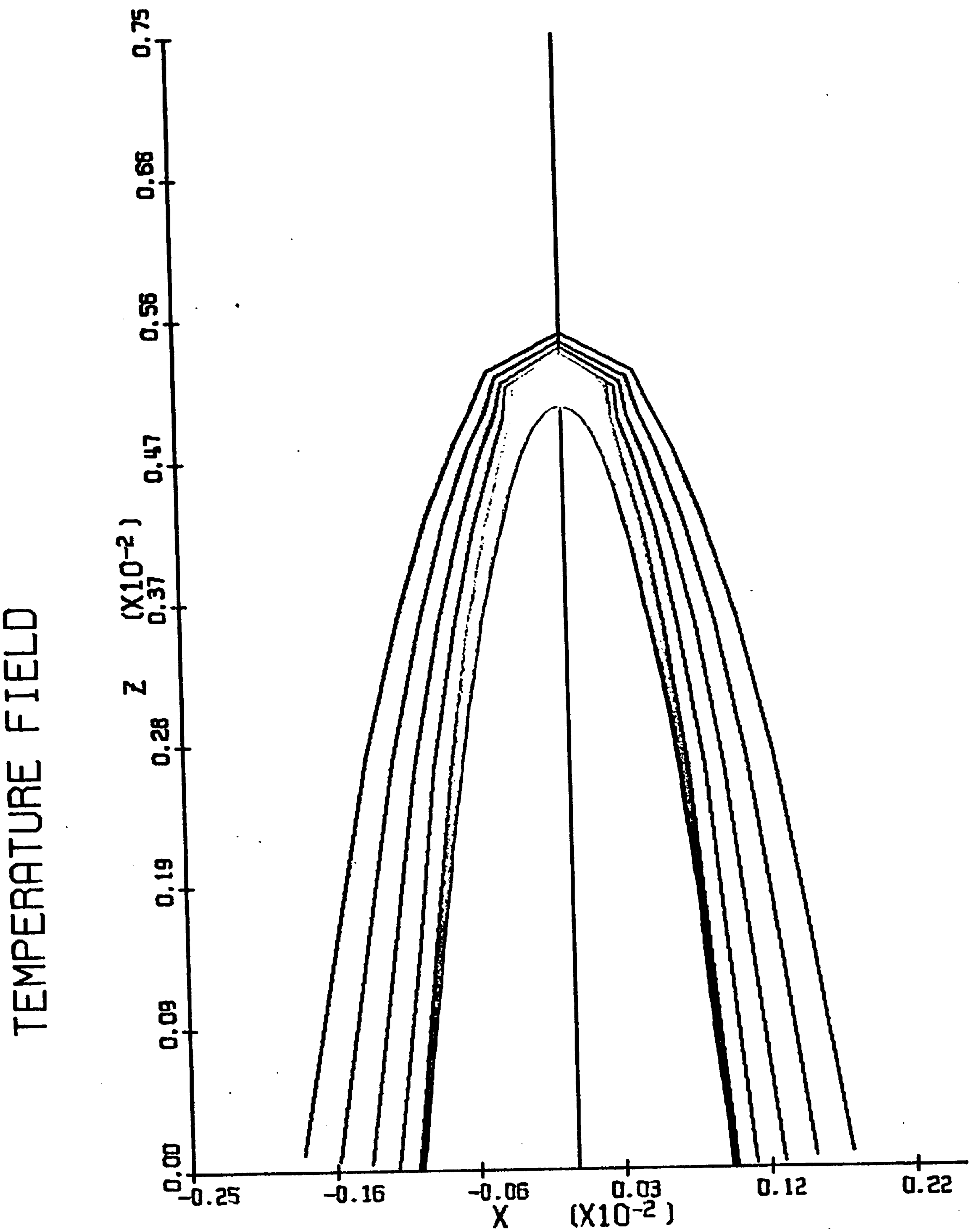

FIGURE 51. THE EXTENT OF CRYSTAL GROWTH DURING THE SIMULATION

near the tip. In consequence, the curvature of the projections cannot be properly estimated. This is made clear by Figure 51, which shows the tip shape to be triangular. Also noteworthy is the small extent of growth in the regions distant from the tip. Although the axial growth was fairly uniform over the whole surface, the rate tangential to the surface falls off drastically. This observation suggests that branches are unlikely to originate far from the crystal tip because perturbations have a very low rate of growth even if they are stable. This was exemplified by this study; axial growth rates did vary along the surface although the effect cannot be seen in the plots of the crystal shape.

CHAPTER X: THE DEVELOPMENT OF CRYSTAL SHAPE

1. The Maximum Velocity Principle

Previous treatments of dendrite growth such as that of Temkin[32] and Bolling and Tiller[39] and others have always given a relationship between growth velocity and tip curvature, without indicating a unique velocity at which the crystal must grow. Mathematically, the solution was unspecified; there were always two unknowns, the velocity and the tip radius. The dilemma was overcome by the arbitrary choice of the maximum velocity and the consequent tip radius as the velocity with which a crystal would grow. The basis for this assumption lay in the physical nature of the problem. It was assumed that in some way the crystal would "optimize itself". The need for such an assumption derives from a simplification introduced into the treatment of the problem, namely that a specific crystal could be assumed. A whole family of problems exist which face the same difficulties, for the same sort of reasons, and which require the postulation of principles such as "maximum penetration", "maximum rate of entropy production", each selected to fit the physical nature of the problem in hand.

The present treatment did not involve any of the arbitrary principles mentioned and should not have needed one because none of the physical variables were fixed arbitrarily. The study of the computer calculation shed new light upon the natural optimization process.

2. "Natural Selection" of Tip Shape

In the calculations described, it was found to be impossible to maintain an excessively sharp tip curvature. This is illustrated by

Figure 48. The tip velocity fell rapidly because of the depression of melting temperature, which not only reduced the temperature gradient in front of the tip, but also tilted forward the direction of maximum temperature gradient at each side of the tip, constricting the heat flow channel for the tip region. This is a description of one part of the selection process--an excessively sharp crystal tip falls back and consequently the curvature is reduced.

There seemed to be no penalty attached to excessively flat tip curvature. As illustrated by Figures 49, 50, and 51, it seems that the tip can become progressively flatter apparently without any process which can restore the tip shape and increase its velocity. It is believed that this is due to a flaw in the computer model and that in nature there does exist a mechanism which restores the tip sharpness. Figures 50 and 51 show that the slowing of the tip velocity (and reduction of its curvature) causes "buds" to form at the shoulders of the crystal. In the calculations, these projections accelerated continually and they were forming side branches on the main crystal. If they had been properly described by an adequate number of points on the crystal surface, they would have been penalized in precisely the same way as the crystal tip when it had excessive curvature. The consequence would be the same; primarily the orthogonal lines (the lines of steepest descent through the temperature field) would be tilted outwards, reducing the width of the heat flow channels for the "buds". In tilting sideways, they open up the heat flow channels for the tip region, driving the terminal region forward in a new burst of growth.

3. Oscillatory Growth

The study of dendrite growth by a computer model gave no hint that the crystal would ever attain a stable shape which would grow with a uniform velocity. Instead, a clear picture of dynamic development emerged in which the tip shape and velocity appeared to oscillate between two extremes. This picture is consistent with the observed dendrite morphology, since each oscillation leads to a side branch. Thus the branching frequency is the same as the oscillatory frequency. The model also showed clearly that branching must take place near the tip, because of the very slow growth of perturbations on the crystal stem. It seemed that the very flat temperature field adjacent to the stem of the crystal changed very slowly, and that side growth must be initiated near the tip if it is to lead to massive branches.

Because of the limitations of the model which was studied (not fundamental to the simulation of the problem) it was impossible to show the cyclic growth of the crystal. The model did, however, give strong clues concerning the basis for cyclic growth. The mechanisms of the cycle have already been discussed. The driving force for such a process exists in the increased mean rate of precipitation possible in such a sequence. A dendrite growing in a pure melt is limited by its ability to liberate latent heat of freezing. In oscillatory growth, the cycle through high and low curvature regimes incorporates the maximum amount of the liberated energy into the solid crystal as surface energy. This can be regarded as a means of carrying energy away from the growing surfaces. This is particularly easy to visualize if a moving coordinate system is referenced on the crystal tip. The curved surface and its associated energy continually moves down the crystal. The energy can also be seen as bands of high pressure at the root of side arms and low pressure in the regions between the arms. Such ideas can be extended to include the presence of solute (predicting bands of high and low solute content by analogy with pressure). When there is a density change upon solidification, oscillatory growth would cause the generation of a sonic wave in the liquid. For pure tine, dendrites growing into a bath undercooled 5°C, the frequency would be in the kilocycle range. Such sonic waves have never been sought in properly designed experiments.

Oscillatory growth of dendrites suggested by this model, recently received experimental backing from the work of Morris and Winegard[40]. Studying the growth of dendrites in a succinonitrile-5% camphor melt, they clearly showed the sequence followed in the generation of side branches. Their illustration of the steps of a growth cycle is shown in Figures 52(a)-(d). The branching process followed that suggested by the model with some precision. First the tip moved forward (Figure 52a). Then it slowed due to excessive curvature and "buds" formed at the shoulders. These "buds" grew rapidly outwards (Figures 52 c) and then the tip was again driven forward (Figure 52 d).

Ideas such as these give clues about analytical approaches which might bear fruit in the study of side branching. Clearly, the optimization of the oscillation frequency to give the maximum growth rate should give the optimum side branch rate, which with the rate of crystal growth would predict the crystal side branch spacing. They also predict that the mean rate of crystal growth should be higher than Temkin forecast, since some

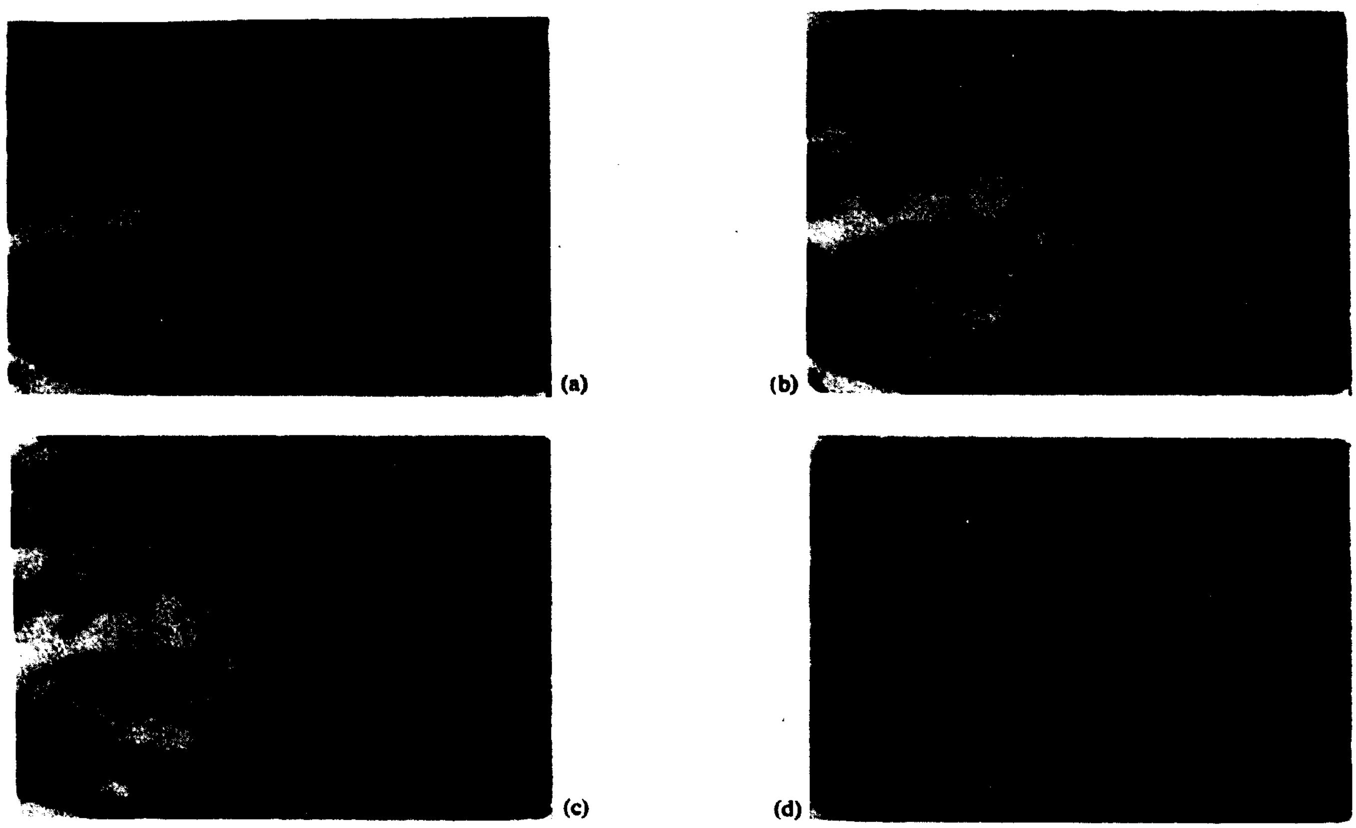

FIGURE 52. TIP OF A DENDRITE SHOWING PROGRESSIVE STEPS IN TIP MORPHOLOGY DURING THE COURSE OF ONE "PULSE CYCLE". THE TIME INTERVAL BETWEEN a AND b WAS 1.2 sec, BETWEEN b and c 1.2 sec, AND BETWEEN c and d 2.1 sec. MAGNIFICATION - 310X

After L. R. Morris and W. C. Winegard, J. Crystal Growth, (1967) 245-246 energy is removed by pressure waves in the solid, and by sonic energy in the liquid. This may well remove the need for the somewhat artificial reduction of the surface energy constant (see Chapter VII) which was necessary for Temkin to achieve agreement between theory and experiment.

CHAPTER XI: SPECIAL FORMS OF DENDRITE GROWTH

1. Varieties of Dendrite Growth

As far as this work is concerned, the characteristic which identifies dendrite growth is the direction of the gradients in the surrounding field. When the gradients slope away from the crystal, removing growth products, the growing crystal should possess some or all of the characteristics of a dendrite. Many of the special forms of dendrite have great commercial and theoretical interest. However, the case which has been simulated is perhaps the most simple form of dendrite; this has proved to be difficult to treat analytically. Therefore, the more complicated forms are even more suitable candidates for the model approach than the simple situation which has just been treated.

Special forms of dendrite growth result from three broad (and overlapping) groups of reasons. The first form derives from special types of attachment mechanism, which cause anisotropic growth. Examples of dendrites whose morphology is controlled in this way are to be found in whiskers, many of which result from the development of a single screw dislocation.[29] A second class (which includes all real dendrites) involves anisotropic crystal properties. In the model, which has just been made, the crystal was assumed to be isotropic, and hence, a body of revolution. In reality, there would be anisotropy in both of the possible angular directions. This controls the direction of growth[41] and strongly affects the branching of the crystal. The third class is one in which the far field boundary condition is not uniform. In this class are arrays of dendrites (in which the crystal is influenced by its neighbors), spherulities (where the members of the array are arranged at noncrystallographic angles), and in fact all highly branched single dendrites.

All the special forms of dendrite mentioned above can be simulated with varying amounts of difficulty by extension and modification of the model.

2. Arrays and Spherulites - Discussion

Dendritic arrays and spherulites are members of the same class of problem, in which the far field boundary conditions are modified. The new feature is the presence of a surface of symmetry, which lies between members of the array. In other words, the crystal and thermal field lying within such a surface forms the building block from which the whole array can be constructed. Repetition of this unit allows the construction of the whole array. This is illustrated by Figure 53, which shows schematically some of the isotherms and lines of heat flow of a parallel array of dendrites growing into a pure supercooled melt. The dotted lines are sections through the surface of symmetry and will be termed symmetry lines. Isotherms cross the surface of symmetry at right angles. The lines of heat flow tend to become parallel to the surface of symmetry as they move away from the crystal. The symmetry line has the properties of an orthogonal (heat flow) line, representing the line of heat flow from the roots of the two adjacent crystals, assumed to be an "infinite" distance from the tips in this parallel array.

The dendrite model which has already been described possessed an immovable orthogonal line which had many of the properties of the symmetry line. The lower orthogonal line was fixed, and the isotherms were allowed

UNDERCOOLED LIQUID BATH

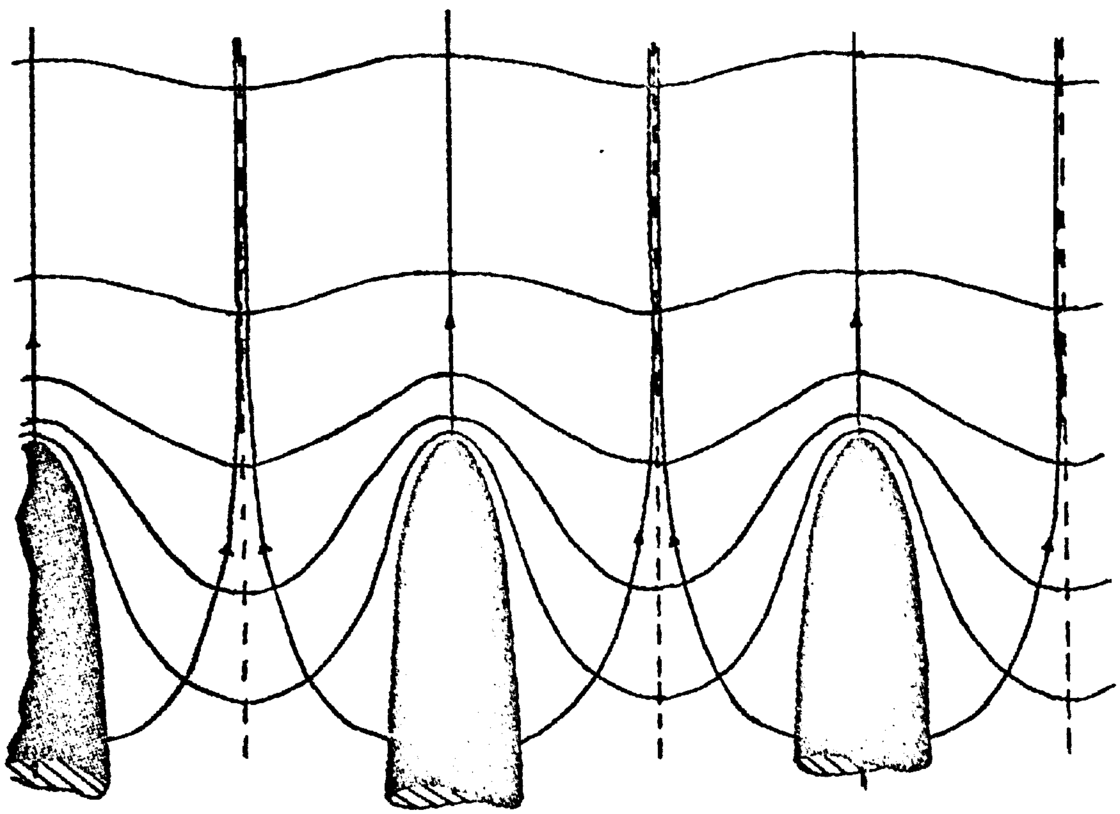

Figure 53 PARALLEL ARRAY OF DENDRITES: LINES OF HEAT FLOW AND ISOTHERMS (SCHEMATIC)

to slide along it like beads on a string. This suggested a simple modification which would permit simulation of arrays. If the orthogonal line from the root of the crystal were initially set up correctly, it would have the properties of the symmetry line, and the model would simulate a single member of an array of dendrites. One major reservation must be made, concerning the "body of revolution" assumption. Clearly, an array of dendrites of finite size and spacing does not have cylindrical or conical surfaces of symmetry. However, a cylinder or cone may not be a very bad approximation to the 6-sided "tubes" of an isotropic array.

3. Arrays and Spherulites - Initial Conditions

Preparation of the initial conditions presented the major problem in simulation of an array. Although some analytical studies have been made, there is no mathematical description of the thermal field, which is both general enough to treat parallel and spherulitic arrays, and simple enough to be readily employed in the preparation of initial conditions. A simple approach was eventually formulated which employed a numerical transformation of the coordinate system.

Referring to Figure 54, the position of the symmetry line was described by a reference point and its angle to the X ordinate. This line is shown dotted in the figure. Orthogonal (heat flow) lines were next fitted within the symmetry line. The lower orthogonal line was assumed to have a parabolic form, leaving the crystal surface at right angles, and approaching the symmetry line to touch at a remote point in the liquid bath. The orthogonal line adjacent to the tip was assumed to be unaffected by the neighboring dendrites. A series of cones (or cylinders) was then constructed.

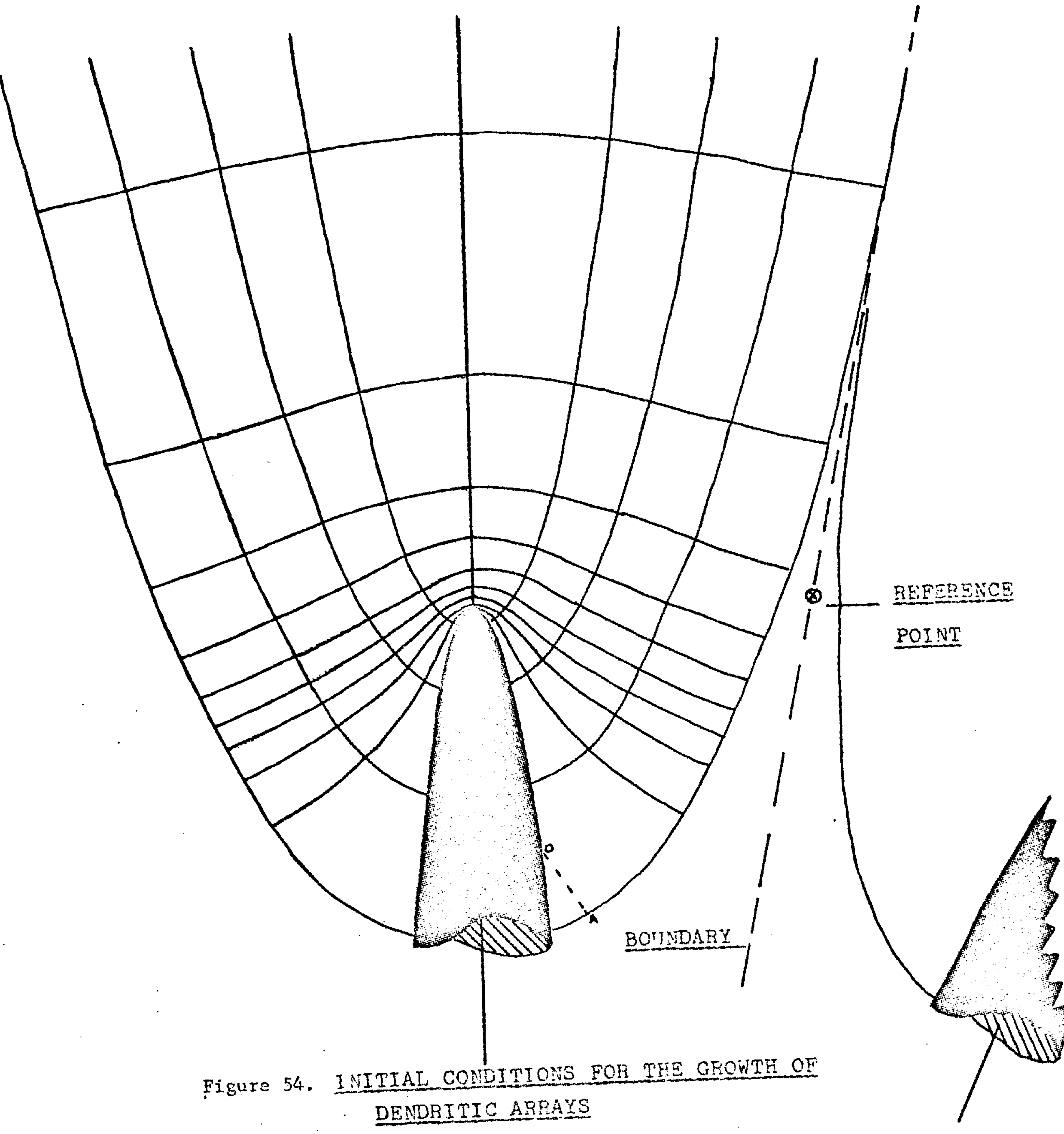

Figure 54. INITIAL CONDITIONS FOR THE GROWTH OF DENDRITIC ARRAYS

The cones were members of a family with a common apex (the meeting point of the symmetry lines which is the centre of a spherulitic system of dendrites). The apertures of the cones were spaced smoothly between the cone (or cylinder) of symmetry and the orthogonal adjacent to the axis, (K=3). Orthogonal lines from all reference points on the crystal surfaces were then constructed as parabolae, derived in the same manner as the lower orthogonal.

The isotherms were next produced. The positions of the isotherms on the axis of the crystal were assumed to be unaffected by the neighboring crystals and found from the E1 functions as before (Chapter VIII). Now the isotherms had to be projected from the axis, through the set of orthogonals. This was done numerically using a form of the "shooting" method described in Chapter VIII, Section 10. Part of the resulting network is shown in Figure 54, where the cone angle was 80 degrees, the reference point was 0.015 cm, and the tip radius was 1.0×10^{-4} cm.

4. Arrays and Spherulites - Results and Discussion

The sharp curvature of the orthogonal lines at the root of the crystal violated one of the assumptions of the model; i.e., that they could be approximated by straight lines running from one orthogonal to the next. Nearer the crystal tip, this problem disappeared, because the isotherms lay more closely together. The difficulty was overcome by moving the root of the crystal out to the dotted position O-A (Figure 54). This line also is at right angles to the lower orthogonal line.

The growth of the spherulite model shown in Figure 54 was simulated. Figure 55 shows a single crystal stem and the first four isotherms at the start of the calculation, and Figure 56 the same features after 100 loops

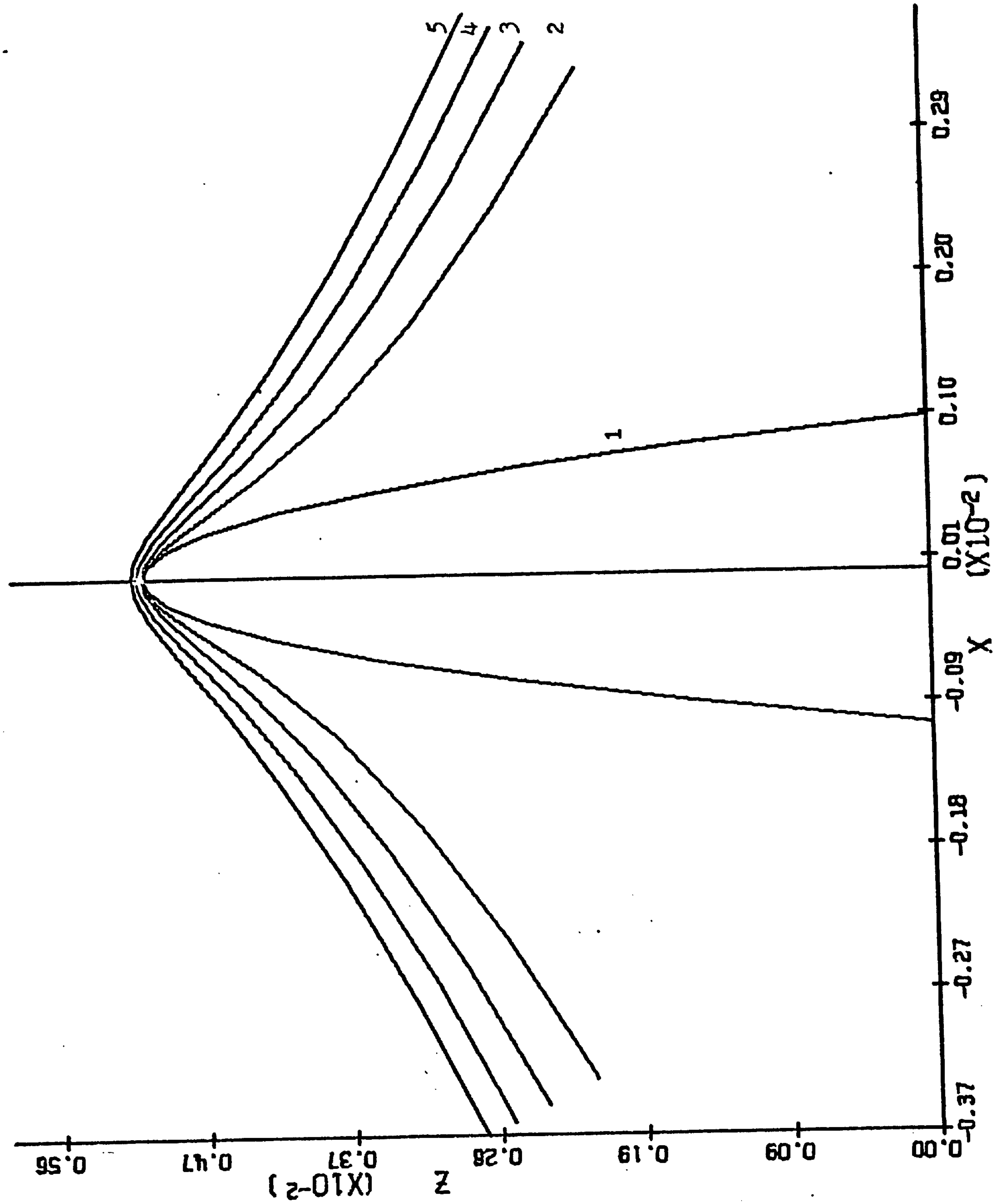

Figure 55. INITIAL CRYSTAL SHAPE AND ISOTHERM DISTRIBUTION

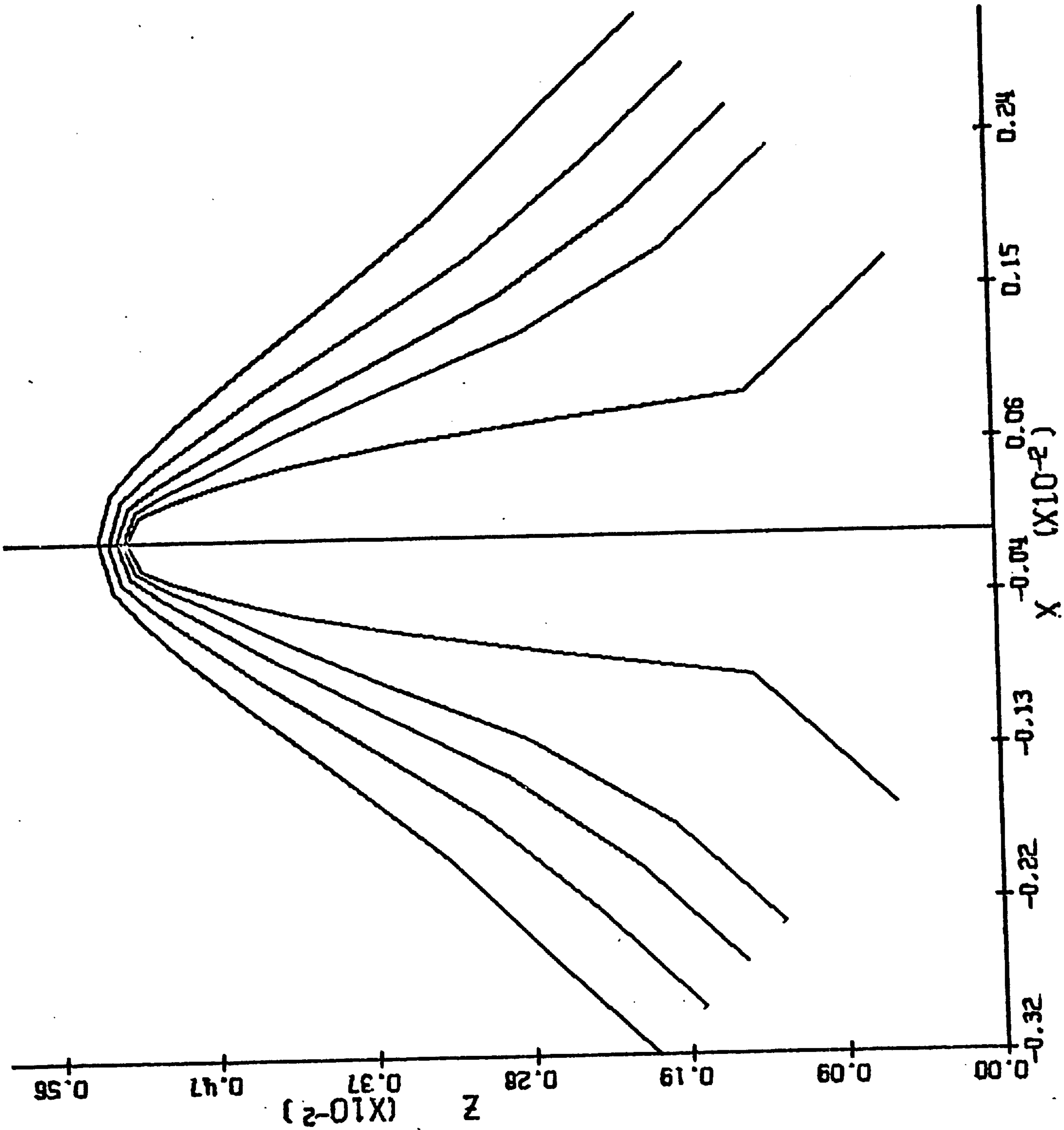

Figure 56. FINAL CRYSTAL SHAPE AND ISOTHERM DISTRIBUTION

(After 0.297×10^{-4} sec of growth) through the simulation. The distribution of the isotherms has changed considerably, tending to smooth the temperature profile along the orthogonals near the root of the crystal. The tip became progressively blunter (Figure 57) and the velocity slowed as shown in Figure 58. As might be expected, the tip velocity was slightly lower than for the single needle (about 4.5 compared to 6.5 cm sec^{-1}) and the axial velocity fell towards the root, finally being about half the axial velocity of the shoulders of the crystal.

The model used in this simulation is probably unrealistic, because it does not include a treatment of fluid flow. When an array of needles freezes with a density difference between solid and liquid, fluid is extruded from or sucked into the space near the roots of the needles[(42)]. Consequently, diffusive flow of heat (or particulary solute) may become of less significance than heat removal by fluid transport.

5. Anisotropic Crystals

Axial anisotropy is included in the model fairly readily. For example, surface energy was related to the angle of the tangent to the surface by the fairly simple law[(43)]:

$$\gamma_m = \gamma_t \cos \theta + \gamma_s \sin \theta \quad ,$$

where γ_m is the surface energy of the surface, γ_t is that of the tip of the crystal, γ_s that of the side face (at right angles to the tip). θ is the angle made by the tangent to the surface with the X axis. Inclusion of this law had a negligible effect upon the growth of the crystal, even when

$$\frac{\gamma_s}{\gamma_t} = 5 \quad ,$$

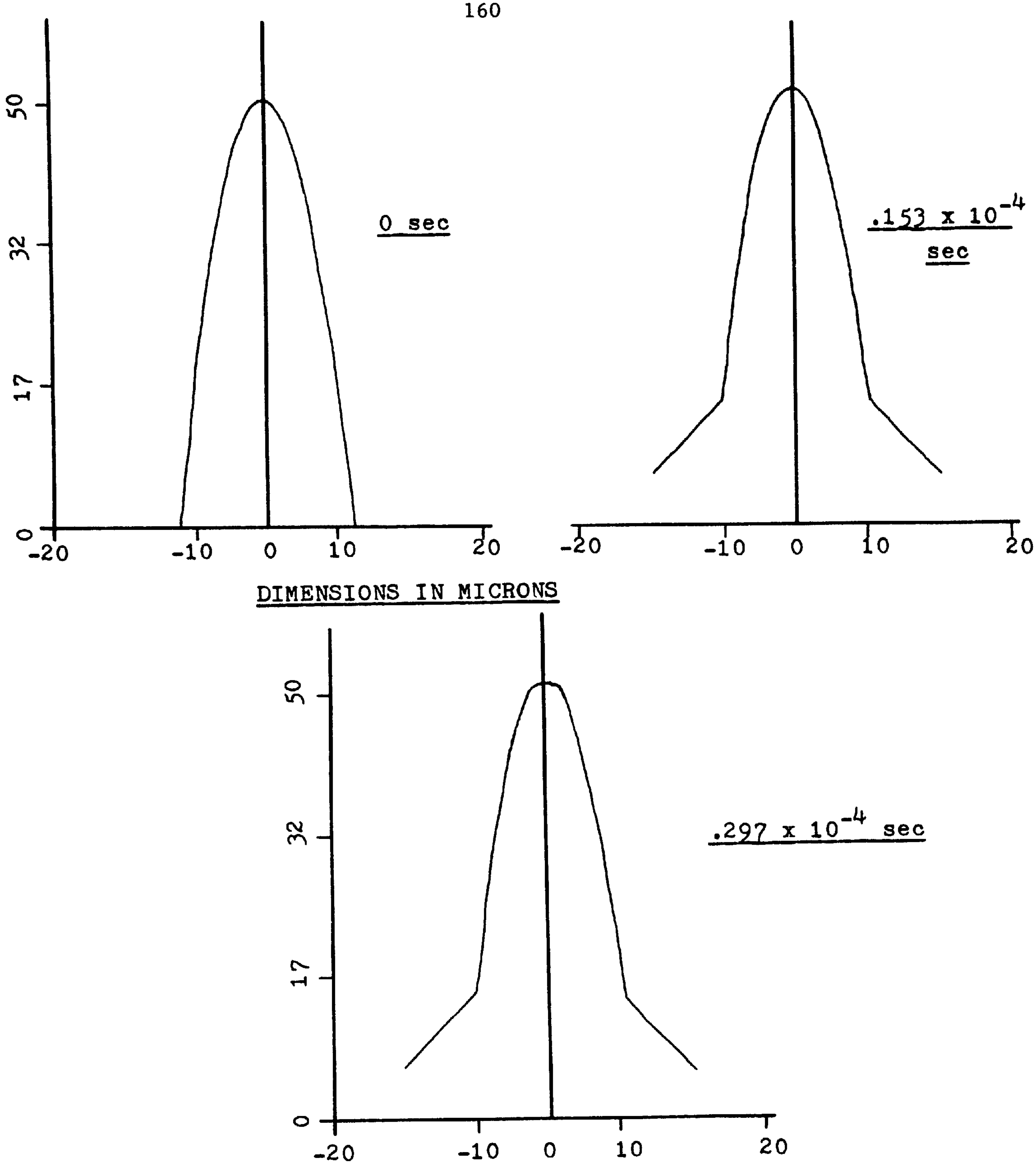

Figure 57 DEVELOPMENT OF CRYSTAL SHAPE IN THE ARRAY SIMULATIONS

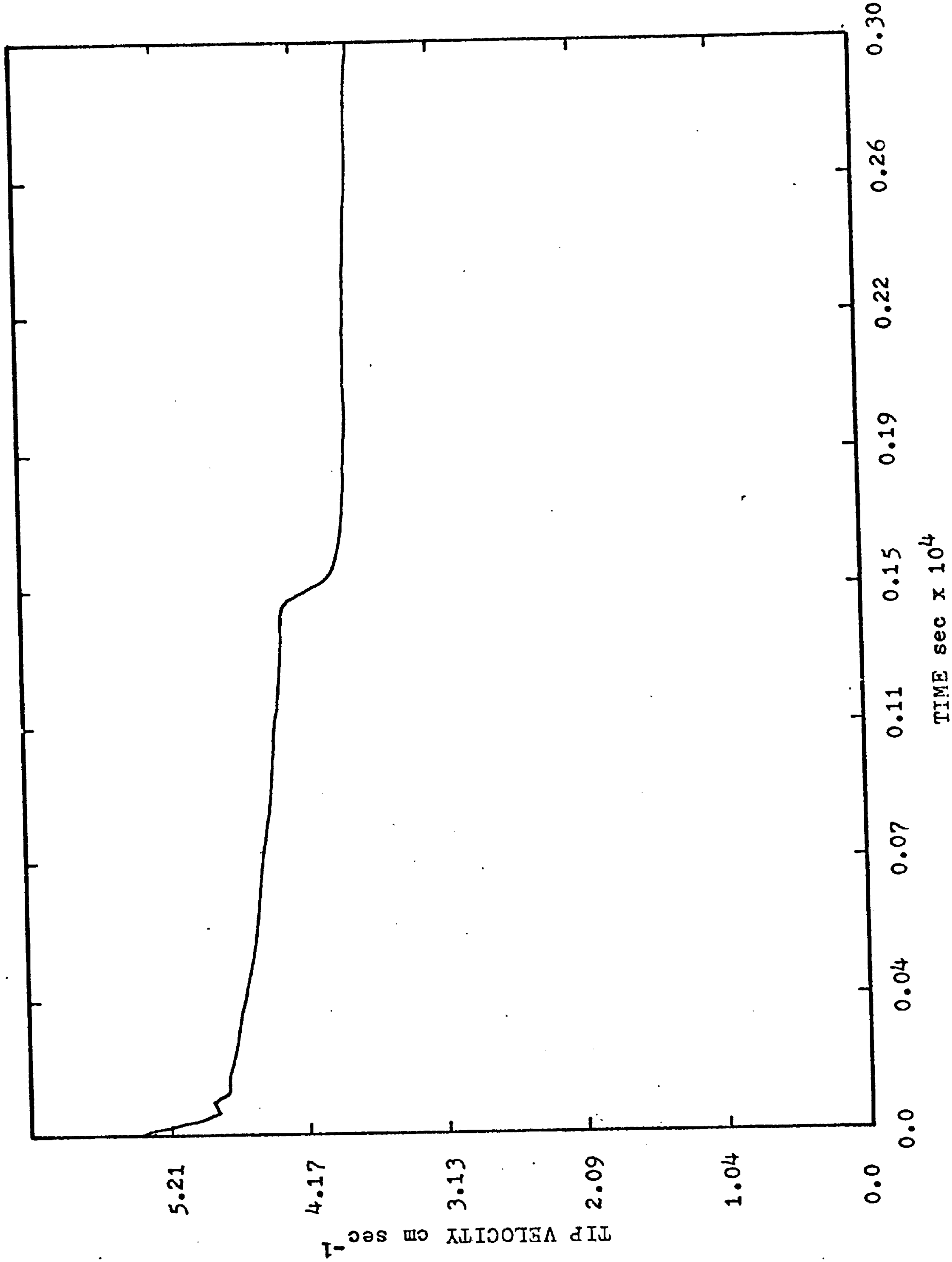

Figure 58. SIMULATION OF A DENDRITIC ARRAY: VELOCITY-TIME RELATIONSHIP

provided that γ_t was the same as in the isotropic crystal model. It would undoubtedly alter the frequency of any velocity fluctuation and hence the spacing of the side branches. This unfortunately could not be determined with the model which was employed.

The simple surface energy relationship was employed for illustrative purposes only. In a more meaningful examination of the effect of anisotropy, a more sophisticated model would be used. Certainly, the limiting feature would not be the computer model, since at the limit it could interpolate from a table of values with the expenditure of a trivial amount of computer time compared to the more complex routines which have already been described. A more difficult problem would be presented by the existence of "rotational" anisotropy, so that the crystal could no longer be simulated by a body of revolution. The preparation of an additional set of orthogonal planes to give a fully three-dimensional model would be a major undertaking.

SECTION D

GENERALIZATION OF THE IDEAS

CHAPTER XII: BUBBLE GROWTH AND ELECTRON BEAM DIFFRACTION

1. The Generality of Modelling Methods

The introductory section (Chapter II) defined two main areas of application of computer models. These were the use of models to enable basic knowledge to be extended to more complex situations of technological importance, and the use of models to study complicated materials problems on a basic level. The ideas were subsequently developed by the modelling of a casting system and by the more basic study of dendrite growth. Both of these problems were oriented towards the science and technology of solidification. The closing chapter will be devoted to the viewpoint that the particular application of the methods is unimportant, and that the problems which have been examined in detail are representative of classes of problems which occur in all areas of materials science.

One of the examples which will be briefly described here is primarily of interest because of the techniques which it illustrates. The Runge-Kutta method was mentioned in Chapter IX. This example illustrates the use of iterative procedures and the Predictor-Corrector method in a situation where there are large numbers of unknown quantities, representing a major stability problem. However, because this model was developed from the model of a casting described in Section B and applied to a problem of general interest in kinetics, it also illustrates the general utility of the modelling methods. That is, despite the fact that a model is developed for a specific situation only, the routines so developed can often be used in a wide range of simulations with only a small amount of modification.

Furthermore, although no attempt will be made to itemize methods and approaches, certain features will be seen to crop up with regularity.

A second example which pertains to electron microscopy highlights this comment. The treatment of electron beam patterns by the column method is strikingly similar to the model for dendrite growth which was developed independently.

2. Ostwald Ripening and Bubble Growth

A study of irradiated nuclear fuel material provided an interesting exercise in the stability of a numerical computation. In this problem, an array of bubbles of a range of sizes was assumed to be present in irradiated fuel material containing an excess of dissolved gas. The fuel was heated (out of the nuclear pile) to a temperature below the melting point. The aim was to simulate the behavior of real fuel in real experiments as a preliminary to the further development of the model for simulating the fuel behavior in-pile. The model followed the time variation of the bubble size distribution, the matrix gas content, and the swelling of the fuel. The assumptions upon which the model was based were that the bubbles were independent, with nonoverlapping diffusion fields, and that the material was isothermal. Both of these assumptions could be removed in a more complex model. Size changes occurred through the coupled diffusion of gas atoms and vacancies. This situation has been studied theoretically by Saralidze, et al.[44] who derived solutions to the terminal states but was unable to solve the problem for intermediate conditions.

Suppose the model to be set to study the development of an array of, say, 100 bubble sizes, each size group containing large numbers of bubbles. This approximates to a continuous size distribution. Consider the development of this array of bubbles during a time interval. Relationships exist for the change of gas content for a bubble of fixed radius and with fixed matrix gas content. Similarly, relationships exist for the change in radius of a bubble of fixed gas content. Conservation of gas atoms dictates the change in matrix gas content with change of gas content of all the bubbles. Thus, in this example, there are 201 unknowns and 201 equations. However, simultaneous solution of the equations is extremely time consuming and the process would have to be repeated many times to simulate the development of the array for any extensive period of time. Therefore, the equations were not solved simultaneously. If the matrix gas content were known throughout the time interval, and the radius of each of the bubbles were also known (this assumes that the time dependence is known) then the gas content change is specified for each size group. Taking the time dependence of radius and matrix gas content from the first terms of a Taylor series expansion of these variables, the unknowns are the terminal radii for each size group and the terminal gas content. For this example, these yield 101 unknowns. The computation can therefore be regarded as a calculation which cannot be expressed in closed form (Chapter IX) and treated as a stability problem. However, after a few cycles through the calculation, the rate of change in size of each group of bubbles is quite accurately known. Similarly, the change in matrix gas content with time is also known. Hence, the final size of all the bubbles and the final matrix gas content can be predicted with some accuracy. These predicted values are used in the first calculation to predict the changes in radii and matrix gas content which actually occur. The predicted values are then employed in a repeated calculation to obtain a more accurate estimate. This sequence is termed the Predictor-Corrector method.[38]

The results of simulations using this model give good agreement with experiment, and it is interesting to compare its predictions with the more simplified analytical results. Figure 59 shows the relationship between the mean bubble radius and time, compared to the result forecast by Speight (1968).[43] The analytical model simplified the problem to a single bubble radius. The computer model, for an array of sizes, showed the same general form of behavior, as would be expected. The mean radius at saturation (after a long period of time) was lower than the calculated value, as predicted by qualitative arguments. The change in matrix gas content with time is analogous to a dispersed spherical precipitate. The results are shown in Figure 60, revealing that the gas content change tended to follow an exponential law after an initial "ripening" period. This is in accord with simple kinetic theory.[46]

3. The Transmission of an Electron Beam Through a Foil

The variation in the transmitted intensity of electron beams after passage through a foil has been studied by Whelan, et al.[47], by Amelinckx[48], and other workers. The observations cannot be explained by simple theory, but require the dynamic theory of diffraction[47] (which takes into account the diffraction and attenuation of the beam on passage through the foil) in order to give even a qualitative explanation of the observations. The first quantitative descriptions were achieved for simple

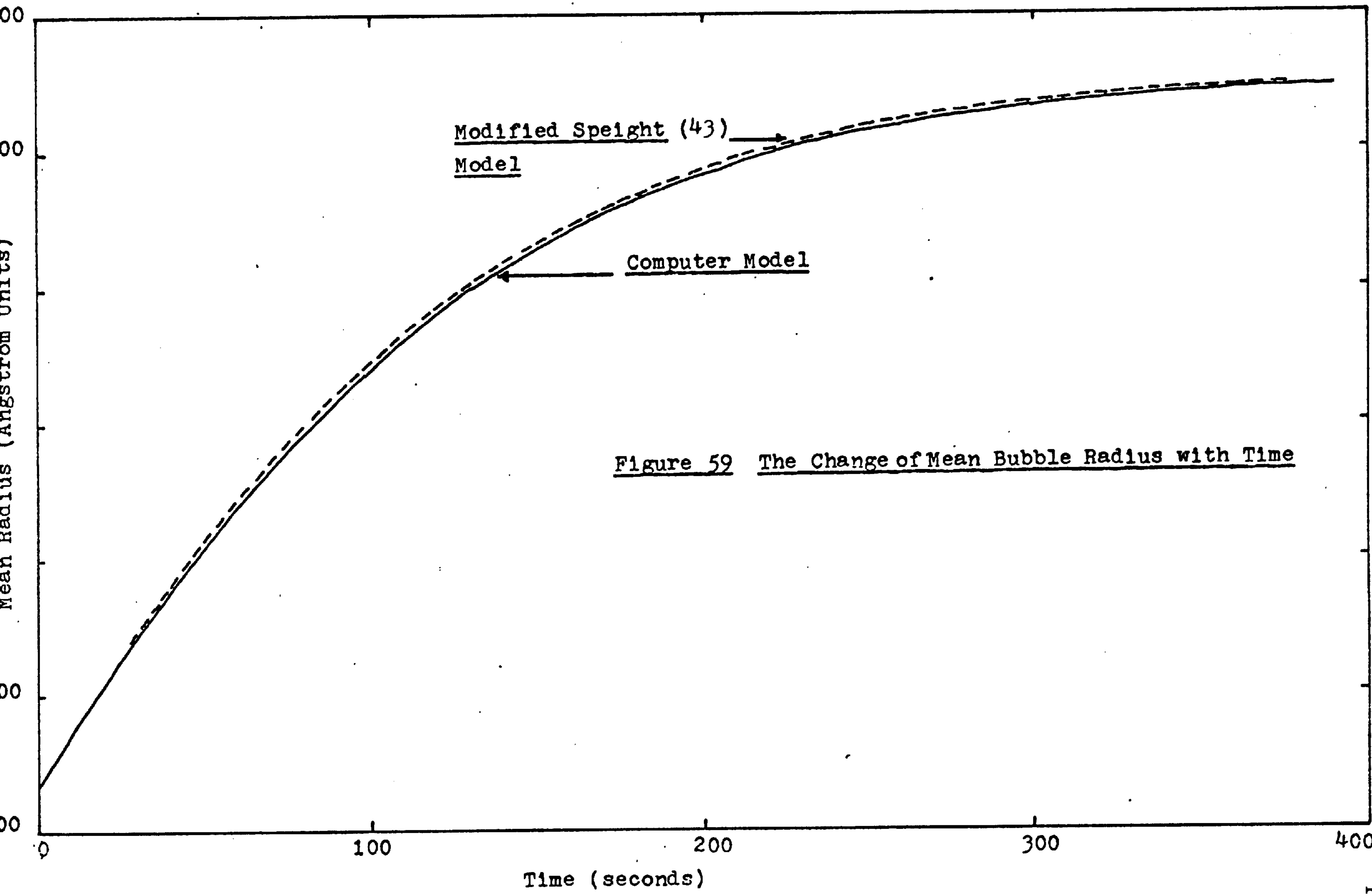

Figure 59 The Change of Mean Bubble Radius with Time

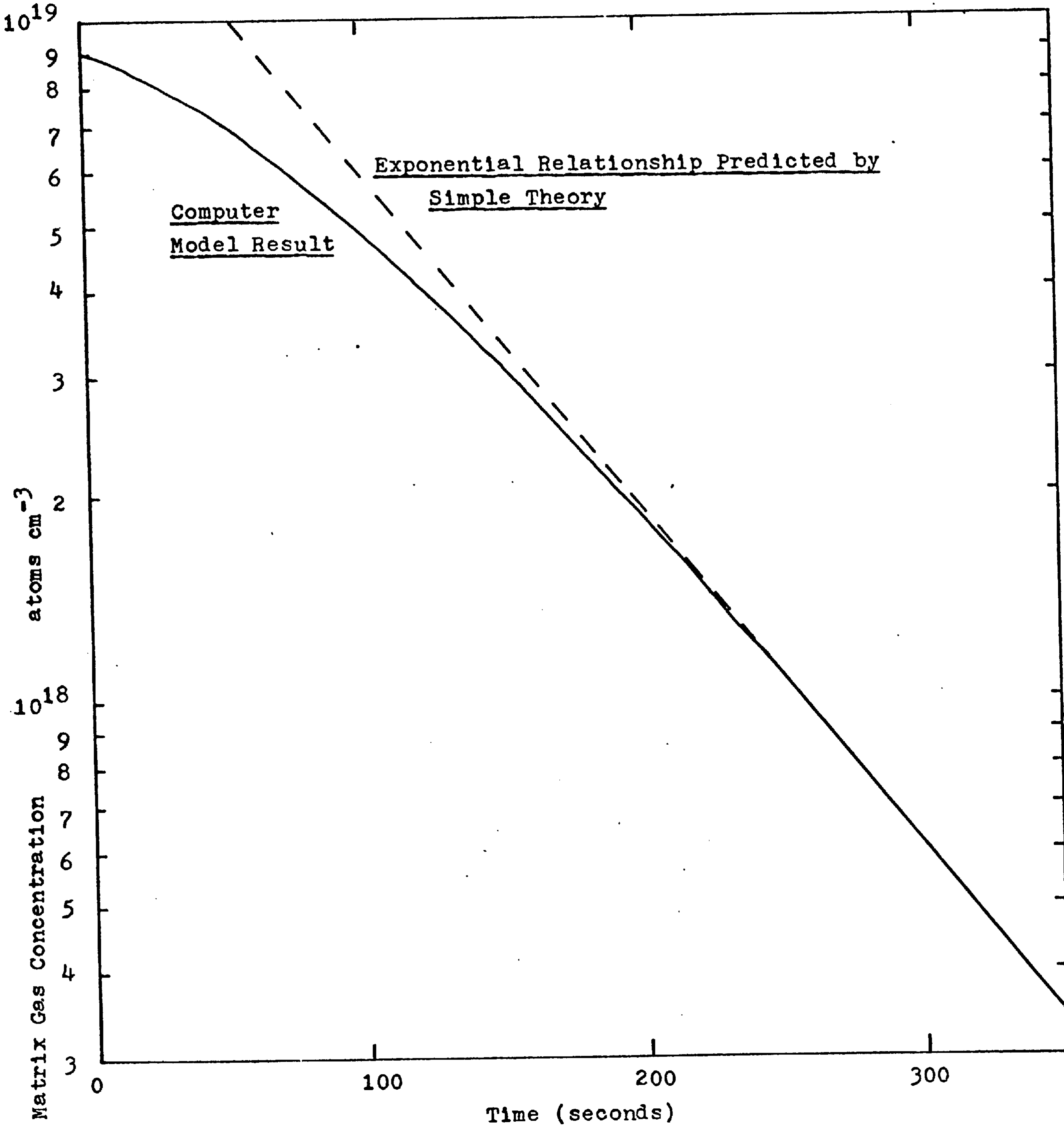

Figure 60 The Decay of Matrix Gas Supersaturation with Time

dislocation ribbons by Whelan and his coworkers using a computer model approach called the Column Method. This approach has been extended to the study of other more complex defects by Amelinckx and other workers. Further extension has been made by Dingley, Amelinckx, and Oldfield in unpublished work.

The Column Method is very analogous to the one-dimensional treatment of diffusive flow used in the study of dendrite growth in Chapter VII. A slice of a foil specimen is considered to be subdivided into a series of noninteractive columns. The individual columns are equivalent to the heat flow channels constructed orthogonally to the isotherms, and they have similar properties. However, because of the small angular scattering of the electron beam, they are constructed parallel to the incident beam. Each column is further subdivided into a set of thin layers which form compartments which are analogous to the compartments of the heat flow calculation. The compartments are treated by the computer in sequence--the intensity of the incident electron beam is determined by the previous history of the beam in passing through the preceding compartments. Using the value of the incident beam and assuming that the thickness of the compartment was very small (permitting first order approximations to be made to the Schrödinger equation), the transmitted and scattered components of the beam could be determined. The intensity of the transmitted beam was then used as the incident intensity for the next compartment and so on through the foil thickness. However, a compartment might differ from its neighbors, possessing a dislocation, stacking fault or other defect. This alters the extent of phase change and the scattering of the compartment. By incorporating defects in compartments as they occur in the foil, the trace to be expected from any defect or combination of defects can be synthesized. The synthetic traces can then be used to identify the defects present in real foils by characterizing the traces. This is illustrated by the results of Figure 61 taken from the book by Amelinckx[48]. This compares the experimental electron micrograph and synthetic traces for a foil containing dislocations.

The major difference between this model and that for diffusive flow is in the treatment of the conservation equations for the sets of compartments. In the diffusion problem, the set of equations is solved simultaneously. In this model, they are solved independently by neglecting the small doubly scattered portion of the beam. This approximation would result in instability in repeated calculations like those used to study the time variation of the temperature distribution. However, the passage of the electron beam is effectively independent of time and only one pass is made through the calculation. Thus, instabilities do not have the opportunity to develop.

4. Extension of the Ideas

In the second part of this chapter, the computer model for bubble growth was likened to the model for freezing cast iron from which it was developed. The similarity between these models likes in the spherical nature of the precipitates (bubbles in one case and eutectic cells in the other), and in the nucleation and growth features which will be present in the final simulation of a fuel material in a nuclear reactor. However, the models can be extended to other types of problems which possess common features. The bubbles can be compared to a set of noninteracting sites, which permit adsorption of other species. Adsorption of the species can be likened to

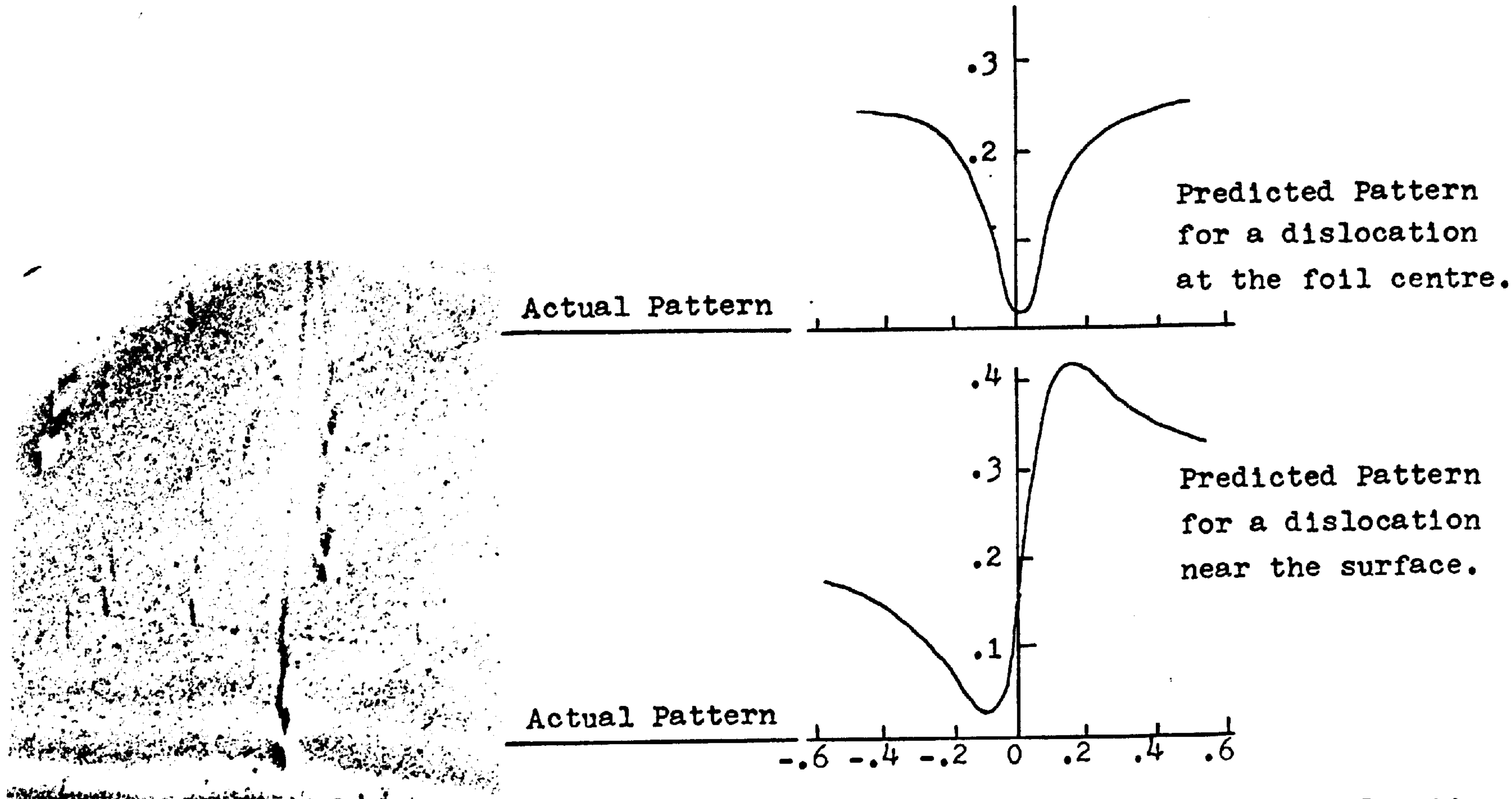

Oscillatory contrast observed as a screw dislocation approaches the surface of a tin disulphide crystal. The observed patterns can be compared to the computer predictions for the centre and edge regions of the foil. The predicted intensity is plotted against distance, with a total scale of about 1200 Angstroms.

Figure 61

the coupled diffusion of gas atoms and vacancies. Thus, this type of model could form the basis for the study of lattice statistics. Similarly, a whole class of problems could be studied by models of this type.

The study of dendrite growth indicates pathways to the study of many other sectors of materials science. The most obvious generalization stems from the similarity of growing voids in solids to growing dendrites. Whereas a dendrite growing in a liquid is an anisotropic crystal in an isotropic medium, a void or crack is an isotropic "crystal" of vacancies growing in an anisotropic medium. Thus, the dendrite model has a potential application in crack mechanics and in void migration in nuclear fuels. Extending the ideas further, the numerical transformation of coordinates developed within this model could be applied to a range of mathematical problems.

5. Summary and Conclusions

Computer model methods are an extension of the classic scientific approach, whereby a quantitative understanding of an unknown phenomenon can be gained by means of a conceptual system of well understood, simple processes. In this dissertation, computer model methods have been presented from a physical and relatively nonmathematical point of view. The objective was to emphasize the ease with which they can be applied to extend our knowledge of materials in situations which cannot be treated analytically.

To attain the objective set out for this work, the approach was developed in four stages.

(1) The first stage was designed to demonstrate that computer model methods are a simple extension of the analytical mathematical approach.

This was done by comparing the solution of a simple heat flow problem by Fourier methods with a solution by a computer model. Both approaches were shown to given identical results (Table 1) and to be similar in principle.

(2) In the second stage, a computer model was used to study the freezing of a casting. The basis for this section was that a complex phenomenon such as casting solidification embodies the interaction of a number of subprocesses. An understanding of each (expressed through a conceptual model) was included in a computer model to give an understanding of the system. A model for cast iron solidification was developed which accounted for all the main features experimentally observed in real castings. The model showed how some impurities such as sulphur impede eutectic growth by segregating at the solid-liquid interfaces;it also forecast the changes in microstructure which would result. Finally, it was used to predict the interaction between the eutectic nucleation and the solidification patterns within the castings. All these predictions could be checked experimentally or against published results. Certain discrepancies between the computer predictions and published results led to an experimental study of primary phase solidification. The computer predicted that the recalescence of the castings should lead to fragmentation of the primary austenite structure of the castings. This was confirmed by a series of experiments in which small ingots were quenched during the period of recalescence. This fragmentation has an important implication with regard to the mechanical properties of the material relating the modulus to the eutectic nucleation. The study of solidification patterns also provided a new explanation for the swelling of castings during freezing, an explanation which differed sharply from the accepted one.[51] A new description of cast iron solidification evolved from the computer study.[52]

(3) The third stage involved the application of computer model methods to more basic work. The objective was to use the computer model to eliminate the onerous mathematics (required in this case to solve diffusion problems) and allow the emphasis to be placed upon the more interesting aspects of the work (in this case the study of crystal growth). A model of a growing dendrite was developed. This problem was chosen because of the great difficulty experienced in the conventional treatments in the solution of the diffusion equations which govern the development of the crystal. The choice was reinforced by the widespread occurrence of this crystal morphology, which has great technological importance.

The dendrite growth problem was simplified, so that only the essential features of the growth process were included within the model. A needle of isotropic, pure material was considered to grow into a pure, undercooled melt. Thermal conductivity in the solid was assumed to be negligible. The computer model approach was then used to study the growth of such a dendrite, without the shape constraints which are normally required by the analytical approach. The results from the model were compared (when appropriate) within the predictions of the Temkin(32) and Ivantsov(31) equations.

Using the Ivantsov(31) equations to give initial conditions for the computation, the tip growth velocity for any crystal with tip radius smaller than or equal to the radius for optimum predicted by Temkin, rapidly blunted and assumed the radius and growth velocity predicted by his analytical treatment. Subsequently, the growth velocity fell more slowly, and the initial needle crystal developed branches just behind the tip. No branches developed nearer to the root of the crystal, because of the slow rates of crystal growth at positions distant from the tip. When the branches had developed, the model was no longer a good representation of the crystal, because the crystal had "grown out" of most of the original network points used to represent the tip region of the crystal. There were clear indications, however, that the tip region would have been driven forward again shortly after branching. Thus, it was surmised that the dendrite grows with a cyclic fluctuation in velocity, forming a new branch in each phase of slow growth.[53] This surmise was confirmed for dendrites of an organic material by Morris, et al.[40].

The model was then adapted to study some special types of dendrite growth. Dendritic arrays are of special interest. Dendrites become arrays through branching in definite crystallographic directions, and form a single crystal array. In some circumstances, the branches become oriented radially[52] and become spherulites. The model was adapted to simulate array growth and the growth velocity of a spherulite was studied. Using the appropriate physical constants for tin (as a matter of convenience to link with the preceding work), the growth of a spherulite was found to be slower than the corresponding single crystal needle. The particular case studied was slowed by approximately 20%. This result agrees with the observations made by Geering[54] in a study of ice spherulites. The model was also adapted to simulate non-isotropic crystals (in this case with varying surface energy).

(4) In the final stage, the preceding examples of basic and applied research were developed into new areas. The intention was to show that these models had more general application through the brief description of other situations into which they were adapted and by revealing analogous

phenomena which have not yet been studied by a computer model method.

The development of an array of bubbles of varying sizes, subject to coupled vacancy and gas migration, was discussed first. This was an extension of the model for casting solidification. The model had been developed in connection with nuclear fuels, and it has demonstrated good agreement with experiment and also with calculations which can be made to relate to terminal situations. The problem treated by this model is an example of a situation in which there is a statistical distribution of energy states which particles (in this case gas atoms and vacancies) can occupy, and processes (diffusion in this case) by which the occupancy of the states can change. The particular case which was described was a member of the family of problems in which a supersaturated matrix decays to give an array of spherical precipitate particles. Other applications might include lattice statistics and other nonequilibrium thermodynamic work.

Finally, the computer simulation of transmission electron microscopy was briefly discussed as an extension of the model for dendrite crystal growth. This approach, which has become almost a standard laboratory tool, illustrates an application to the solution of the wave equation. A similar approach could be applied to radiative heat transfer and particularly to coupled processes in which energy is transmitted through a medium by several mechanisms, including radiation.

It can be concluded that model methods have already demonstrated their utility in the study of materials. The method is still in its infancy--there is no question that as the procedures are further developed and as computers become more powerful, many of the most difficult materials problems will be solved by the use of computer models. Furthermore, the application of scientific ideas to technology through computer models promises to give real meaning to the title "Applied Science".

REFERENCES

1. A. A. Chernov and J. Lewis, J. Phys. Chem. Solids, 28, 2185-98 (1967).

2. H. S. Carslaw and J. C. Jaeger, Conduction of Heat in Solids, Clavendon Press (1947).

3. W. Oldfield, Graphite-Austenite and Iron Carbide-Austenite Eutectic Reactions During the Solidification of Cast Iron, Research in Cast Iron Seminar, Detroit (1964), Gordon and Breach.

4. H. Morrogh and W. Oldfield, Iron and Steel, 32 (September and October, 1959).

5. W. Oldfield, BCIRA Journal, 10, 17-27 (1962).

6. W. Oldfield, M.Sc. Thesis, University of Manchester (1961).

7. J. V. Dawson, BCIRA Journal, 9, 199-236 (1961).

8. J. V. Dawson and W. Oldfield, BCIRA Journal, 8, 221-231 (1960).

9. R. Vogel and G. Ritzau, Archiv fur das Eisenhuttenwesen, 4, 549-557 (1931).

10. W. A. Tiller, Research in Cast Iron Seminar, Detroit, 1964 (Gordon and Breach).

11. I. Minkoff, Joint Conference on Solidification, Brighton (England), December, 1967 (Iron and Steel Institute).

12. W. A. Johnson and R. F. Mehl, AIMME Tech. Pub., 1089, 5 (1939).

13. U. R. Evans, Trans. Faraday Soc., 41, 365 (1945).

14. W. Oldfield and J. G. Humphries, BCIRA Journal, 10, 315-324 (1962).

15. W. Patterson and D. Amman, Geisserei-Technisch-Wissenschaftliche Beiheft, 23, 1247-1275 (1959).

16. H. D. Merchant and J. F. Wallace, Modern Castings, 39, 63-72 (June, 1961).

17. J. W. Dews and A. G. Fuller, BCIRA Journal Res. and Dev., 7, 292-299 (1958).

18. A. G. Fuller, ibid, 7, 157-170 (1958).

19. I.C.H. Hughes, K.E.L. Nicholas, A. G. Fuller, and T. Szajda, AFS Transactions, 67, 149-165 (1959).

REFERENCES (Continued)

20. H. Morrogh, BCIRA Journal Res. and Dev., 5, 655-673 (1955).

21. M. Wilkinson and A. Helliwell, BCIRA Journal, 11, 439-450 (1963).

22. K. D. Lakeland, J. Austr. Inst. Metals, 10, 55-63 (1965), BCIRA Journal, 12, 634-650 (1964).

23. A. Boyles, "The Structure of Cast Iron", American Society for Metals (1947).

24. J. V. Dawson, B. Bach, and L.W.L. Smith, BCIRA Journal of Res. and Dev., 6, 249-258 (1956).

25. W. Oldfield, BCIRA Journal, 8, 177-192 (1960).

26. H. D. Keith and F.J. Padden, J. Appl. Phys., 34, 2409 (1963).

27. W. A. Tiller and J. W. Rutter, Can. J. Phys., 34, 96 (1956).

28. K. A. Jackson, J. D. Hunt, D. L. Uhlmann, and T. P. Seward III, Trans. AIME, 236, 149 (1966).

29. S. Amelinckx, J. Appl. Phys., 29, 1610 (1958), see also Ref. 46.

30. M. E. Glicksman and R. J. Schaefer, Joint Conference on Solidification, Brighton, England, December, 1967 (Iron and Steel Institute).

31. G. P. Ivantsov, Dokladi Akadamii Nauk, 58, 567-569 (1947).

32. D. E. Temkin, Soviet Physics-Crystallography, 7, 354-357 (1962).

33. D. Turnbull, Thermodynamics in Physical Metallurgy, American Society for Metals (1950).

34. G. R. Kotler and W. A. Tiller, Crystal Growth, Pergamon (1967).

35. G. R. Kotler, Ph.D. Thesis, Stanford University (1967).

36. M. Abramowitz and I. A. Stegun, Handbook of Math. Functions, Nat. Bur. of Standards, Appl. Math. Series 55 (1965).

37. B. Carnahan, et al., Applied Numerical Methods, Wiley (1964).

38. S. D. Conte, Elementary Numerical Analysis, 220, McGraw-Hill (1965).

39. G. F. Bolling and W. A. Tiller, J. Appl. Phys., 32, 2587 (1961).

REFERENCES (Continued)

40. L. R. Morris and W. C. Winegard, J. Cryst. Growth, 1, 245 (1967).

41. S. O'Hara, Acta. Met., 15, 231 (1967).

42. W. A. Tiller and S. O'Hara, Joint Conference on Solidification, Brighton, England, December, 1967 (Iron and Steel Institute).

43. Metal Interfaces, American Society for Metals (1952).

44. Z. K. Saralidze and V. V. Slezov, Soviet Physics-Solid State, 7, 1299 (1965).

45. M. V. Speight, Metal Science J., 2, 73 (1968).

46. F. S. Ham, J. Phys. Chem. Solids, 6, 335 (1958).

47. A. Howie and M. J. Whelan, Proc. European Conf. on Electron Microscopy, Delft, 1, 194 (1961).

48. S. Amelinckx,"The Direct Observation of Dislocations", Solid State Physics, Suppl. 6 (1964).

49. A. Art, R. Gevers, and S. Amelinckx, Phys. Stat. Solid, 3, 697 (1963).

50. W. Oldfield, ASM Trans. Quarterly, 59, 945 (1966).

51. K. E. L. Nicholas, BCIRA Journal of Res. and Dev., 9, 103-116 (1961).

52. W. Oldfield, G. T. Geering, and W. A. Tiller, Joint Conference on Solidification, Brighton, England, December, 1967 (Iron and Steel Institute).

53. W. Olfield, Numerical Study of Dendrite Growth, ibid.

54. G. T. Geering,Ph.D. Dissertation, Stanford University (1968).

APPENDIX A

MODEL FOR HEAT FLOW ACROSS A PLATE

APPENDIX A-1

MODEL FOR HEAT FLOW ACROSS A PLATE

OS/360 FORTRAN H

```
C ***MAIN PROGRAM
      COMMON R(100),AZ(100),BZ(100),CA(100),T(100),COND,TON(2),S,AI
      DIMENSION X(100)
C INSERT CONSTANTS
      TIME=0.0
      DTIME=0.1
      CONST=0.005
      S=1.0
      QT1=1.0
      QT2=1.0
      W=1.0
      J=20
      LAST=100
      IDRAW=10
C PUT IN INITIAL CONDITIONS
      DEL=W/FLOAT(J)
      TINIT=100.0
      DO 1 I=1,J
      S(I)=0.5*DEL+FLOAT(I-1)*DEL
      R(I)=DEL
      T(I)=TINIT
```

```
1      CONTINUE
       J1=J-1
       DO  100   LOOP=1,LAST
       DTIME=DTIME+0.2*DTIME
       TIME=TIME+DTIME
       COND=CONST*DTIME
       WRITE(6.20)  LOOP,TIME
C MODEL FOR THE OUTER BOUNDARY
       CALL BOUND2(QT1,DTIME,J)
       DO  2  I=2,J1
       N=J-I+1
C MODEL FOR A CENTRAL BOUNDARY
2      CALL CENTRE(N)
C MODEL FOR AN INNER BOUNDARY
       CALL INNER2(QT2,DTIME,1)
C SOLVE THE TWO EQUATIONS GOVERNING THE INNER COMPARTMENT'S TEMPERATURE
       DT=(CZ(1)-CZ(2))/(AZ(2)/BZ(2)-AZ(1)/BZ(1))
       T(1)=T(1)+DT
       J4=1
       WRITE(6,10)T(1),DT.J4
       DO  3  I=2,J
C CHANGE THE TEMPERATURES PRIOR TO A NEW LOOP
       DT=DT*AZ(I)/BZ(I)+CZ(I)
       T(I)=T(I)+DT
```

```
3     WRITE(6,10)  T(I),DT,I
      IF(FLOAT(LOOP)/IDRAW-LOOP/IDRAW.NE.0)  GO TO 100
      DO  4  I=1,J
      PX=X(I)
      PY=T(I)
4     CALL POINT1(I,PX,PY)
      CALL CURVE1(I,1,5)
100   CONTINUE
      CALL TITLE1('TEMP')
      CALL TITLE1('ERAT')
      CALL TITLE1('URE')
      CALL TITLE1('V X ')
      CALL GRAPH1(10.,'     T',7.0'     X')
10    FORMAT(10X,'T = ',E14.7,10X,'DT =',E14.7,10X,'J =',I4)
20    FORMAT(////,10X,'LOOP IS     ',I5,10X,'TIME IS ',E14.7)
      RETURN
      END
```

```
SUBROUTINE CENTRE(/N/)
COMMON R(100),AZ(100),BZ(100),CZ(100),T(100),COND,TON(2),S,AI
CLINF(RI,RO,P1,P2,P3)=(P2-P )/RO+(P3-P1)/(RI+RO)+(P2-P1)/RI
CSQF(RI,RO,P1,P2,P3)=(RI*(P3-P2)-RO*(P2-P1)/(RI*RO*(RI+RO))
SLOPEF(A,B,POS)=A+2.0*B*POS
VOLUME(AI,AO,U)=(AI+AO)*U/2.0
SLNC=CLINF(R(N),R(N+1),T(N-1),T(N),T(N+1))
SQC =CSQF(R(N),R(N+1),T(N-1),T(N),T(N+1))
TON(2)=TON(1)
POS=R(N)/2.0
TON(1)=SLOPEF(SLNC,SQC,POS)
AO=AI
AI=AREA(N,2)
WIDTH=(R(N)+R(N+1))/2.0
V=VOLUME(AI,AO,WIDTH)
AZ(N)=AI*COND/(2.0*R(N))
BZ(N)=AZ (N)+COND*AO*(1.0-AZ(N+1)/BZ(N+1))/(R(N)*2.0)+V*S
CZ(N)=COND*(AO*(TON(2)+CZ(N+1)/(2.0*R(N)))-AI*TON(1))/BZ(N)
RETURN
END
```

```
      SUBROUTINE BOUND2(QT1,DTIME,N)
      COMMON R(100),AZ(100),BZ(100),CZ(100),T(100),COND,TON(2),S,AI
      CLINF(RI,RO,P1,P2,P3)=(P2-P3)/RO+(P3-P1)/(RI+RO)+(P2-P1)/RI
      CSQF(RI,RO,P1,P2,P3)=(RI*(P3-P2)-RO*(P2-P1))/(RI*RO*(RI+RO))
      SLOPEF(A,B,POS)=A+2.0*B*POS
      VOLUME(AI,AO,U)=(AI+AO)*U/2.0
      SLNC=CLINF(R(N-1),R(N),T(N-2),T(N-1),T(N))
      SQC=CSQF(R(N-1),R(N),T(N-2),T(N-1),T(N))
      TB=SQC*(R(N)+R(N-1))**2+SLNC*(R(N)+R(N-1))+T(N)
      POS=R(N)/2.0+R(N-1)
      TON(1)=SLOPEF(SLNC,SQC,POS)
      AO=AREA(N,1)
      AI=AREA(N,2)
      WIDTH=R(N)
      V=VOLUME(AI,AO,WIDTH)
      AZ(N)=AI*COND/(2.0*R(N))
      BZ(N)=AI*COND/(2.0*R(N))+S*V
      CZ(N)=(-COND*AI*TON(1)+AO*QT1*DTIME)/BZ(N)
      WRITE(6,1)  TB
1     FORMAT(50X,'TEMPERATURE OF OUTER SURFACE IS ',E14.7)
      RETURN
      END
```

A-7

```
SUBROUTINE INNER(QT2,DTIME,N)
COMMON R(100),AZ(100),BZ(100),CZ(100),T(100),COND,TON(2),S,AI
VOLUME(AI,AO,U)=(AI+AO*U/2.0
TON(2)=TON(1)
AI=AREA(N,1)
AO=AI
WIDTH=R(N)
V=VOLUME(AI,AO,WIDTH)
BZ(N)=COND*AO/(2.0*R(2))
AZ(N)=BZ(N)+S*V
CZ(N)=(-COND*AO*TON(2)+AI*QT2*DTIME)/BZ(N)
RETURN
END
```

APPENDIX B

HEAT FLOW ACROSS A CYLINDER

APPENDIX B

HEAT FLOW ACROSS A CYLINDER

Referring to Figure B-1, R_1 is the radial diameter, R_{n+1} is the center line, equal to zero. R_1' is the radial center of mass of the outer annulus, R_2' of the next annulus, and so on.

Let the temperature of each annular volume (at the radial center of mass) be T_1, T_2, ...T_n, prior to a time increment in which heat is removed through the outer surface, latent heat liberated, and temperature changes occur.

Considering the outer shell:

$$-Q + J_2 + (LH)_1 - S\ V\ \Delta T_1 = 0 \quad , \qquad \text{(A-1)}$$

where

Q is the heat crossing the outer boundary into the mold

J_2 is the heat crossing the surface formed by radius R_2

$(LH)_1$ is the latent heat liberated in annulus 1

S is the specific heat per unit volume

V_1 is the annular volume

ΔT_1 is the change in temperature which takes place in the annulus of outer radius R_1.

$$J_2 = \Delta t\ k_1 \left\{ \frac{(T_2 - 1/2\Delta T_2) - (T_1 + 1/2\Delta T_1)}{R_1' - R_2'} \right\} A_1 \quad , \qquad \text{(A-2)}$$

where

k_1 is the mean thermal conductivity between R_1' and R_2'

Δt is the time increment

A_1 is the surface area of the interface between annuli 1 and 2.

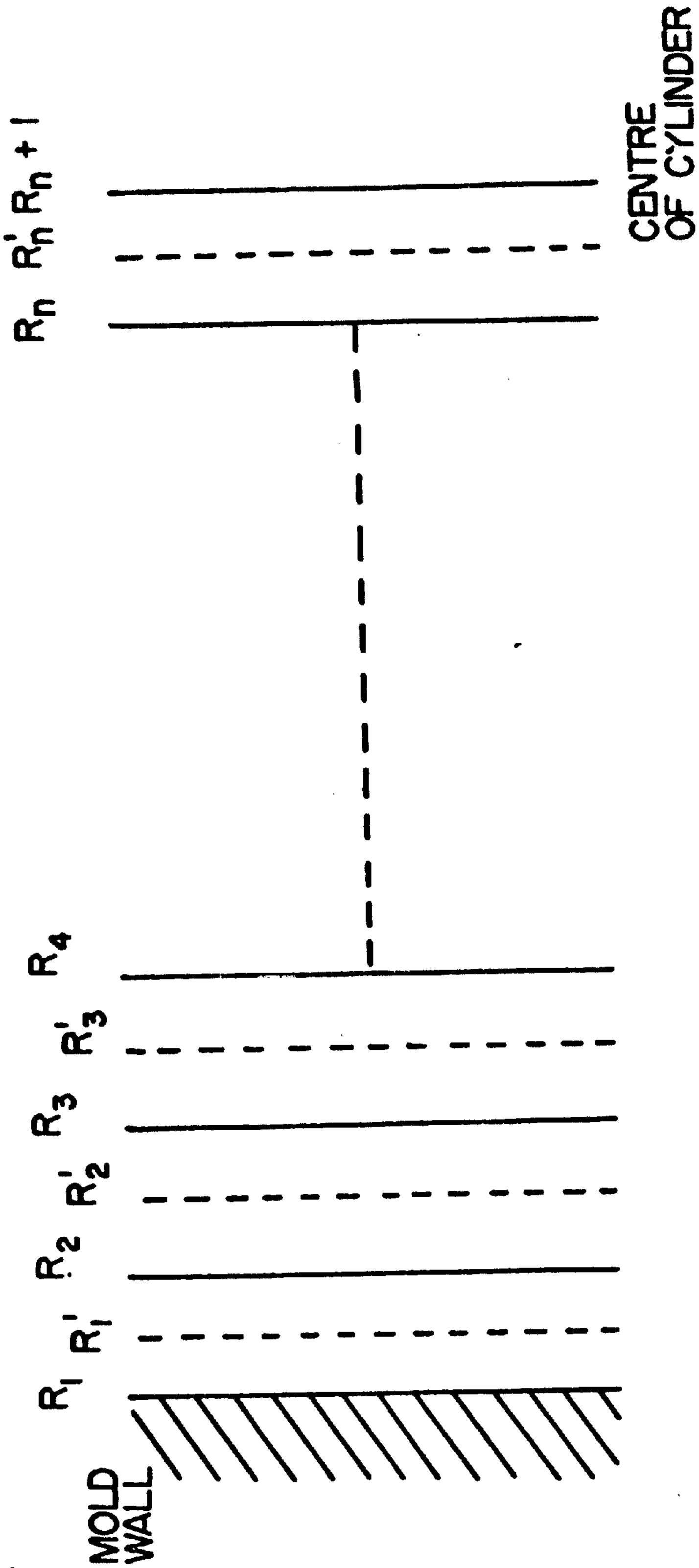

FIGURE B-1. HEAT FLOW ACROSS A CYLINDER

Substitution of equation (B-2) into equation (B-1) gives:

$$-Q + \alpha_1 \left\{ 2\,(T_2 - T_1) + (\Delta T_2 - \Delta T_1) \right\} + (LH)_1 - S\ V\ \Delta T_1 = 0 \quad .$$

In this expression:

$$\alpha_1 = \frac{\Delta t\ k_1\ A_1}{2(R_1{}' - R_2{}')} \quad .$$

Then:

$$\Delta T_1(\alpha_1 + S\ V) = \Delta T_2\ \alpha_1 + 2\alpha_1\ (T_2 - T_1) - Q + (LH)_1 \quad .$$

Rearranging:

$$\Delta T_1 = \frac{\alpha_1}{\beta_1}\ \Delta T_2 + \gamma_1 \quad .$$

In this expression,

$$\beta_1 = \alpha_1 + S\ V$$

$$\gamma_1 = \frac{(LH)_1 - Q + 2\alpha_1\ (T_2 - T_1)}{\beta_1} \quad .$$

Similar expressions can be derived for the other annuli. Using the same symbols, but replacing the 1 by i:

$$-J_i + J_{i+1} + (LH)_i - S\ V_i \Delta T_i = 0 \quad .$$

Retaining the definition of α:

$$2\alpha_i(T_{i+1} - T_i) + \alpha_1(\Delta T_{i+1} - \Delta T_i) - 2\alpha_{i-1}(T_i - T_{i-1}) - \alpha_{i-1}$$
$$(\Delta T_i - \Delta T_{i-1}) + (LH)_i - S\ V_i\ \Delta T_i = 0 \quad . \qquad \text{(B-4)}$$

However, ΔT_{i-1} can be related to ΔT_i as shown in the first calculation:

$$\Delta T_{i-1} = \frac{\alpha_{i-1}}{\beta_{i-1}}\ \Delta T_i + \gamma_{i-1} \quad .$$

Substituting this relation into equation (B-4)

$$-\Delta T_i \left[\alpha_i - (1 - \frac{\alpha_{i-1}}{\beta_{i-1}}) + \alpha_1 + S\ V_i\right] + \Delta T_{i+1}\ \alpha_i + 2\alpha_i(T_{i+1} - T_i)$$

$$- 2\alpha_{i-1}(T_i - T_{i-1}) + (LH)_i = 0 \quad .$$

Hence, the result is again obtained:

$$\Delta T_i = \gamma_i + \frac{\alpha_i}{\beta_i}\Delta T_{i+1} \quad , \tag{B-5}$$

where

$$\beta_i = \alpha_{i-1}(1 - \frac{\alpha_{i-1}}{\beta_{i-1}}) + \alpha_i + S\ V_i$$

$$\gamma_i = \frac{2\alpha_i(T_{i+1}-T_i) - 2\alpha_{i-1}(T_i-T_{i-1}) + \alpha_i\gamma_{i-1} + (LH)_i}{\beta_i}$$

Finally, the center annulus can be treated. In this case, there is no inner surface, so that a heat flux flows only into the n-1 annulus. The conservation equation can be written:

$$-J_n + (LH)_n - S\ V_n\ \Delta T_n = 0 \quad .$$

Substituting the equation for J_n (equation B-2):

$$-2\alpha_{n-1}(T_n-T_{n-1}) - \alpha_{n-1}(\Delta T_n-\Delta T_{n-1}) + (LH)_n - S\ V_n\Delta T_n = 0 \quad .$$

Substituting for ΔT_{n-1}:

$$-\Delta T_n\ \ \alpha_n - (1 - \frac{\alpha_{n-1}}{\beta_{n-1}}) + S\ V_n \quad - 2\alpha_{n-1}(T_n-T_{n-1}) + \gamma_{n-1}\alpha_{n-1} + (LH)_n = 0.$$

Rearranging:

$$\Delta T_n = \frac{2\alpha_{n-1}(T_n-T_{n-1}) - \gamma_{n-1}\alpha_{n-1} - (LH)_n}{\alpha_{n-1}(1 - \frac{\alpha_{n-1}}{\beta_{n-1}}) + S\ V_n} \quad .$$

This result gives the change in temperature at the center of the bar. Since all the coefficients α, β, and γ are stored in the computer memory, they can be used in conjunction with equation (B-5) to yield the new temperature at all stations across the bar.

APPENDIX C

PROGRAM LISTING - MAIN PROGRAM FOR THE PLOTTING OF COOLING CURVES

APPENDIX C

MAIN PROGRAM FOR THE PLOTTING OF COOLING CURVES

OS/360 FORTRAN H

```
C      MODEL FOR FREEZING SPHERICLE CELLS, ROUND BAR DIAM D, WITH GAMMA
       INTEGER IN(60,13)
       DIMENSION R(300,20),X(20),COND(20),S92),FVS(20),XMIN(20),J(20),
      1C(2),P(300,20),SA(20),NE(20),E(20),V(20),DX(20),ALH(20),RAD(21),
      2ATEMP(19),BTEMP(19),TIME(19),AZ(20),BZ(20),CZ(20),RID(20),
      3BLH(20),CLOST(20),AG(20),DAT(13)
       COMPO(TEMP)=CEU+(TEMP-1153.0)/SLOPEV
       READ(5,1)  DAT(1),(IN(K,1),K=1,60)
       NRUNS=DAT(1)
       DO  95  KOUNT=1,NRUNS
C      INITIALLIZATION
       IPLOT=KOUNT+1
       WRITE(6,6)
       DO  1000  I=2,13
       READ(5,1)  DAT(I),(IN(K,I),K=1,60)
 1000  WRITE(6,1) DAT(I),(IN(K,I),K=1,60)
       WRITE(6,6)
       D=DAT(2)*2.54
       DQ=DAT(3)
       A=DAT(4)
       B=DAT(5)
       BB=DAT(6)
       AA=DAT(7)
```

```
      TLIQ=DAT(8)
      SLOPEV=DAT(9)
      BL=DAT(10)
      CEU=DAT(11)
      SK=DAT(12)
      NDIV=DAT(13)
      RAD(NDIV+1)=0.0
      NIP=0
      LOP=0
      EU=1153.0
      C(1)=0.378
      C(2)= 0.189
      S(1)=1.66
      S(2)=1.44
      AL=430.0
      DQ=DQ*3.1459*D*D/240.0*(S(1)-AL/(SLOPEV*(1.0-SK)*COMPO(1158.0)))
      DT=3.142*D*D*0.20 /DQ*BB
      Q=DQ*DT
      DO  49  K=1,NDIV
      RID(K)=D/2.0*SQRT(FLOAT(2*NDIV+1-2*K)/FLOAT(2*NDIV))
49    RAD(K)=D/2.0*SQRT(FLOAT(NDIV+1-K)/FLOAT(NDIV))
      DO  210  K=1,NDIV
210   CLOST(K)=(RAD(K)*RAD(K)*RAD(K)-RAD(K+1)*RAD(K+1)*RAD(K+1))*2.0/3.0
     1/(RAD(K)*RAD(K)-RAD(K+1)*RAD(K+1))
      DO  50  K=1,NDIV
      AG(K)=0
```

```
      E(K)=OXMIN(K)=EU
      ALH(K)=1.0E-9
      FVS(K)=1.0E-9
      V(K)=3.142*(RAD(K)*RAD(K)-RAD(K+1)*RAD(K+1))
      X(K)=1170.0
      FVS(K)=0
      J(K)=0
      SA(K)=0
      DO  50  L=1,300
      R(L,K)=0
50    P(L,K)=0
      AT=DT
      II=1
      WRITE(6,4)D,DQ,Q,B,BB,C(1),C(2),S(1),S(2),EU,AL,TLIQ,SLOPEV,BL
     1,CEU,SK
      WRITE(6,6)
      WRITE(6,2)
C     END OF INITIALLIZATION
C     SCANS THE SUBVOLUMES IN TURN
C     I IS THE SUBVOLUME INDEX
C     M IS THE SIZE INDEX
51    DO  61  I=1,NDIV
      IF (TLIQ-X(I)) 52,52,53
52    ASSIGN 101 TO NEXT
C     X(I) IS ABOVE THE LIQUIDUS (NEXT=101)
      GO TO 57
```

```
53     ASSIGN 54 TO NEXT
C      X(I) IS AT OR BELOW THE LIQUIDUS (NEXT=54)
57     IF (EU-X(I)) 100,100,58
58     IF(1.0-FVS(I)) 59,59,60
C      X(I) BELOW THE EUTECTIC TEMPERATURE
59     II=2
C      COMPLETELY SOLID
       NIP=1+NIP
       GO TO 101
60     IF (300-J(I))
100    GO TO NEXT,(101,54)
C      X(I) AT OR ABOVE THE EUTECTIC TEMPERATURE
54     CALL GAMM(V,DX,SLOPEV,ALH,AG,FVS,BL,I,AMOUNT,CEU,SK,X,EU)
C      X(I) ABOVE THE EUTECTIC BUT BELOW THE LIQUIDUS
C      COOL
101    COND(I)=C(II)
C      X(I) ABOVE BOTH EUTECTIC AND LIQUIDUS
       ALH(I)=0
       GO TO 61
C      END OF COOL
C      FREEZE
150    SA(I)=0
       IF (X(I)-XMIN(I)) 151,153,153
151    J(I)=J(I)+1
       JI=J(I)
```

```
C APPLY THE NUCLEATION LAW
      P(JI,I)=(1.0-FVS(I)*A*(2.0*(EU-X(I))*(XMIN(I)-X(I))+(XMIN
     1/(I)-X(I))*(XMIN(I)-X(I)))*V(I)
      IF   (P(JI,I)-0.01) 152,149,149
 149  XMIN(I)=X(I)
      E(I)=E(I)+P(JI,I)
      GO TO 153
 152  P(J I,I )=0
 153  DR=B*((EU-X(I))**AA)*DT
      JI=J(I)
      DO  156  M=I,JI
      R(M,I)=R(M,I)+DR
C     CORRECT FOR CELL-MOLD WALL CONACT
      FLOST=(R(M,I)+CLOST(I)-D/2.0)/(2.0*R(M,I))
      IF  (FLOST)154,154,155
 154  SA(I)=12.566*R(M,I)*R(M,I)*P(M,I)+SA(I)
      GO TO 156
 155  SA(I)= 12.566*R(M,I)*R(M,I)*P(M,I)*FLOST+SA(I)
 156  CONTINUE
C     CORRECT FOR CELL-CELL CONTACT
      SA(I)=SA(I)*(1.0-FVS(I))
      FVS(I)=SA(I)*DR/V(I)+FVS(I)
      BLH(I)=SA(I)*DR*AL
      COND(I)=C(1)-FVS(I)*(C(1)-C(2))
      NIP=0
C     END OF FREZZE
```

```
      CALL GAMMA(V,DX,SLOPEV,ALH,AG,FVS,BL,I,AMOUNT,CEU,SK,X,EU)
      AL(I)=ALH(I)+BLH(I)
61    CONTINUE
C     SOLVE
200   CONTINUE
      DO  199  K=2,NDIV
      L=NDIV-K+1
199   COND(L)=(COND(L)*(RAD(L)-RID(L)+COND(L-1)*(RID(L-1)-RAD
     1(L)))/(RID(L-1)-RID(L))
      DO  198  K=2,NDIV
198   AZ(K)=COND(K)*DT*3.142*RAD(K)/(RID(K-1)-RID(K))
      MOL=NDIV-1
      BZ(NDIV)=AZ(NDIV)+V(NDIV)*(S(1)-FVS(NDIV)*(S(1)-S(2)))
      CZ(NDIV)=(ALH(NDIV)-AZ(NDIV)*(X(NDIV)-X(MOL))*2.0)/BZ
     1(NDIV)
      DO 201 LI=2,MOL
      I=NDIV+1-LI
      BZ(I)=AZ(I+1)*(1.0-AZ(I+1)/BZ(I+1))+AZ(I)+V( I)*(S(1)
     1-FVS(I)*(S(1)-S(2)))
201   CZ(I)=(AZ(I+1)*(X(I+1)-X(I)+CZ(I+1)*0.5)+ALH(I)*0.5-AZ
     1(I)*(X(I)-X(I-1)))/BZ(I)*2.0
      BZ(1)=AZ92)*(1.0-AZ(2)/BZ(2))+V(1)*(S(1)-FVS(1)*(S(1)-S(2)))
      CZ(1)=(AZ(2)*(2.0*(X(2)-X(1))+CZ(2))+ALH(1))/BZ(1)
      DX(1)=DZ(1)-Q/BZ(1)
      X(1)=X(1)+DX(1)
      DO 202   I=2,NDIV
```

```
      DX(I)=CZ(I)+AZ(I)/BZ(I)*DX(I-1)
202   X( I)=X( I)+DX( I)
C     END OF SOLVE
      DO 62  K=1,NDIV
      IF(X(K).LT.1070.0    GO TO 87
      IF(X(K).GT.1170.0)   GO TO 88
62    NE(K)=E(K)/V(K)+0.5
      LOP=1+LOP
      IF(LOP-4)    64,63,63
63    WRITE (6,3)AT,(RAD(I),X(I),NE(I),V(I),AG(I)    ,FVS(I),
     1SA(I),I=1,NDIV)
      CALL POINT1(1,AT,X(1))
      CAL POINT1(IPLOT,AT,X(NDIV))
      LOP=0
64    AT=AT+DT
      IF   (NDIV-NIP)89,89,51
C     END OF MAIN PROGRAM
85    WRITE (6,5)
      GO TO 90
87    WRITE (6,7)
      WRITE (6,3)AT,(RAD(I),X(I),NE(I),V(I),AG(I)   ,FVS(I),
     1SA(I),I=1,NDIV
      GO TO 90
88    WRITE (6,8)
      WRITE (6,3)AT,(RAD(I),X(I),NE(I),V(I),AG(I)   ,FVS(I),
     1SA(I),I=1,NDIV)
      GO TO 90
```

```
89     WRITE (6,9)
       WRITE (6,3)AT,(RAD(I),X(I),NE(I),V(I),AG(I)   ,FVS(I),
      1SA(I),I=1,NDIV)
90     WRITE (6,4)    (XMIN(I),I=1NDIV)
       CALL CURVE1(1,1,5)
       CALL CURVE1(IPLOT,1,5)
       CALL TITLE1('TEMP')
       CALL TITLE1('V TI')
       CALL TITLE1('ME  ')
       CALL GRAPH1(8.0,'TIME',6.0,'TEMP')
1      FORMAT(E20.7,60A1)
2      FORMAT (25X,23HFREEZING OF A ROUND BAR/12X,4HTIME,9X,
      16HRADIUS,9X,4HTEMP,9X,5HCELLS,9X,6HVOLUME,9X,3HFGS ,
      111X,3HFVS,11X,2HSA)
3      FORMAT (4X,F14.2,20(F14.6,  F14.3,I14,F14.6,F14.6,F14.8,
      1F14.4/18X))
4      FORMAT (8(1 X,F14.8))
5      FORMAT (4X,11HJ TOO LARGE)
6      FORMAT('1')
7      FORMAT (4X,16HX LESS THAN 1070)
8      FORMAT (4X,12HX ABOVE 1170)
9      FORMAT (4X,19HNIP 0+, NORMAL EXIT)
95     CONTINUE
       IF(NRUNS.EQ.1)  GO TO 301
       DO  300  NPLOT=2,IPLOT
       CALL CURVE1(NPLOT,1,5)
```

```
300   CONTINUE
      CALL TITLE1('TEMP')
      CALL TITLE1('V TI')
      CALL TITLE1('ME  ')
      CALL GRAPH1(8.0,'TIME',6.0,'TEMP')
301   RETURN
      END
```

SUBPROGRAM TO CALCULATE THE AMOUNT OF AUSTENITE LIBERATED

```
SUBROUTINE   GAMMA(V,DX,SLOPEV,ALH,AG,FVS,BL,I,AMOUNT,CEU,SK,X,EU)
DIMENSION  V(20),DX(20),ALH(20),AG(20),FVS(20),X(20)
COMPO(TEMP)=CEU+(TEMP-1153.0)/SLOPEV
DELTA=1.0-(COMPO(X(I))/COMPO(X(I)+DX(I)))**(1.0/(1.0-SK))
AMOUNT=V(I)*DELTA*(1.0-FVS(I))
ALH(I)=AMOUNT*BL
AG(I)=AG(I)+DELTA
FVS(I)=FVS(I)+DELTA
RETURN
END
```

TYPICAL SET OF DATA CARDS FOR A CALCULATION

```
    4.0THE NUMBER OF RUNS,  NRUNS
    0.6THE DIAMETER OF THE BAR IN INS, D                          50
  311.0THE COOLING RATE, DEG. C./MIN                              51
   2.86THE NUCLEATION CONSTANT                                    52
29.0E-5THE GROWTH CONSTANT (PRE-EXPONENTIAL)                      53
    1.0THE SENSITIVITY-DETERMINES THE TIME INCREMENT              54
   0.78THE GROWTH RATE EXPONENT                                   55
 1165.0THE LIQUIDUS TEMPERATURE FOR THE ALLOY DEG C               56
 -171.0THE SLOPE OF THE LIQUIDUS LINE                             57
  430.0THE LATENT HEAT OF FUSION OF THE PRIMARY PHASE             58
```

3.7THE EUTECTIC CARBON CONTENT		59
0.25THE PARTITION COEFFICIENT		60
5.0THE NUMBER OF RADIAL SUBDIVISIONS		61
0.875THE DIAMETER OF THE BAR IN INS, D	1	50
185.0THE COOLING RATE, DEG. C./MIN	1	51
2.86THE NUCLEATION CONSTANT	1	52
29.0E-5THE GROWTH CONSTANT (PRE-EXPONENTIAL)	1	53
1.0THE SENSITIVITY-DETERMINES THE TIME INCREMENT	1	54
0.78THE GROWTH RATE EXPONENT	1	55
1165.0THE LIQUIDUS TEMPERATURE FOR THE ALLOY DEG C	1	56
-171.0THE SLOPE OF THE LIQUIDUS LINE	1	57
430.0THE LATENT HEAT OF FUSION OF THE PRIMARY PHASE	1	58
3.7THE EUTECTIC CARBON CONTENT	1	59
0.25THE PARTITION COEFFICIENT	1	60
5.0THE NUMBER OF RADIAL SUBDIVISIONS	1	61
1.20THE DIAMETER OF THE BAR IN INS, D	1	62
77.0THE COOLING RATE, DEG. C./MIN	1	63
2.86THE NUCLEATION CONSTANT	1	64
29.0E-5THE GROWTH CONSTANT (PRE-EXPONENTIAL)	1	65
1.0THE SENSITIVITY-DETERMINES THE TIME INCREMENT	1	66
0.78THE GROWTH RATE EXPONENT	1	67
1165.0THE LIQUIDUS TEMPERATURE FOR THE ALLOY DEG C	1	68
-171.0THE SLOPE OF THE LIQUIDUS LINE	1	69
430.0THE LATENT HEAT OF FUSION OF THE PRIMARY PHASE	1	70
3.7THE EUTECTIC CARBON CONTENT	1	71
0.25THE PARTITION COEFFICIENT	1	72

```
    5.0THE NUMBER OF RADIAL SUBDIVISIONS                    1     73
    1.6THE DIAMETER OF THE BAR IN INDS, D                         62
   43.4THE COOLING RATE, DEG. C./MIN                              63
   2.86THE NUCLEATION CONSTANT                                    64
29.0E-5THE GROWTH CONSTANT (PRE-EXPONENTIAL)                      65
    1.0THE SENSITIVITY-DETERMINES THE TIME INCREMENT              66
   0.78THE GROWTH RATE EXPONENT                                   67
 1165.0THE LIQUIDUS TEMPERATURE FOR THE ALLOY DEG C               68
 -171.0THE SLOPE OF THE LIQUIDUS LINE                             69
  430.0THE LATENT HEAT OF FUSION OF THE PRIMARY PHASE             70
    3.7THE EUTECTIC CARBON CONTENT                                71
   0.25THE PARTITION COEFFICIENT                                  72
    5.0THE NUMBER OF RADIAL SUBDIVISIONS                          73
```

APPENDIX D

SAMPLE OF OUTPUT DATA

FREEZING OF A ROUND BAR

TIME	RADIUS	TEMP	CELLS	VOLUME	FGS	FVS	SA
0.24	0.762000	1166.357	0	0.364876	0.0	0.0	0.0
	0.681553	1167.311	0	0.364876	0.0	0.0	0.0
	0.590242	1168.195	0	0.364876	0.0	0.0	0.0
	0.481931	1168.945	0	0.364876	0.0	0.0	0.0
	0.340777	1169.552	0	0.364876	0.0	0.0	0.0
0.48	0.762000	1164.165	0	0.364876	0.001145	0.00114489	0.0
	0.681553	1165.176	0	0.364876	0.0	0.0	0.0
	0.590242	1166.167	0	0.364876	0.0	0.0	0.0
	0.481931	1167.132	0	0.364876	0.0	0.0	0.0
	0.340777	1168.078	0	0.364876	0.0	0.0	0.0
0.72	0.762000	1162.171	0	0.364876	0.005470	0.00546998	0.0
	0.681553	1163.195	0	0.364876	0.003198	0.00319785	0.0
	0.590242	1164.215	0	0.364876	0.001044	0.00104427	0.0
	0.481931	1165.231	0	0.364876	0.0	0.0	0.0
	0.340777	1166.264	0	0.364876	0.0	0.0	0.0
0.96	0.762000	1160.225	0	0.364876	0.009636	0.00963634	0.0
	0.681553	1161.252	0	0.364876	0.007362	0.00736159	0.0
	0.590242	1162.279	0	0.364876	0.005193	0.00519288	0.0
	0.481931	1163.309	0	0.364876	0.003088	0.00308800	0.0
	0.340777	1164.365	0	0.364876	0.001023	0.00102282	0.0
1.20	0.762000	1158.291	0	0.364876	0.013754	0.01375443	0.0
	0.681553	1159.319	0	0.364876	0.011484	0.01148432	0.0
	0.590242	1160.348	0	0.364876	0.009317	0.00931680	0.0
	0.481931	1161.381	0	0.364876	0.007209	0.00720865	0.0
	0.340777	1162.442	0	0.364876	0.005134	0.00513381	0.0
1.44	0.762000	1156.359	0	0.364876	0.017852	0.01785231	0.0
	0.681553	1157.386	0	0.364876	0.015588	0.01558805	0.0
	0.590242	1158.416	0	0.364876	0.013427	0.01342702	0.0
	0.481931	1159.450	0	0.364876	0.011323	0.01132321	0.0
	0.340777	1160.512	0	0.364876	0.009251	0.00925124	0.0

TIME	RADIUS	TEMP	CELLS	VOLUME	FGS	FVS	SA
1.68	0.762000	1154.426	0	0.364876	0.021938	0.02193820	0.0
	0.681553	1155.454	0	0.364876	0.019680	0.01967990	0.0
	0.590242	1156.484	0	0.364876	0.017526	0.01752597	0.0
	0.481931	1157.518	0	0.364876	0.015428	0.01542801	0.0
	0.340777	1158.581	0	0.364876	0.013362	0.01336223	0.0
	0.681553	1117.618	3359	0.364876	0.098420	0.14594591	2.8479
	0.590242	1118.557	3190	0.364876	0.096561	0.13613355	2.4922
	0.481931	1119.428	3035	0.364876	0.094904	0.12770492	2.1720
	0.340777	1120.256	2891	0.364876	0.093426	0.12036771	1.8792
10.06	0.762000	1116.797	3546	0.364876	0.100240	0.16811424	3.6628
	0.681553	1117.815	3359	0.364876	0.098125	0.15512794	3.2324
	0.590242	1118.740	3190	0.364876	0.096294	0.14401364	2.8427
	0.481931	1119.587	3035	0.364876	0.094684	0.13446969	2.4904
	0.340777	1120.382	2891	0.364876	0.093270	0.12616086	2.1666
10.30	0.762000	1117.188	3546	0.364876	0.099558	0.17971164	4.0989
	0.681553	1118.293	3359	0.364876	0.097448	0.16508085	3.6344
	0.590242	1119.115	3190	0.364876	0.095643	0.15254694	3.2116
	0.481931	1119.939	3035	0.364876	0.094080	0.14178175	2.8275
	0.340777	1120.701	2891	0.364876	0.092729	0.13240319	2.4730
10.54	0.762000	1117.767	3546	0.364876	0.098498	0.19217646	4.5456
	0.681553	1118.780	3359	0.364876	0.096394	0.17578572	4.0491
	0.590242	1119.679	3190	0.364876	0.094609	0.16172165	3.5947
	0.481931	1120.482	3035	0.364876	0.093090	0.14963573	3.1799
	0.340777	1121.214	2891	0.364876	0.091801	0.13909668	2.7952
10.78	0.762000	1118.527	3546	0.364876	0.097068	0.20545048	4.9970
	0.681553	1119.539	3359	0.364876	0.094967	0.18719661	4.4715
	0.590242	1120.428	3190	0.364876	0.093204	0.17150962	3.9876
	0.481931	1121.211	3035	0.364876	0.091721	0.15800989	3.5435
	0.340777	1121.915	2891	0.364876	0.090491	0.14622742	3.1299

TIME	RADIUS	TEMP	CELLS	VOLUME	FGS	FVS	SA
11.02	0.762000	1119.456	3546	0.364876	0.095294	0.21945739	5.4471
	0.681553	1120.468	3359	0.364876	0.093190	0.19925237	4.8961
	0.590242	1121.348	3190	0.364876	0.091443	0.18186021	4.3854
	0.481931	1122.115	3035	0.364876	0.089994	0.16687155	3.9142
	0.340777	1122.793	2891	0.364876	0.088815	0.15377027	3.4732
11.26	0.762000	1120.535	3546	0.364876	0.093207	0.23409671	5.8901
	0.681553	1121.549	3359	0.364876	0.091095	0.21187347	5.3178
	0.590242	1122.424	3190	0.364876	0.089359	0.19271100	4.7835
	0.481931	1123.177	3035	0.364876	0.087939	0.17617142	4.2876
	0.340777	1123.833	2891	0.364876	0.086800	0.16168535	3.8212
34.26	0.762000	1124.561	3546	0.364876	0.084080	0.89477175	2.6416
	0.681553	1126.318	3359	0.364876	0.072800	1.00002480	0.0286
	0.590242	1128.462	3190	0.364876	0.076119	0.99552673	0.3390
	0.481931	1131.056	3035	0.364876	0.070938	0.96477699	1.9165
	0.340777	1134.031	2891	0.364876	0.065086	0.90175682	4.1543
34.50	0.762000	1123.502	3546	0.364876	0.086177	0.90358543	2.5148
	0.681553	1125.260	3359	0.364876	0.072800	1.00002480	0.0286
	0.590242	1127.376	3190	0.364876	0.078283	0.99822372	0.1627
	0.481931	1129.956	3035	0.364876	0.073136	0.97072482	1.6438
	0.340777	1132.960	2891	0.364876	0.067235	0.91151488	3.8451
34.74	0.762000	1122.366	3546	0.364876	0.088421	0.91238058	2.3760
	0.681553	1124.126	3359	0.364876	0.072800	1.00002480	0.0286
	0.590242	1126.213	3190	0.364876	0.080003	1.00008297	0.0356
	0.481931	1128.774	3035	0.364876	0.075495	0.97637349	1.3728
	0.340777	1131.799	2891	0.364876	0.069556	0.92114896	3.5255
34.98	0.762000	1121.157	3546	0.364876	0.090816	0.92111754	2.2252
	0.681553	1122.926	3359	0.364876	0.072800	1.00002480	0.0286
	0.590242	1124.997	3190	0.364876	0.080003	1.00008297	0.0356
	0.481931	1127.514	3035	0.364876	0.078013	0.98168838	1.1053
	0.340777	1130.543	2891	0.364876	0.072065	0.93061906	3.1961

TIME	RADIUS	TEMP	CELLS	VOLUME	FGS	FVS	SA
35.22	0.762000	1119.880	3546	0.364876	0.093340	0.92972815	2.0637
	0.681553	1121.659	3359	0.364876	0.072800	1.00002480	0.0286
	0.590242	1123.714	3190	0.364876	0.080003	1.00008297	0.0356
	0.481931	1126.177	3035	0.364876	0.080676	0.98662484	0.8445
	0.340777	1129.195	2891	0.364876	0.074758	0.93985957	2.8586
35.46	0.762000	1118.526	3546	0.364876	0.096007	0.93817669	1.8919
	0.681553	1120.317	3359	0.364876	0.072800	1.00002480	0.0286
	0.590242	1122.353	3190	0.364876	0.080003	1.00008297	0.0356
	0.481931	1124.758	3035	0.364876	0.083498	0.99116969	0.5918
	0.340777	1127.749	2891	0.364876	0.077640	0.94881159	2.5151
35.70	0.762000	1117.085	3546	0.364876	0.098837	0.94642979	1.7102
	0.681553	1118.889	3359	0.364876	0.072800	1.00002480	0.0286
	0.590242	1120.906	3190	0.364876	0.080003	1.00008297	0.0356
	0.481931	1123.245	3035	0.364876	0.086496	0.99531579	0.3486
	0.340777	1126.197	2891	0.364876	0.080726	0.95742089	2.1675

APPENDIX E

COMPUTER PROGRAM TO MODEL DENDRITE GROWTH

APPENDIX E

COMPUTER PROGRAM TO MODEL DENDRITE GROWTH

Main Program

OS/360 FORTRAN H

```
C   THIS PROGRAM IS DESIGNED TO CALCULATE THE GROWTH OF A DENDRITE
C   AS A RESULT OF HEAT FLOW.  IT CAN BE MODIFIED TO TREAT SOLUTE
C   DIFFUSION PROBLEMS, BUT THE DIFFUSION PARAMETERS MUST BE CHOSEN
C   WITH CARE TO AVOID UNDER AND OVERFLOW PROBLEMS.  IT WILL TREAT
C   DENDRITE ARRAYS, AND CRYSTALS WITH NON-ISOTROPIC SURFACE ENERGIES.
C   IF SOLID FLOW IS TO BE CONSIDERED, A FURTHER PROCEDURE IS NEEDED
C   WHICH IS NOT INCLUDED WITH THIS PACKAGE.
      INTEGER IN(60,15)
      REAL*8 RI,RO,P1,P2,Pe,CSQF
      REAL*8X,Z,AZ,BZ,XSURF,ZSURF
      COMMON X(50,50),Z(50,50),XSURF(50),ZSURF(50),AZ(50),BZ(50),CZ(50),
     1ZM(50),XM(50),SM(50),NPAR,NORTH,ZO,FO,TS,TINF,COND,E,G,TEQ,AH,
     2TON(2),S,AI,DT,JIN,DTIME,CEFF,CS1,SLOP1,CHANGA,CONDS,SS,BASE,TOP,
     3OUT,FLOIN,CHANGE,DPREST,BEFF,DELTAT(50,50),T(50,50)r(50,50)
      DIMENSION DAT(15)
      CSQF(RI,RO,P1,P2,P3)=(RI*(P3-P2)-RO*(P2-P1))/(RI*RO*(RI+RO))
      READ(5,2)  NRUNS,(IN(K,1),K=1,60)
      WRITE(6,16)
      DO 130 KOUNT=1,NRUNS
C   READ IN DATA FOR EACH CASE TO BE STUDIED
      READ(5,2)  NPAR,(IN(K,2),K=1,60)
      READ(5,2)  NORTH,(IN(K,3),K=1,60)
```

```
      READ(5,2)  LOOPS,(IN(K,4),K=1,60)
      WRITE(6,2) NRUNS,(IN(K,1),K=1,60)
      WRITE(6,2) NPAR,(IN(K,2),K=1,60)
      WRITE(6,2) NORTH,(IN(K,3),K=1,60)
      WRITE(6,2) LOOPS,(IN(K,4),K=1,60)
      DO  30  I=1,15
      READ(5,3) DAT(I),(IN(K,I),K=1,60)
30    WRITE(6,3) DAT(I),(IN(K,I),K=1,60)
C   NOW CHANGE THE INPUT DATA INTO THE TRIVIAL TERMS USED IN THE CALCUL-
C   ATION.
      OMEG=DAT(1)
      FO=DAT(2)
      ZO=DAT(3)
      TINF=DAT(4)
      TS=DAT(5)
      TEQ=DAT(6)
      S=DAT(7)
      AH=DAT(8)
      COND=DAT(9)
      BEFF=DAT(10)
      SS=DAT(11)
      CEFF=DAT(12)
      DTIME=DAT(13)
      WRITE(6,8)
      NCONE=1
      COND=COND*DTIME
```

```
      IF(DAT(14).LE.0.0)    GO TO 64
      IF(DAT(14)-90.0)    57,58,61
57    A2=TAN(DAT(14)*3.14159/180.0)
      GO TO 59
58    A2=1.0E6
C   THIS IS FOR PARALLEL ARRAYS AND SETS THE BOUNDARIES AT A VERY SLIGHT
C   ANGLE TO ONE ANOTHER FOR CONVENIENCE.
59    BOUND=DAT(15)/2.0
      NCONE=2
64    CONTINUE
C   SET UP THE INITIAL NETWORK.  NETCOM MAKES THE TIP TEMPERATURE PROFILE
C   FOLLOW THE E1 FUNCTION, AND FOR SINGLE NEEDLES EXTENDS THE CRYSTAL
C   AND THE ISOTHERMS AS CONFOCAL PARABOLAE.  THE ORTHOGONALS ARE STARTED
C   ON THE CRYSTAL SURFACE WITH SPACING GIVEN BY A POWER SERIES, THE
C   POWER ADJUSTED TO MAKE THE ISOTHERM-ORTHOGONAL SPACING RATIO AT THE
C   TIP BE 1:15.
      CALL NETCOM(NCONE,BOUND,A2,&13)
      LAST=NPAR-1
      LOWER=NORTH-1
      DO 63  J=1,LAST
      XM(J)=X(J,NORTH)
      ZM(J)=Z(J,NORTH)
63    SM(J)=(Z(J+1,NORTH)-Z(J,NORTH))/(X(J+1,NORTH)-X(J,NORTH))
      CALL MOVER(&13)
      CALL HUNT(&13)
      ACT=0.0
      HUMP=50.0*DTIME
```

```
C   HUMP IS A CONSTANT WHICH DETERMINES WHEN THE ARRAYS ARE PRINTED.
         TIME=0.0
         ZSURF(2)=R(2,2)/2.0
C   THE START OF THE MAIN CALCULATION
         CALL POINT1(9,0.0,0.0)
         DO  12  LOOP=1,LOOPS
         IWAY=1
         IF(ACT.GT.HUMP)   CALL PUTOUT(ACT)
         WRITE(6,6)
999      CONTINUE
C   THE FOLLOWING STATEMENTS CALCULATE THE TEMPERATURE DEPRESSION DUE TO
C   CURVATURE AT THE TIP.  VALUES FOR OTHER STATIONS DOWN THE CRYSTAL
C   ARE CALCULATED IN INNER AND INNER2 ROUTINES.
         DAR=CSQF(X(1,3),X(1,3),Z(1,3),Z(1,2),Z(1.3))
         DPREST=-4.0*CEFF*DAR
         RHO=-0.5/DAR
         ANEWT=TEQ-DPREST
C   CHANGA IS USED WHEN HEAT FLOW IN THE SOLID IS BEING CONSIDERED
         CHANGA=T(1,2)-ANEWT
         T(1,2)=ANEWT
         WRITE(6,14)
         WRITE(6,4) DPREST,ANEWT,CHANGA,RHO
         GO TO 909
7        COND=COND*DTIME
909      CONTINUE
```

```
      SLOP1=0.0
      CS1=1.0
      DO 10 K=2,LOWER
C     OUTER APPLIES THE FAR FIELD BOUNDARY CONDITION. JIN IS THE INDEX
C     OF THE THIRD ISOTHERM FROM THE NON-ISOTHERMAL SURFACE, AND IS
C     CALCULATED IN OUTER.
      CALL OUTER(NPAR,K)
      JEND=JIN+1
      DO 9 M=JEND,LAST
      N=LAST-M+JEND
C     CENTRE APPLIES THE CONSERVATION EQUATION FOR THE CENTRAL COMPARTMENTS
9     CALL CENTRE(N,K)
C     INNER APPLIES THE CONSERVATION CONDITION FOR THE SURFACE BOUNDARY
C     AND CHANGES ALL TEMPERATURES.  IT CALCULATES SURFACE GROWTH.
      GO TO (40,50),IWAY
40    CALL INNER(K,&19,TIME)
10    CONTINUE
      IF(IWAY.EQ.1) GO TO 60
      TIME=TIME+DTIME
      ACT=ACT+DTIME
C     MOVER FINDS THE NEW POSITIONS FOR THE ISOTHERMS
60    CALL MOVER(&13)
C     HUNT IS THE MOST COMPLEX ROUTINE USED.  IT FINDS THE NEW ORTHOGONALS
      IF(IWAY.EQ.2)GO TO 12
      CALL CRECT1(&13,IWAY)
      GO TO 999
```

```
C   PUTOUT WRITES AND PLOTS THE TEMPERATURE FIELD
19      CONTINUE
        WRITE(6,15) DTIME,ACT,TIME
        GO TO 7
12      WRITE(6,1)LOOP
        GO TO 62
61      WRITE(6,17)
62      WRITE(6,16)
C   AFTER THE CALCULATION HAS BEEN COMPLETED, THE DATA ARE REPRINTED
        DO 31 I=1,15
31      WRITE(6,3) DAT(I),(IN(K,I),K=1,60)
        CALL PUTOUT(ACT)
13      WRITE(6,18)
        CALL CURVE1(9,1,3)
        CALL TITLE1('VELO')
        CALL TITLE1('CITY')
        CALL TITLE1(' V T')
        CALL TITLE1('IME')
        CALL GRAPH1(8.0,'TIME',6.0,'VEL ')
130     WRITE(6,20)
1       FORMAT(50X,5HLOPP=,I5)
2       FORMAT(I20,60A1)
3       FORMAT(E20.7,60A1)
4       FORMAT(4+20.9)
5       FORMAT(10X,5f20.9)
6       FORMAT(///)
8       FORMAT(//.10X,'THIS CALCULATION GENERATES ITS OWN NETWORK',//)
```

```
14      FORMAT(10X,6HDPREST,14X,5HANEWT,15X,6HCHANGA,14X,6HRADIUS)
15      FORMAT(2X,6HDTIME=,E12.5,10X,4HACT=,E12.5,10X,5HTIME=,E12.5)
16      FORMAT('1',30X,'INPUT DATA',//)
17      FORMAT(5X,'THE INPUT DATA WAS FAULTY.  THE CONE ANGLE WAS GREATER
       1THAN 90 DEGREES.')
18      FORMAT(2X,'NON-STANDARD RETURN FROM HUT OR MOVER')
20      FORMAT('1')
        RETURN
        END
```

Line of Steepest Descent Through a Temperature Field From a Non-Isothermal Surface

The computer calculation fits a quadratic relationship between the Z and X coordinates of the three adjacent points on the crystal surface (taking the two points on either side of the desired portion). Differentiating, the slope of the tangent is found, and thence the sine and cosine of the angle of the tanget line with the X and Z coordinates. In a similar fashion, taking the three nearest points lying outwards in the temperature field, the sine and cosine of the angle at the surface made by a line through the points outwards into the thermal field can be calculated. Using a radial coordinate system (taking the radial distances between the points) the temperature gradients in the two directions can be found. These quantities are sufficient to allow the calculation of the line of steepest descent through the temperature field.

Consider the diagram of Figure E-1. This shows in three dimensions the relationships near the surface. The circle of radius dR is intersected by the two lines at angles α and β with the X ordinate. At the points of intersection, the temperature change dT is shown as a vertical projection. $dT\alpha$ and $dT\beta$ are the temperature decreases at a distance dR from the origin at angles α and β to the X axis. Figure E-2 shows the isothermal surface which passes through both of the points and through the origin. This can be imagined to form an ellipse when the dR circle is projected on to it. The line of steepest descent is the major axis of the ellipse. In the calculation which follows, the direction of the minor axis will first be found, and from it the gradient of the major axis.

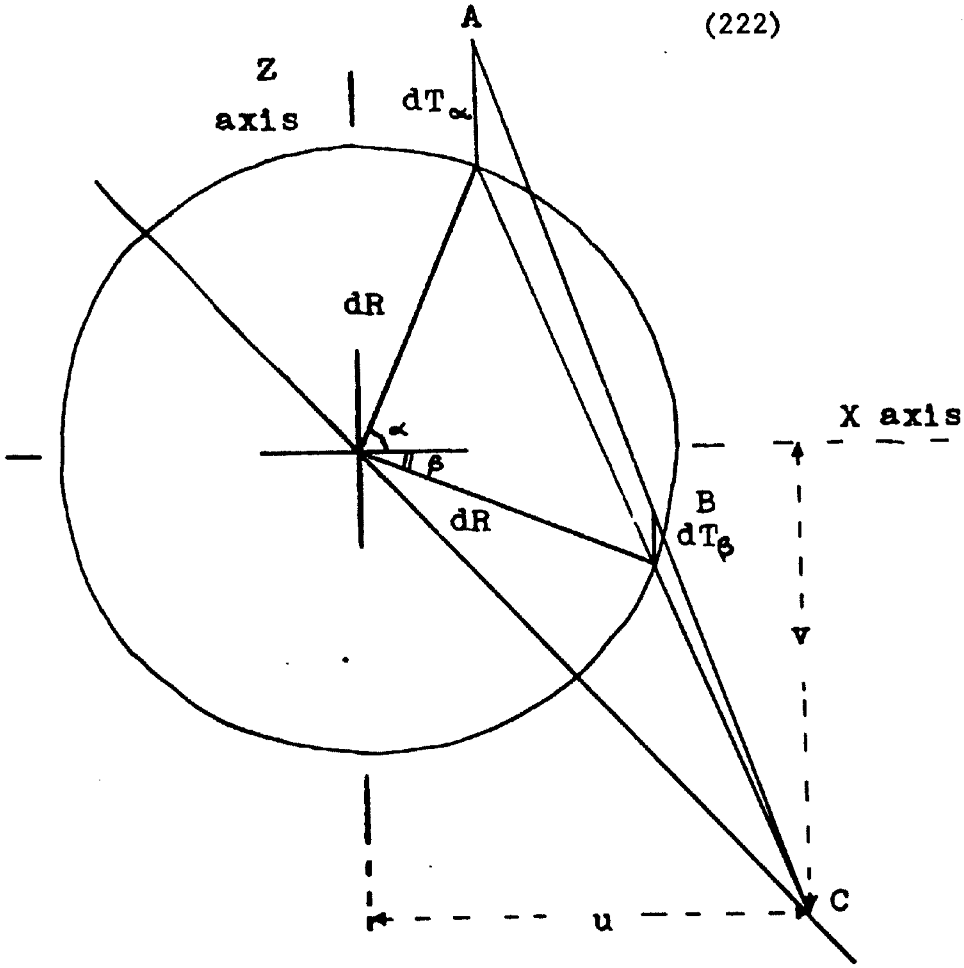

Figure E-1 Finding the Axis of Zero Temperature Gradient from the Temperature Gradients in Two Known Directions

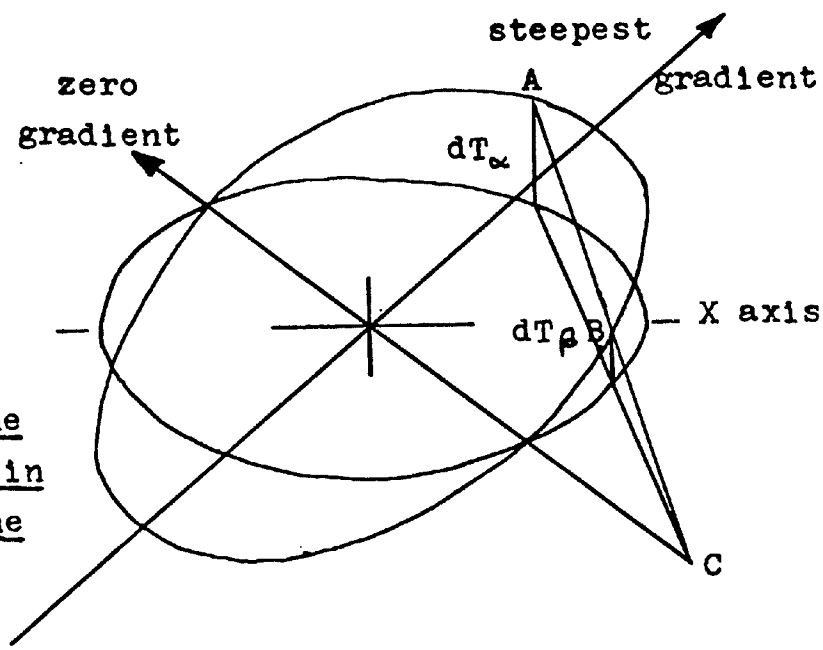

Figure E-2 The Direction of Steepest Descent as the Major Axis of an Ellipse in the Zero Temperature Plane

Consider the projection of the points A and B to a point C for which dT is zero. Let the coordinates of C be u and v for the X and Z axes, respectively. In the Z coordinate only:

$$\frac{dT_\alpha}{v+dR\sin\alpha} = \frac{dT_\beta}{v+dR\sin\beta} \quad . \qquad \text{(E-1)}$$

Similarly, taking the X ordinate:

$$\frac{dT_\alpha}{u-dR\cos\alpha} = \frac{dT_\beta}{u-dR\cos\beta} \quad . \qquad \text{(E-2)}$$

Suitable manipulation of (E-1) and (E-2) yields:

$$-\frac{v}{u} = -\left\{\frac{\cos\alpha\ dT_\beta - \cos\beta\ dT_\alpha}{\sin\beta\ dT_\alpha - \sin\alpha\ dT_\beta}\right\} \quad . \qquad \text{(E-3)}$$

Equation (E-3) is the direction of steepest descent through the thermal field. Further manipulation leads to the form which was most convenient for computation:

$$\text{Gradient} = \left\{\left(\frac{\cos\alpha}{\cos\beta.Am}\right) - 1 \ / \left\{\tan\beta - \frac{\sin\alpha}{\cos\beta.Am}\right\}, \qquad \text{(E-4)}$$

where

$$Am = \frac{dT_\alpha}{dT_\beta} \quad .$$